CHARACTERIZATION OF ION CHANNELS IN MDCK CELLS AND OF THE EFFECTS OF AMPHOTERICIN B ON ION CONDUCTION IN THESE CELLS USING THE PATCH-CLAMP TECHNIQUE

by

SHYUE-FANG HSU

A thesis submitted in partial fulfillment of the
requirements for the degree of

Doctor of Philosophy

(Pharmacy)

at the

University of Wisconsin-Madison

1993

phar
AW
#78

A dissertation entitled

Characterization of Ion Channels in MDCK Cells and of the Effects of Amphotericin B on Ion Conduction in These Cells using the Patch-Clamp Technique

submitted to the Graduate School of the
University of Wisconsin-Madison
in partial fulfillment of the requirements for the
degree of Doctor of Philosophy

by

Shyue-Fang Hsu

Degree to be awarded: December 1993 May 19___ August 19___

Approved by Dissertation Readers:

Major Professor

Aug. 16, 1993
Date of Examination

Dean, Graduate School

CHARACTERIZATION OF ION CHANNELS IN MDCK CELLS AND OF THE EFFECTS OF AMPHOTERICIN B ON ION CONDUCTION IN THESE CELLS USING THE PATCH-CLAMP TECHNIQUE

by

SHYUE-FANG HSU

A thesis submitted in partial fulfillment of the
requirements for the degree of

Doctor of Philosophy

(Pharmacy)

at the

University of Wisconsin-Madison

1993

To my parents and Bruce

ACKNOWLEDGMENTS

I am deeply indebted to many people who gave generously of their time, knowledge, and support during my pursuit of this degree, and I cannot find words to express my gratitude to them. First I would like to mention my advisor, Professor Ronald R. Burnette; Professors Meyer B. Jackson, Theodore Sokoloski, and Bill Chiu; Professor Marcelino Cereijido and Dr. Arturo Ponce in Mexico City; and Professor Robert Turner in the Mathematics Department.

I would also like to thank all of the professors in the School of Pharmacy, especially Professors Connors, Heath, Mukerjee, and Zografi, for their teaching and inspiration.

I will not forget the warm friendship of my fellow graduate students. They shared with me the ups and downs of life as a graduate student and made my life more enjoyable than otherwise.

I am extremely grateful for the love and tremendous support which my parents and my husband, Bruce, gave during this turbulent period. My mother and father traveled half of the globe to help out so that I could concentrate on being a graduate student. My husband lost countless nights of sleep correcting my clumsy writing, tolerating my bad moods and sharing my good ones, and most of all teaching me how to write for people who can't read my mind.

Characterization of Ion Channels in MDCK Cells and of the Effects of Amphotericin B on Ion Conduction in these Cells using the Patch-Clamp Technique

Shyue-Fang Hsu

Under the Supervision of Associate Professor Ronald Ray Burnette

at the University of Wisconsin-Madison

The primary objective of this research is to characterize the ion channels present in the membranes of cultured MDCK cells and to identify the effects, if any, of Amphotericin B on these channels.

We demonstrated previously the presence of ion channels that constitute the ionic conduction pathway across MDCK cell membranes. Based on our whole cell and cell-attached single channel studies, we concluded that MDCK cells can serve as a model to study the effects of Amphotericin B on ion channels in kidney epithelium. The thrust of this research, a continuation of our previous studies, is to characterize fully the ion channels in these cells and to study the effects of Amphotericin B on these ion channels.

Our interest in Amphotericin B concerns its widely accepted mode of action - that is, pore forming. Creation of aqueous membrane-spanning pores in bilayer lipid membranes has long been seen as the mechanism for the toxicity of Amphotericin B. These pores are thought to cause leakage of certain electrolytes from viable cells, and to increase the uptake of other drug molecules when these drug molecules are coadministered with Amphotericin B. A detailed examination of the data obtained in studies of the mechanism of Amphotericin B, however, reveals certain phenomena associated with Amphotericin B which cannot be explained by pore formation.

The purpose of this research is to evaluate the effects of Amphotericin B on ion channels in a model cell system, because Amphotericin B may alter ion transport through transport proteins of a cell membrane. We hypothesize that Amphotericin B either disturbs lipid ordering in cell membranes or binds to ion channel proteins, leading to conformational changes in ion transport proteins, and as a result upsetting the intracellular ion balance.

This thesis is divided into two chapters. Chapter One describes the transport of potassium ions across kidney tubular membranes, emphasizing in particular renal potassium channels. The functional roles of these potassium channels are of particular interest to us because we have identified, in our model cells (MDCK cells), various types of potassium channels; we found that, among the different channels, two types of channels increased their opening with either intracelluar Ca^{+2} or ATP (adenosine triphosphate). Chapter Two concerns the study of Amphotericin B on our model cells. The effects of Amphotericin B on whole cell ion conduction as well as on single channel conduction are presented.

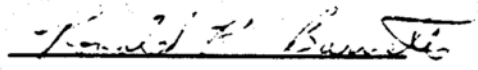

TABLE OF CONTENTS

Chapter One
Potassium channels in kidney tubules

Abstract

Using the inside-out patch-clamp technique, we found, in the membranes of cultured MDCK cells, three types of potassium channel which are sensitive to intracellular adenosine 5'-triphosphate (ATP) in the mM range. Two of these channels, whose open probability increased with intracellular ATP concentration, turned out to be Ca^{+2}-activated potassium channels. The open probability of the third type of potassium channel decreased, however, in the presence of intracellular ATP in the same range.

The two Ca^{+2}-activated potassium channels were found to be capable of reversible activation by intracellular adenosine 5'-triphosphate (ATP) together with low intracellular Ca^{+2} (~130nM). Covalent modification (phosphorylation) was ruled out as the mechanism of activation since the channels could be activated by non-hydrolyzable ATP (AMP-PCP), as well as by ATP in the absence of Mg^{+2}. The dissociation constants for the activation for these channels were found to be in the range of 0.5 - 1mM. The nucleotides ADP and AMP also increased the open probabilities of these channels with relative potencies as follows: ATP $\approx$ ADP > AMP. However, c-AMP and adenosine had no effect on these Ca^{+2} channels.

These two Ca^{+2}-activated potassium channels were distinguishable by their conductance values, 49 pS and 240 pS. The 49 pS channel was found to be inwardly rectifying in the presence of a bathing and pipette potassium solution of 160mM on both sides of the membrane, and was relatively voltage-independent. ATP increased this channel's open probability without altering its voltage-independence. In contrast, the 240 pS conductance channel was relatively voltage-sensitive. In the absence of

ATP, its open probability increased slightly with depolarization with a $V_{1/2}$ of greater than 100 mV. ATP binding shifted the voltage-dependence of this channel toward a more negative potential. A $V_{1/2}$ shift of approximately -90 mV, observed for a change in ATP concentration from 0.5 mM to 4 mM, reflects ATP's efficacy in activating this channel. The Hill's coefficient of ATP binding is ~ 1.87 for the K channel with smaller conductance, and ~ 3.8 for the K channel with larger conductance.

These two Ca^{+2}-activated channels were different from many K_{ATP} channels reported in the literature in that their activity was enhanced rather than suppressed by intracellular ATP. Only four other Ca^{+2}-activated channels have been reported so far as susceptible to activation by intracellular ATP in a concentration range of 0.5 - 5 mM (38, 39, 40, 41). Three of these channels are modulated by phosphorylation, not by direct binding, which has been the consensus mechanism for the effects of intracellular ATP on K_{ATP} channels.

The third channel found in the MDCK cells had a conductance of 40 pS and an ATP sensitivity similar to that of K_{ATP} channels found in other cell types. Intracellular ATP at millimolar concentrations closed this channel. Because high intracellular potassium also suppressed the opening of this channel, we avoided the use of high levels of intracellular potassium during our study on the sensitivity of this channel to ATP. We believe that, in vivo, inactivation caused by ATP is not likely to be an important mode of regulation for this channel since, in normal physiological conditions, the intracellular potassium concentration is generally high.

Introduction

The kidney tubule is a common site of Amphotericin B nephrotoxicity. Our focus of study was the effects of Amphotericin B in MDCK cells, a cultured cell line, obtained from dog kidneys, that in many respects resembles distal tubular cells (31-34).

Two factors led us to narrow our focus to Amphotericin B's effects on potassium channels. First, no other channels are found in MDCK cells (4, 35, 36). Second, Amphotericin B is known to cause potassium wasting from cells (37). Hypokalaemia is among the forms of nephrotoxicity of Amphotericin B that is related to disturbances of ion transport across kidney tubules. Our studies using MDCK cells indicate that these effects may be caused by the malfunctioning of certain potassium channels in these cells (see experimental results). Since potassium channels play a significant role in regulating ion transport across cell membranes in kidney epithelial tissue, we believe that the ion imbalances induced by Amphotericin B are partly related to this abnormal potassium channel activity.

The following sections review the interdependence of the functions of potassium channels and various transporters in kidney tubular cells. The purpose of this review is to emphasize that potassium channels play significant roles in the transport of ionic species and neutral molecules across kidney epithelium; hence Amphotericin B's disturbance of the functioning of potassium channels can lead to a dramatic change in the functioning of the transport epithelium.

Part I: Physiology of renal potassium channels and their roles in the transport of nutrients and ions across renal epithelium.

A. The proximal renal tubules

The activity of most of the transporters in the membranes of proximal tubular cells are indirectly coupled to and modified by the activity of potassium channels (4). This is because the majority of these transporters are sensitive to potential differences across cell membranes, and potassium channels play a major role in controlling cell membrane potential (4, 13).

Several lines of evidence suggest that various potassium channels found in the proximal tubules of kidneys have distinct roles in regulating ion transport across the tubular cells (Table 1) (4). The distributions of these potassium channels in apical and basolateral membranes were found to vary according to the position of the proximal tubular cells relative to the glomerulum (6, 7). Potassium conductance was found to increase with the distance between the tubular cells and the glomerulum. Hence, there can be an increasing influence of potassium channels on cell membrane potential and consequently, an increasing influence of potassium channels on other transport mechanisms of these cells. Also, because of the paracellular shunt pathway among the proximal tubular cells, the main transcellular potassium conductance, which is associated with the basolateral membrane, can affect any potential-sensitive transport processes across both the basolateral and the apical cell membranes. This effect is produced via the generation of a circular current, which may be substantial because of the leaky nature of the tight junctions between proximal tubular cells. Thus, the current flowing through the basolateral potassium channels can circulate across the tight junction of the cell and affect the membrane potential of the apical membrane (8, 9). The activity of potential-sensitive transporters thus can be altered by changes in the

opening and closing of potassium channels residing at either site in the proximal tubular cell membrane.

Many factors can regulate the activity of potassium channels. These factors can thus indirectly modulate various transporters through a change in membrane potential. The potassium channels observed to date along the kidney tubules are found to be controlled by membrane potential, intracellular pH, intracellular calcium, potassium and sodium concentrations, cell volume, hormones, and second messengers such as c-AMP (4, 10). The potassium channels of the kidney, like those of other tissues, are often classified according to modes of activation: (a) voltage-gated channels, (b) calcium-activated potassium channels, (c) ligand-gated channels, (d) nucleotide-gated channels (K_{ATP} and K_{nuc}) (10). Thus, a change in concentration of any regulators mentioned above inside a renal cell can indirectly modify the activities of a variety of transporters through the action of potassium channels.

One such scenario is the change of the transport direction of the basolateral $(HCO_3^-)_3$ cotransporter, as a result of a decrease in potassium channel activity (4). The Na^+-$(HCO_3^-)_3$ cotransporter is one of the major pathways for ion translocation across the basolateral membranes of proximal tubular cells. It is very sensitive to potential differences across the basolateral membrane since its driving force for the normal outward transport of Na^+ and HCO_3^- arises from the potential difference between the transporter's equilibrium potential (-58mV) and the resting membrane potential (-70mV). Hence, a change in membrane potential caused by a decreased potassium channel activity can reverse the direction of transport and cause alkalinization of the proximal tubular cells. Further changes in ion transport can also occur because of the higher pH environment of the tubular cells. These include

shutting down of the Na^+/H^+ exchanger and reduction of the activity of the Na^+/citrate cotransporter.

Potassium channels also play a role in physiological homeostasis during stimulated transport (4). An illustration of this role is the stimulation of Na^+ transport by increased physiological uptake of phenylalanine, which is mediated through activation of Na^+-coupled amino acid transporters (11, 12). Increased Na^+ uptake by proximal tubular cells results in membrane depolarization. The ensuing sequence of events differs depending on the location in the cells. In the basolateral membrane, depolarization eventually leads to a reduction in Na^+ entry. The mechanism of this reduction is as follows. Depolarization of the basolateral membrane leads to an initial decrease in the potassium conductance because of the voltage-sensitive potassium channels in this membrane (Table 1). As a consequence, there is a reduction in the cellular loss of potassium across the basolateral membrane, further depolarizing the basolateral membrane. A reduced electrochemical driving force for the Na^+-$(HCO_3^-)_3$ cotransporter hence results, leading to accumulation of HCO_3^-, and thus a reduction in the Na^+/H^+ exchange. These events culminate in reduced Na^+ entry. If a continued stimulation of Na^+ entry leads to acidosis after a time lag, then potassium conductance across the basolateral membrane can recover, eventually leading to recovery of H^+ secretion (12).[1] However, in the apical membrane, in contrast to the basolateral membrane, depolarization caused by the initial Na^+ entry helps to maintain the driving force for further Na^+ entry. In the apical membrane, depolarization

---

[1]This delayed recovery is believed to be, in part, due to cell swelling brought about by the entry of Na^+ and organic substrates into the cells. The swelling leads to the opening of stretch-activated potassium channels and calcium-conducting channels in the basolateral membrane, repolarizing the membrane potential and hence resurrecting the H^+ secretion.

activates certain potassium channels (Table 1). The increased potassium conductance repolarizes the apical membrane, thus helping to sustain the driving force for Na^+ entry. The decreased Na^+ entry in the basolateral membrane and the sustained or increased Na^+ entry in the apical membrane combine to determine the final level of Na^+ entry, which is achieved through an interplay between the potassium channels of the apical membrane and the basolateral membrane.

B. Henle's Loop

The potassium channels in the tubular cell membranes of Henle's Loop play significant roles in the transport of NaCl, potassium and divalent ion transport (4,13). The three major functions of these potassium channels are as follows. First, their presence makes possible high levels of potassium in the glomerular filtrate in the region of Henle's Loop, thus ensuring a high level of activity of the Na^+-K^+-$2Cl^-$ cotransporter and maintaining adequate reabsorption of Na^+, Cl^- and K^+. Second, these potassium channels participate in creating the transepithelial potential that is the driving force for Na^+ and some divalent ions across the paracellular shunt pathways among tubular cells. Third, these potassium channels regulate the net intake of K^+.

High potassium levels in the glomerular filtrate are made possible only by apical potassium channels. Thus it is no surprise that all potassium channels found in the region of Henle's Loop are located in the apical membranes (Table 2). This highly polarized distribution reflects the important role of these channels in maintaining a high level of potassium recycling (13). Since the luminal potassium concentration is low compared with the concentration of Na^+ and Cl^-, the potassium ion is the limiting ion for the activity of the Na^+-K^+-$2Cl^-$ cotransporter, which is the major reabsorption mechanism in Loop of Henle. The apical potassium channels allow the recycling of the absorbed potassium ions, and thus create a locally high potassium environment which permits reabsorption through Na^+-K^+-$2Cl^-$ cotransporter.

The paracellular shunt pathway provides a nonspecific mechanism for ion reabsorption in the region of Henle's Loop, and is an important route for reabsorption of cations besides potassium. This non-selective reabsorption mechanism is driven by the transepithelial potential difference created by the previously mentioned outward potassium flux across the apical potassium channels and a outward Cl^- flux across the

basolateral chloride channels. Because the tight junctions between tubular cells here also allow leakage, Na^+, Ca^{+2}, and Mg^{+2} can all be driven by this potential difference across the tight junctions.

The potassium channels in Henle's Loop also play a significant role in determining the net potassium intake into the body. This regulation is discussed here in three different situations: (a) potassium depletion, (b) normal potassium levels, and (c) potassium surplus.

When potassium is depleted, Na^+ transport via the Na^+-K^+-$2Cl^-$ cotransporters is reduced. The reduction in Na^+ entry diminishes the transepithelial potential because of the low level of potassium available for recycling through the apical potassium channels. Thus the reabsorption of potassium through the paracellular shunt pathway is compromised.

When a normal concentration of potassium is present in the glomerular filtrate, net reabsorption of potassium occurs in Henle's Loop. This potassium reabsorption is driven by the transepithelial potential difference through the paracellular pathway, and the potassium is reabsorbed into the peritubular capillaries.

If a high level of potassium is present in the organism, reabsorption of potassium stops along the Loop of Henle, to be replaced by net secretion. Two mechanisms are responsible for this reversal. First, an increase in extracellular potassium lessens the potassium gradient across the basolateral membranes of tubular cells. This reduces back-leakage of potassium ions from inside the cells through the basolateral membrane. Since potassium constantly enters the cells, a higher concentration of intracellular potassium results. This in turn increases the efflux of potassium through the apical membrane. The second mechanism involves the hormone aldosterone. After high potassium loading, aldosterone is secreted by the zona glomerulosa cells of

the adrenal cortex to regulate potassium secretion. Aldosterone stimulates the apical Na^+/H^+ exchanger, and thus leads to intracellular alkalosis. The alkalosis leads to the activation of existing apical potassium channels and triggers the incorporation of new potassium channels into the apical membrane. Both lead to an increase in the outflow of potassium ions through the apical membrane.

C. Distal convoluted tubules and collecting ducts

Potassium channels are crucial in integrating the transport functions of distal nephrons in order to maintain proper ion levels in the body. For example, in sodium reabsorption, since the tight junctions between cells here are much tighter than those in the proximal tubules and Henle's Loop, the reabsorption occurs only through the apical membranes. As with the selective Na^+ reabsorptions in both the proximal tubules and Henle's Loop, the driving force for Na^+ increases with the activity of the apical potassium channels.

As another example, potassium secretion requires the participation of all potassium channels of both the apical and the basolateral membranes, as well as the basolateral Na^+-K^+-ATPase (Table 3). Potassium secretion is initiated by the electrogenic pump Na^+-K^+-ATPase. Since this pump transports Na^+ and K^+ with a stoichiometry of 3:2, it causes hyperpolarization of the basolateral membrane, thus activating the basolateral potassium channels. Because this hyperpolarization can go beyond the equilibrium potential for potassium, potassium can enter the cells through the inwardly rectified channels of the basolateral membranes. At the same time, secretion of potassium occurs because Na^+ enters from the other side of the membrane, creating a depolarized apical membrane potential that causes the activation of apical voltage-gated and Ca^{+2}-activated potassium channels.

D. Summary

In summary, concerted cooperation between all the specialized transport mechanisms in renal tubular cells is required for an organism to conserve internal ions and nutrients. These specialized transport mechanisms can influence each other by mutual modification of driving forces and other regulatory factors. In this complex interplay, potassium channels play a key role, since they maintain the cell membrane potential and thus the electrical driving force for the electrogenic transport systems. It is thus likely that a disturbance in potassium channels can lead to overall ion imbalance in the body.

Table 1. Potassium channels identified in proximal renal tubules or various cells

Species	Conductance, pS	rf	Inhibitors	Activating or Inactivating Factors
Apical membrane				
Rabbit	33	ir	Ba	
Mouse	33	ir		
	60	nr		
Necturus	60			+Depolarization, $+Ca^{+2}$
	100			+Depolarization, $+Ca^{+2}$
Basolateral membrane				
Rabbit	10-55	ir	TEA, Ba, Cs	+Depolarization, $-H^{+}$
	36			
Amphibian	30-50	nr	Ba	+Hyperpolarization, +Stretch
	20	ir		
Isolated or cultured cells				
Rabbit	40		Ba, Apa	
	200		Ba, TEA, CTX, Qui	+Depolarization, $+Ca^{+2}$, $-H^{+}$
OK	15	or		$+Ca^{+2}$
	120	nr		$+Ca^{+2}$
	80	ir		$-Ca^{+2}$, +MgATP, $-H^{+}$
JTC-12	200	nr		+Depolarization, $+Ca^{+2}$
Frog	5	ir		

rf, rectification; ir, inwardly rectifying; nr, nonrectifying; CTX, charybdotoxin; Qui, quinidine; Apa, apamine; TEA, tetraethylammonium; + activating; -, inactivating.

Table 2. Potassium channels identified in mammalian thick ascending limbs and amphibian diluting segments or related cells

Species	Conductance, pS	rf	Inhibitors	Activating or Inactivating Factors
Tubules (all potassium channels are found in the apical membrane)				
Amphibian	200		Ba	+Depolarization, $+Ca^{+2}$, -ATP, $-H^+$, $-Na^+$
	8-30	ir	Ba	+Depolarization, $-H^+$
Rat	60	ir	Ba, Qui, VP, TEA, Rb, NH_4^+	+Depolarization, $-Ca^{+2}$, -ATP, $-H^+$
Rabbit	20	ir	Ba	-ATP
Cultured cells (all in apical membrane)				
Clone A3	130	nr	TEA, Ba, CTX, Qui	+Depolarization, $-H^+$, $+Ca^{+2}$, +stretch, +C-AMP

rf, rectification; ir, inwardly rectifying; nr, nonrectifying; CTX, charybdotoxin; Qui, quinidine; TEA, tetraethylammonium; Vp, verapamil, + activating; -, inactivating.

Table 3. Potassium channels identified in distal convoluted tubules and collecting ducts and related cells

Species	Conductance, pS	rf	Inhibitors	Activating or Inactivating Factors
Tubules (all potassium channels are found in the apical membrane)				
Rat PC CD	140	nr	Ba, TEA, Nai	+Ca, +depolarization
	15-35	ir	Ba	-H^+, -ATP, -PKC, +PKA
Rabbit PC CD	40	nr	Ba	+Ca, +depolarization
	4	or		
	9-25	ir		
Rat, Rabbit IC CD	Maxi		TEA	+Ca
Tubular: basolateral				
Rabbit DCT	50-60	nr	Ba	
	77	nr		
Rabbit CD	30	ir		+Hyperpolarization
Cultured cells				
MDCK	60	ir	OAG, MxSO4	+Ca
	26	nr		-Depolarization
	31	nr		
	80	or		+Ca
	109	nr		+depolarization
	250	nr	TEA, Qui	+Ca, +depolarization
Rabbit PC	180	or	Ba, Nai	+Ca, +depolarization
	20	nr		
Rabbit CD	60	nr		+Ca, +depolarization, +AA

rf, rectification; ir, inwardly rectifying; nr, nonrectifying; Qui, quinidine; TEA, tetraethylammonium; OAG, oleoyl-2-acetyl-glycerol; Nai, intracellular Na^+; $MxSO_4$, minoxidil sulfate; AA, arachidonic acid; + activating; -, inactivating.

Part II: Calcium-activated and ATP-gated potassium channels in renal epithelial cells

A. Calcium-activated potassium channels in renal cells

In Part I, we explained our focus on potassium channels. For our work with renal epithelial cells, we further limited our attention to potassium channels activated by Ca^{+2} (K_{Ca} channels). These are among the most common channels found in MDCK cells (Table III) (4, 13). We chose to investigate this type of channel in MDCK cells for the following three reasons. First, it is experimentally easy to identify a K_{Ca} potassium channel. Second, because of their wide distribution in many cell types and tissues such as neurons, muscles and secretory glands, the responses of K_{Ca} channels to regulators such as Ca^{+2} and membrane voltage have been well characterized through extensive studies. These studies can serve as a guide in characterizing the properties of K_{Ca} channels in MDCK cells. Third, the results of our study can be compared to reports on similar types of channels in the literature.

In Part II, the characteristics of K_{Ca} channels are reviewed in brief to help understand the design of our single channel experiments and the logic behind single channel data analysis. The review begins with an introduction to the types of K_{Ca} channels. Since channels with similar conductance values may share similar conduction properties, one may adapt approaches from studies of other channels of the same conductance category. Next, current knowledge of the physiological roles of K_{Ca} channels is introduced as they relate to renal cell functioning. The modes of regulation of these channels are directly related to their physiological roles - that is, their effects on the overall functioning of organs where these channels are located. However, this study did not emphasize the physiological roles of K_{Ca} channels because we believed that information about them cannot be extrapolated from data obtained from single channel experiments alone. Single channel data do offer an excellent approach to understanding the biochemical characteristics of channel

conduction, so the biochemical basis of K_{Ca} channel conduction is described next. The final part of this review explains the logic behind typical single channel data analysis.

A.1 Types of Ca^{+2}-activated potassium channels

Since quite a number of K_{Ca} channels have been found in various tissues, categorizing these channels according to their pharmacological and physiological properties can accelerate the identification of new channels. One classification of K_{Ca} channels is based on single channel conductance: (1) Maxi K channels (conductance > 150 pS), (2) Intermediate K (IK) channels (conductance 50 - 100 pS) and (3) Small K (SK) channels (conductance < 50 pS) (10, 16). Each group is characterized by common pharmacological and physiological properties. For example, Maxi K channels can often be blocked by external submillimolar concentrations of tetraethylammonium ion (TEA) or nanomolar concentrations of charybdotoxin (CTX), whereas SK channels are more likely to be blocked by nanomolar concentrations of apamin instead of by TEA or CTX. In addition to the differences in sensitivity to the various blockers, the three types of channels have distinct Ca^{+2} sensitivities as well. Maxi K channels are also voltage sensitive, the opening probability increasing with depolarization potential, and they have lower Ca^{+2} sensitivity than SK channels, which have high Ca^{+2} sensitivity.

A.2 Types, characteristics and possible physiological roles of Ca^{+2}-activated potassium channels in renal cells

Many single channel studies on isolated renal cells or intact tubules have indicated that K_{Ca} channels predominate in kidney epithelium. For example, in MDCK cells, half of the six channel types reported so far are K_{Ca} channels (Table III), including a Maxi-K channel and two IK channels. However, aside from the

conductance values and some qualitative indications showing the sensitivities of these channels to Ca^{+2} and to some agonists or antagonists, the biochemical aspects of channel conduction in renal cells have never been studied. Presumably, this is because the purpose of these experiments was to identify single channels that could account for macroscopic potassium transport across kidney epithelium, and hence to infer their physiological roles. Attention in these studies was on identifying the factors regulating channel activity, rather than on understanding the mechanism of channel conduction. This type of channel investigation can be illustrated by the study of Guggino et al. (14). Guggino et al. performed one study concerned with the physiological role of K_{Ca} channels, using cultured chick kidney cells. They found that both ADH (antidiuretic hormone) and forskolin activated a certain K_{Ca} channel located in the apical membrane of these cells. Because the conduction characteristics of the single channel, including its Ba^{+2} sensitivity and ADH activity, match those of the macroscopic potassium secretion, they concluded that this K_{Ca} channel plays a major role in the secretion of potassium ions from distal nephrons.

There is evidence that at least one of the three types of K_{Ca} channels present in MDCK cells resembles the channel that Guggino et al. concluded to be responsible for the main functions of distal nephrons (19). The question thus arises as to why MDCK cells need all three types of channels if one type can fulfill the main function of distal tubular cells. The reason may be that each channel type is regulated differently. It turns out that the K_{Ca} channels are subject to multiple forms of metabolic regulation besides Ca^{+2} and voltage, which are probably intimately related to their individual physiological roles in the kidneys (16). Hormones, neurotransmitters, lipids and nucleotides have been found capable of modifying K_{Ca} channels in different renal epithelial cells (4, 13, 14). In the case of MDCK cells, Lang et al. found that extracellular serotonin, ephinephrine, bradykinin and ATP all can activate K_{Ca}

channels in MDCK cells (17). But, because of a lack of understanding of the molecular details of multiple regulation, a sufficiently elaborate physiological model of these K_{Ca} channels remains to be constructed.

A.3 Regulation of Ca^{+2}-activated potassium channels by calcium ions.

The regulation of K_{Ca} channels by Ca^{+2} is better understood than is their regulation by metabolites. This is largely due to the fact that these channels can be opened directly by increasing the concentration of Ca^{+2} on the intracellular side of the channel. During single channel recording, the intracellular Ca^{+2} concentration can be manipulated easily using either the inside-out patch clamp technique or the lipid bilayer technique. Thus the effects of intracellular Ca^{+2} on K_{Ca} channels can readily be studied.

The equilibrium and kinetic properties of single channel opening for K_{Ca} channels at various Ca^{+2} concentrations can reveal many basic features concerning the mechanism of activation of the channel by Ca^{+2}. These features include the number of Ca^{+2} ions participating in opening the channel, the number of major conformational states traversed by the channel protein between closed and final open states, and the rate constants associated with these conversions - provided that not many states are involved in the pathway of channel activation (16).

The number of Ca^{+2} ions binding to a channel protein can be calculated from the dose-response curve for Ca^{+2}. Because it is generally believed that Ca^{+2} activates the K_{Ca} channel by direct binding, dose response curves are usually analyzed using the Hill equation (Equation 1)(16, 20, 21). The slope factor (n) of the Hill's plot, also named the Hill coefficient, is taken as the minimum estimate of the number of Ca^{+2} ions participating in maximally activating the channel. The affinity constant K and its

n^{th} root, which provides an estimate of the midpoint of the activation curve, provide an indication for the sensitivity of the channel to Ca^{+2}.

Extensive studies on various K_{Ca} channels indicate large variations for both the Hill coefficient and Ca^{+2} sensitivity, depending on the types and sources of the K_{Ca} channels (16).

$$P_{open} = \frac{P_{max.}\,[Ca^{+2}]^n}{K^n + [Ca^{+2}]^n} \qquad \text{(Equation 1)}$$

For example, in the Maxi K channel, the Ca^{+2} requirement for half-maximal opening varies from ~ 0.01 to ~ 200 μM. This difference of four orders of magnitude has been attributed to differences in the local membrane environment of a channel (16). Lipid composition and membrane surface charge both have been found to alter the gating of Maxi K channels (21,22). Differences in the local membrane environment, however, do not completely account for the variation observed. Smaller but significant variations in the Ca^{+2} sensitivity, on the order of 10-fold, exist for channels obtained from the same tissue (16). Possible reasons for such variation include (a) different subclasses of Maxi K channels in a single tissue or cell type (24, 25), (b) spontaneous kinetic mode shifts (23), and (c) slow rundown of Maxi K channels. Among these, the spontaneous mode shifts and slow rundown are related to single channel properties that are not well understood. The phenomenon of channel rundown (described in Section A.4) has hindered progress toward an understanding of both the equilibrium and kinetic properties of single channels because the steady state, a condition required for analyzing both the kinetic and equilibrium properties of a channel, can no longer be assumed.

As seen with Ca^{+2} sensitivity, channels from similar tissue sources can have different Hill coefficients. The largest variations seen for the Hill coefficient occur

among Maxi K channels, ranging from 1 to 5.8. However, IK and SK channels appear to have much smaller variations in the value of n. IK channels have a value of n very close to 3, and SK channels, very close to 1. The variations observed in the value of n among Ca^{+2}-activated channels may be due to both differences in number of and cooperativity between binding sites.

A.4 Single channel data analysis

The conformational change of a channel from closed to open states after its binding to Ca^{+2} is often analyzed by constructing open and closed dwell time histograms from continuous single channel recordings. Because a given dwell time is probabilistically independent of previous dwell times, a channel's opening or closing can be viewed as a stochastic process, so that the dwell time distributions of single-channel opening or closing events can be described by fitting them to multiexponential expressions. Certain relationships exist between these expressions and properties of dwell times and openings and closings. The number of open or closed states of a channel turns out to equal the number of exponential terms in an expression fitted to describe the dwell time histogram of this channel's open or closed events, and the rate constants for the various exponential terms, in the simplest case of one open state and one closed state, are the reciprocals of the mean dwell times for the individual open or closed states. Knowing the number of exponential terms and the number of ligands bound to the channel as discussed in Section A.3, one can propose reasonable models to describe the kinetics of activation for a channel under investigation.

A more detailed explanation of these points follows. The reciprocal relationship between the rate constants and the mean dwell time is derived from probability theory. Because transitions between different conformational states of a channel protein occur

at random, the rate constants describing the transitions of this single molecule must be interpreted in a probabilistic way (26).

$$\text{Closed} \underset{\alpha}{\overset{\beta}{\rightleftharpoons}} \text{Open} \qquad \text{(Scheme I)}$$

As in scheme I, rate constant α should be regarded as a measure associated with the probability that an open channel will close during a given unit of time. However, α itself is not a probability because α is given in units of time^{-1}. Thus, the probability that an open channel will close during time Δt is associated with the expression $(\alpha \cdot \Delta t)$. This also is not a probability, since it can be greater than 1. The rate constant α can be expressed as the following expression:

$$\alpha = \lim_{\Delta t \to 0} [\text{prob (channel closed at } t+\Delta t \mid \text{open at } t) / \Delta t],$$

where prob represents probability.

This equation can be generalized to all rate constants within a kinetic scheme similar to scheme I:

$$q_{ij} = \lim_{\Delta t \to 0} [\text{prob (channel in state } j \text{ at } t+\Delta t \mid \text{in state } i \text{ at } t) / \Delta t].$$

Since the length of time that a channel stays in a particular state can be regarded as a random variable, this variability can be described by a probability distribution. A probability density function is often used in the analysis of single channel recording. The area under the probability density curve from time zero up to any time t represents the probability that the lifetime is less than or equal to t. Mathematically, the probability density function (pdf) can be expressed as

$$f(t) = \lim_{\Delta t \to 0} [\text{prob (lifetime is between } t \text{ and } t+\Delta t) / \Delta t],$$

which can be solved by combining probability theory with the above equations. Function f(t) has the following form for the open configuration described in kinetic scheme I:

$$f(t)_{open} = \alpha \exp(-\alpha t), \quad (t \geq 0).$$

With similar arguments, the pdf for the closed configuration in scheme I can be expressed as follows:

$$f(t)_{closed} = \beta \exp(-\beta t), \quad (t \geq 0).$$

The functional forms of the pdfs of the two states allow determination of the exact mean life times for each state. These are $1/\alpha$ and $1/\beta$, respectively, for the open and closed states. Based on the same arguments, a more generalized conclusion can also be reached, that regardless of the number of conformational states assumed by a channel along its activation pathway, the lifetime of any single state is always exponentially distributed with a mean equal to 1/(the sum of transition rate constants leading away from the state). This is the reason that, in single channel data analysis, dwell time histograms are always constructed and fitted to multiexeponential expressions. The number of exponential terms thus reflects the minimum number of states a channel of interest will traverse during the process under study.

Not all single channel data yield a reasonable kinetic model that describes both the equilibrium and kinetic properties of the channel under investigation. As the number of states increases, discrimination among kinetic models becomes difficult. In addition, the time constants from the exponential fit of the dwell time histograms may not have physical meaning. In the ligand binding study, it is thus difficult to discern the effects of certain activators along the activation pathway. The following example illustrates how rate constants may be found for a proposed model of the transitions

between various closed and open states of a channel. For instance, if the proposed model contains two closed states that are not interconnected, and one open state, as depicted in scheme II,

(Scheme II)

$$\text{Closed state 1} \underset{\alpha}{\overset{\beta}{\rightleftharpoons}} \text{Open state} \underset{k_{-B}}{\overset{k_{+B}X_B}{\rightleftharpoons}} \text{Closed state2},$$

one may first calculate the pdf for the closed state 1 (f (t)):

$$f(t) = \left(\frac{\alpha}{\alpha + k_{+B}X_B}\right)\beta \exp(-\beta t) + \left(\frac{k_{+B}X_B}{\alpha + k_{+B}X_B}\right) k_{-B} \exp(-k_{-B}t).$$

By equating the fitted multiexponential expression with the above expression, the rate constants connecting each state may be obtained. Notice that in this scheme, the time constants happen to be the rate constants. This is because the two closed states are not interconnected. However, this simplicity disappears when closed states are interconnected.

The derivation of the kinetic scheme relies on the assumption that the rate constants are genuine constants, i.e., that they do not vary over time. This is sometimes not true for channels present in excised membrane patches. Channel activity very often decreases over time even at fixed membrane voltages in identical experimental conditions. This is referred to as channel rundown. In single channel recording using the cell-attached configuration, rundown may be avoided. Channel rundown is believed to be caused by the loss of certain cellular components upon excision of the membrane from the rest of a cell, some of which are crucial for optimal

channel activity. Channel rundown often renders single channel kinetic analysis difficult. Even in equilibrium studies such as construction of a dose-response curve, channel rundown can lead to shifts in the sensitivity of the channel to ligands. In this case, normalization of the channel responses becomes crucial.

B. ATP-gated potassium channels in renal cells

In addition to Ca^{+2}-activated potassium channels, we also investigated ATP's effects on single ion channels found in MDCK cells. In an earlier control study, we observed two different types of current responses of the MDCK cells to voltages over time. We suspected that some of these changes in whole cell currents might be related to a loss of intracellular ATP during whole cell current recording. In Type II cells, whole cell current decreased and, in Type III cells, whole cell current increased over time (1). One reason for increased currents over time may be the presence of ATP-sensitive potassium channels (K_{ATP} channels). An intracellular ATP level reduced from its normal range, ~ 2-3 mM (27), to submillimolar levels after membrane breakage - to gain access to the interior of a cell for whole cell current recording - may lead to the activation of K_{ATP} channels, thus increasing whole cell currents over time.

Several renal potassium channels have been identified as sensitive to intracellular ATP. These include a 35 pS channel found in rat collecting ducts (29) and a 22 pS channel found in rabbit thick ascending limbs (28). It has been thought that some of these renal K_{ATP} channels are similar to the K_{ATP} channels commonly observed in both the cardiac muscles and smooth muscles, because non-hydrolyzable ATP increases the activity of K_{ATP} channels found in both renal, and cardiac and smooth muscles (28). In a cell, the opening probability of this type of ATP-gated channel is usually low; however, a reduction in the ATP level inside the cell causes an increase in channel opening (27). Some researchers suggest that the activity of renal K_{ATP} channels is coupled to the activity of basolateral Na^+-K^+-ATPase. Thus, a reduction in the intracellular ATP level, as a result of a sudden increase in the activity of basolateral Na^+-K^+-ATPase, can lead to activation of the K_{ATP} channels, which can increase potassium secretion from the membrane (30).

Statement of the problem

From our earlier studies, we found many types of potassium channels in the membranes of MDCK cells using the patch clamp technique in cell-attached configuration (1). However, besides the respective conductance values and overall open probability at various voltage levels, we had little idea about how these channels were regulated intracellularly and about their physiological function as well as about the biochemical basis of channel conduction. Our inability to explain the observation that, under the same experimental conditions, many of these channels with similar conductances exhibited very different open probabilities reflected our incomplete understanding of the properties of these channels.

To characterize these channels further, we needed to identify factors that activate as well as block the activity of these channels, and to study their equilibrium and kinetic properties. Among the many known regulators for potassium channels, we chose to study the effects of intracellular adenosine triphosphate (ATP) and Ca^{+2} for the following two reasons. First, we felt that quantitative studies of other regulators might be more difficult owing to the nature of the activation (or the inactivation); for example, the activation of potassium channels by various hormones was found to be generally mediated through a second messenger pathway. Depending on the extent of second messenger response to hormone, the effects of constant extracelluar hormone on single - channel activity can vary tremendously in cells. Second, we felt that since a wealth of knowledge had been learned on channels affected by intracelluar Ca^{+2} and ATP, many such studies could be used as a guideline for our study.

Our goal in this part of the study is to investigate whether the potassium channels identified from our previous study are capable of being regulated by intracellular Ca^{+2} and ATP. If so, we will proceed to examine the changes in equilibrium and kinetic properties caused by Ca^{+2} or ATP binding.

Experimental

Material and Methods

A. Tissue Culture

Cloned MDCK (Madin Derby canine kidney), MDCK C-7, cells were kindly contributed by Dr. Cereijido (Department of Physiology, Biophysics and Neuroscience, Center of Investigation, Mexico). The passages used were from 101 to 120. Serial cultures were maintained at 37°C in disposable plastic culture flasks (Costar 3375, Cambridge MA) with an air - 5% CO_2 atmosphere and Dulbecco's Modified Eagle's Medium (Gibco 430-1600EB, Grand Island, NY) supplemented with 0.08 U/ml insulin (Gibco 890-8125IG, Grand Island, NY) , and 10% fetal bovine serum (Gibco 210-6510AJ, Grand Island, NY). Upon reaching confluency, the cells were harvested with 0.1% trypsin (Sigma T0646, St. Louis, MO) prepared in reconstituted Dulbecco's phosphate buffered saline (Sigma D-5652, St. Louis, MO), and plated on 35 X 10 mm culture dishes (Corning Sterile 25000, Corning, NY) for the patch clamp study.

Prior to the patch clamp study, monolayer cells cultured in 35 X 10 mm dishes were first washed 3 to 5 times with a high potassium, low calcium bathing solution that contained no ATP. The monolayers was then allowed to stand at room temperature in the bathing solution for approximately 30 minutes. This led to disruption of the tight junctions between cells and resulted in partial rounding up of the flat monolayer cells which aided gigaseal formation tremendously.

B. Single channel recording

Single channel currents were recorded from the surface membranes of MDCK cells grown in tissue cultures, using the inside-out patch clamp technique (Hamill et al.). The patch clamp pipettes were obtained by pulling glass capillaries (OD 1.5 mm, ID 0.75 mm, Sutter Instruments, Navato, CA) using the Flaming Brown micropipette

puller (Model P - 87, Sutter Instrument, Navato, CA). Prior to use, the pipettes were coated with Sylgard® 184 (ET 030497, Dow Corning, Midland, MI), and then fire polished. These procedures were used to reduce the stray capacitance of the micropipettes, and to ensure the smoothness of the pipette tip. The inner pipette diameters were approximately 1 - 1.5 μm and exhibited 10 - 15 Mohm resistance when filled with various pipette solutions.

The pair of thin Ag/AgCl electrodes used in the patch clamp recording were prepared by passing a constant current of ~ 1 mA for 24 hours between two pairs of thin silver wires (99.9% purity, 0.25 mm in diameter, Aldrich Chemicals, Milwaukee, WI) and slightly thicker silver wires (99.9% purity, 1 mm in diameter, Aldrich Chemicals, Milwaukee, WI) connected in series in 0.5 M KCl solutions. The direction of the constant current was such that Cl^- ions were attracted to the thin silver wires to form AgCl coatings on their surfaces.

The inside-out configuration of the patch-clamp technique was used for all experiments described in this chapter. The procedures used to obtain the inside-out cell membrane patches are summarized briefly as follows: a fire - polished pipette was sealed (seal resistance greater than 1 Gohm) against the cell membrane of a target MDCK cell by applying gentle suction after initial contact. A patch of membrane was then excised from the cell by withdrawing the pipette from the cell surface. The current flow direction across the membrane patch is defined as convention (see Figure 1 for current flow direction).

C. *Electrolyte solutions:*

A high potassium solution with low Ca^{+2} (~ 130 nM) content and no ATP was used to bathe both sides of the membrane at the beginning of each experiment. Unless specified, the bathing solution (the solution in contact with the intracellular side of the

membrane patch) was changed to other bathing solutions with the same compositions, except for their Ca^{+2} or ATP content, during experiments to study the effects of intracellular Ca^{+2} and ATP on ion channel activity. The compositions of the high potassium and low Ca^{+2} solutions used to evaluate the sensitivity of channels to ATP were as follows: potassium gluconate 150 mM, $Ca(OH)_2$ 1.54mM, EGTA 2.3 mM, HEPES 10 mM, and glucose 10 mM. In cases where Mg^{+2} or nucleotides or both were included in the bathing solution for inside-out patches, required amounts of these agents in salt form ($MgCl_2$, sodium nucleotide) were added to this solution. In certain cases, this high potassium solution was found to inhibit single channel activity; a high sodium solution without potassium was used in these cases. Sodium gluconate was substituted for potassium gluconate in the high sodium solution.

For experiments that required varying concentrations of free Ca^{+2}, the level of free Ca^{+2} in solution was adjusted by adding various amounts of the Ca^{+2} chelator EGTA. Table I lists the various amounts of several stock solutions required to prepared the high potassium solutions of varying free Ca^{+2} levels used to study the sensitivities of the channels of MDCK cells to intracellular Ca^{+2}. The high potassium stock solution (5X) contained potassium gluconate 0.75 M, glucose 0.05 M and Hepes 0.05 M. The $CaCl_2$ stock had a concentration of 50 mM, and the two EGTA stocks had concentrations of 50 mM and 5 mM.

All the high potassium solutions were adjusted to pH = 7.35 ± 0.05, and their osmolarities were in the range of 300 ± 15 mOsm per liter of water. The vehicle used for these solutions was double deionized water. The quantities of chemicals used, whenever possible, were corrected for purity as specified by the manufacturers.

D. Voltage control and data aquisition system

Prior to the patch clamp studies, the micropipette was mounted in a pipette holder, and then connected to the head stage of the recording amplifier (EPC-7, List Electronic, Darmstadt, F.R.G.) via a BNC. The whole head stage was attached to a hydraulic micromanipulator (MO 303, Nikon, Japan) to allow positioning of the measuring pipette to target cell surface.

Seal formation and current recordings were monitored with an oscilloscope as depicted in Figure 2. The inside out membrane voltage was controlled directly by adjusting the V-command control of the EPC-7. Filtered current signals (1 KHZ) were digitized through an analog digital converter and collected using the Fetchex program (MCDAS and Pclamp 5.5.1, Axon Instruments) installed in an 80386-based computer (IBM PS2, Model 70). The single channel data were then analyzed with the Fetchan and Pstat programs.

Table I

Volumes of the various stock solutions required to prepare a 500 ml of high potassium solution with various levels of free Ca^{+2}

Stock Solution	Concentration and Volume Required	Free Ca^{+2} Level
high K stock	100 ml	
CaCl2 stock	10 ml	
EGTA	80ml 5mM (0.8mM)	200.25 µM
	90ml 5mM (0.9mM)	100.57 µM
	95ml 5mM (0.95mM)	51.17 µM
	50mM 10ml (1.00mM)	7.93 µM
	5mM 3ml + 50mM 10ml (1.03mM)	1.98 µM
	5mM 7ml + 50mM 10ml (1.07mM)	892 nM
	5mM 10ml + 50mM 10ml (1.1mM)	629 nM
	5mM 25ml + 50mM 10ml (1.25mM)	253 nM
	50mM 15ml (1.5mM)	127 nM
	50mM 20ml (2mM)	63 nM
	50mM 25ml (2.5mM)	42 nM
	50mM 50ml (5mM)	16 nM
adjust pH 7.4 with KOH and qs to 500 ml		

Figure 1. Current flow diagrams for inside-out and outside-out patches which contain specific cation channels and are bathed in symmetric bathing and pipette solutions

(a) For inside-out patches, current flows inward when pipette voltage is held at positive voltage (negative membrane potential), and current flows outward when pipette is held at negative voltage (positive membrane potential).

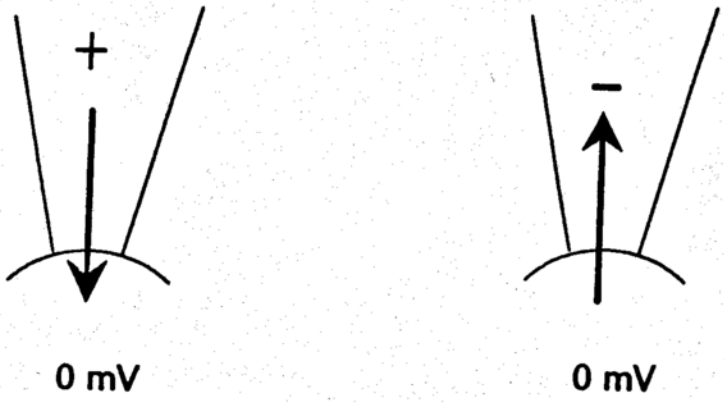

(b) For outside-out patch, current flows inward when pipette voltage is held at negative voltage (negative membrane potential), and current flows outward when pipette is held at positive voltage (positive membrane potential).

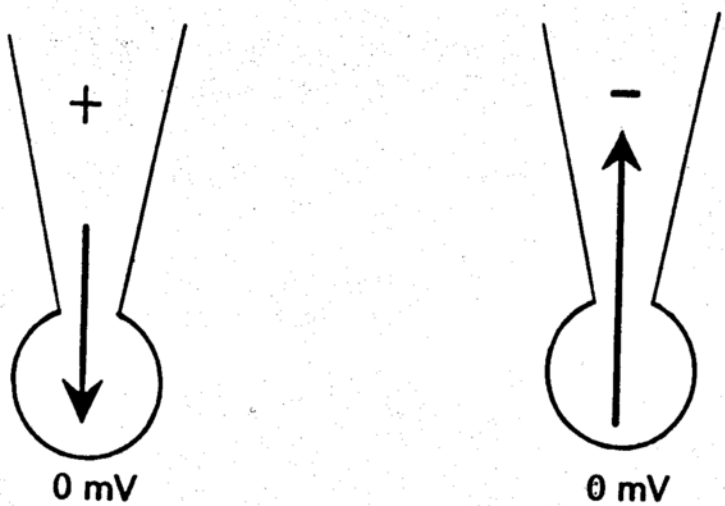

Figure 2

Connections for a typical recording setup

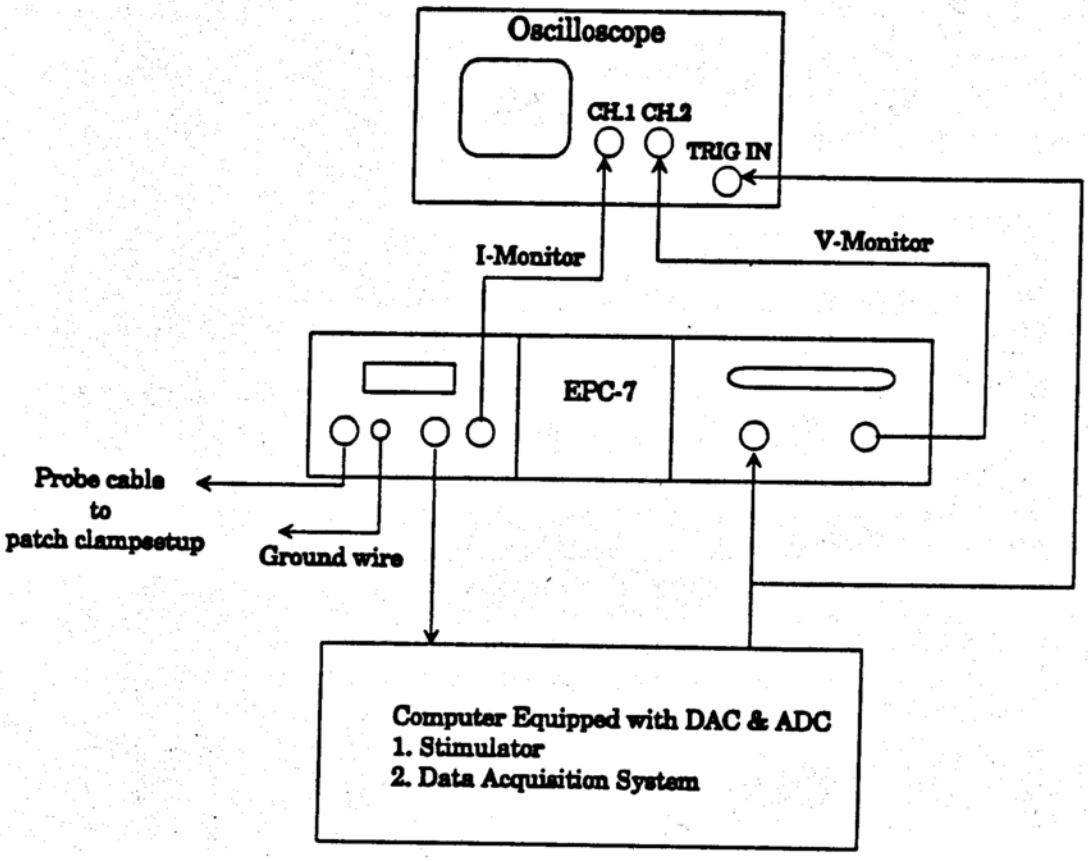

Results

Using the inside-out cell-free patch clamp technique, we found three types of potassium channels in MDCK cloned cells sensitive to either intracellular Ca^{+2} or ATP. The first channel had a conductance of 40 ± 4.6 pS (n=3) at membrane potentials ranging from -60 to -120 mV. The second channel type was inwardly rectified, and its conductance was 49.1 ± 5.1 pS (n= 25) in a similar potential range. The third type of channel had a very large conductance, 241.6 ± 15.4 pS (n=26). This channel type did not exhibit any rectification characteristics in the voltage range studied.

A. The 40 pS ATP-sensitive channels (K_{ATP} channels)

One potassium channel type found using the inside-out patch clamp technique was sensitive to intracellular ATP. This channel's specificity to potassium was indicated by its reversible block by TEA (tetraethyl ammonium ion) (Figure 5), a specific blocker for potassium channels. The opening activity of this channel decreased as intracellular ATP increased (Figure 2), but the ATP effects were reversible; after removal of ATP, the opening of the channel recovered approximately to its level prior to the ATP treatment (Figure 2). The conductance value of this channel was 40 ± 4.6 pS (n=3) (Figure 1a). Figure 3 illustrates the opening probabilities of this channel in various intracellular conditions as the experiment progressed. Figure 3 also shows that the channel's response to reduction of the ATP level decreased over time. This is probably due to gradual channel rundown.

No outward current flow was discernible from the IV relationship of the K_{ATP} channel (Figures 1a and 1b). This was because the channel was bathed in a high sodium bathing solution containing no potassium ions, making outward movement of potassium ions impossible. We avoided high potassium concentrations in the absence of intracellular ATP because they dramatically reduced the channel's opening probability (Figure 3). We avoided them during the ATP study of this channel as well, in order to avoid unnecessary complications arising from effects of intracellular potassium on channel opening.

Both the gating of the K_{ATP} channel and the channel opening probabilities showed little dependence on membrane voltage. As shown in Figure 4, this voltage independence appeared to be unaffected by the presence of intracellular ATP.

Figure 1 Single channel current traces and conductance plot of the 40 pS ATP-sensitive channel

(a) Conductance plot

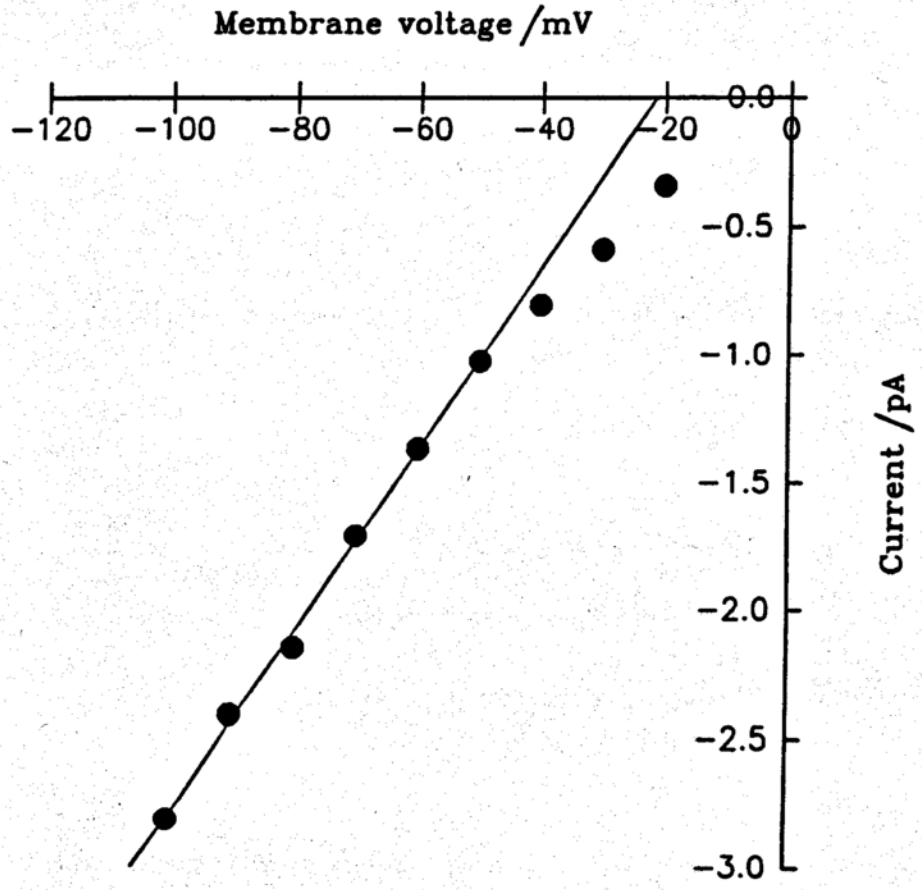

(b) Single channel current traces at various membrane potentials

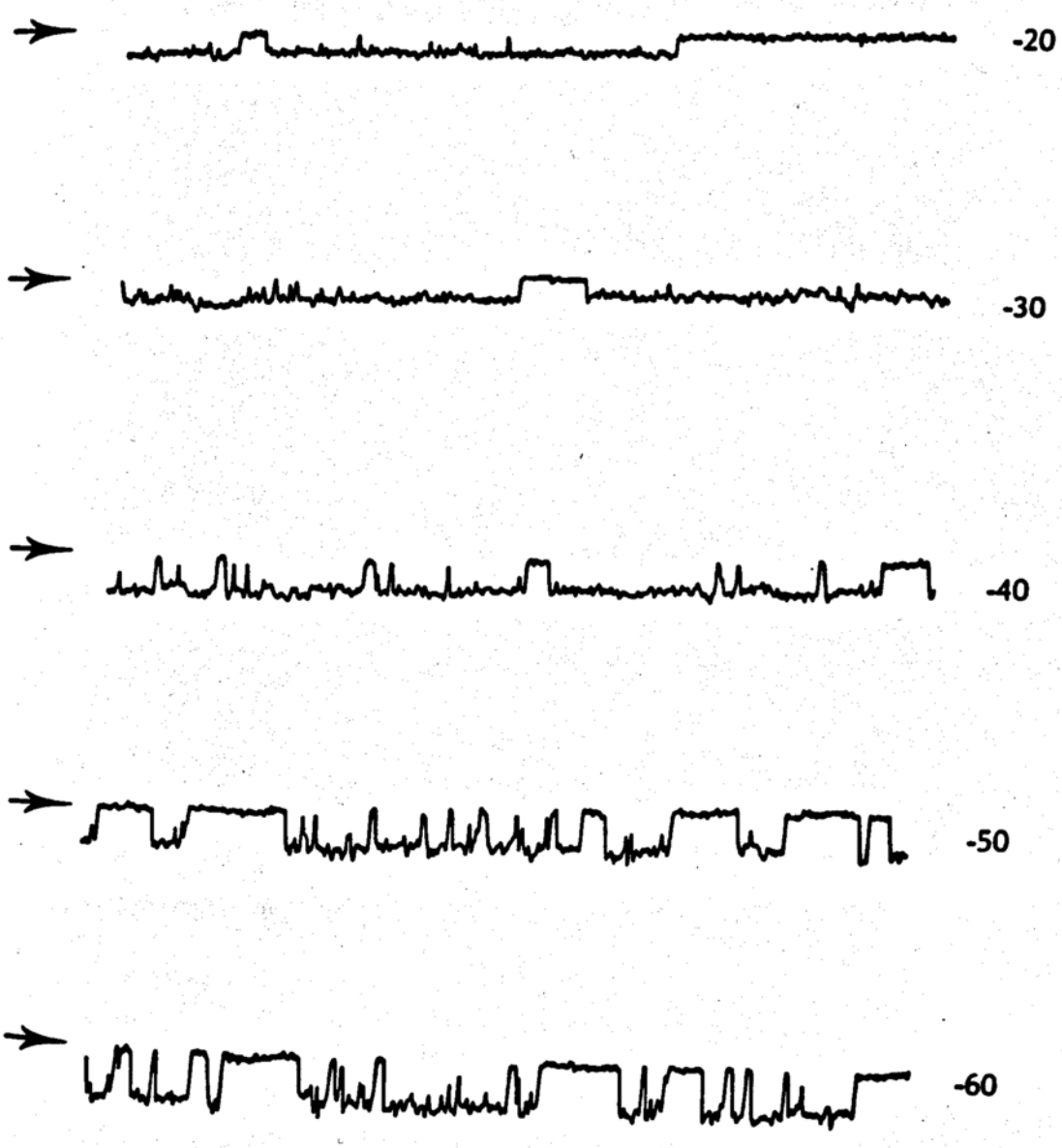

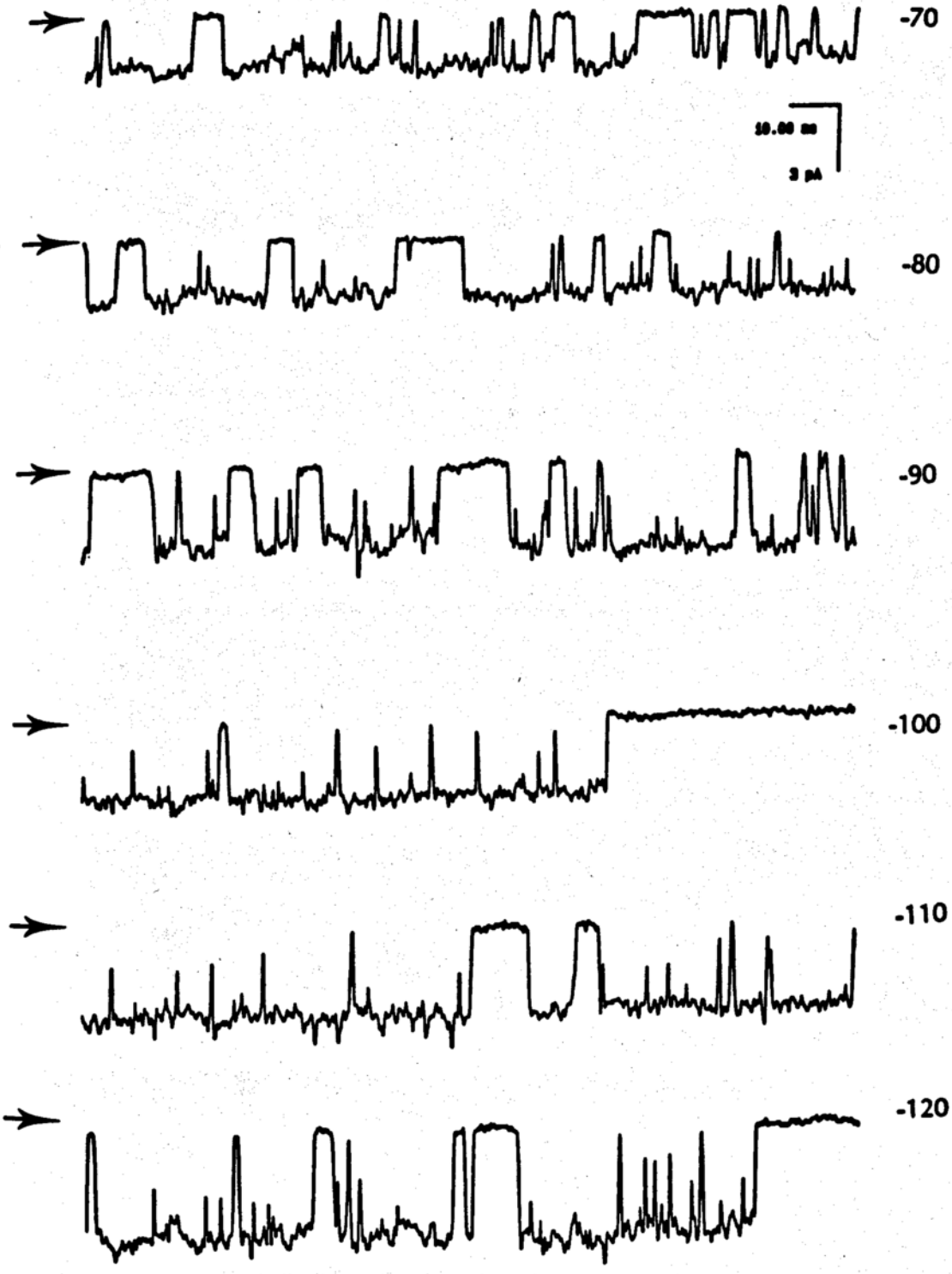
-70
10.00 ms
3 pA
-80
-90
-100
-110
-120

Figure 2 The activity of the 40 pS ATP-sensitive channel can be blocked by intracellular ATP. This blocking can be reversed by simply replacing the ATP-containing high sodium bathing solution with ATP-free high sodium bathing solution.

(a) Channel activity without intracellular ATP

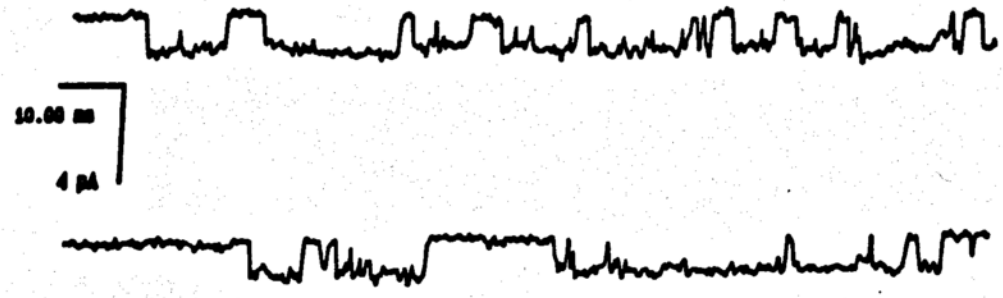

(b) Channel activity blocked by intracellular ATP

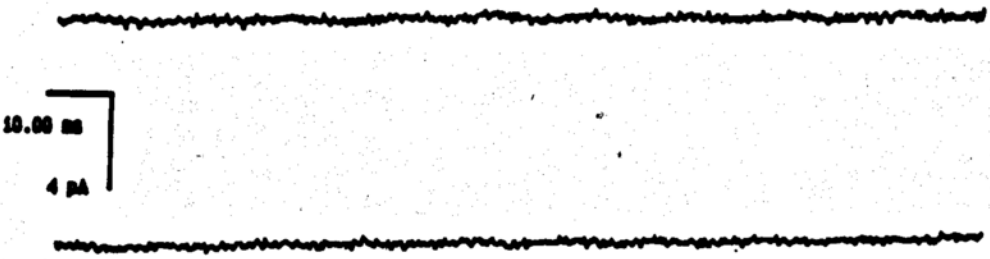

(c) Channel activity recoved after washing off ATP

Figure 3 The opening probabilities of the 40 pS ATP-sensitive channel vary with intracellular conditions as the experiment progressed.

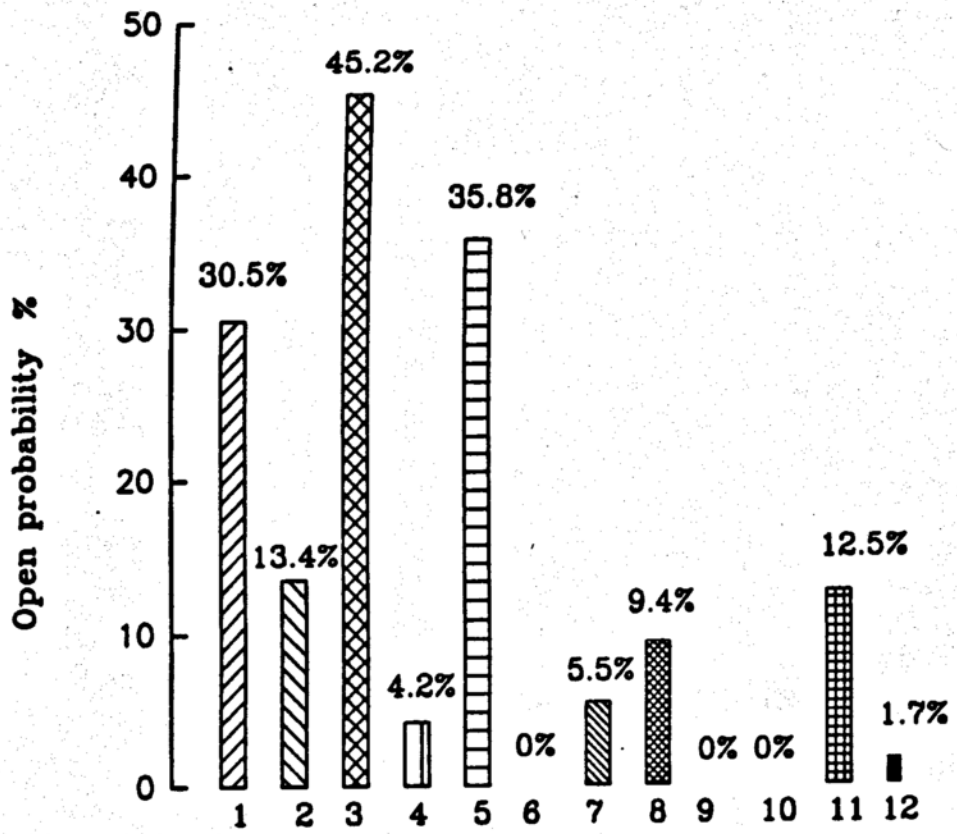

1. high sodium bathing without ATP
2. high sodium bathing with ~ 2mM TEA
3. high sodium bathing (washoff TEA)
4. high sodium bathing with ATP
5. high sodium bathing without ATP (washoff ATP)
6. high potassium bathing without ATP
7. high potassium bathing with ATP
8. high sodium bathing without ATP
9. high potassium bathing without ATP
10 high potassium bathing with ATP
11 high sodium bathing without ATP
12 high sodium bathing with ATP

Figure 4 Probability of opening for the 40 pS ATP-sensitive channel at various voltage levels in high sodium bathing solution containing either 0 mM, or 3 mM, or 6 mM ATP.

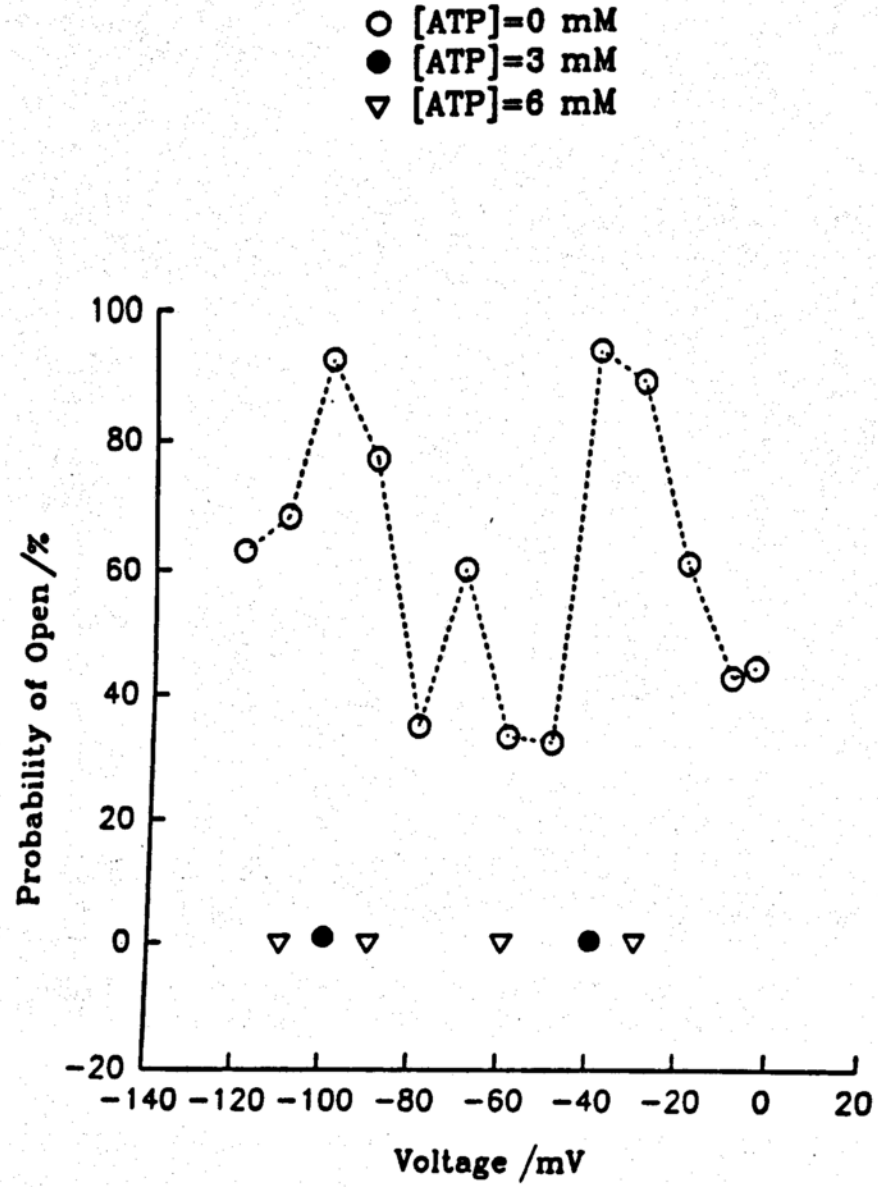

Figure 5 The activity of the 40 pS ATP-sensitive potassium channel can be blocked by the specific potassium channel blocker TEA.

(a) Channel activity in the absence of both ATP and TEA

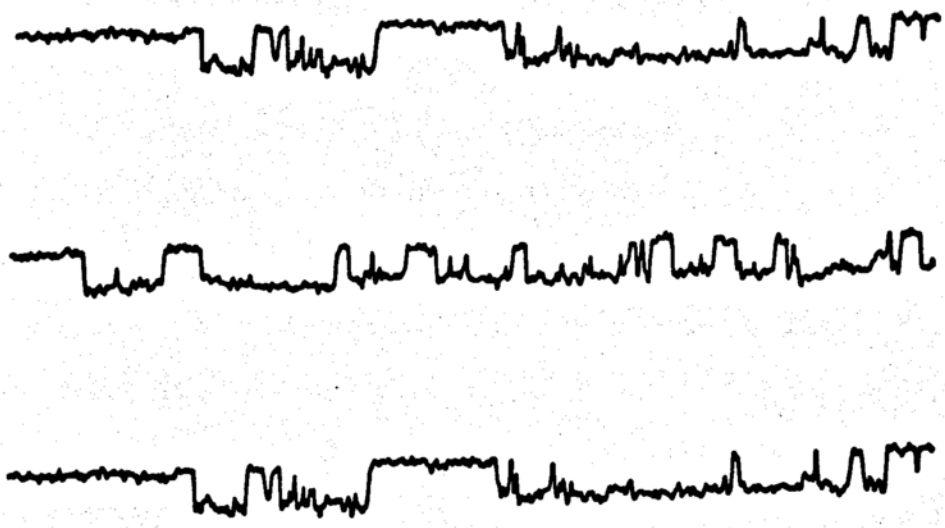

(b) Channel activity blocked by TEA

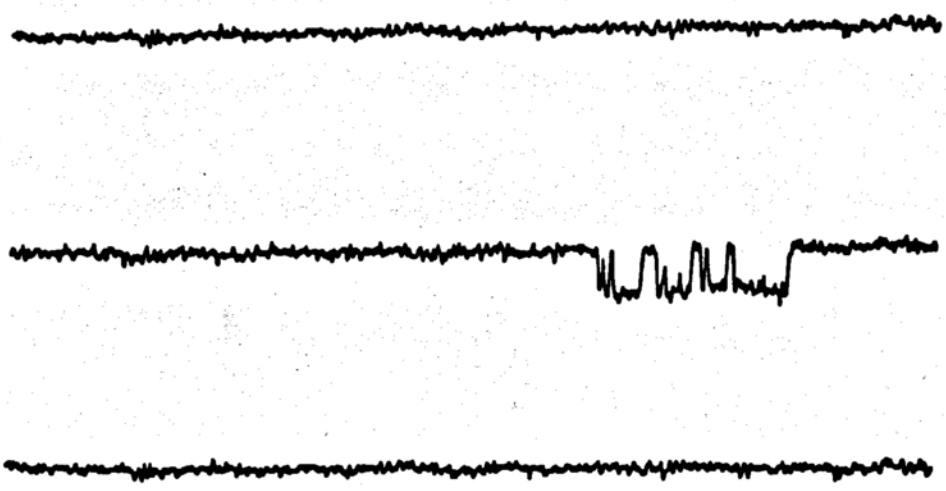

B. The 49 pS ATP-activated potassium channel

The second type of channel found was an ATP-activated K_{Ca} channel (Figure 28, 29, 30). Again its specificity for potassium was demonstrated by blocking the channel current with TEA (Figure 7). Intracellular ATP at a concentration of ~ 0.75 mM caused channel opening to reach 50 % of maximum (Figure 10). The effect of ATP was reversible; upon removal of ATP, the incidence of opening events was reduced to approximately the same level as before the ATP treatment (Figure 8).

The conductance of this channel was 49.1 ± 5.1 pS (n=25) when bathed in symmetric high potassium-low Ca^{+2} solutions (~130 nM) (Figure 6). Since the channel showed inward rectification with very low conductance at depolarizing potentials, the potassium could flow only from the interior of the recording pipette toward the bathing solution. Thus, changes in the bathing potassium concentration had no effect on the conductance measured in a negative potential range, as indicated in the I-V plot (Figure 11). Conductance also remained stable throughout the entire experiment (Figure 12).

The open probabilities were in most cases close to zero, both in the cell-attached configuration and immediately after the formation of inside-out patches. Therefore ATP's effects of increasing channel activity cannot be due to ATP's capability to prevent channel rundown. Millimolar concentrations of ATP are often used to prevent channel rundown in cell-free membrane patches because channel rundown, in many cases, is caused by dephosphorylation of channel proteins (38). Addition of MgATP to the intracellular side of a membrane patch reverses extensive dephosphorylation which leads to the inactivation of some channel proteins.

In our study, we found that the effects of ATP were mediated through direct binding. We discovered that phosphorylation was not required in order to activate this

channel, for the following reasons. First, in addition to ATP, both ADP and AMP also caused channel opening to increase, and their effects were reversible, like those of ATP (Figures 13 and 15). ADP's potency in increasing channel activity was quite comparable to that of ATP, but AMP was a slightly weaker agonist (Figure 16). Since ADP and especially AMP were unlikely to be donors for protein phosphorylation, we concluded that they activate the channel through direct binding. They also reverse TEA channel blocking, as does ATP, which further confirms the role of ADP and AMP in channel activation (Figure 14). Second, hydrolysis of ATP was not required for activation. Mg^{+2}, a cofactor required for ATP hydrolysis, was not required to activate this channel. In the absence of Mg^{+2}, channel activity still increased with the concentration of sodium ATP, when present on the intracellular side of the channel. Third, non-hydrolyzable ATP, AMP-PCP, exhibited a positive effect on channel opening as well (Figure 17).

From an averaged ATP dose-response curve, we obtained a Hill coefficient of 1.85 (Figure 19), indicating that a minimum of two ATP molecules must bind to this channel along the activation pathway. This averaged curve was constructed from dose-response curves from seven out of nine total patches, in which the ATP sensitivity actually varied from patch to patch. In two of the nine cases, the variation in sensitivity was greater than 10-fold, so we excluded these two cases from the average, yielding an averaged curve with a smaller deviation (Figure 18). Figure 9 illustrates a typical dose-response curve for this type of channel from a single patch voltage clamped at -60 mV. Since the opening probability remained constant at various voltages, the dose reponses at other voltages were assumed to be similar to the one at -60 mV (Figure 20).

The effects of ATP on channel opening were studied kinetically. This was done by first constructing dwell time histograms for both closed and open events at various concentrations of intracellular ATP, and then fitting these histograms to multiexponential expressions (see introduction). Figure 21 shows the histograms as well as the fitted curves for single channel events obtained from one membrane patch. As can be seen from these figures, the open time histograms are best described by biexponential expressions, while the closed events are best described by triexponential expressions. This indicates that at least two open states and three closed states were involved along the activation pathway.

We approached our analysis of ATP's effects through changes in the time constants of the various open and closed states, obtained from the data fitting mentioned above (Table 1). We concluded that ATP binding to the channel has no influence on the open states of this channel because both the arithmetic mean open time and the mean residence times of the two open states were relatively independent of ATP concentration (Figure 22 and 23).[1] ATP binding, however, reduced the arithmetic mean closed time as well as the three fitted closed time constants (Figure 22 and 24). Notice that ATP caused decreases in the individual closed time constants without significantly altering the relative distributions of the three states, as can be seen from Figure 27. The maximum decrease in time constant due to ATP binding was associated with the closed state having the longest mean resident time ($\tau_{3,\ closed}$). These decreases were found to be functionally dependent on the reciprocal of ATP concentration. The two shorter mean closed time constants were found to be proportional to the square of the reciprocal of ATP concentration (Figure 25), and the longest mean closed time constant ($\tau_{3,\ closed}$) was found to be proportional to the reciprocal of the ATP concentration (Figure 26). We fitted the dependency of the three

[1]This will be addressed in more detail in the discussion section.

closed time constants on the reciprocal of ATP concentration using linear regression, and obtained the following three expressions:

$$\tau_{1,\,closed} = 0.598 + \frac{0.119}{[ATP]^2},$$

$$\tau_{2,\,closed} = 2.044 + \frac{1.160}{[ATP]^2}, \text{ and}$$

$$\tau_{3,\,closed} = -15.071 + \frac{141.916}{[ATP]}.$$

Figure 6 Single channel current traces and conductance plot for the 49 pS ATP-activated potassium channel

(a) Conductance plot

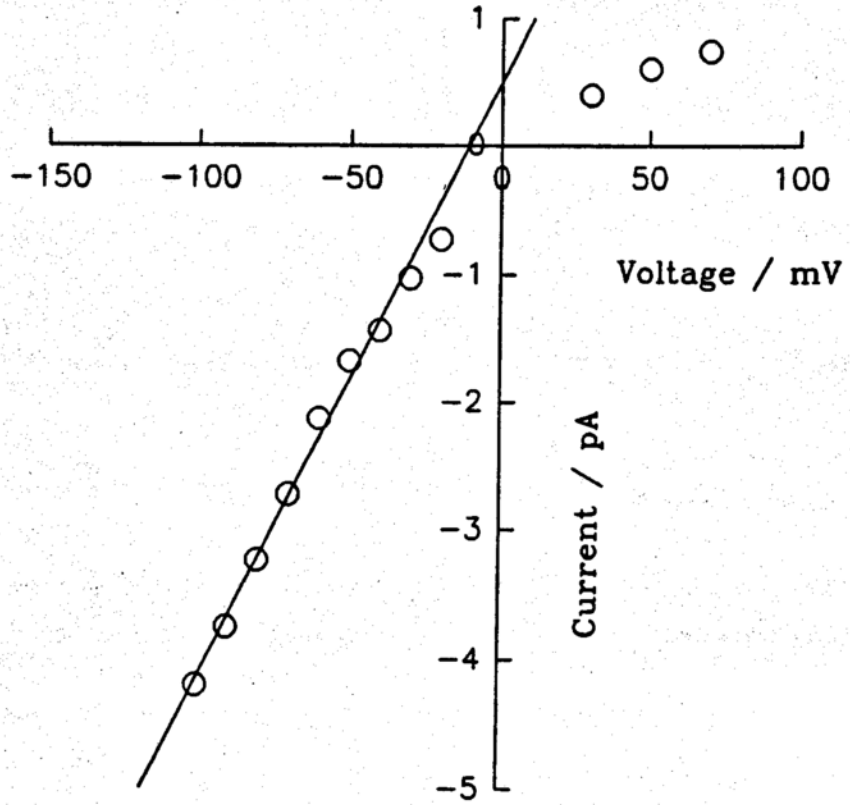

(b) Single channel current traces at various membrane voltages

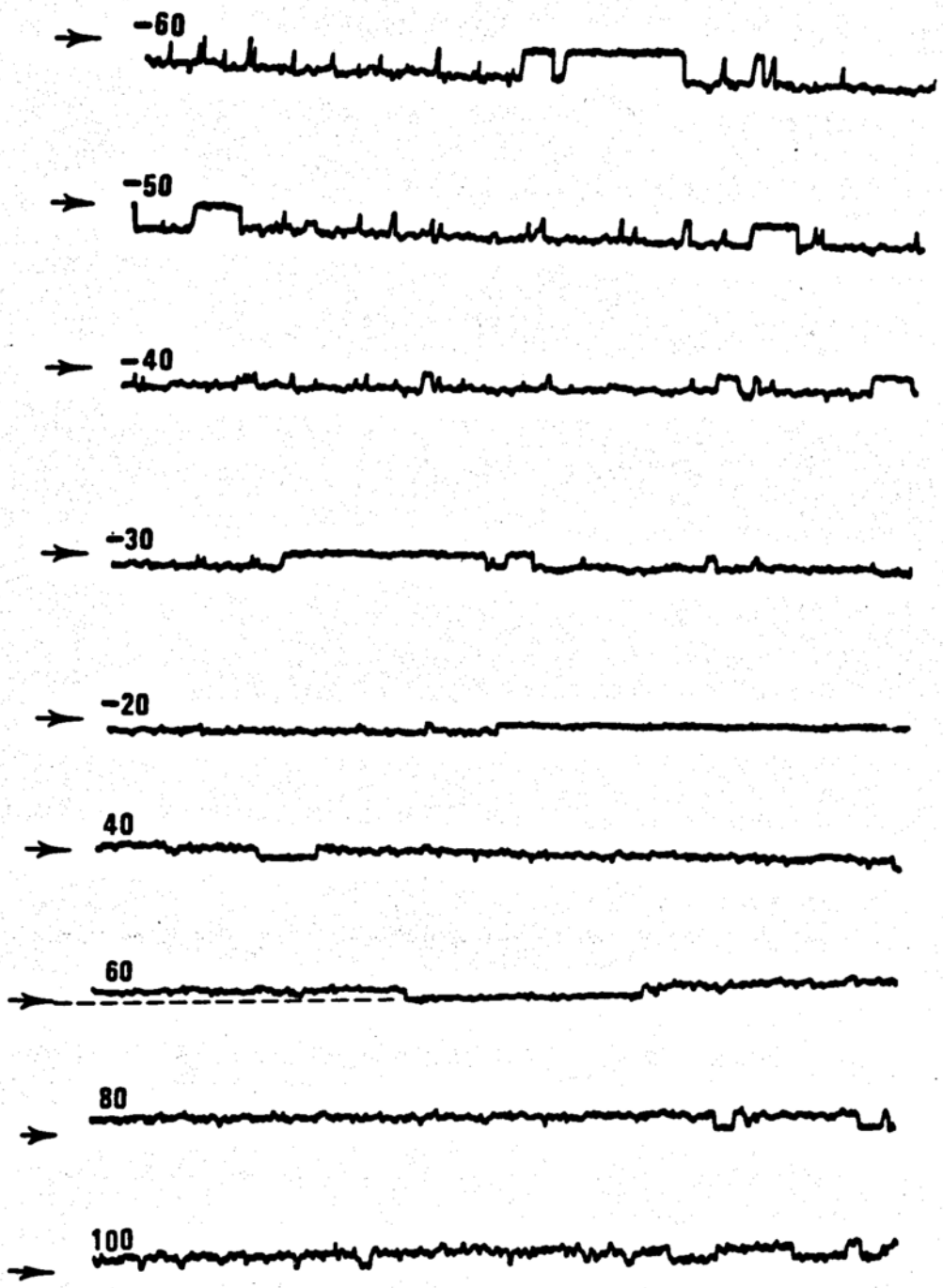

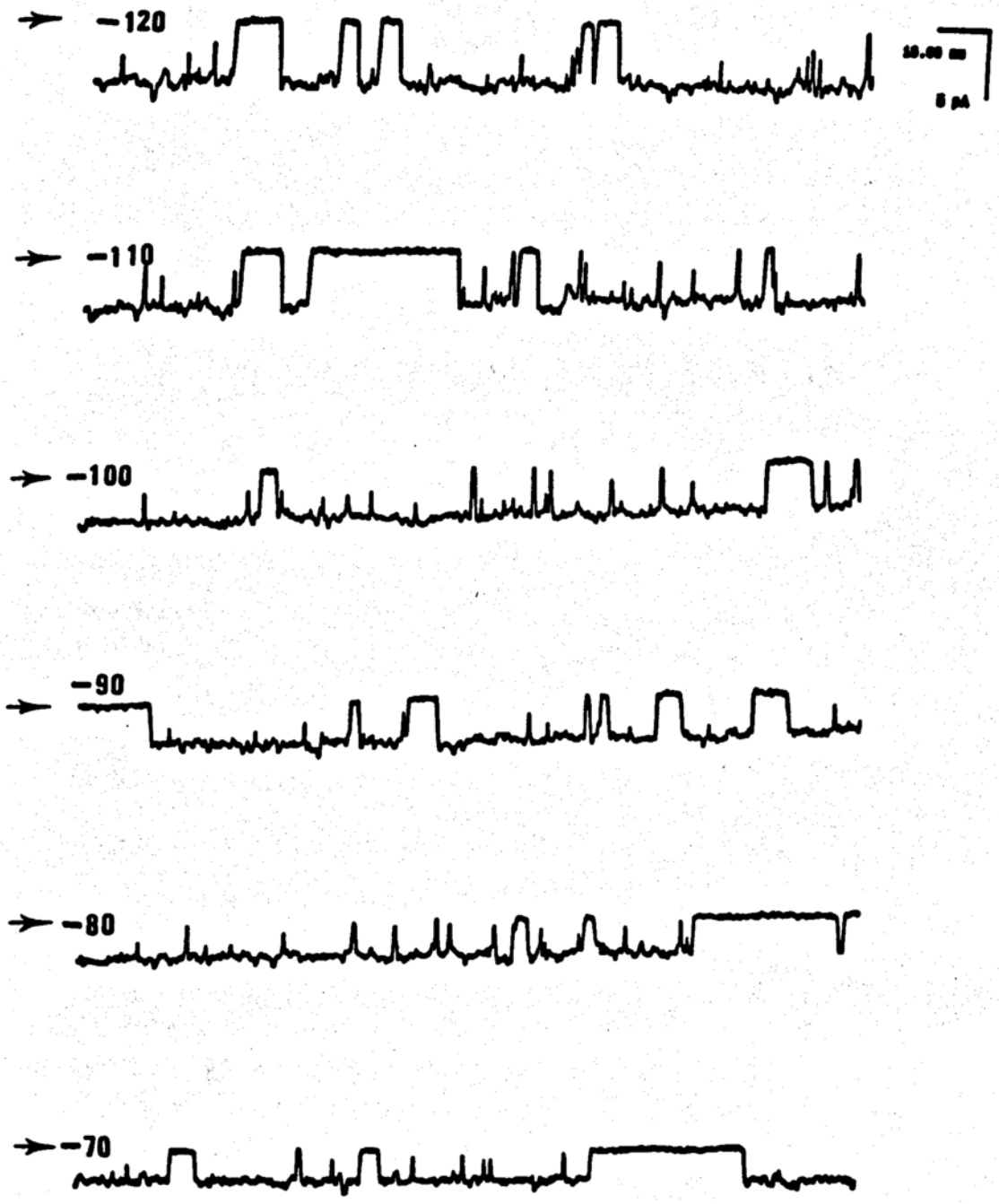
−120
−110
−100
−90
−80
−70

Figure 7 The specificity of the 49 pS ATP-activated potassium channel is demonstrated by using the specific potassium channel blocker TEA. The membrane patch is voltage clamped at -60 mV.

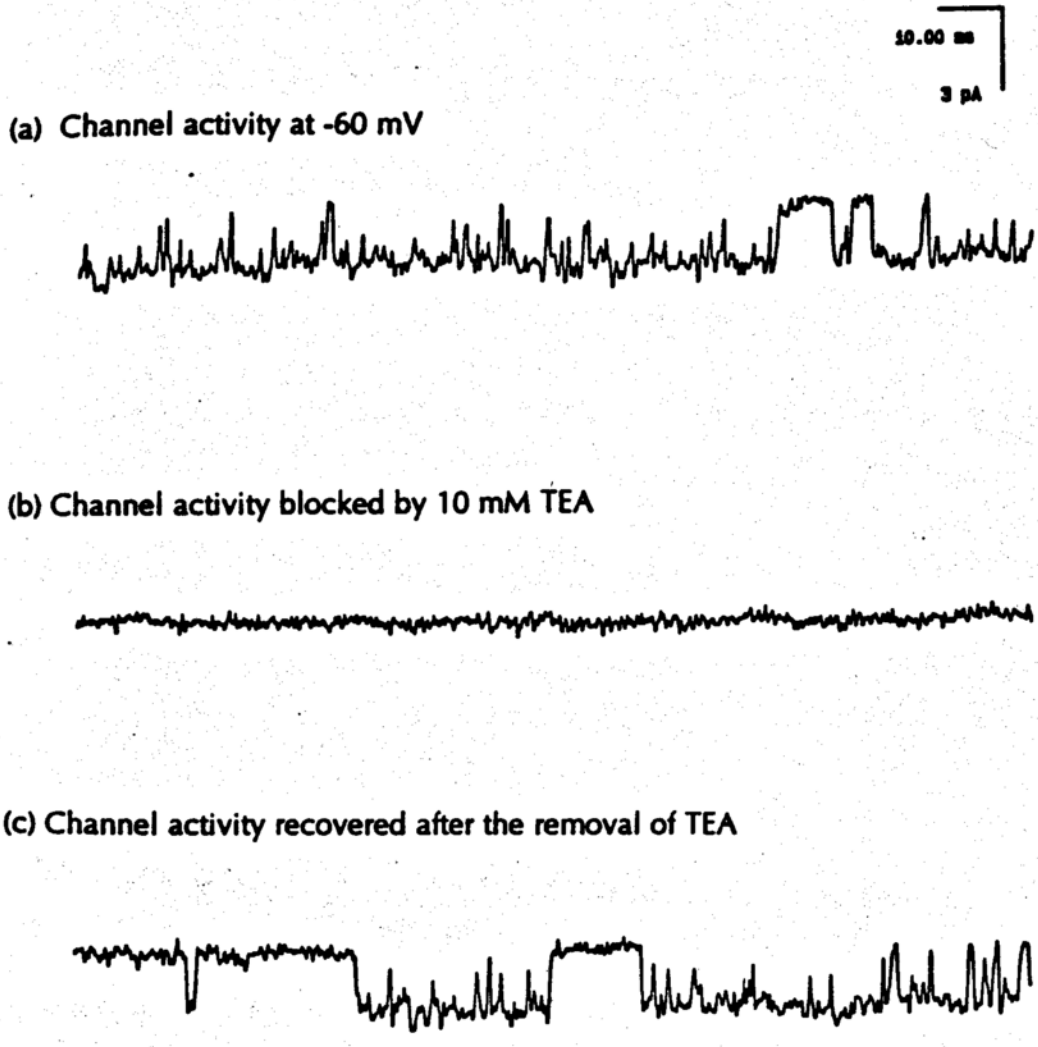

Figure 8 Reversible ATP effect on 49 pS channel opening.

(a) Before ATP addition to the intracellular side of the channel.

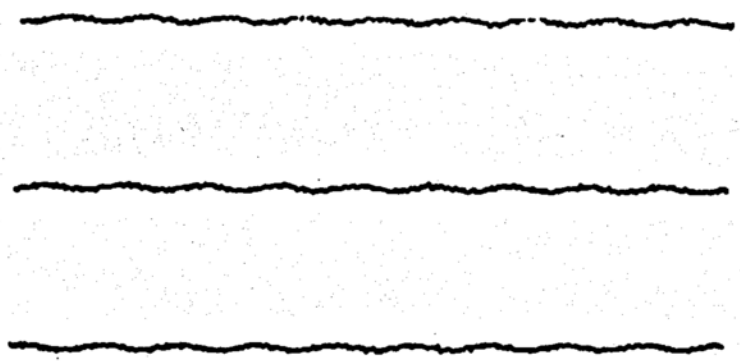

(b) Channel activity increases after the addition of intracellular ATP (~ 1.5 mM).

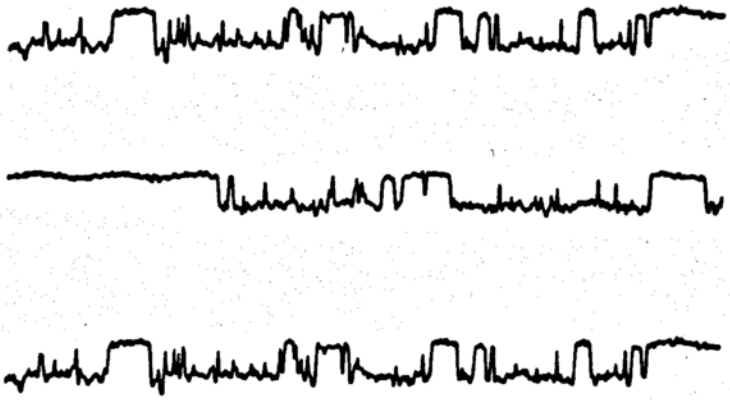

(c) Effect of ATP on channel activity is reversed by replacing the ATP-containing bathing solution with ATP-free bathing solution.

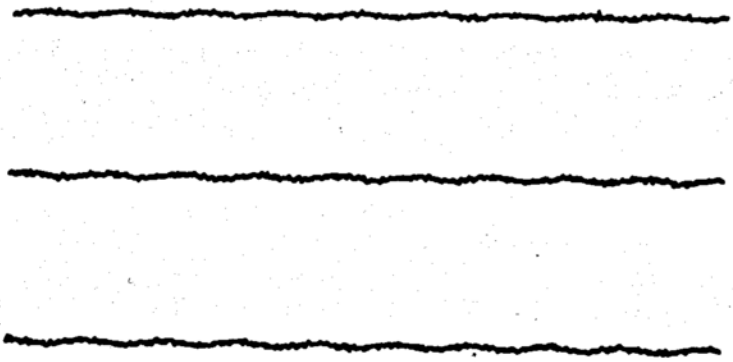

Figure 9 Graded response of the 49 pS channel activity to intracellular ATP.

(a) Opening of the 49 pS channel decreased with the intracellular concentration of ATP.

(a.1) [ATP]= 3 mM

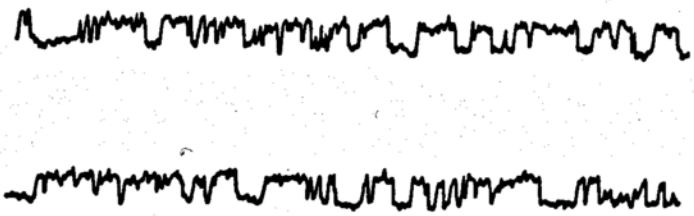

(a.2) [ATP]= 1mM

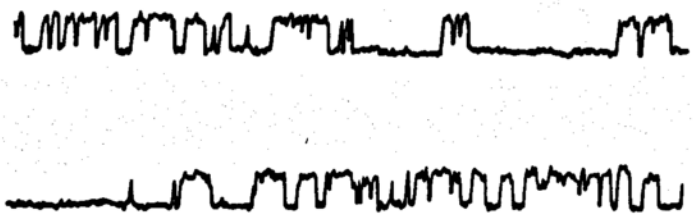

(a.3) [ATP]= 0.5 mM

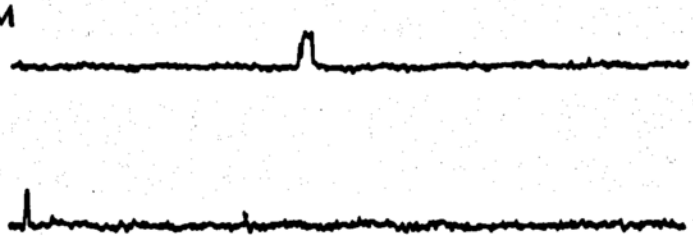

(a.4) [ATP]= 0 mM

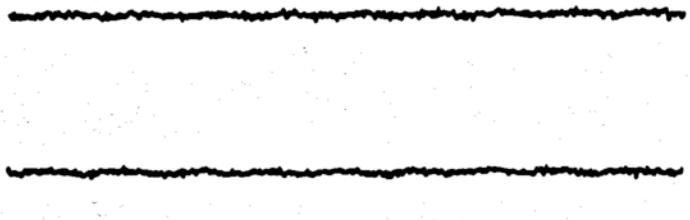

(b) Dose-response curve for one 49 pS channel. Notice that the variations in responses here at various concentrations of ATP are small compared to those seen between different patches (Figure 18).

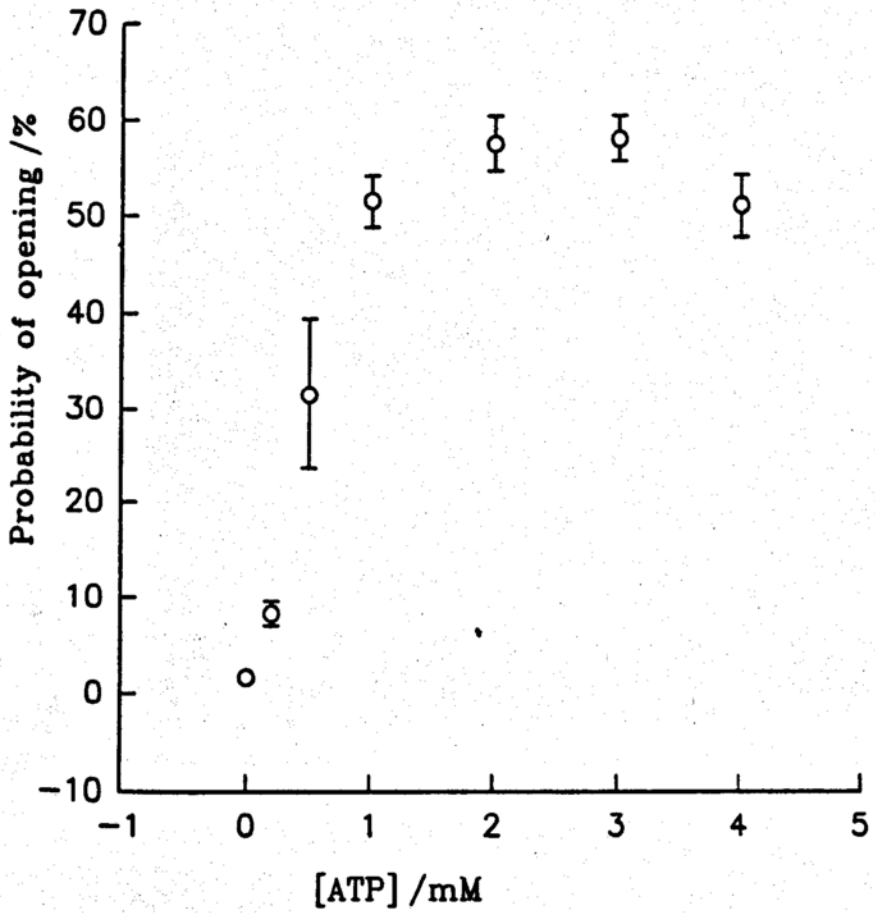

Figure 10 Dose-response of seven different patches containing the 49 pS ATP-activated potassium channel. Notice that the y axis is "normalized response".

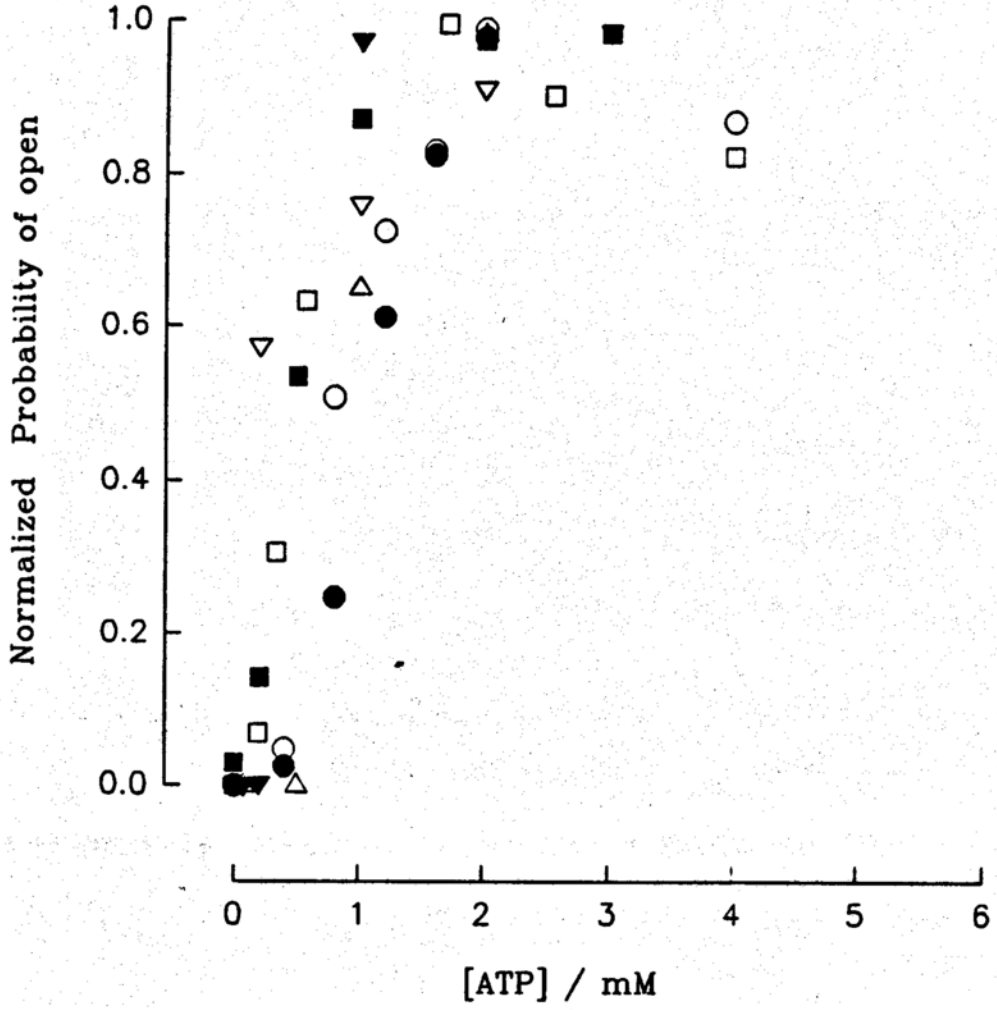

Figure 11 The ionic composition of the solution bathing the intracellular side of the patch has little effect on channel conductance at hyperpolarization potentials.

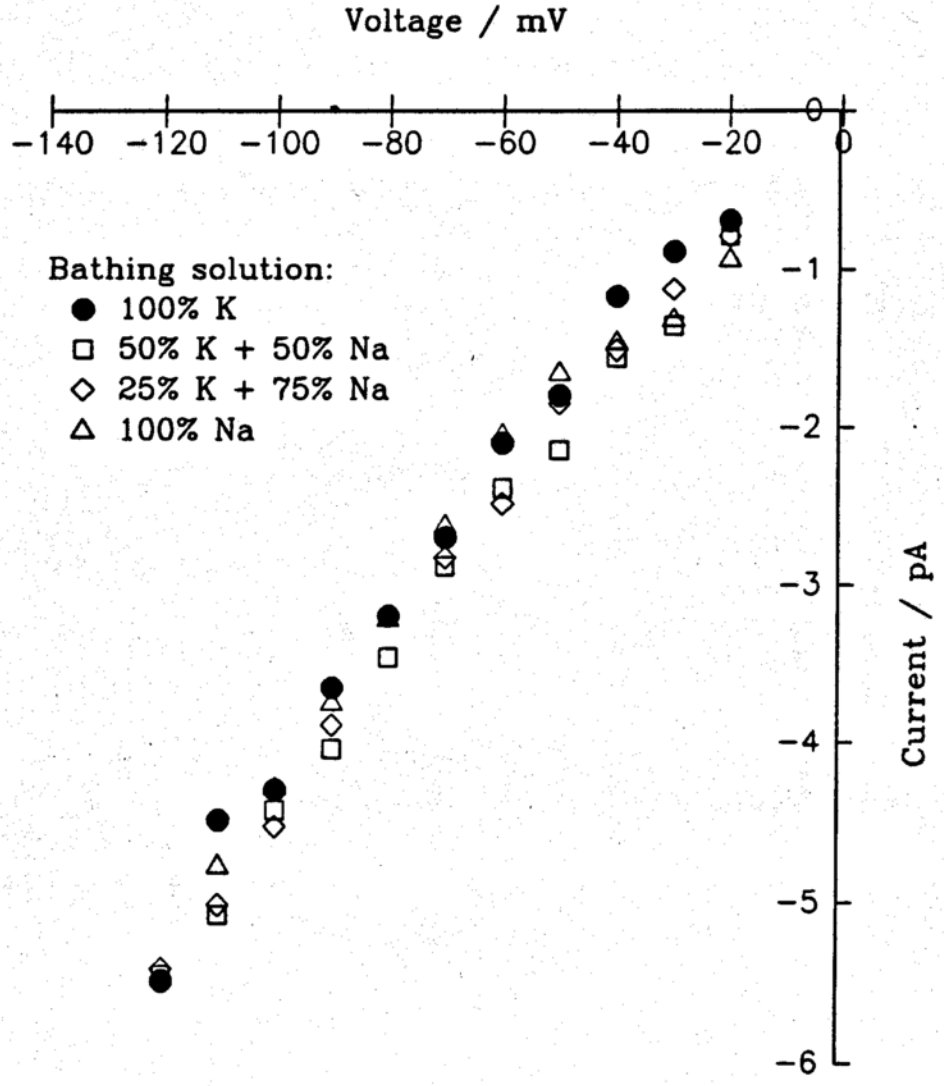

Figure 12 The conductance value remains stable during an entire experiment of ~ 1.5 hours.

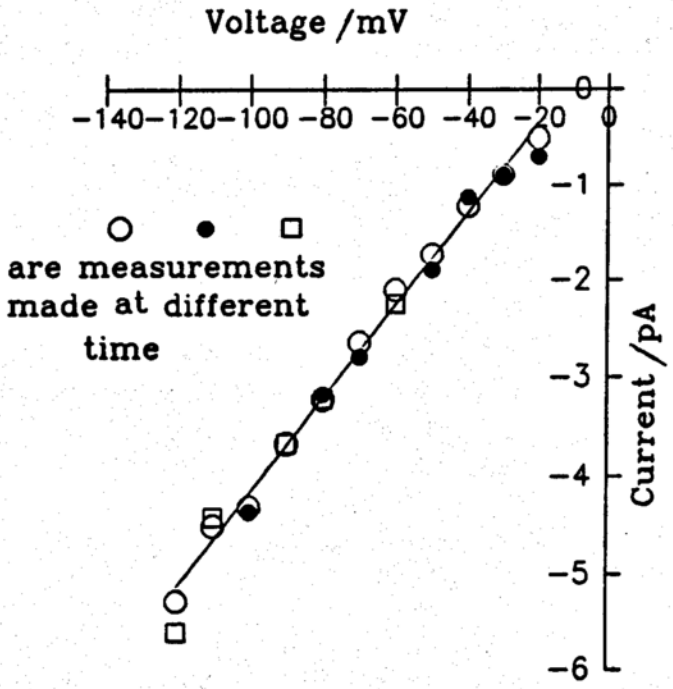

Figure 13 Both ADP and AMP show positive effects on the opening of the 49 pS channel.

(a.1) Control

(a.2) Higher probability of opening due to 3 mM ADP.

(b.1) Control

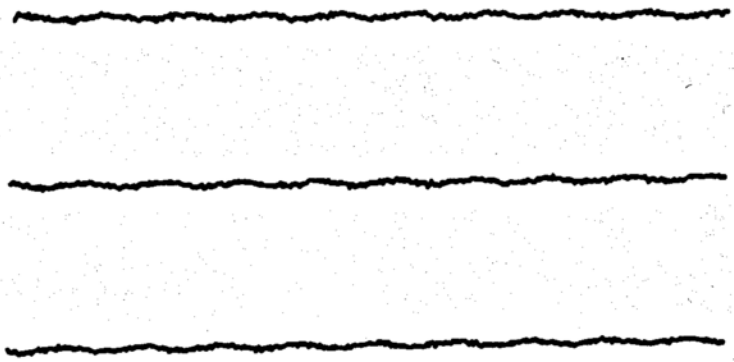

(b.2) Higher probability of opening due to 3 mM AMP

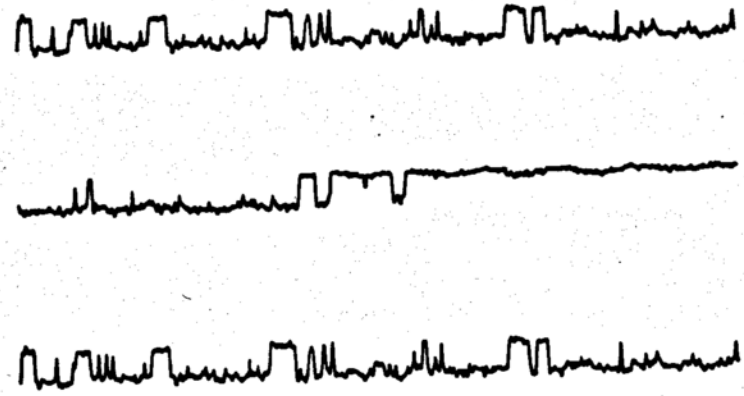

(b.3) Washoff AMP

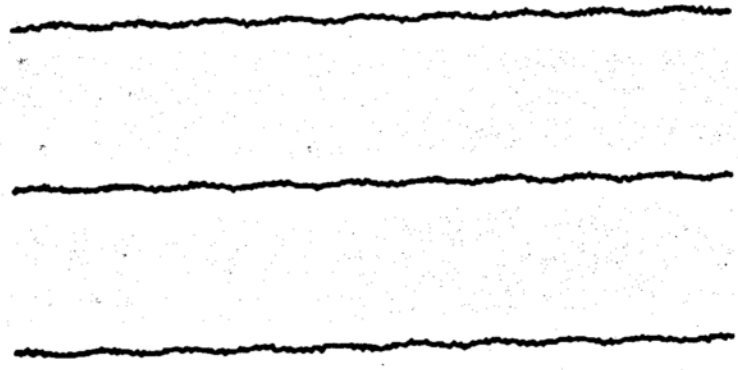

Figure 14 Blockage of channel activity by TEA can be reversed by the addition of intracellular ADP (3 mM).

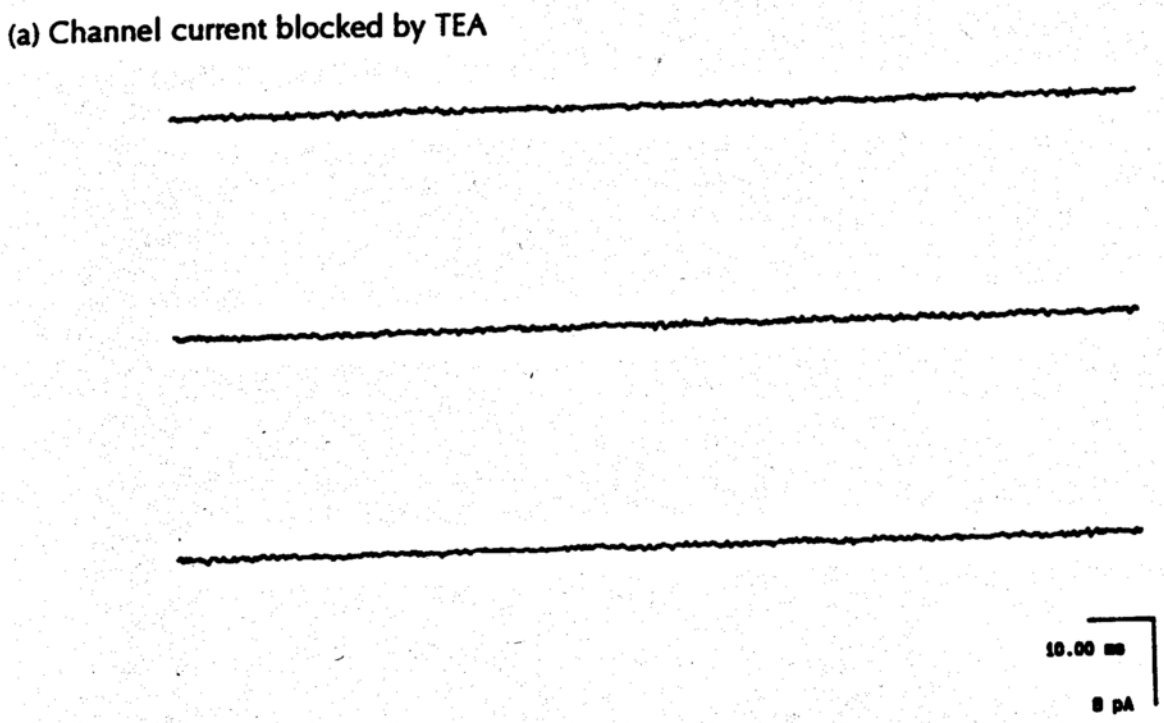

Figure 15 Opening probabilities in various intracellular conditions observed within a single patch as experiment proceeds.

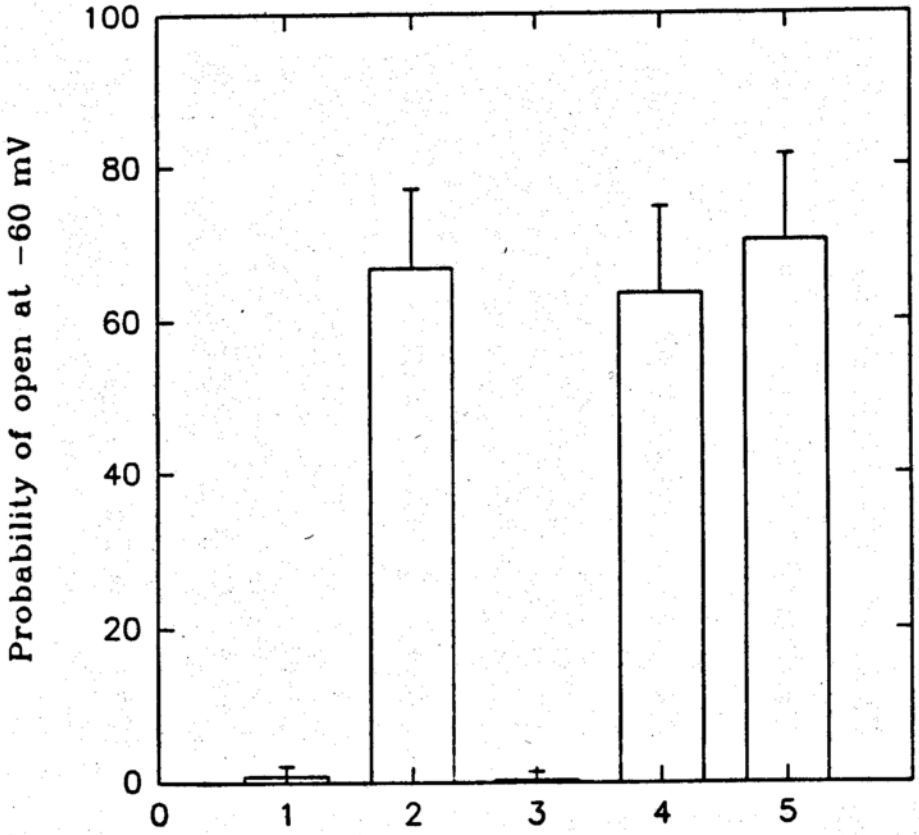

Figure 16 Effects of adenosine, AMP, ADP, and ATP on the opening of the 49 pS channel at various membrane voltages.

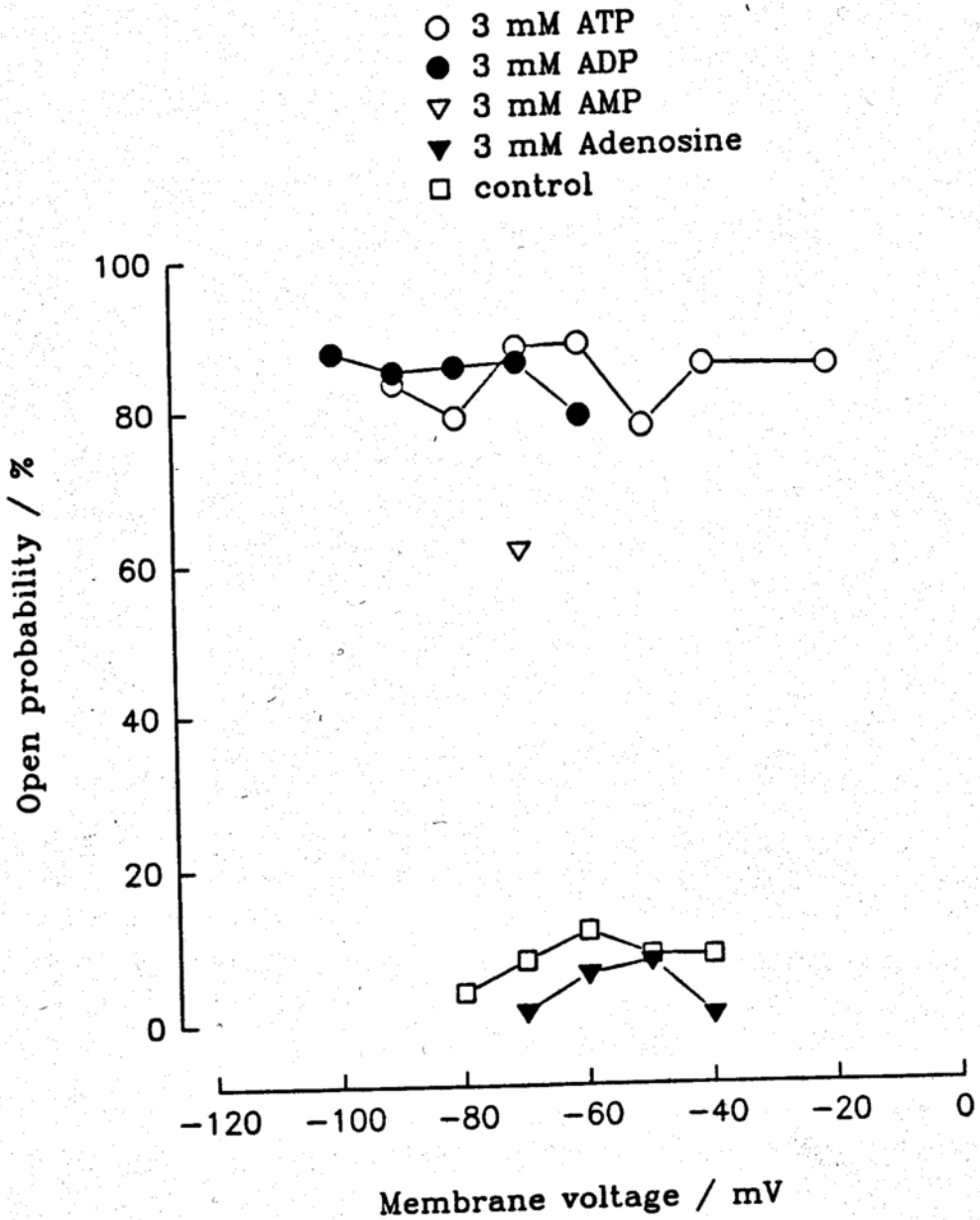

Figure 17 Effects of the non-hydrolyzable ATP analog, AMP-PCP, on the opening of the 49 pS channel.

(a) Control

(b) High probability of opening due to AMP-PCP

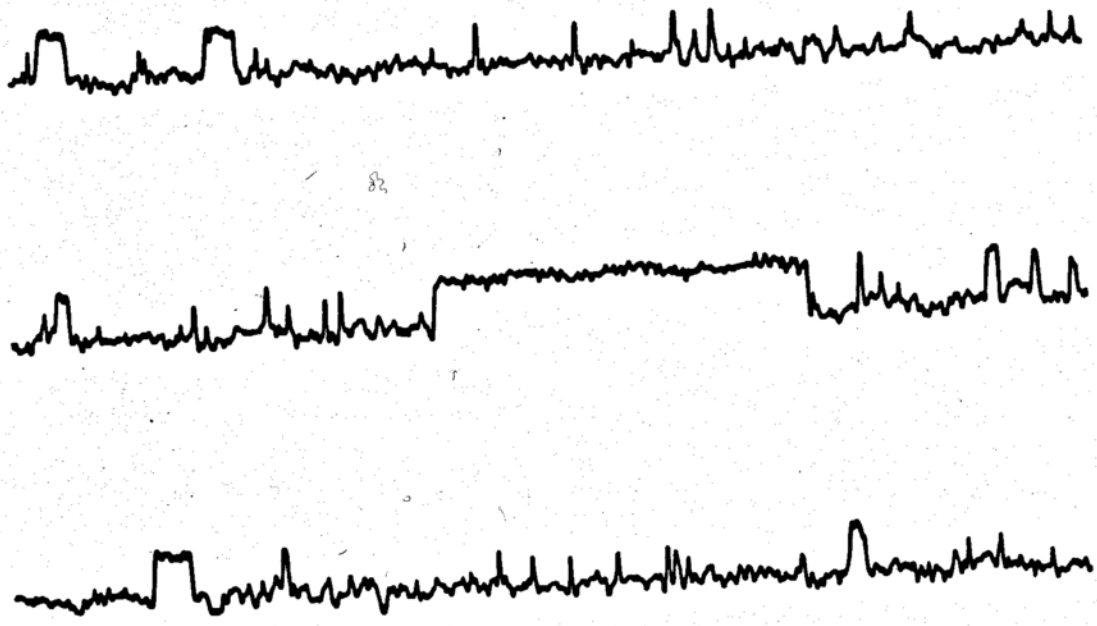

(c) Channel closed upon the removal of AMP-PCP

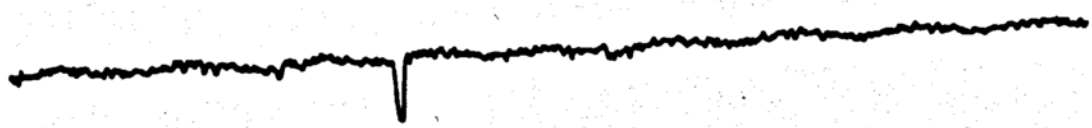

Figure 18 Dose-response curve averaged from the seven different patches shown in Figure 1.10.

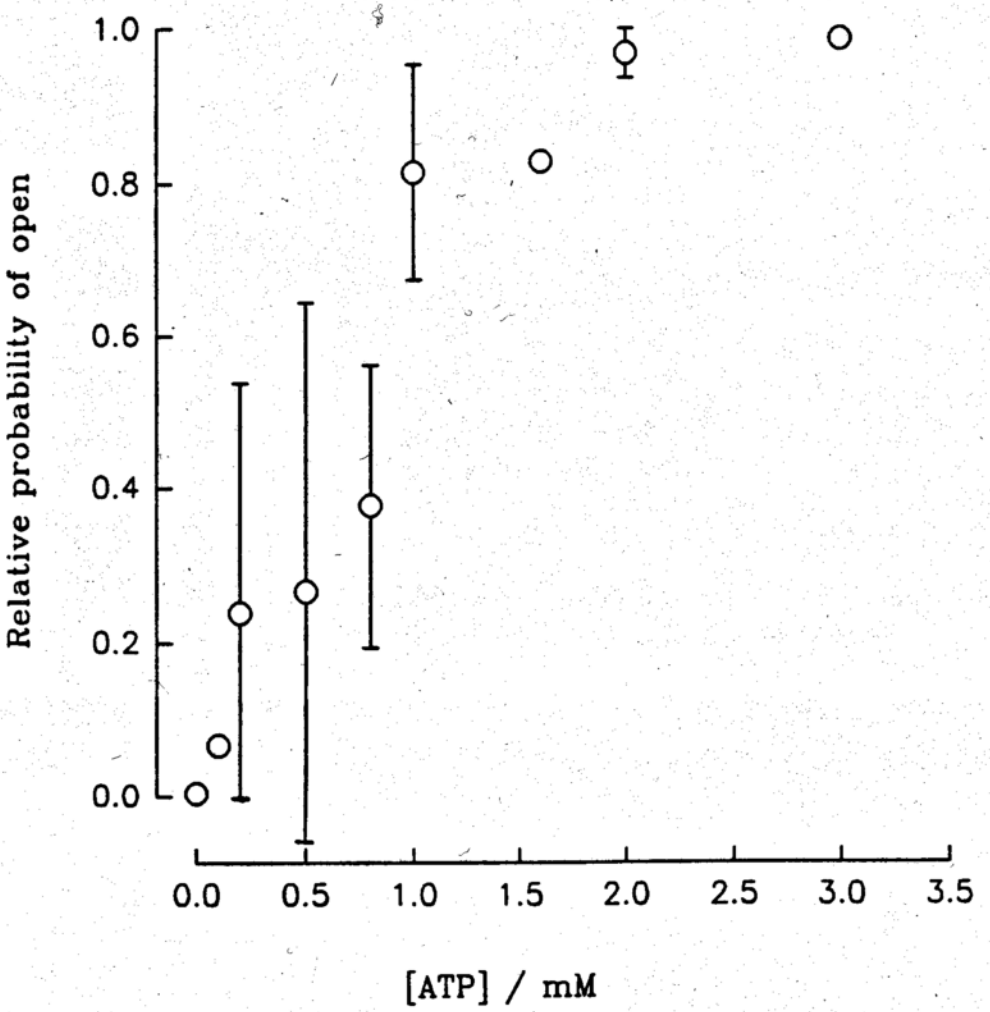

Figure 19 Hill's plot of the averaged dose-response curve for the 49 pS ATP-activated channel. The resulting slope is 1.87.

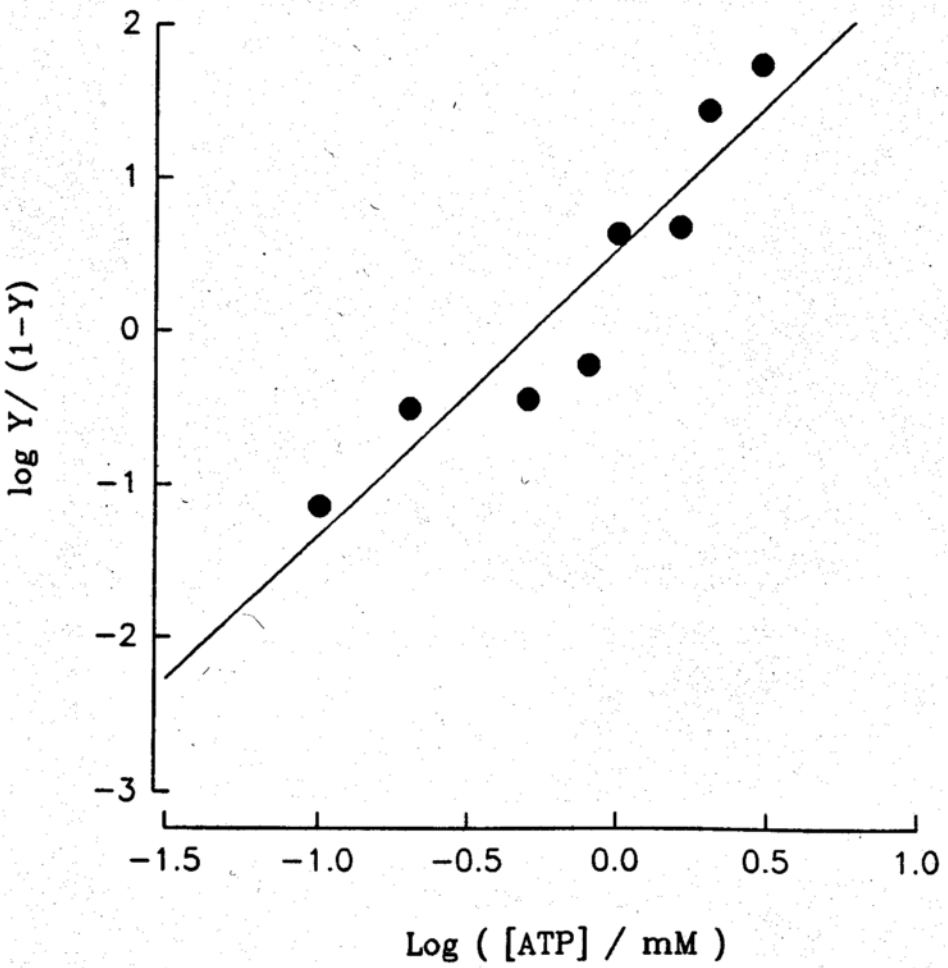

Figure 20 The effect of ATP on the opening of the 49 pS channel is independent of membrane voltage.

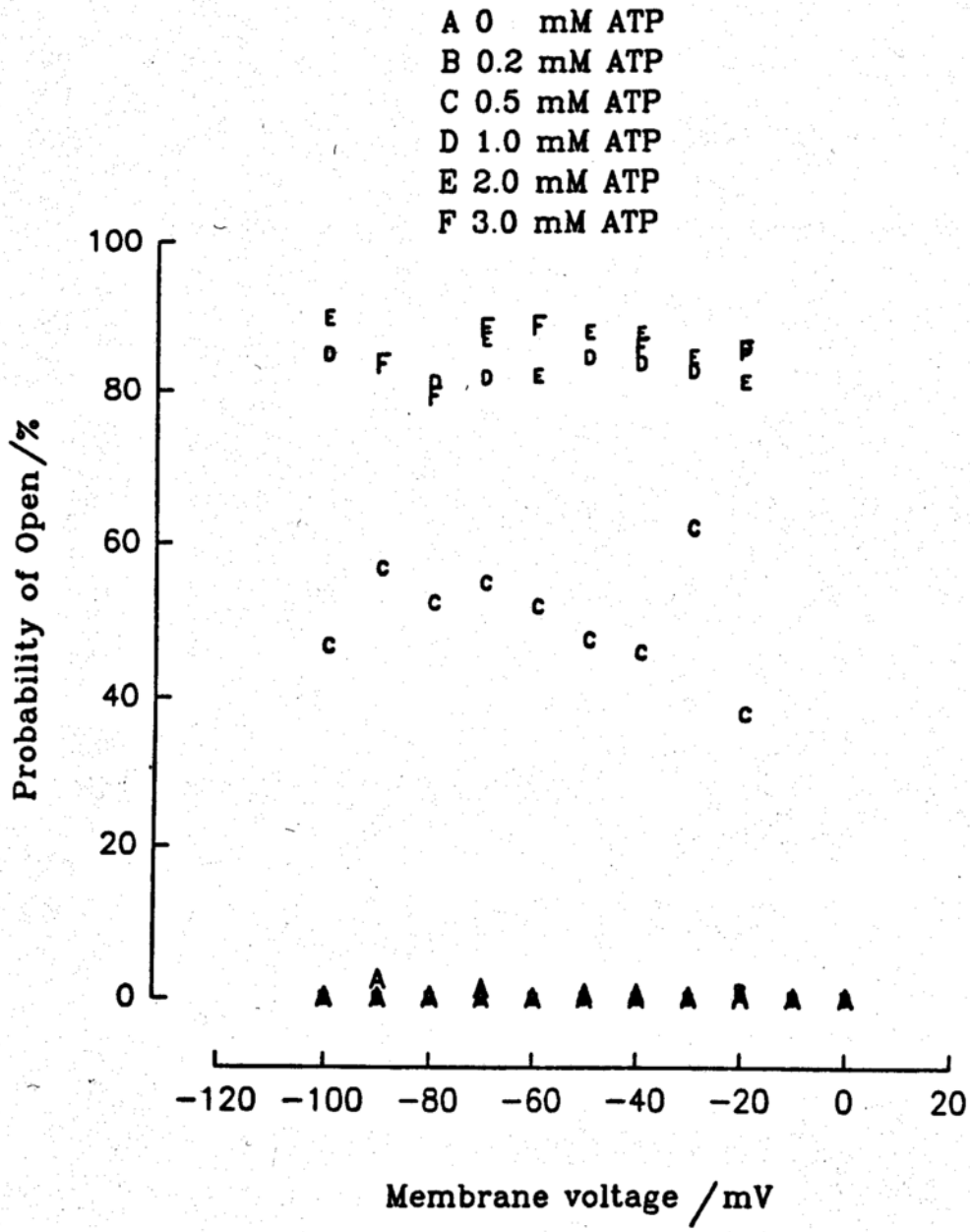

Figure 21 Dwell time histograms of both the open and closed events at various concentrations of ATP, and their fitting to multiexponential expressions: (see Table 1 for values of Wi's and τi's)

$$N_o = \sum_{i=1}^{2} \frac{Wi,o}{\tau_i,o} \text{Exp} \left(-\frac{t}{\tau_i,o} \right) \quad \text{for open}$$

$$N_c = \sum_{i=1}^{3} \frac{Wi,c}{\tau_i,c} \text{Exp} \left(-\frac{t}{\tau_i,c} \right) \quad \text{for closed}$$

Where t is time, Wi's are weighing factors and τi's are time constants.

(a) At intracellular [ATP] = 0.33 mM, the probability density functions (pdfs) of the open events and the closed events are fitted respectively to multiexponential expressions:

$$F(t), o = 0.509 \bullet \exp(-0.848 \bullet t) + 0.491 \bullet \exp(-0.119 \bullet t)$$

$$F(t), c = 0.9491 \bullet \exp(-0.5714 \bullet t) + 0.0493 \bullet \exp(-0.0762 \bullet t) + 0.0016 \bullet \exp(-0.0023 \bullet t)$$

(a.1) Open dwell time histogram and the fitted curve (normal scale)

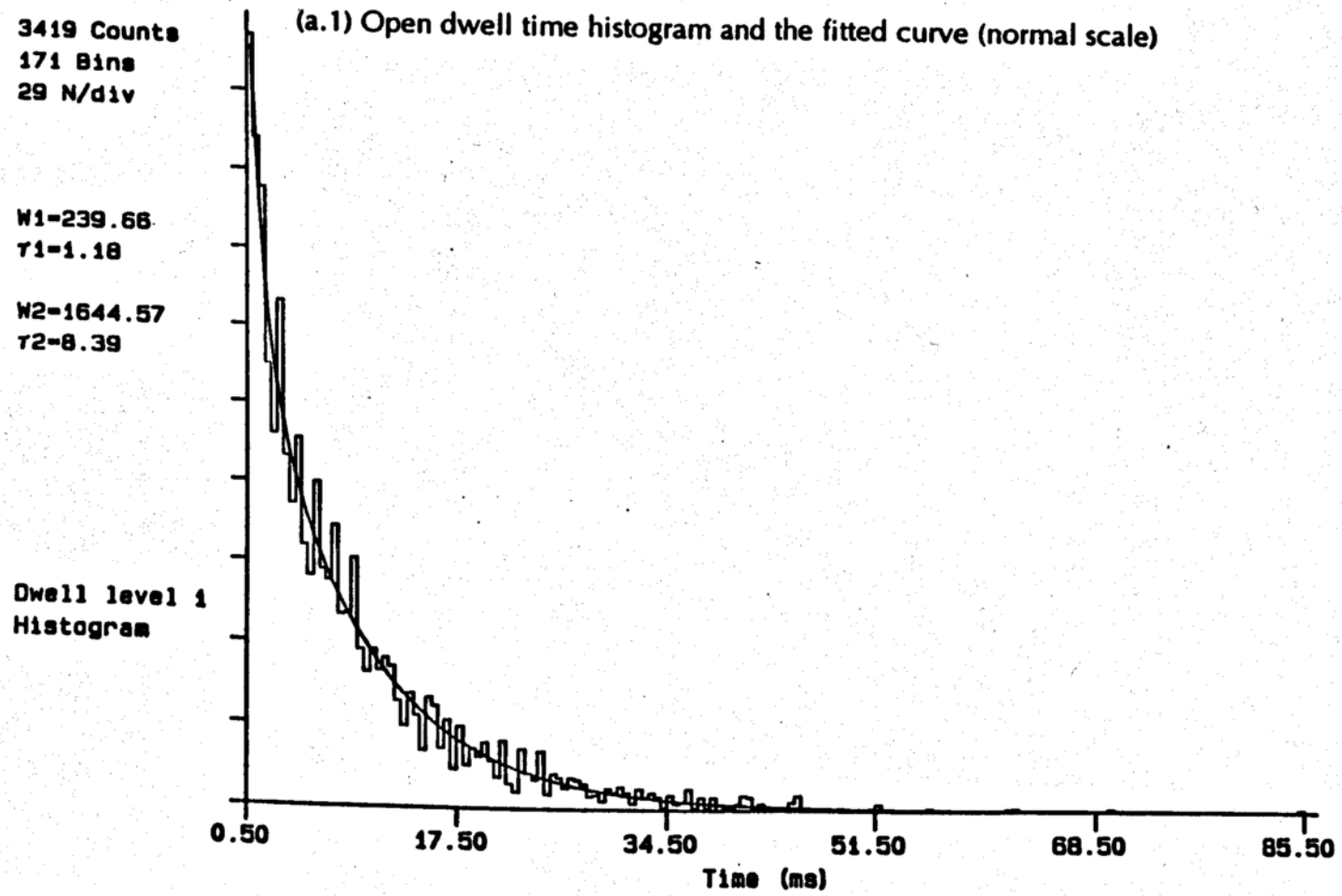

(a.2) Open dwell time histogram and the fitted curve (log scale)

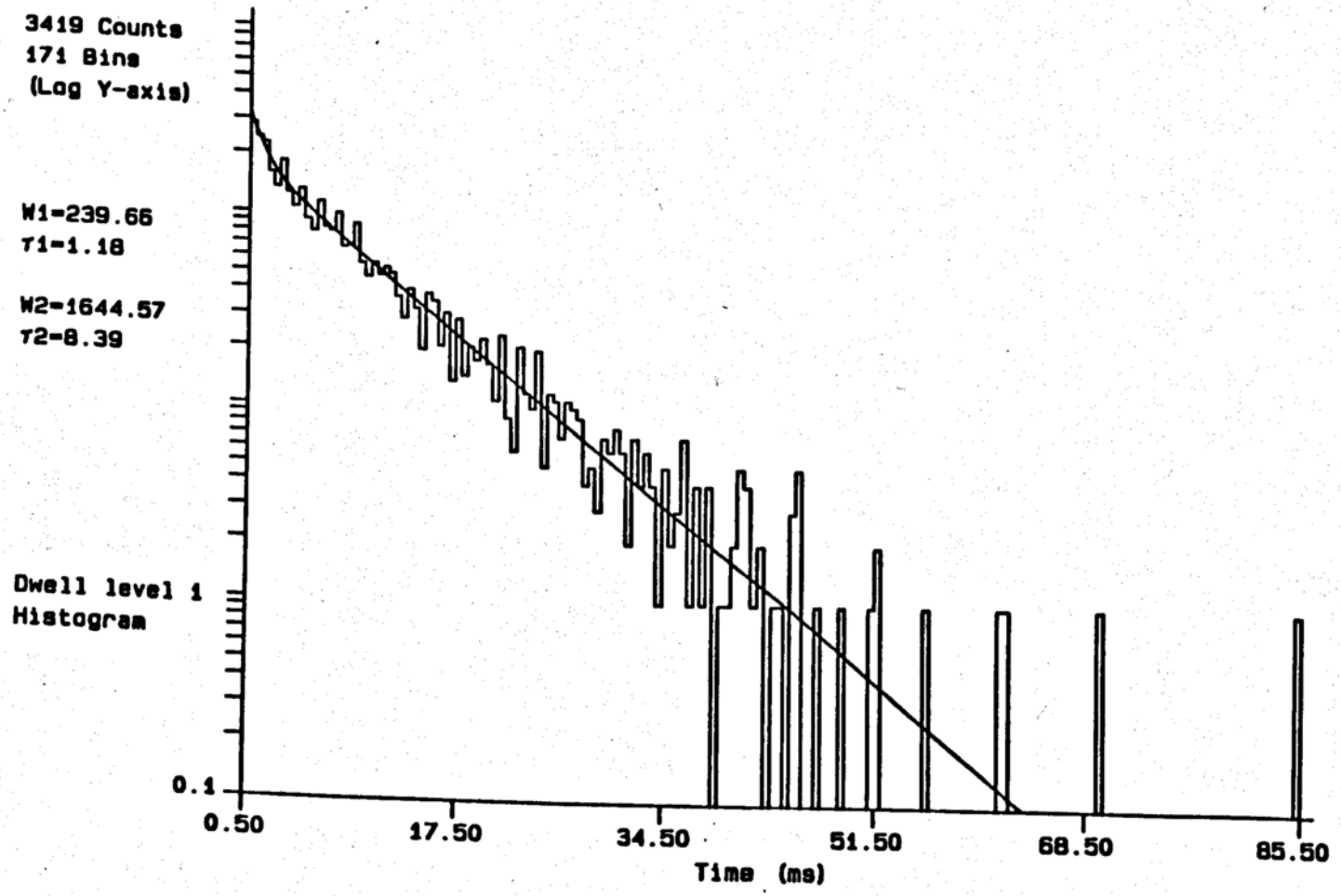

(a.3) Residual plot

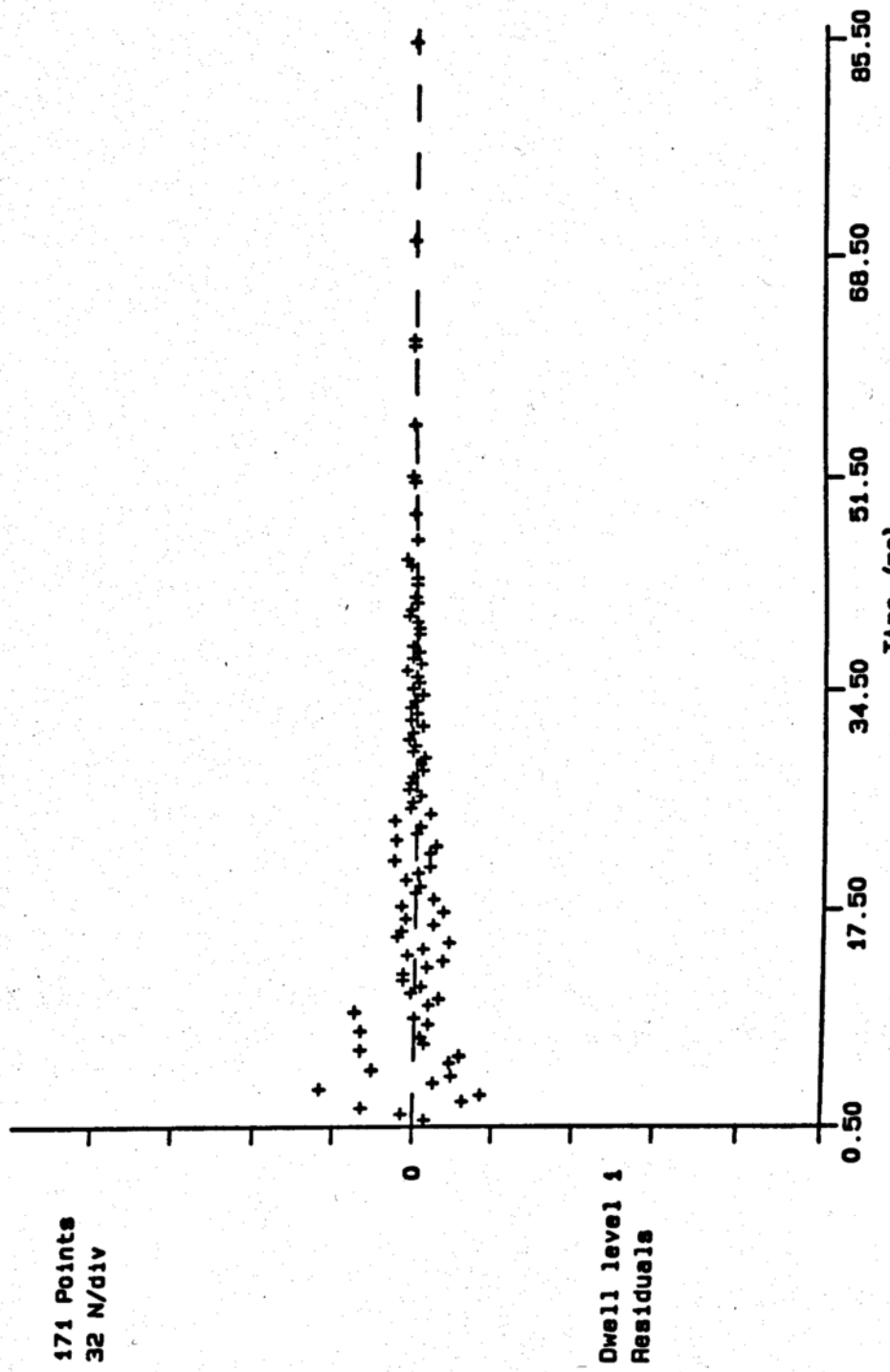

(a.4) Closed dwell time histogram and the fitted curve (normal scale)

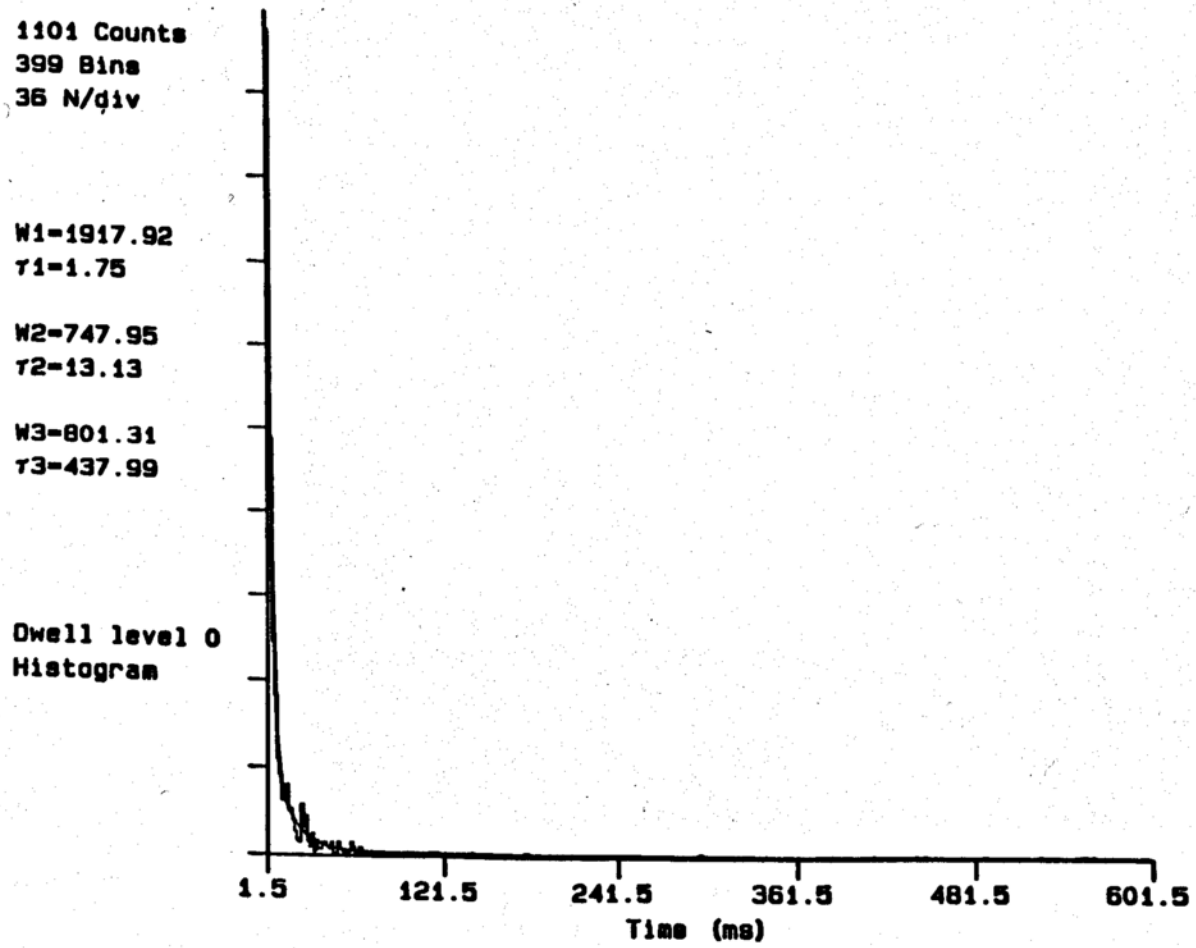

(a.5) Closed dwell time histogram and the fitted curve (log scale)

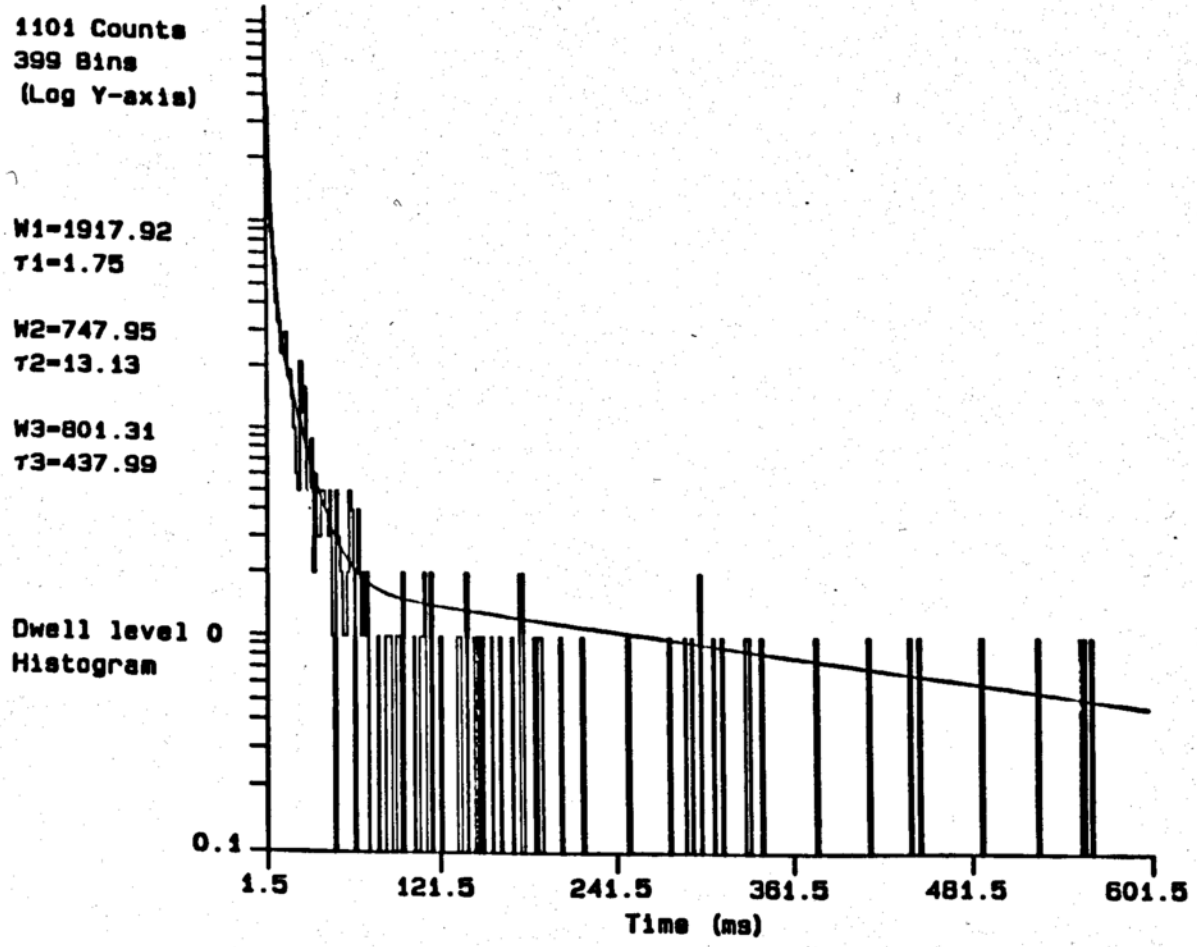

(a.6) Residual plot

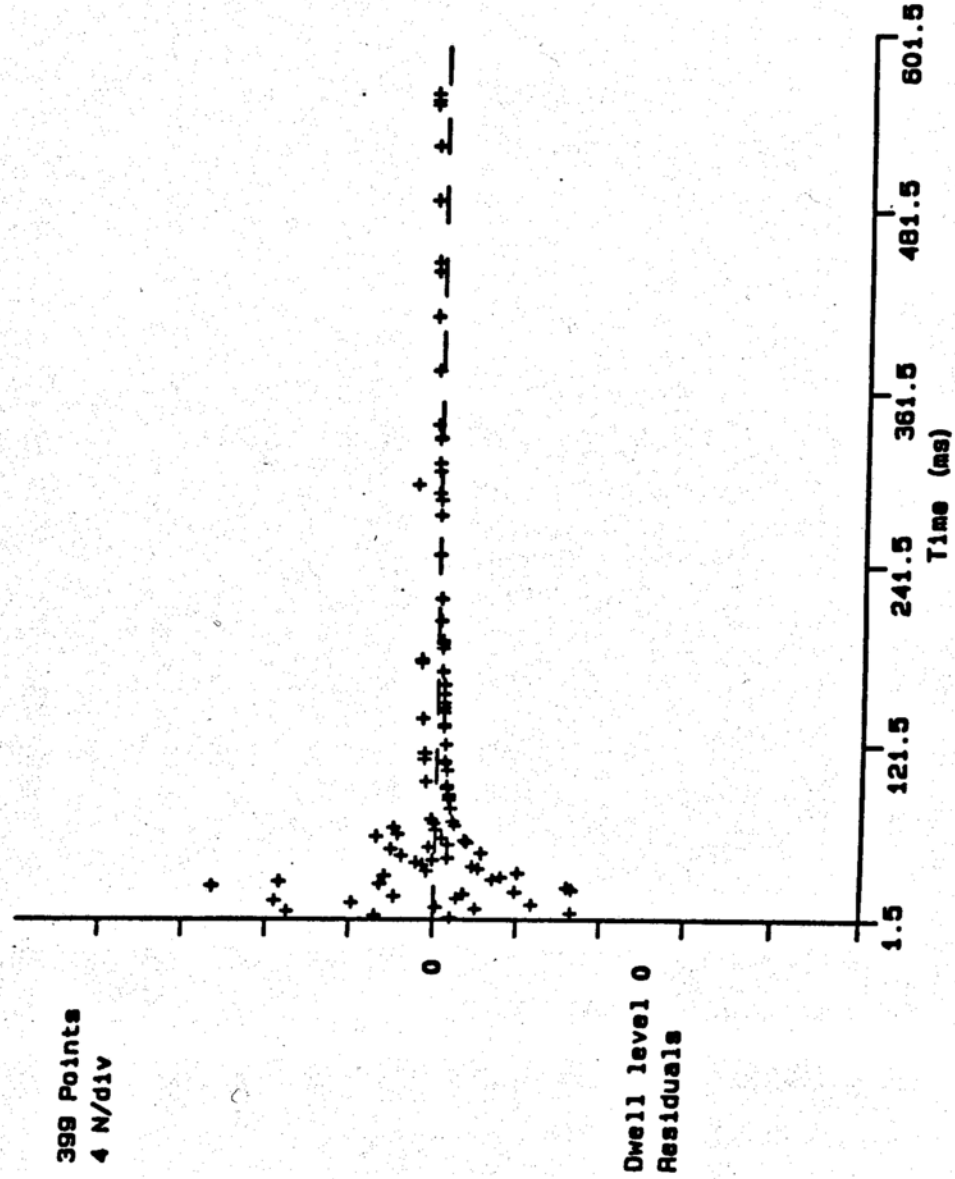

(b) At intracellular [ATP] = 0.57 mM, the probability density functions (pdf) of the open events and the closed events are fitted respectively to multiexponential expressions:

$$F(t), o = 0.336 \bullet \exp(-0.307 \bullet t) + 0.664 \bullet \exp(-0.122 \bullet t)$$

$$F(t), c = 0.9288 \bullet \exp(-1.2331 \bullet t) + 0.0701 \bullet \exp(-0.2392 \bullet t) + 0.0011 \bullet \exp(-0.0074 \bullet t)$$

(b.1) Open dwell time histogram and the fitted curve (normal scale)

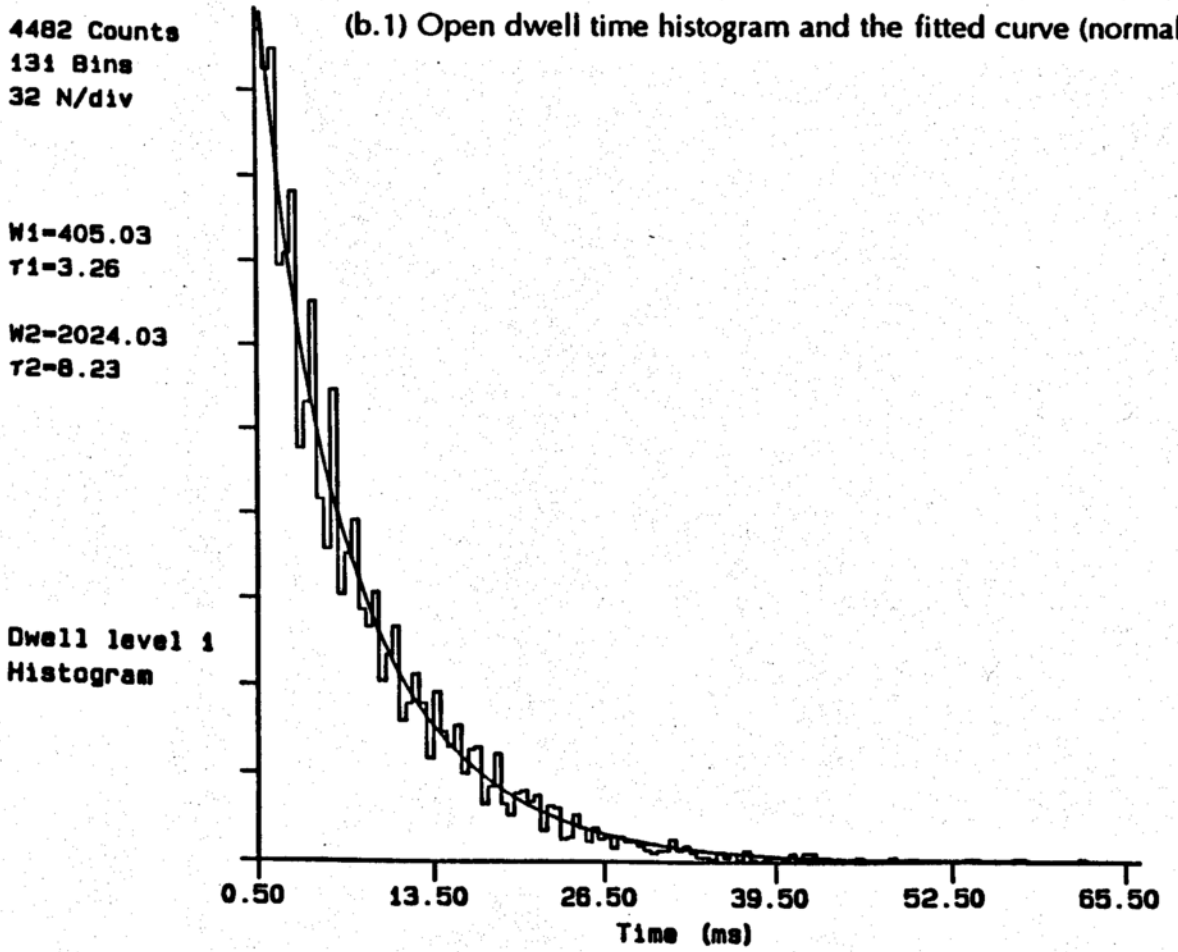

(b.2) Open dwell time histogram and the fitted curve (log scale)

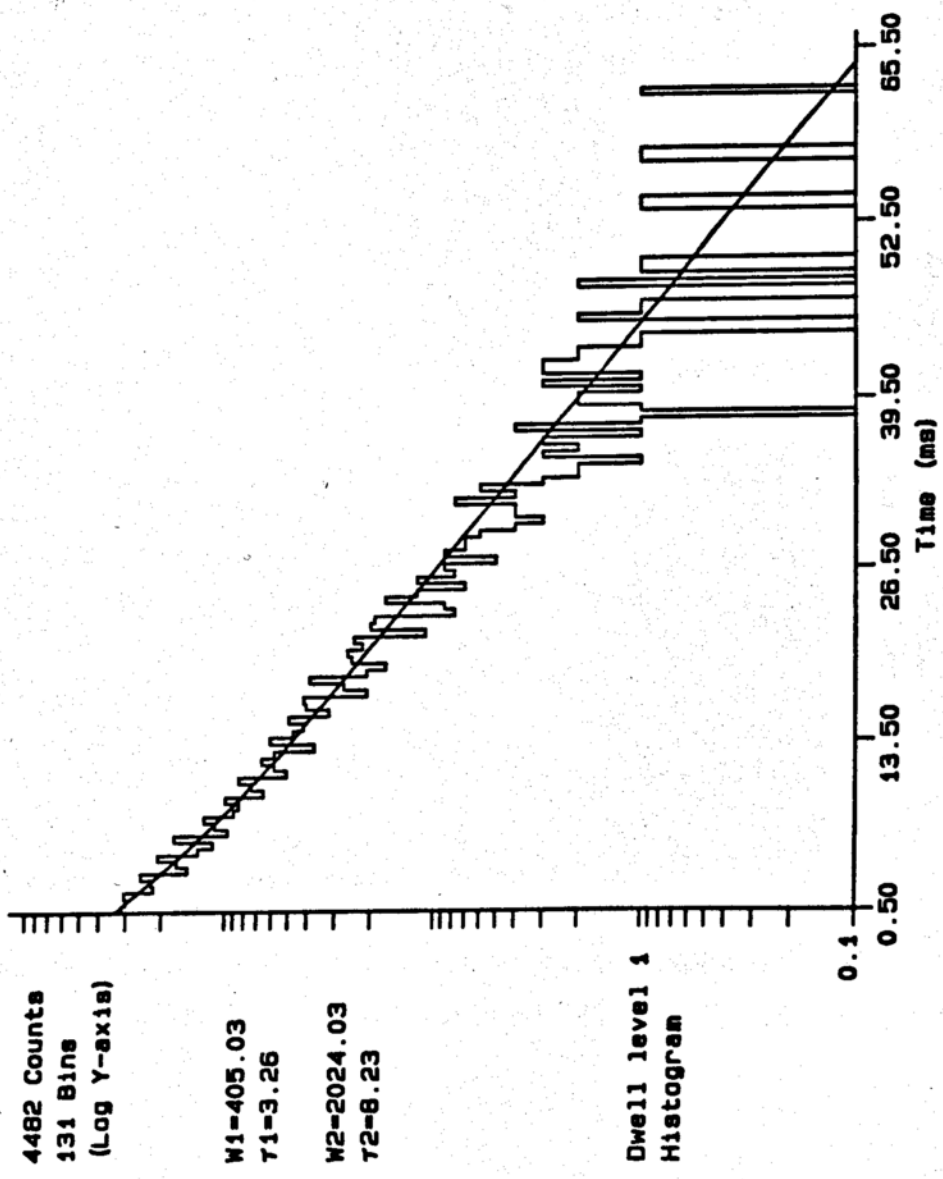

(b.3) Residual plot

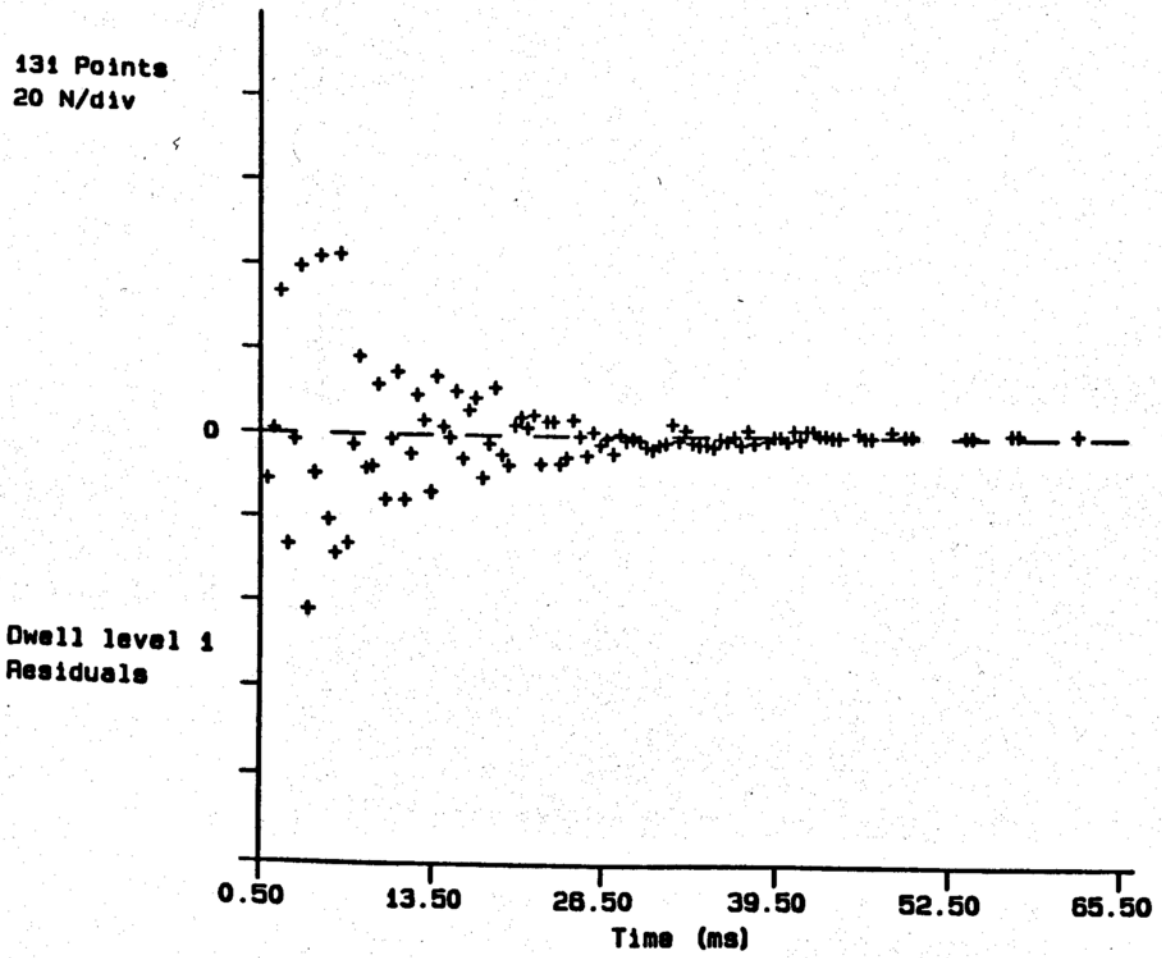

(b.4) Closed dwell time histogram and the fitted curve (normal scale)

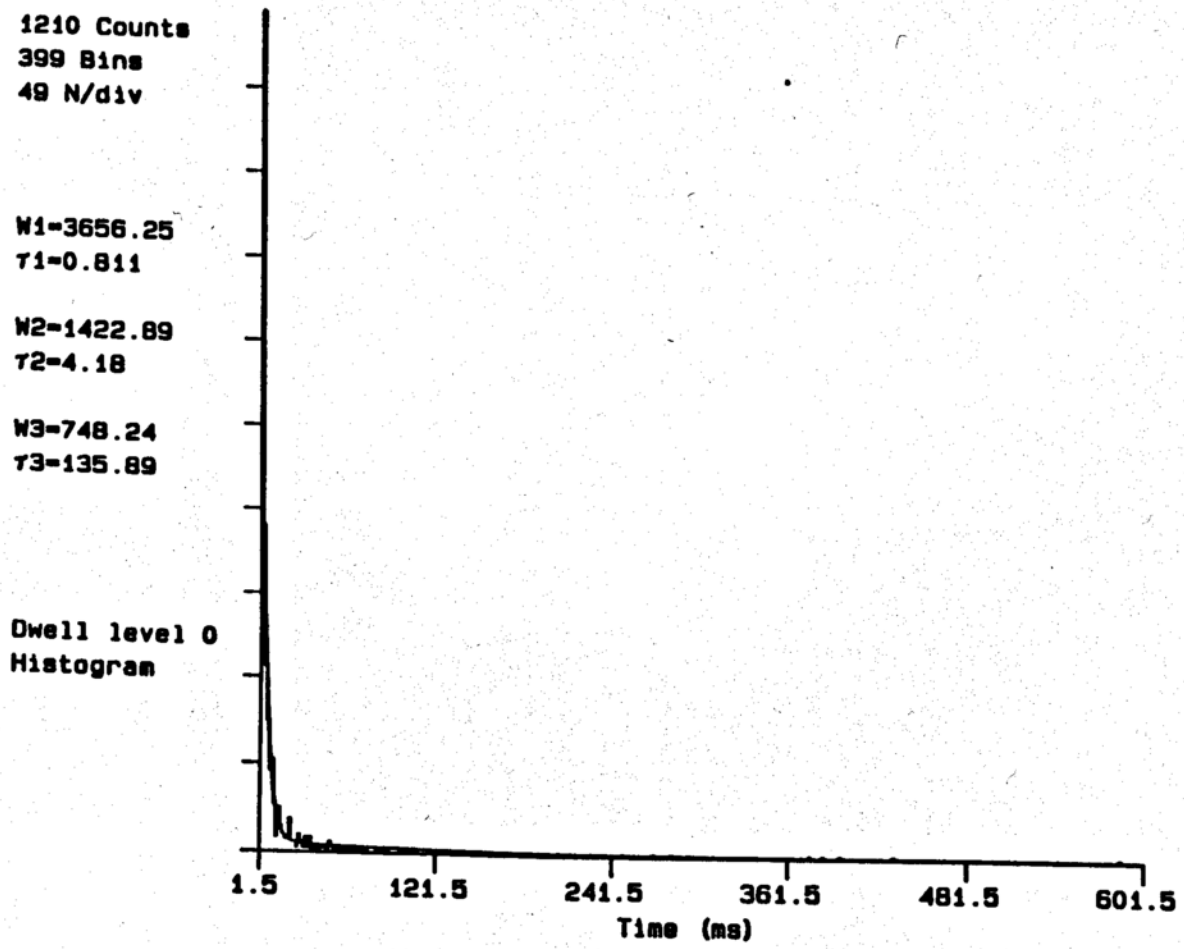

(b.5) Closed dwell time histogram and the fitted curve (log scale)

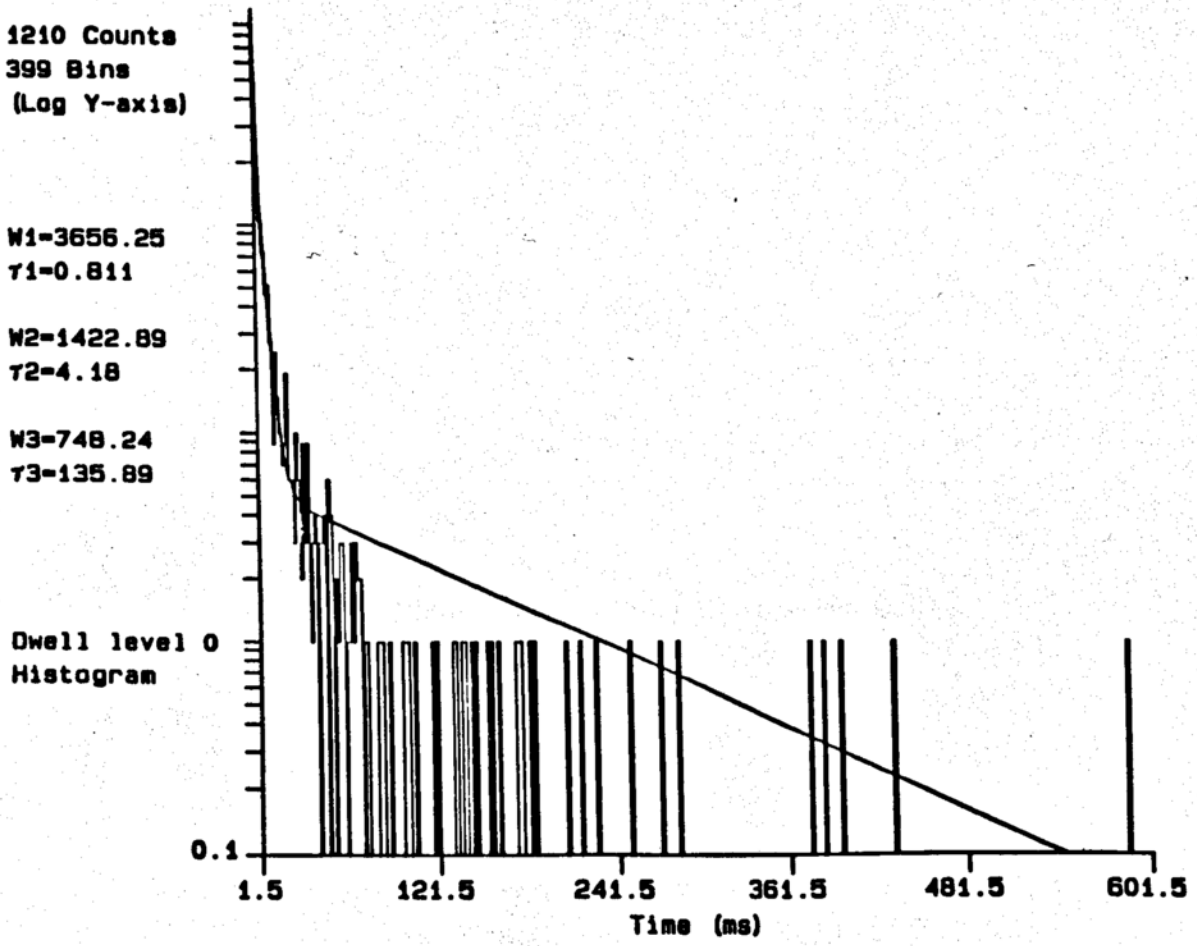

(b.6) Residual plot

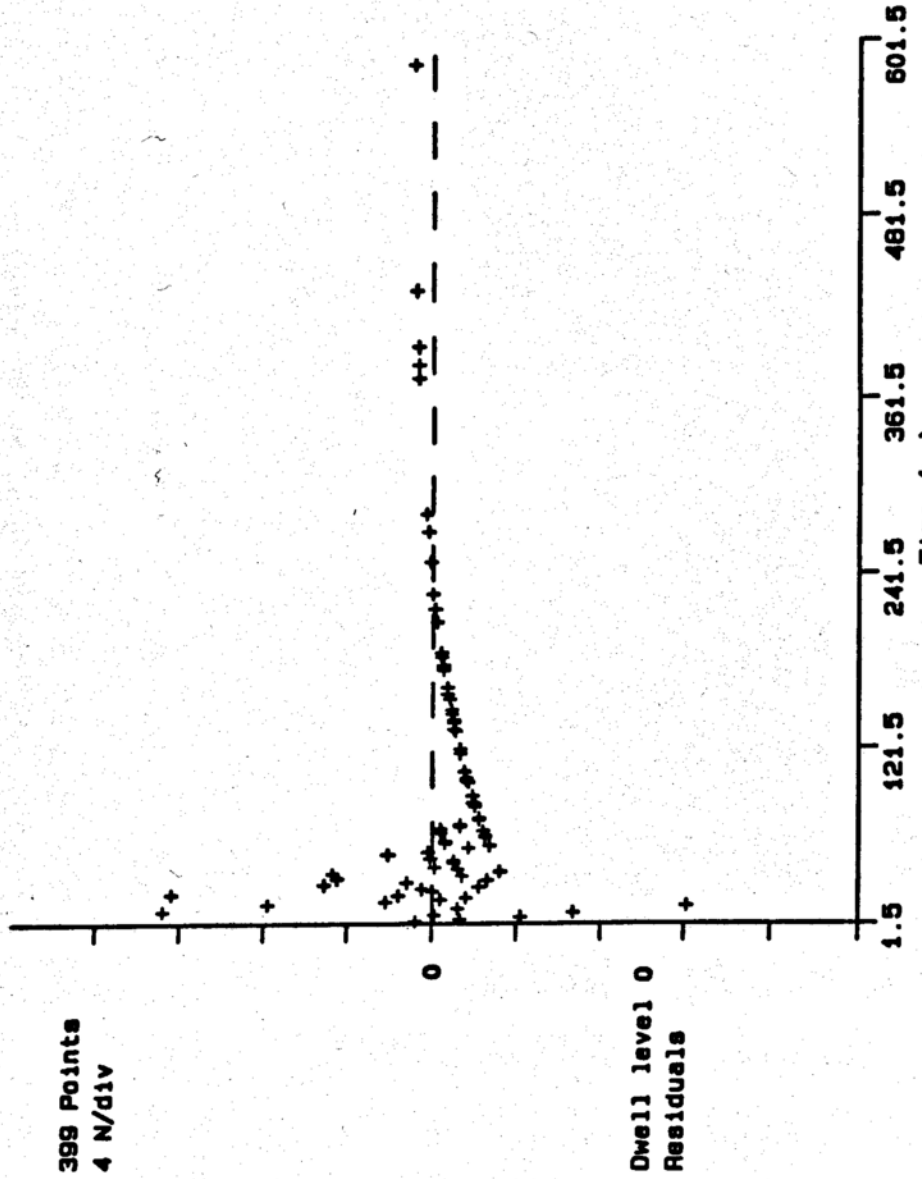

(c) At intracellular [ATP] = 1.7 mM, the probability density functions (pdfs) of the open events and the closed events are fitted respectively to multiexponential expressions:

$$F(t), o = 0.300 \bullet \exp(-0.259 \bullet t) + 0.700 \bullet \exp(-0.119 \bullet t)$$

$$F(t), c = 0.9196 \bullet \exp(-1.3986 \bullet t) + 0.0793 \bullet \exp(-0.3226 \bullet t) + 0.0011 \bullet \exp(-0.0156 \bullet t)$$

(c.1) Open dwell time histogram and the fitted curve (normal scale)

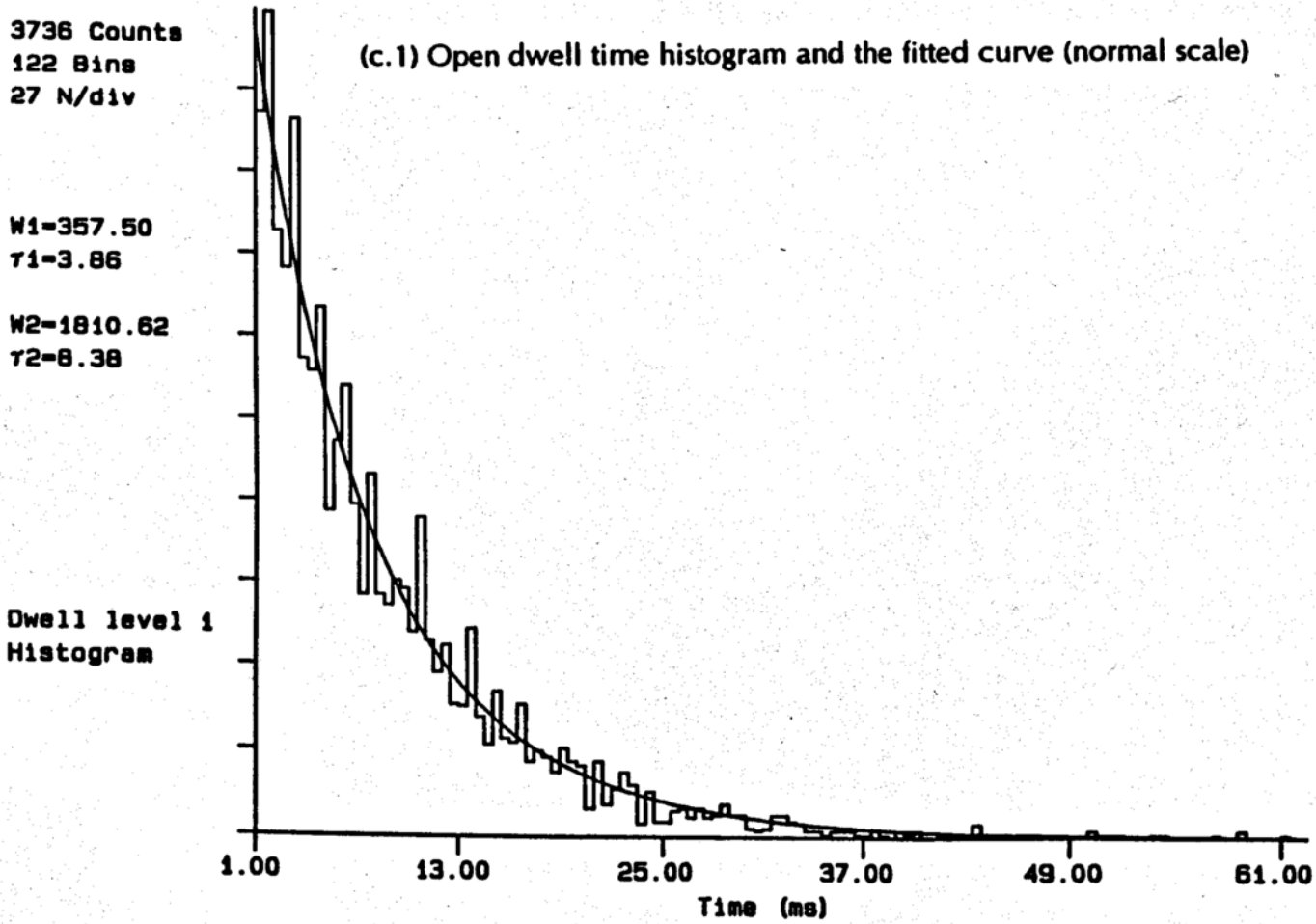

(c.2) Open dwell time histogram and the fitted curve (log scale)

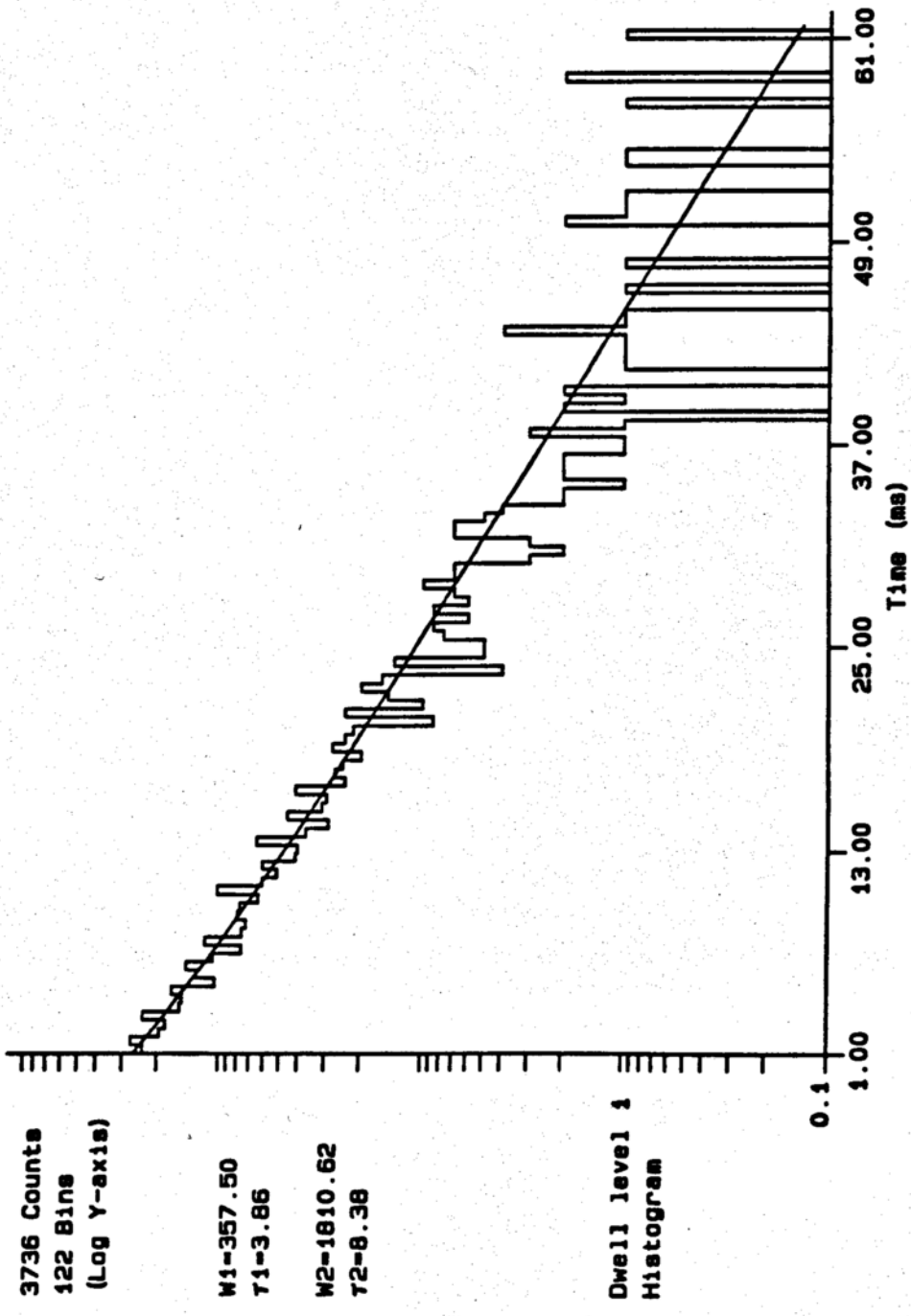

(c.3) Residual plot

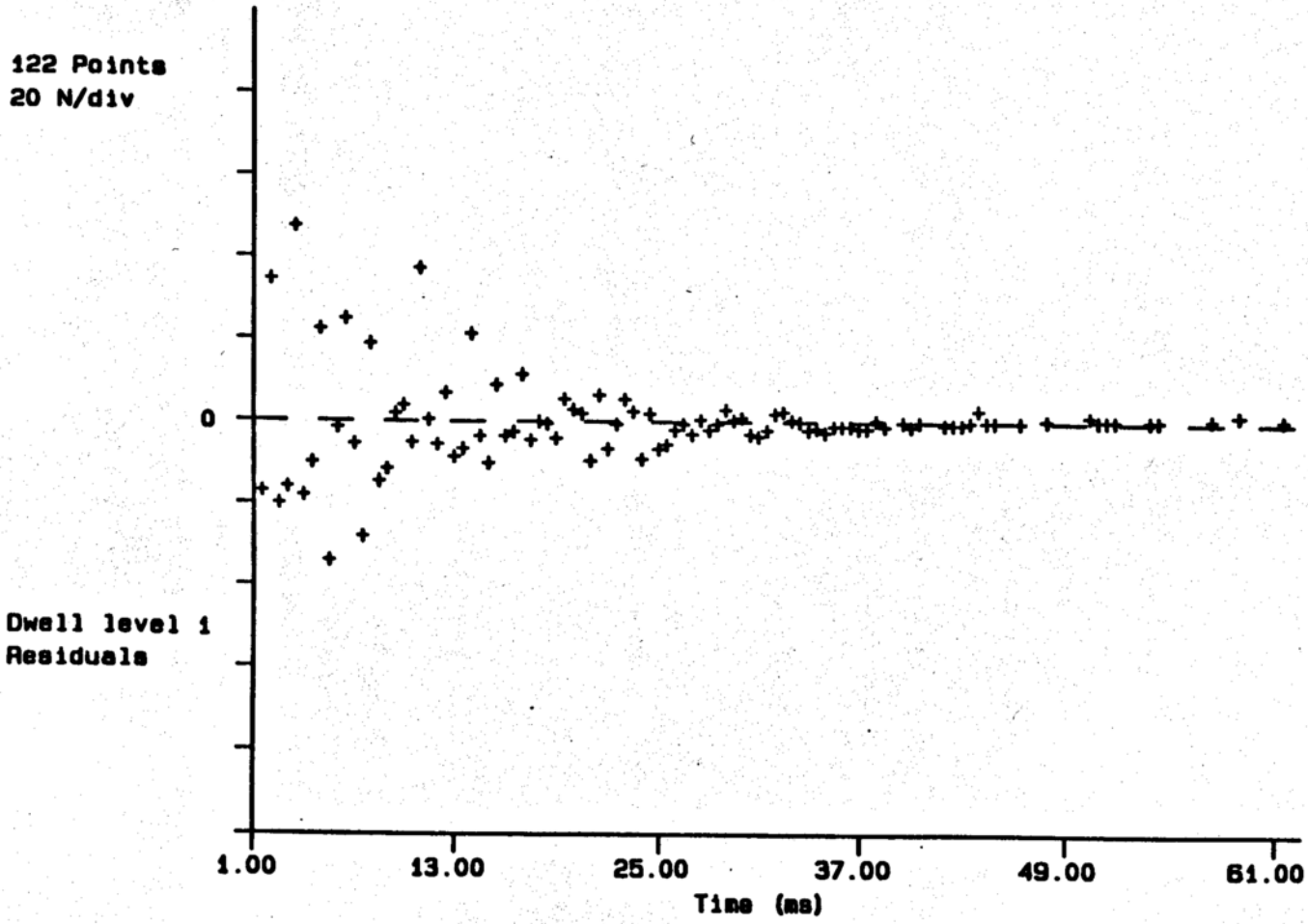

(c.4) Closed dwell time histogram and the fitted curve (normal scale)

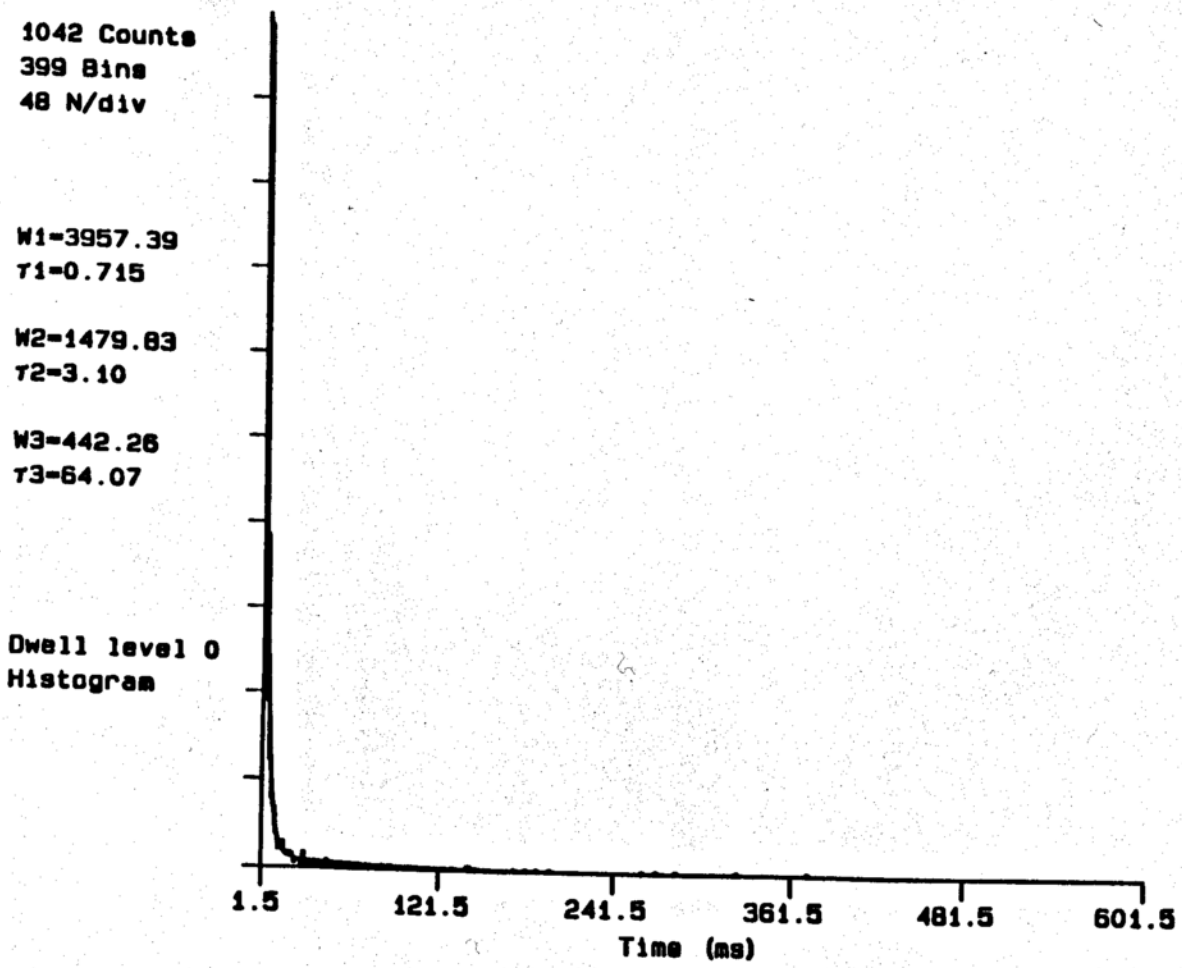

(c.5) Closed dwell time histogram and the fitted curve (log scale)

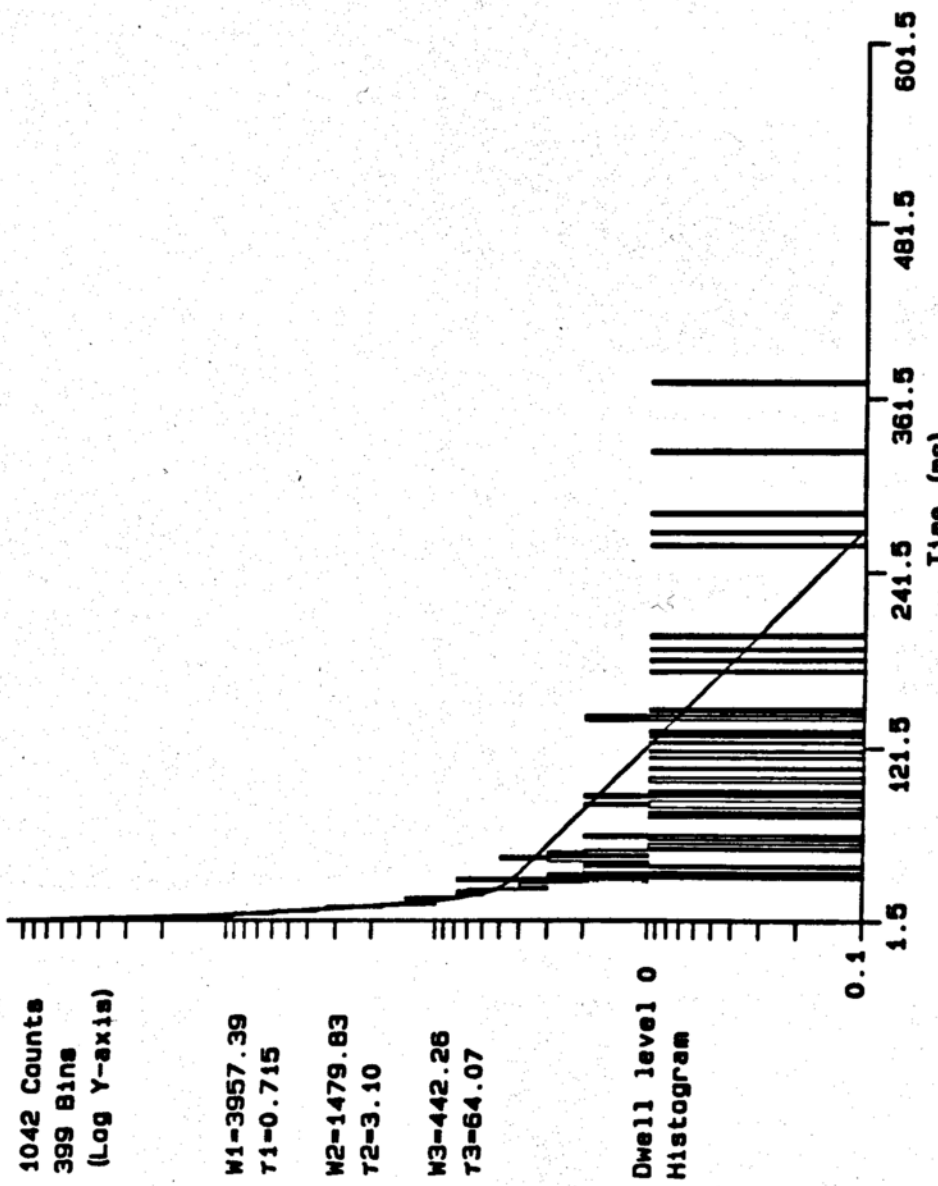

(c.6) Residual plot

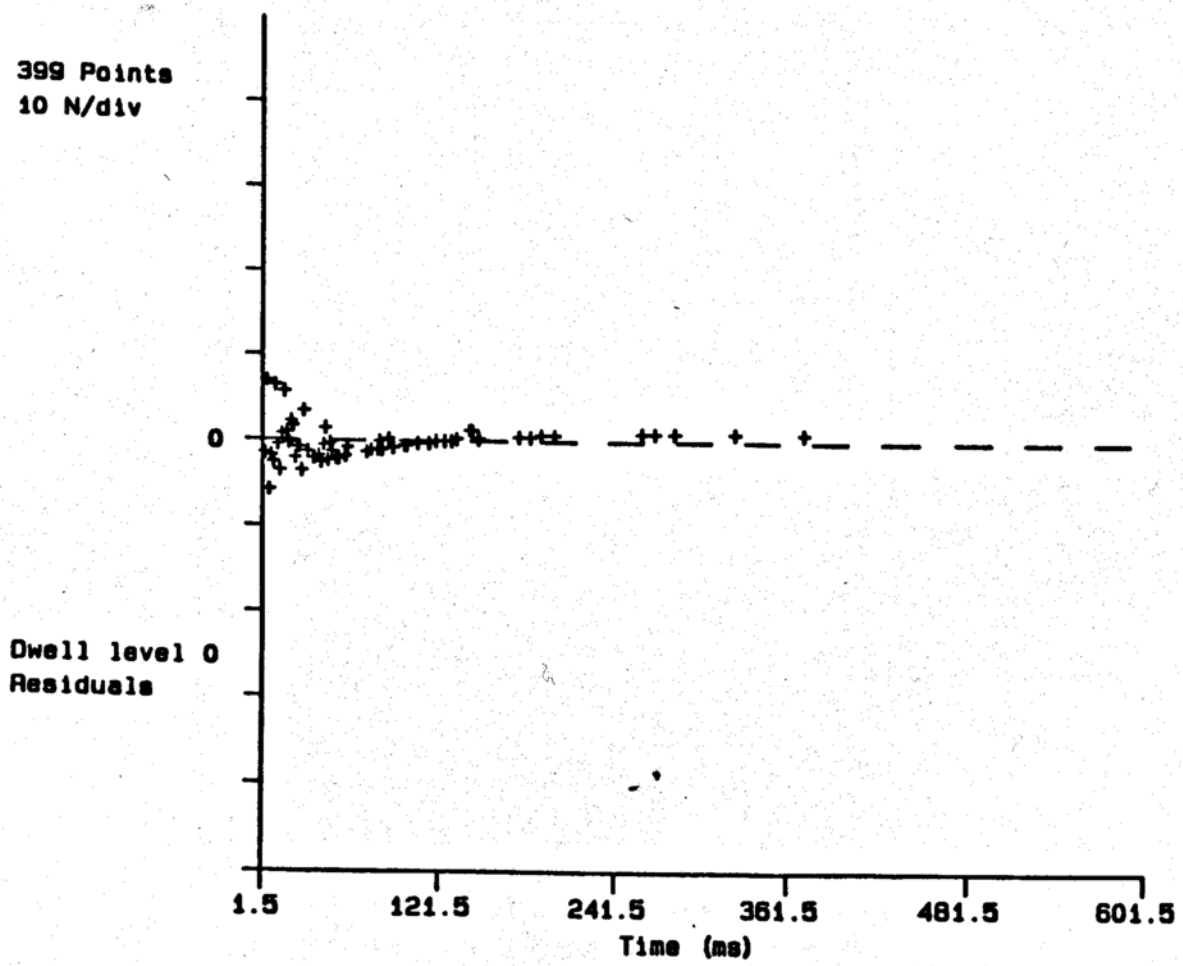

(d) At intracellular [ATP] = 2.55 mM, the probability density function (pdfs) of the open events and closed events are fitted to biexponential and triexponential expressions, respectively:

$$F(t), o = 0.372 \bullet \exp(-0.221 \bullet t) + 0.628 \bullet \exp(-0.113 \bullet t)$$

$$F(t), c = 0.8973 \bullet \exp(-1.5576 \bullet t) + 0.1012 \bullet \exp(-0.3968 \bullet t) + 0.0015 \bullet \exp(-0.0189 \bullet t)$$

(d.1) Open dwell time histogram and the fitted curve (normal scale)

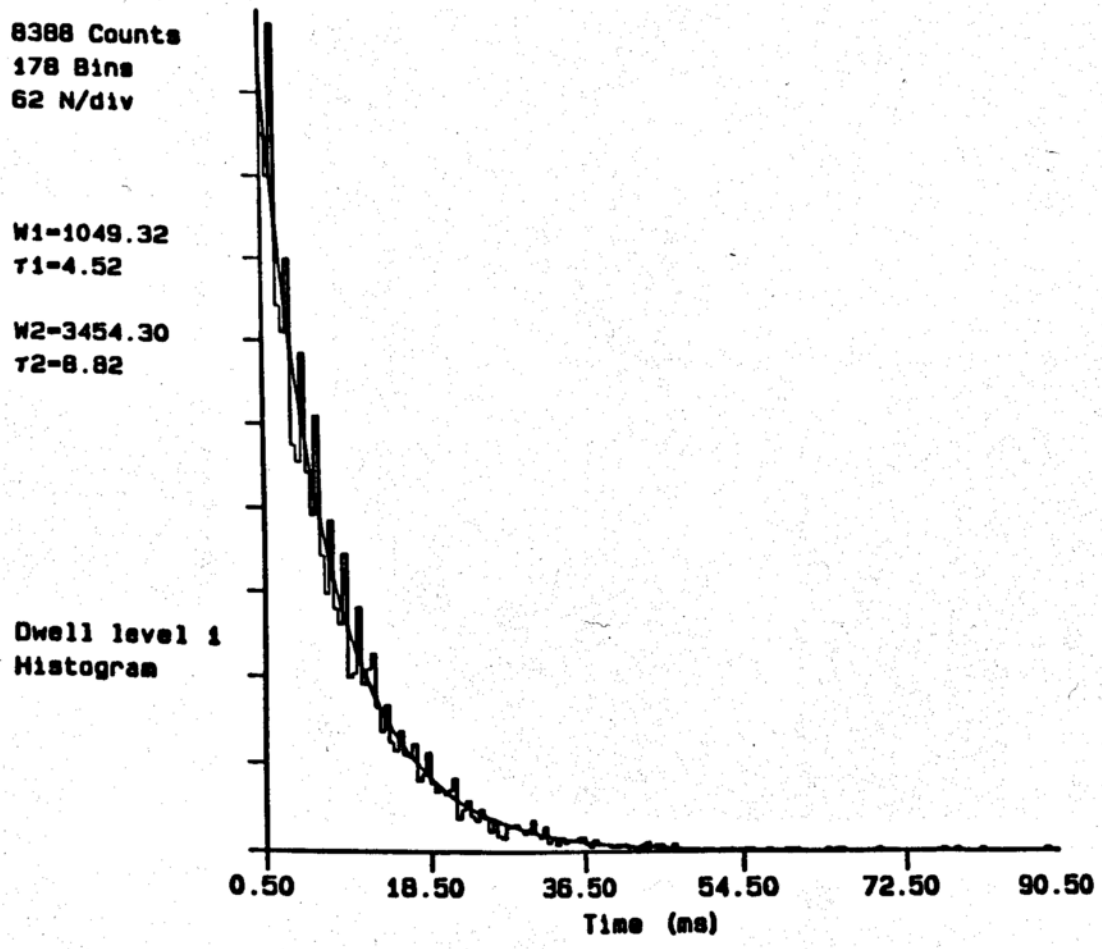

(d.2) Open dwell time histogram and the fitted curve (log scale)

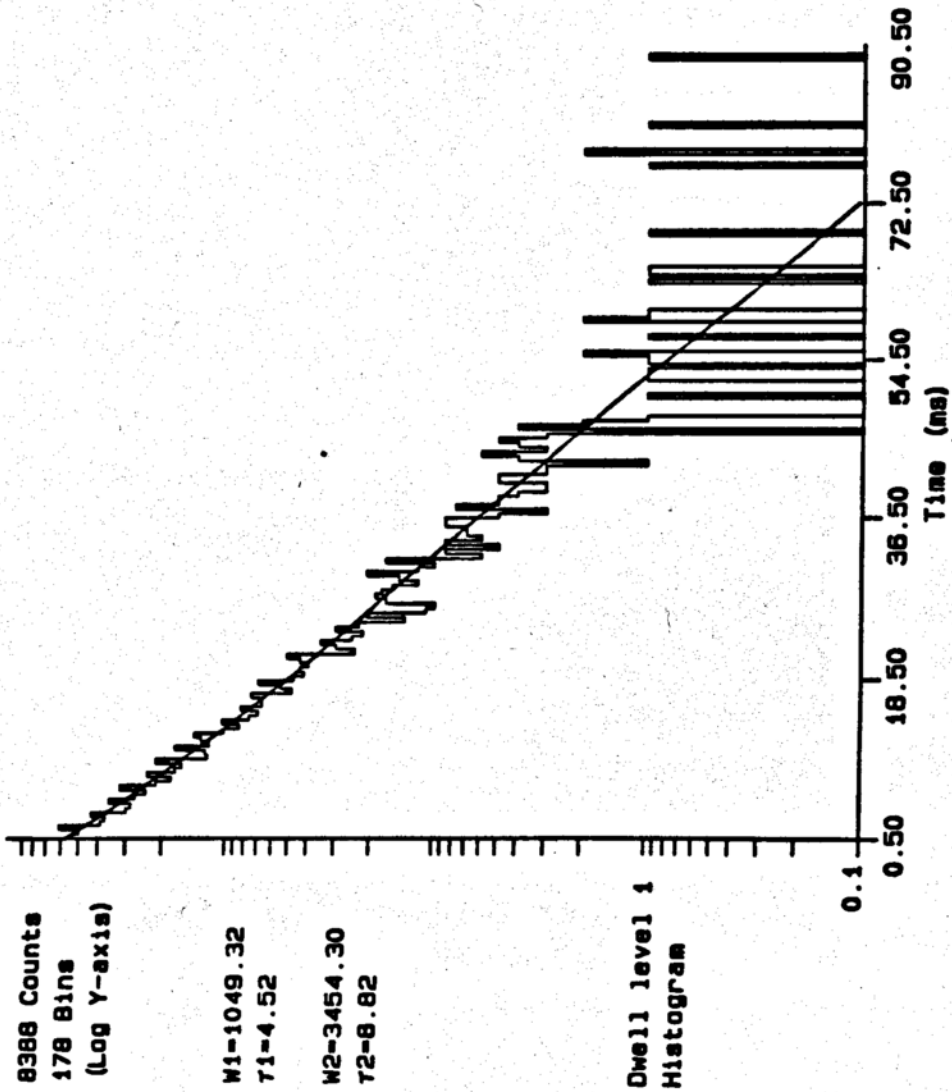

(d.3) Residual plot

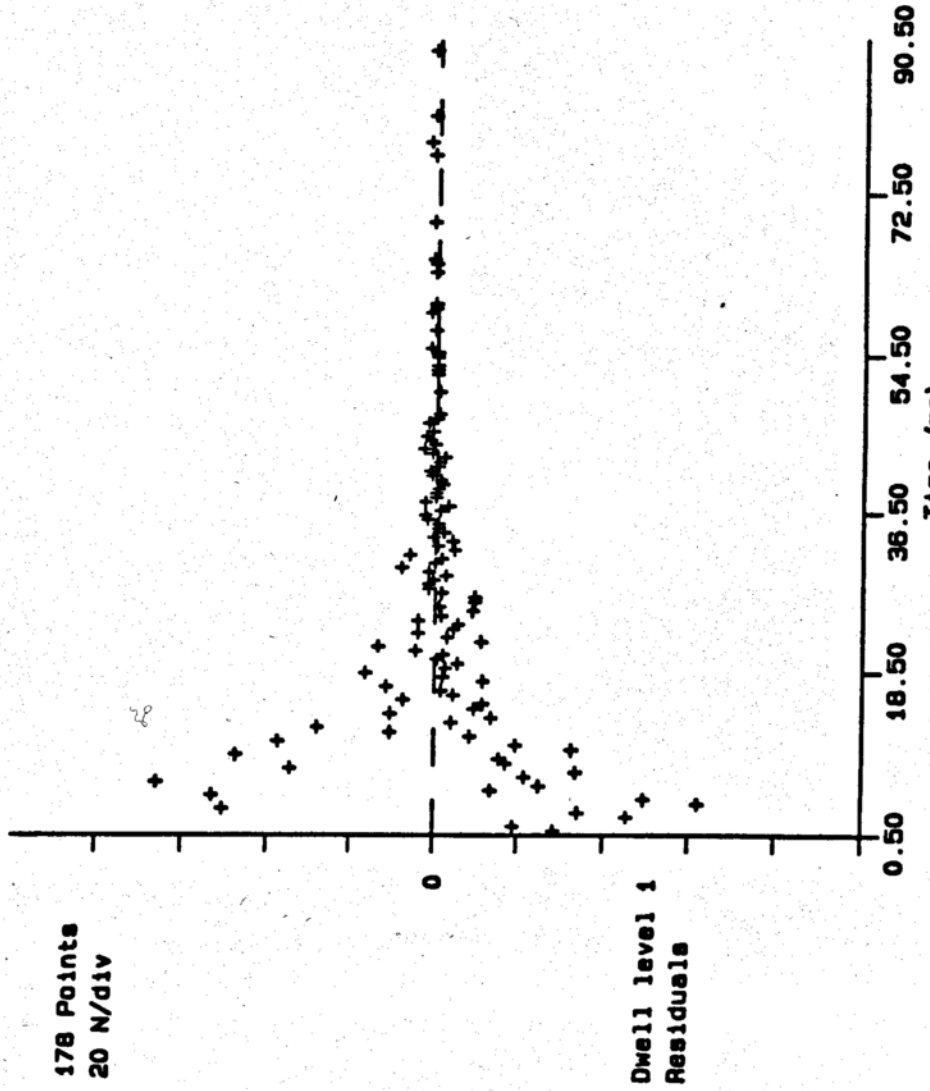

(d.4) Closed dwell time histogram and the fitted curve (normal scale)

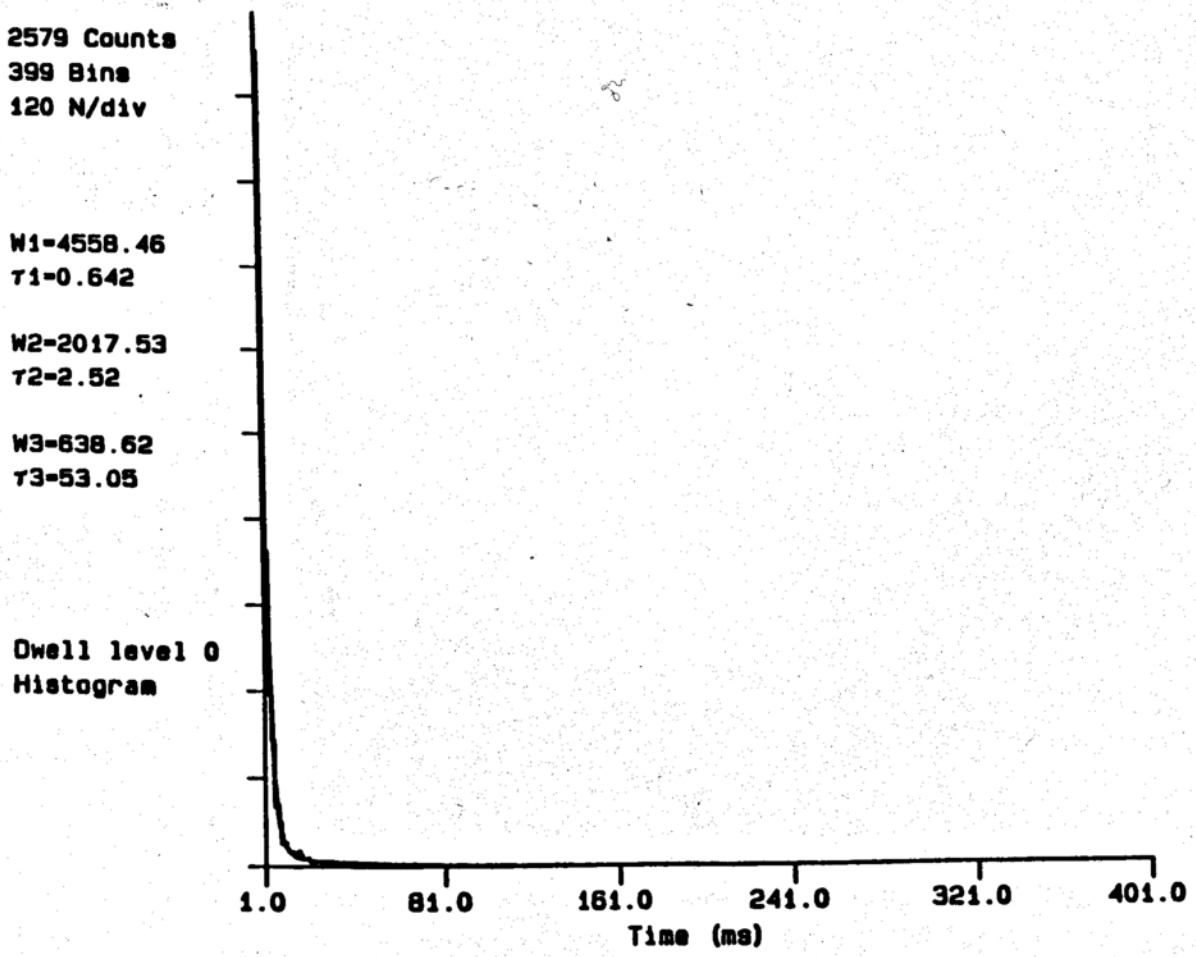

(d.5) Closed dwell time histogram and the fitted curve (log scale)

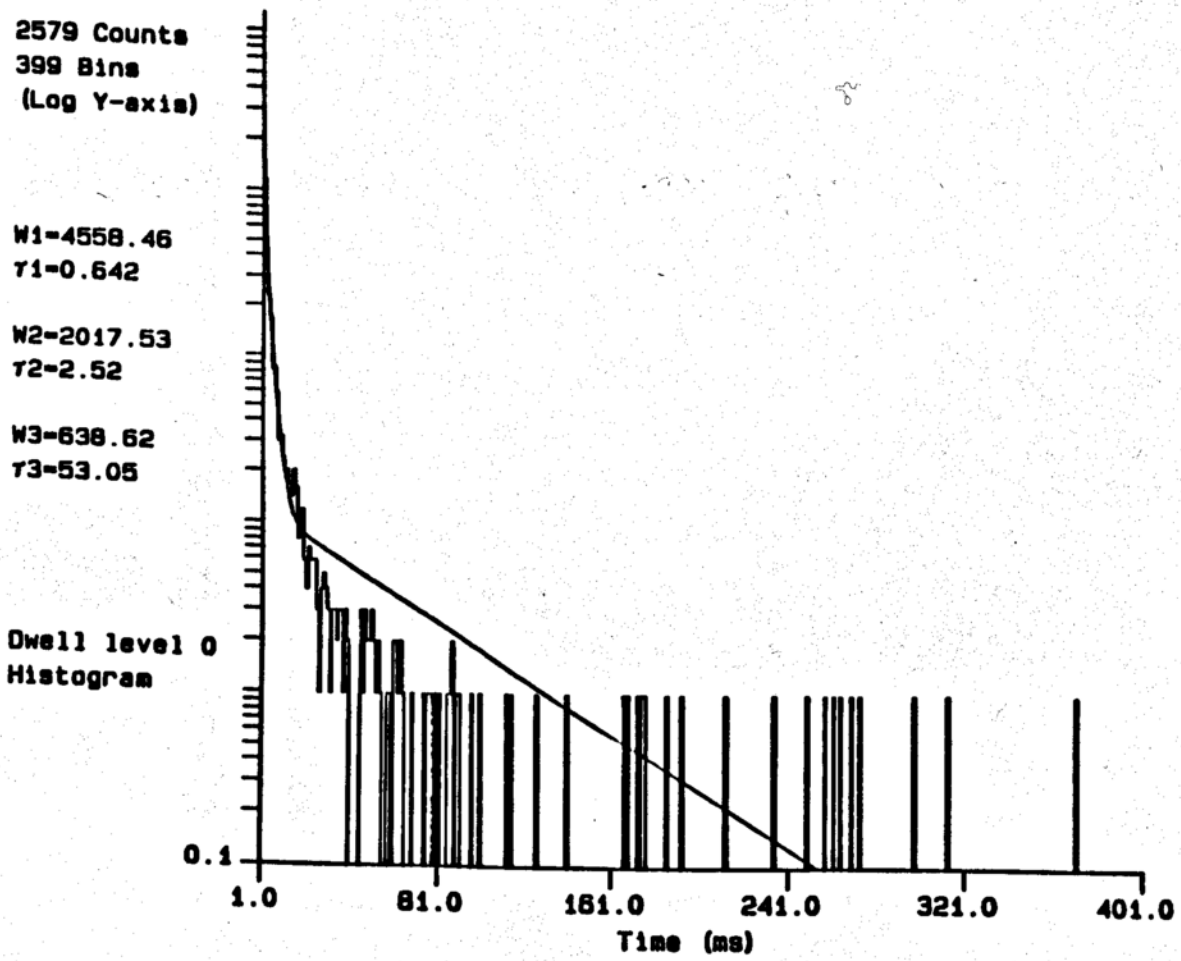

(d.6) Residual plot

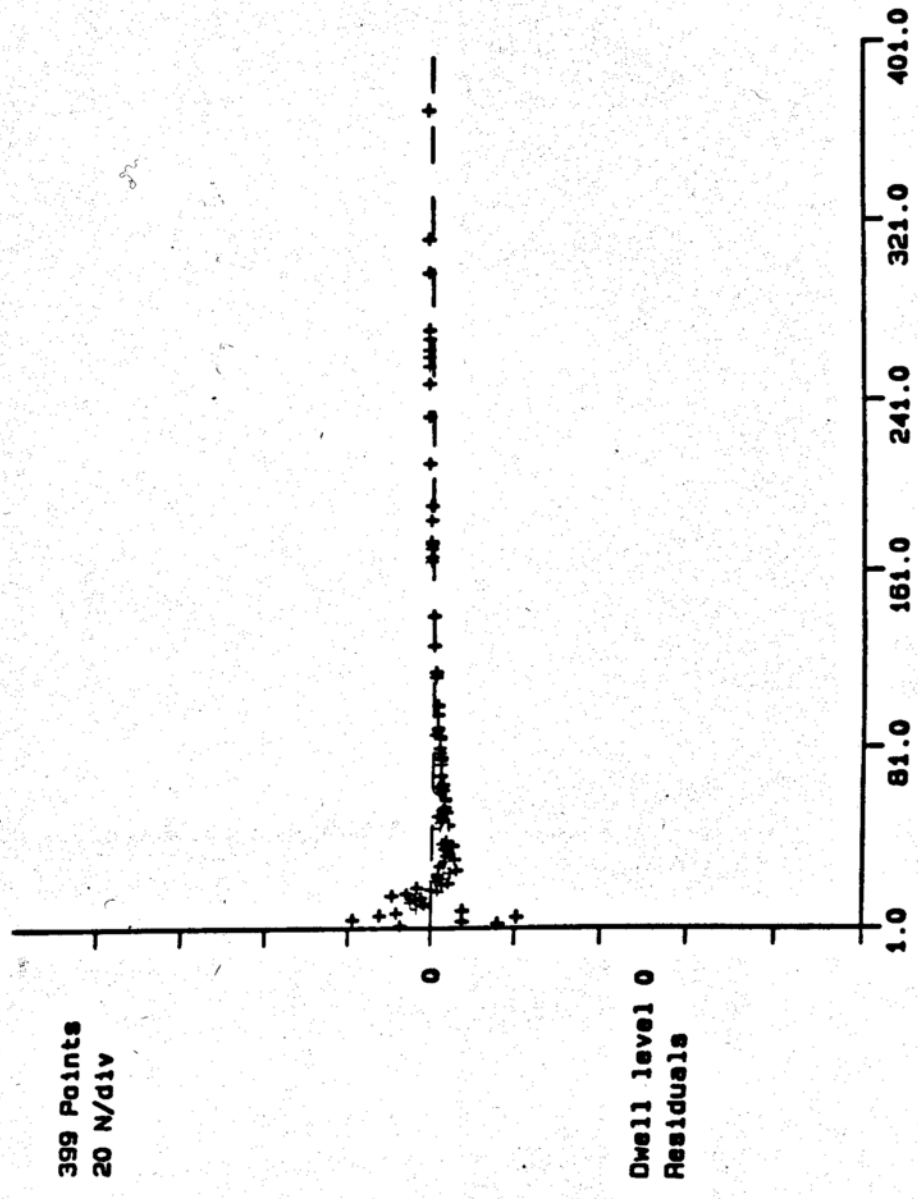

(e) At intracellular [ATP] = 5.09 mM, the probability density functions (pdfs) of the open events and closed events are fitted respectively to multiexponential expressions:

$$F(t), o = 0.874 \bullet \exp(-0.202 \bullet t) + 0.126 \bullet \exp(-0.071 \bullet t)$$

$$F(t), c = 0.9468 \bullet \exp(-2.0619 \bullet t) + 0.0472 \bullet \exp(-0.4329 \bullet t) + 0.0060 \bullet \exp(-0.1405 \bullet t)$$

(e.1) Open dwell time histogram and the fitted curve (normal scale)

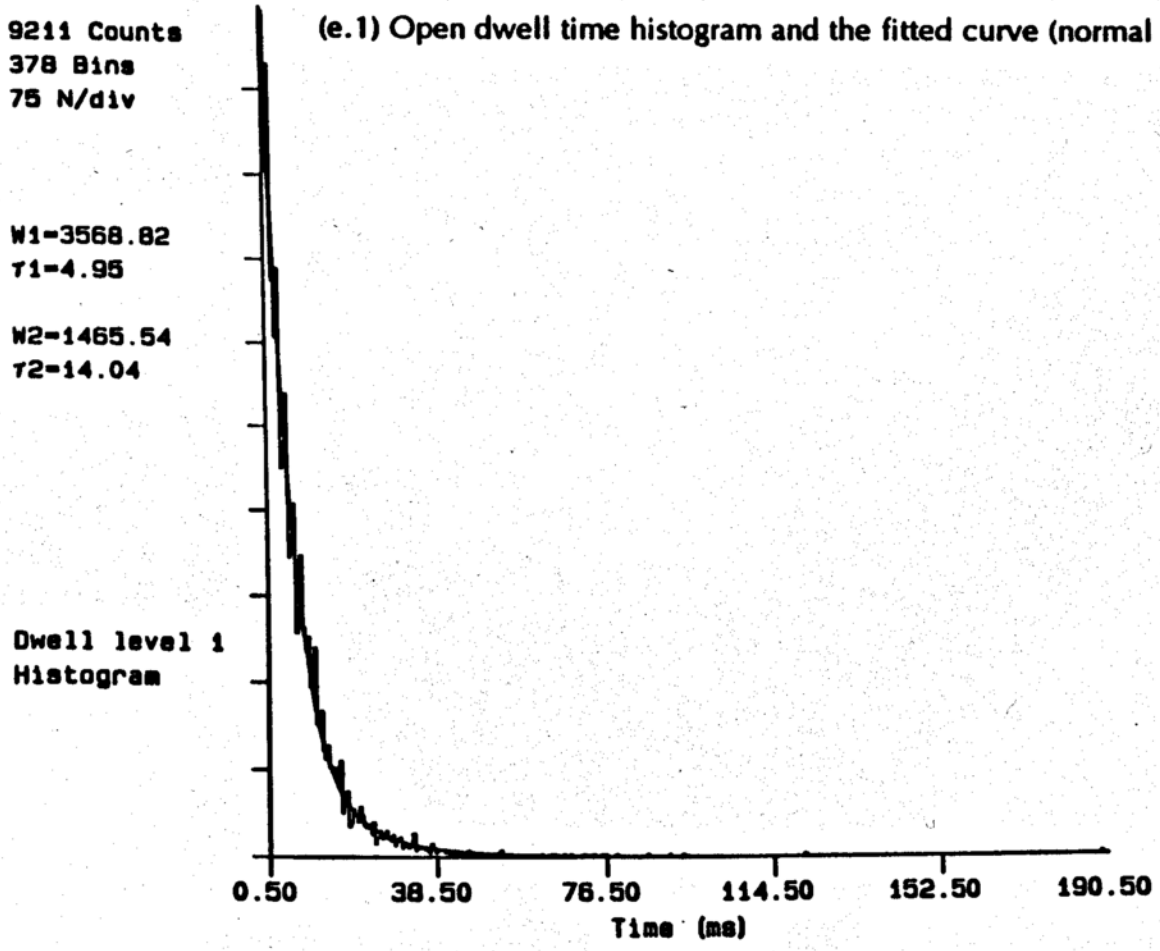

(e.2) Open dwell time histogram and the fitted curve (log scale)

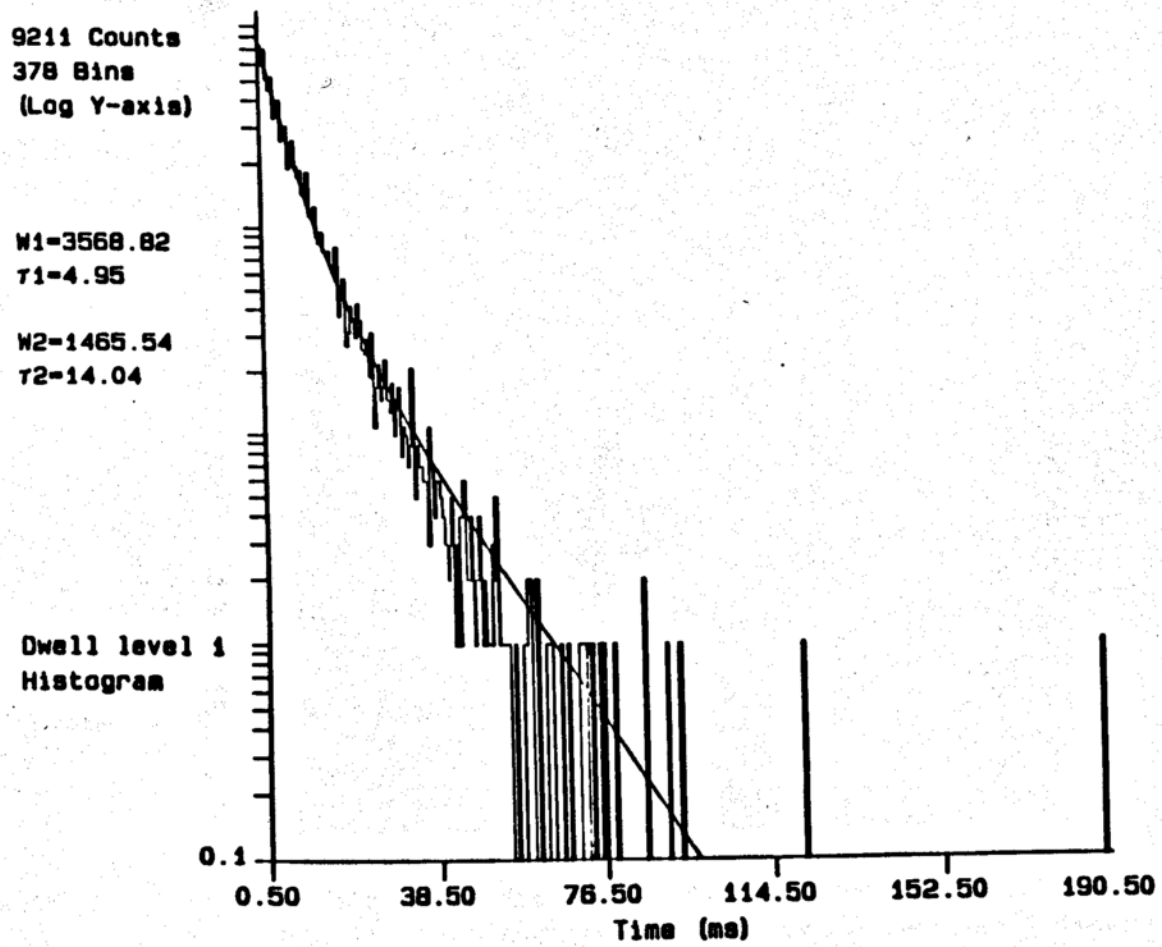

(e.3) Residual plot

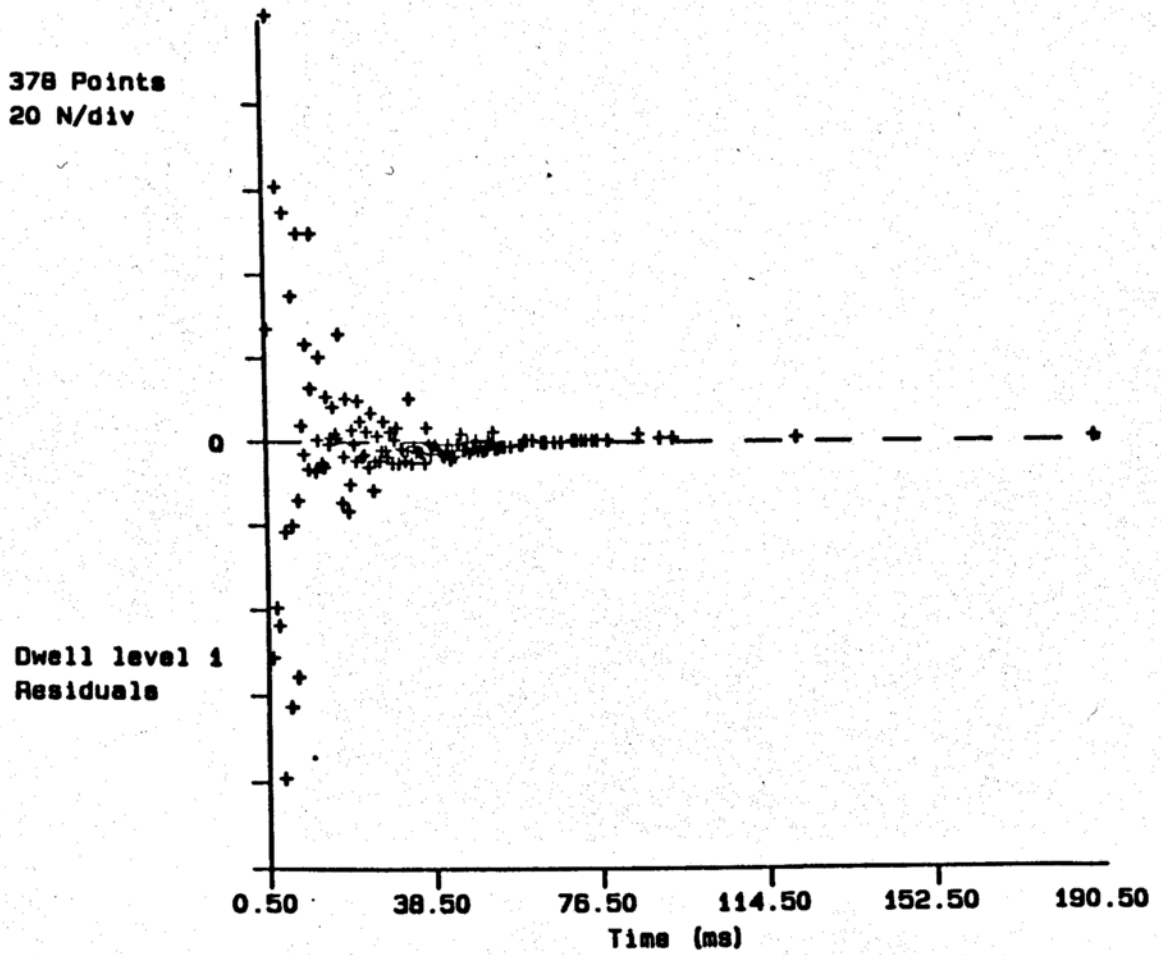

(e.4) Closed dwell time histogram and the fitted curve (normal scale)

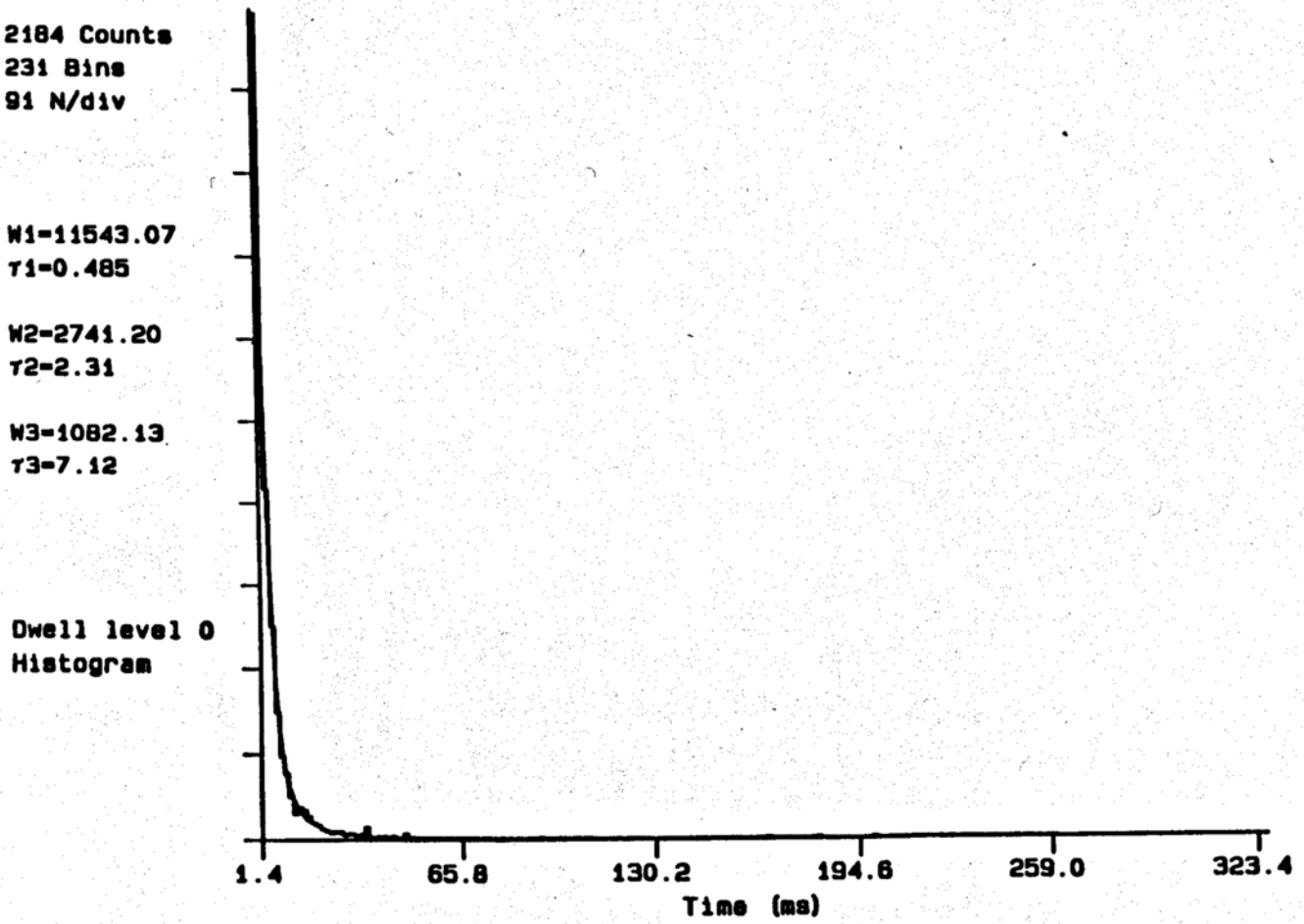

(e.5) Closed dwell time histogram and the fitted curve (log scale)

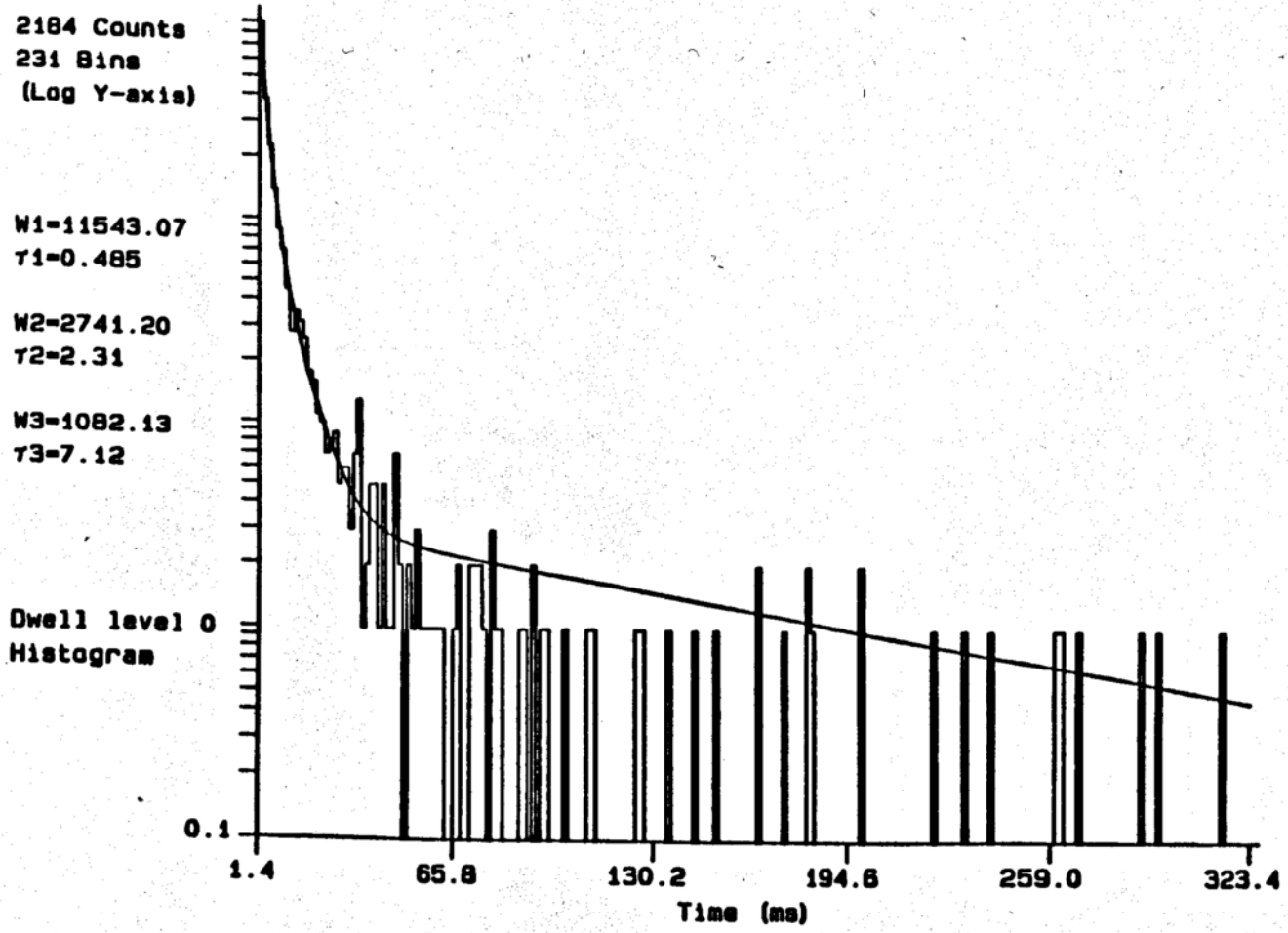

(e.6) Residual plot

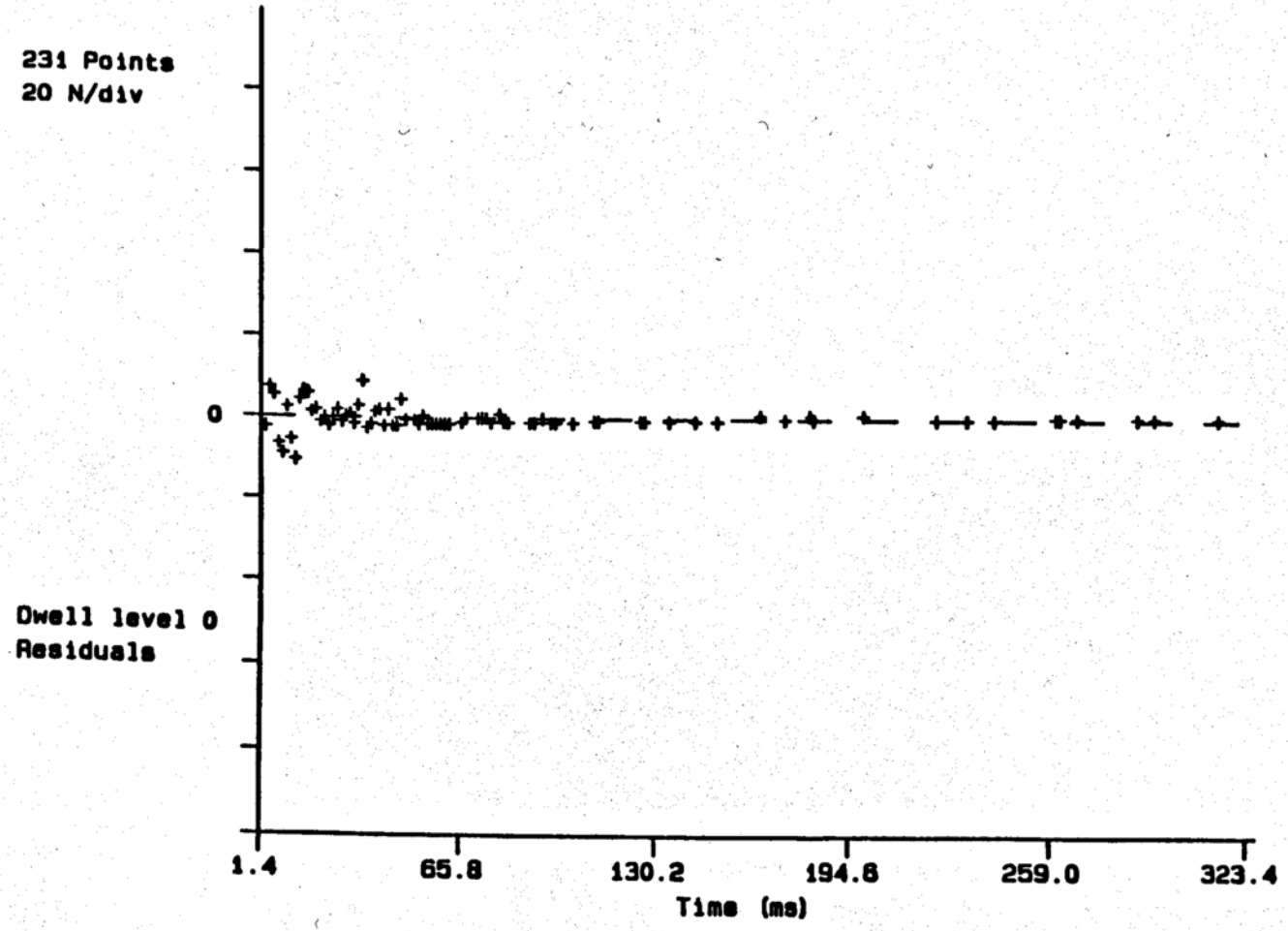

Figure 22 The arithmetic means for open and closed events at various concentrations of ATP.

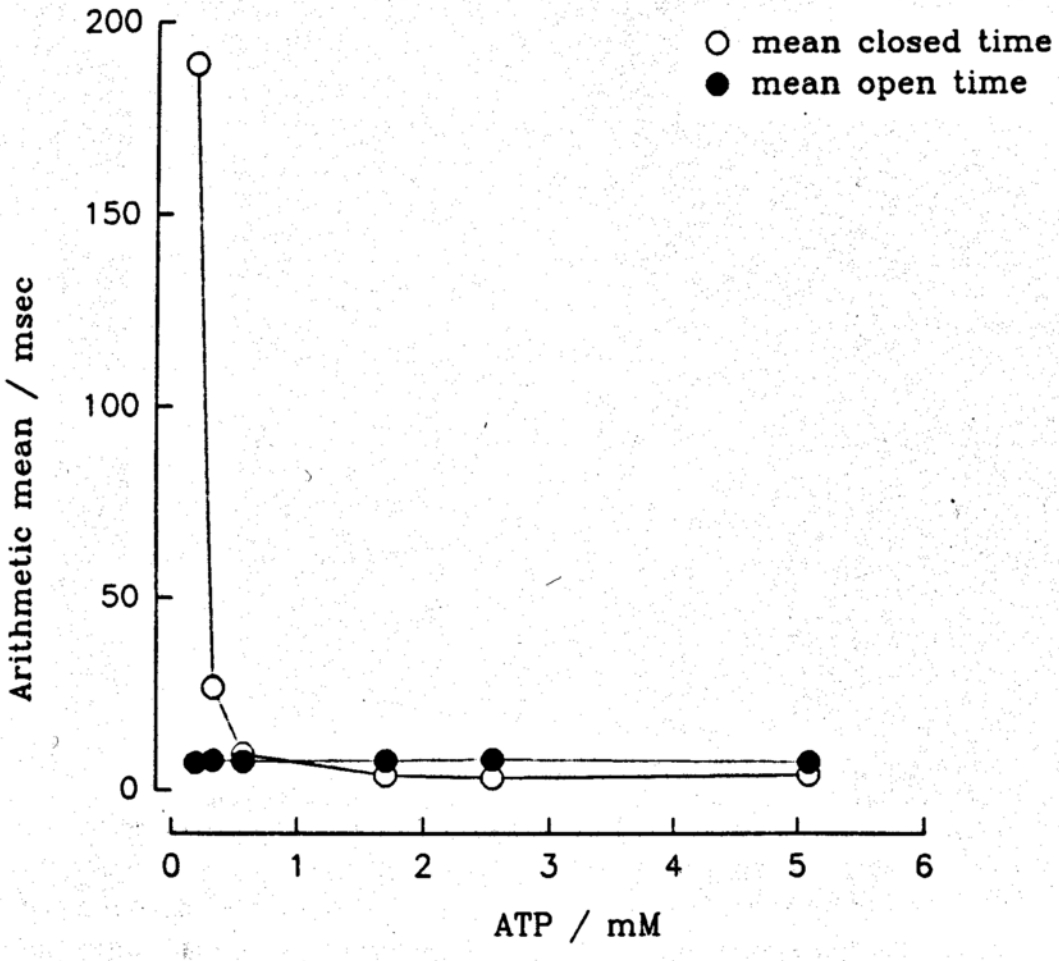

Figure 23 The mean dwell times of the two open states do not vary dramatically with the concentration of ATP.

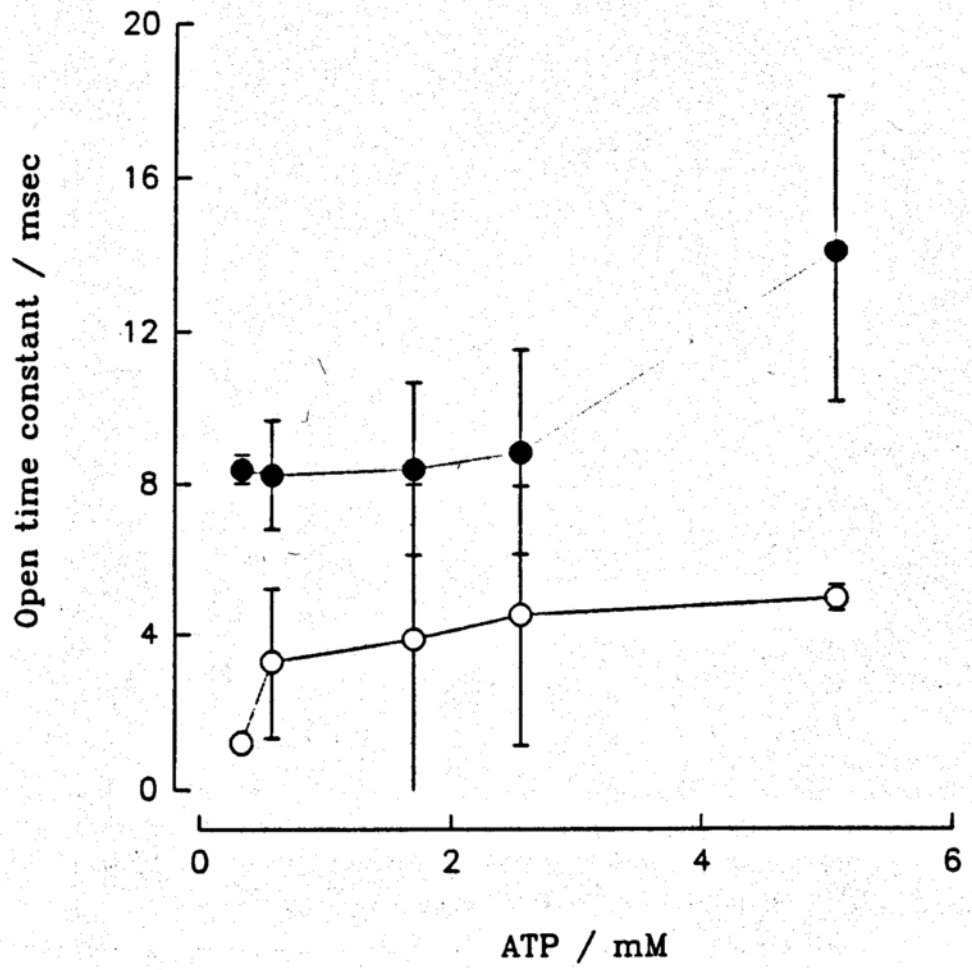

Figure 24 The mean dwell time for one closed state varies dramatically with the concentration of ATP.

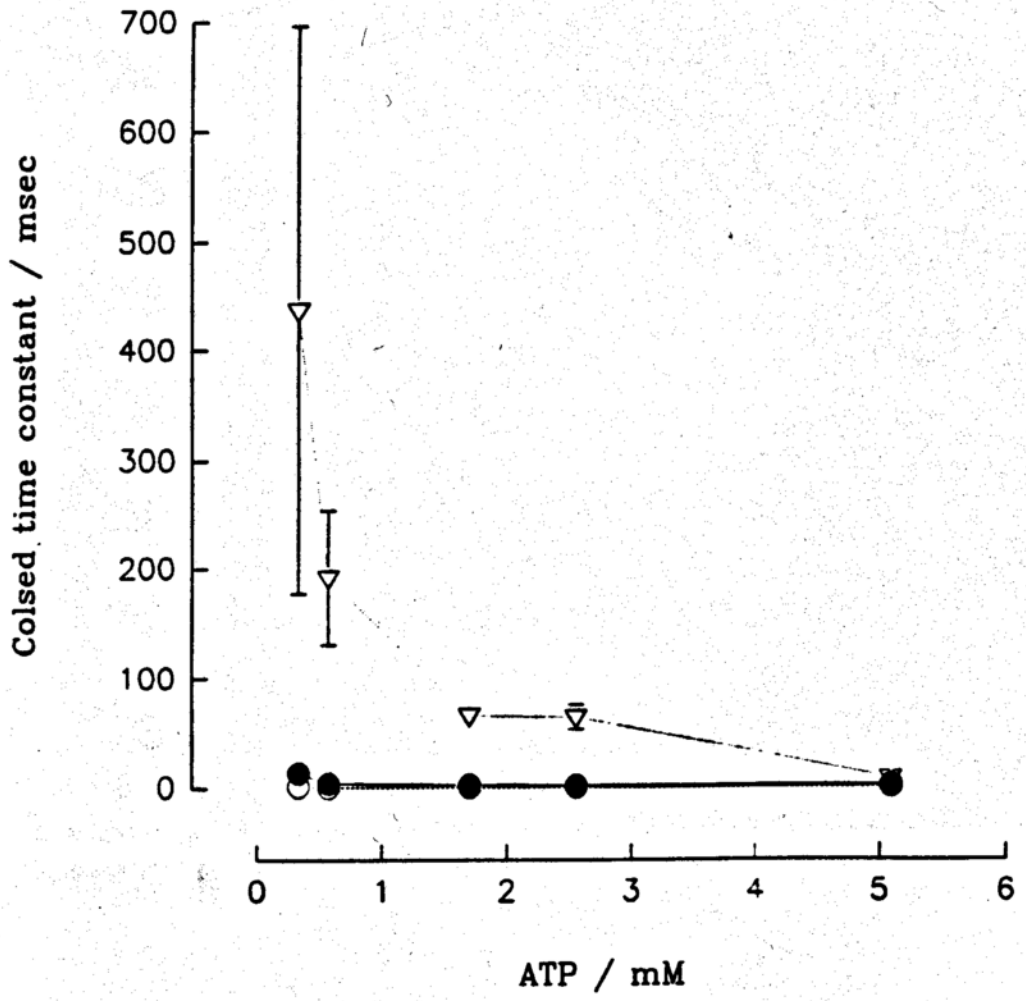

Figure 25 The mean dwell times for two of the closed states are proportional to the reciprocal of the square of the ATP concentration.

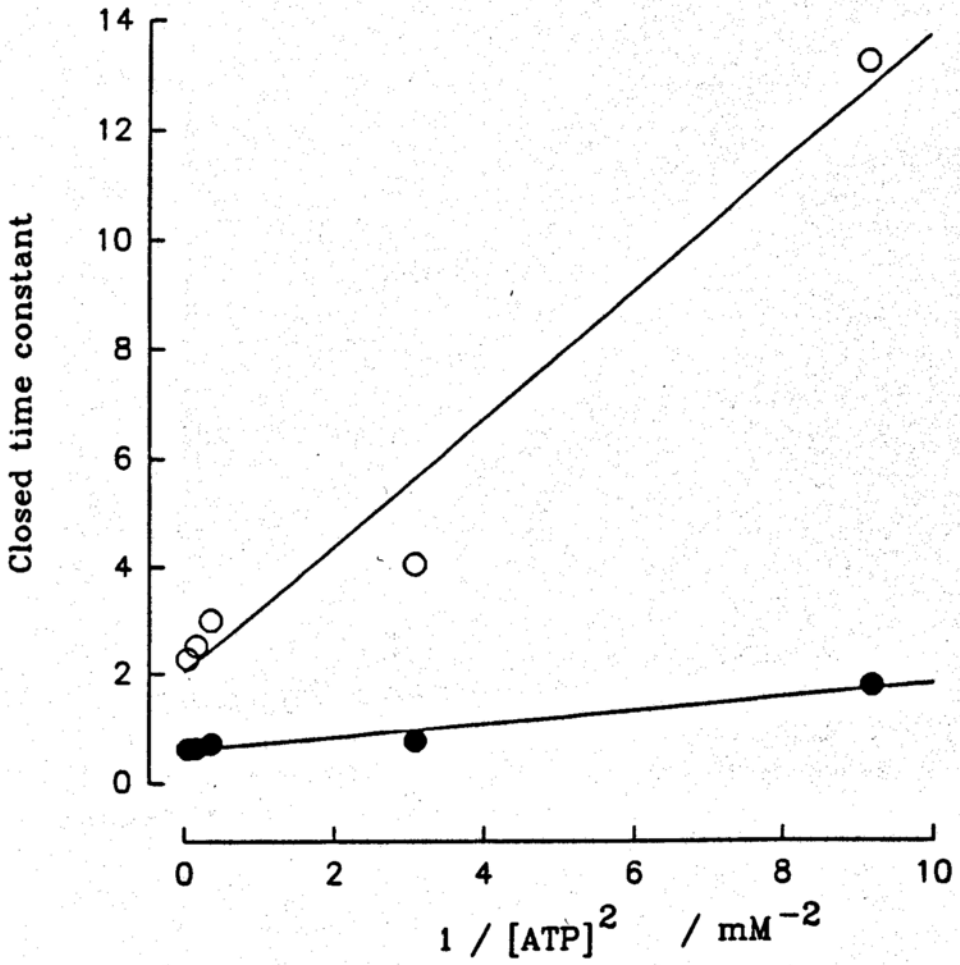

Figure 26 The longest mean dwell time of the three closed states is proportional to the reciprocal of the ATP concentration.

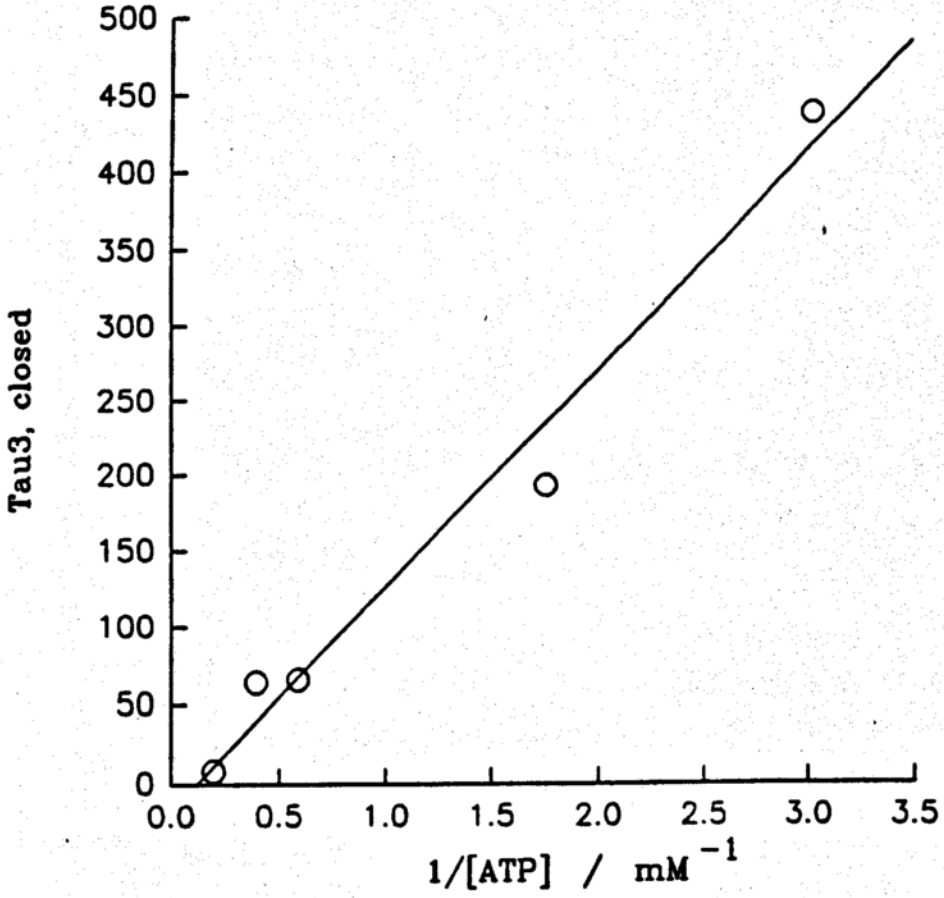

Figure 27 The pre-exponential factors of the three closed states do not vary dramatically with the concentration of ATP.

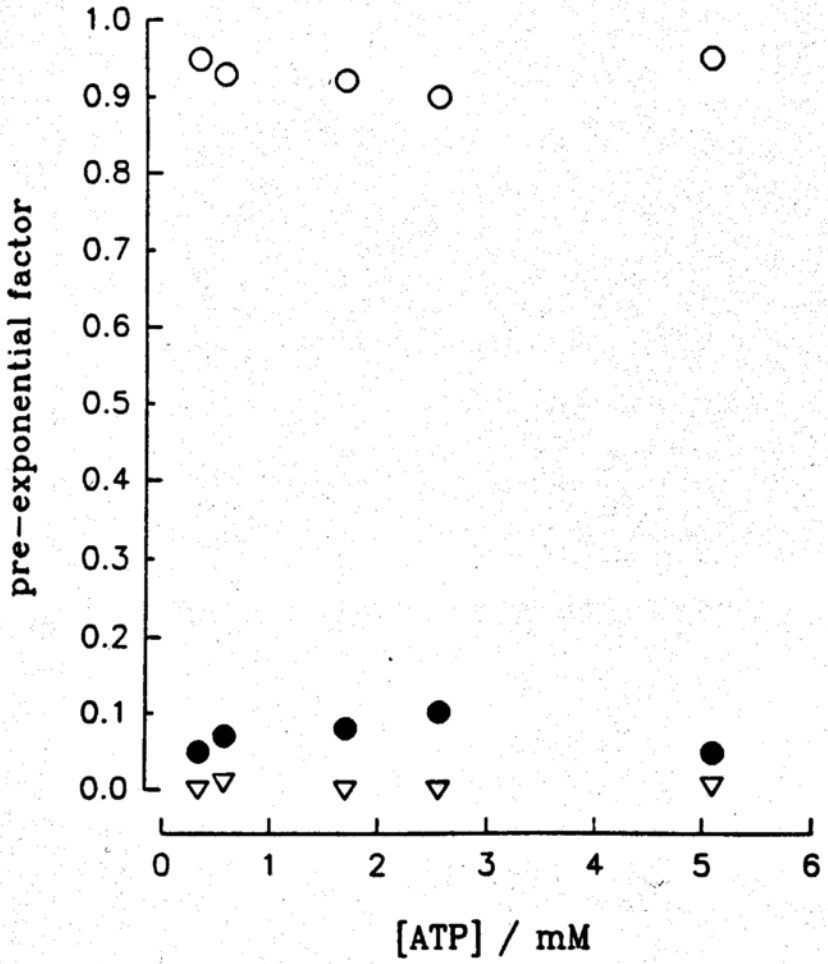

Figure 28 Calcium and ATP dependency of the 49 pS ATP-activated K_{Ca} channel

(a) Calcium dose-response curve for a typical ATP-activated K_{Ca} channel in the absence of ATP:

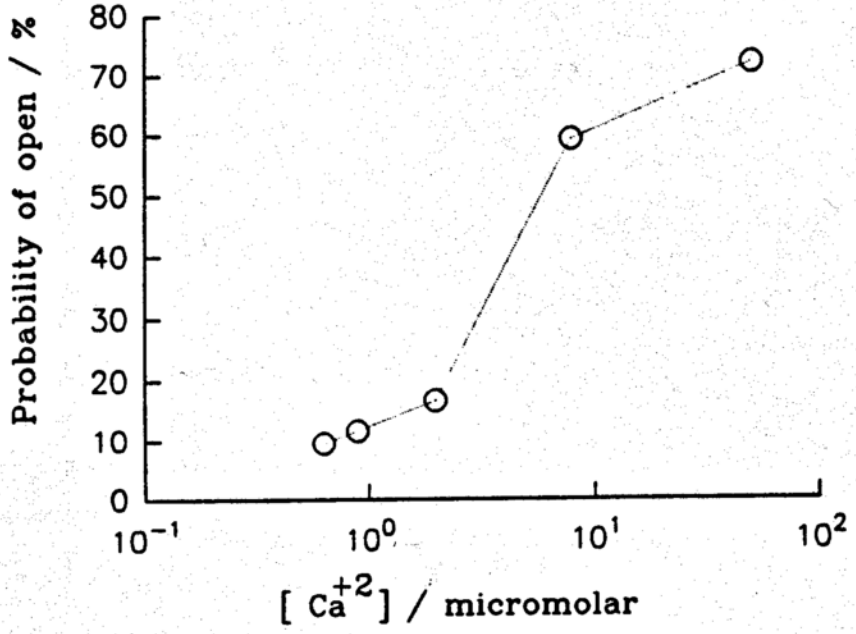

(b)This channel could be activated by ATP at low Ca^{+2} level (~ 130 nM)

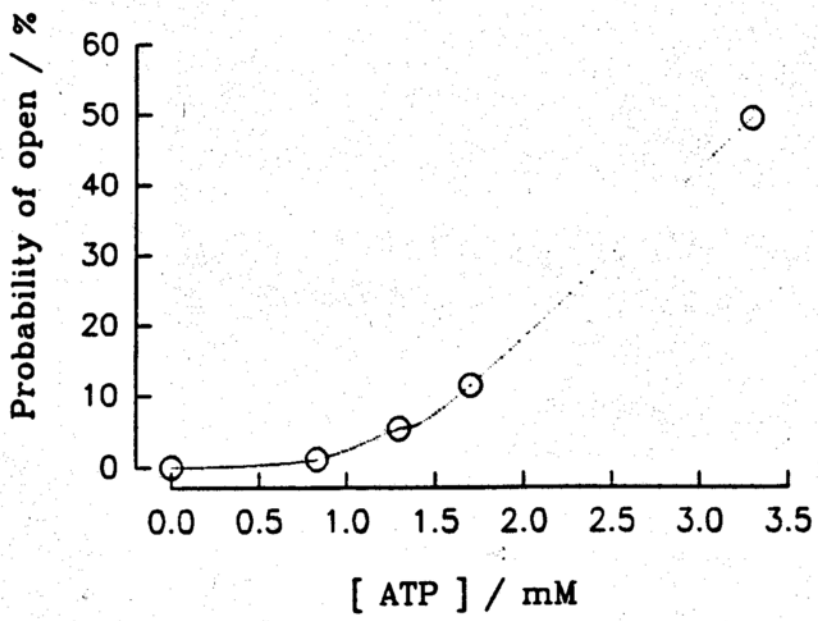

Figure 29 Calcium dose-response of the 49 pS ATP-activated K_{Ca} channel in the absence of ATP (obtained from three different patches)

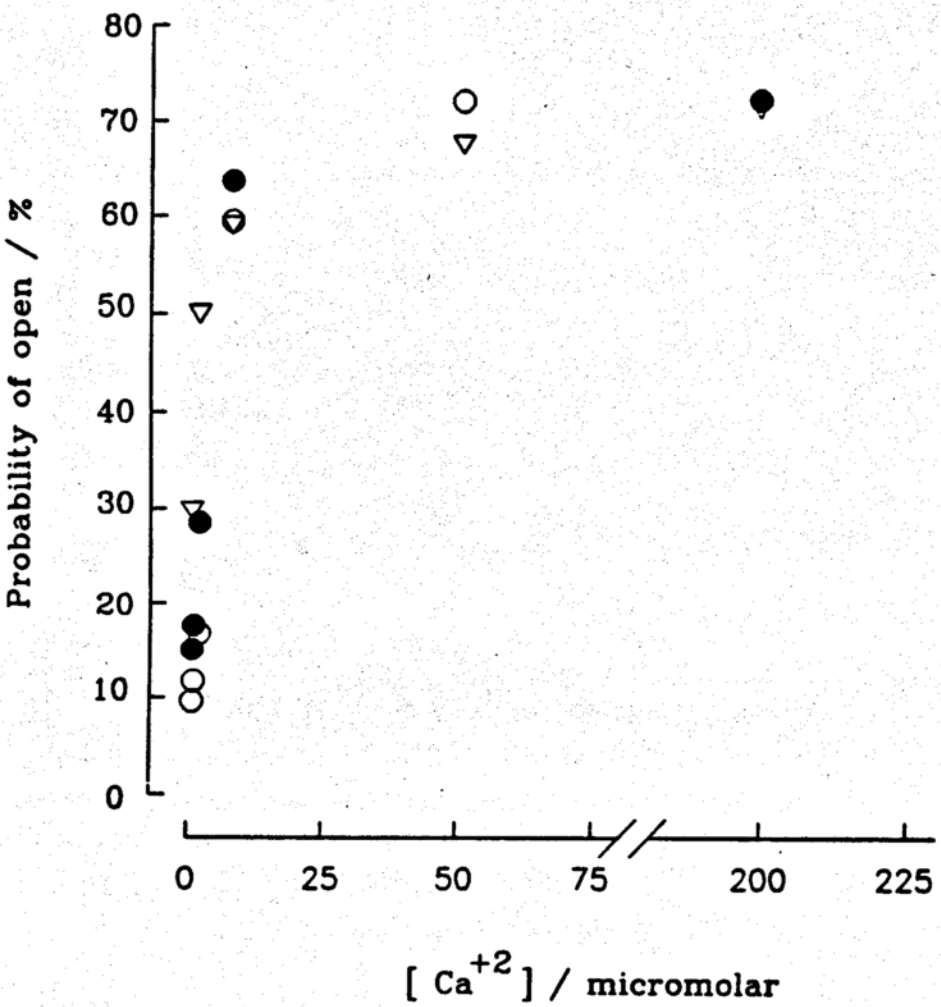

Figure 30 Hill plot of the dose-response of the 49 pS ATP-activated K_{Ca} channel
(The resulting slope is 0.5)

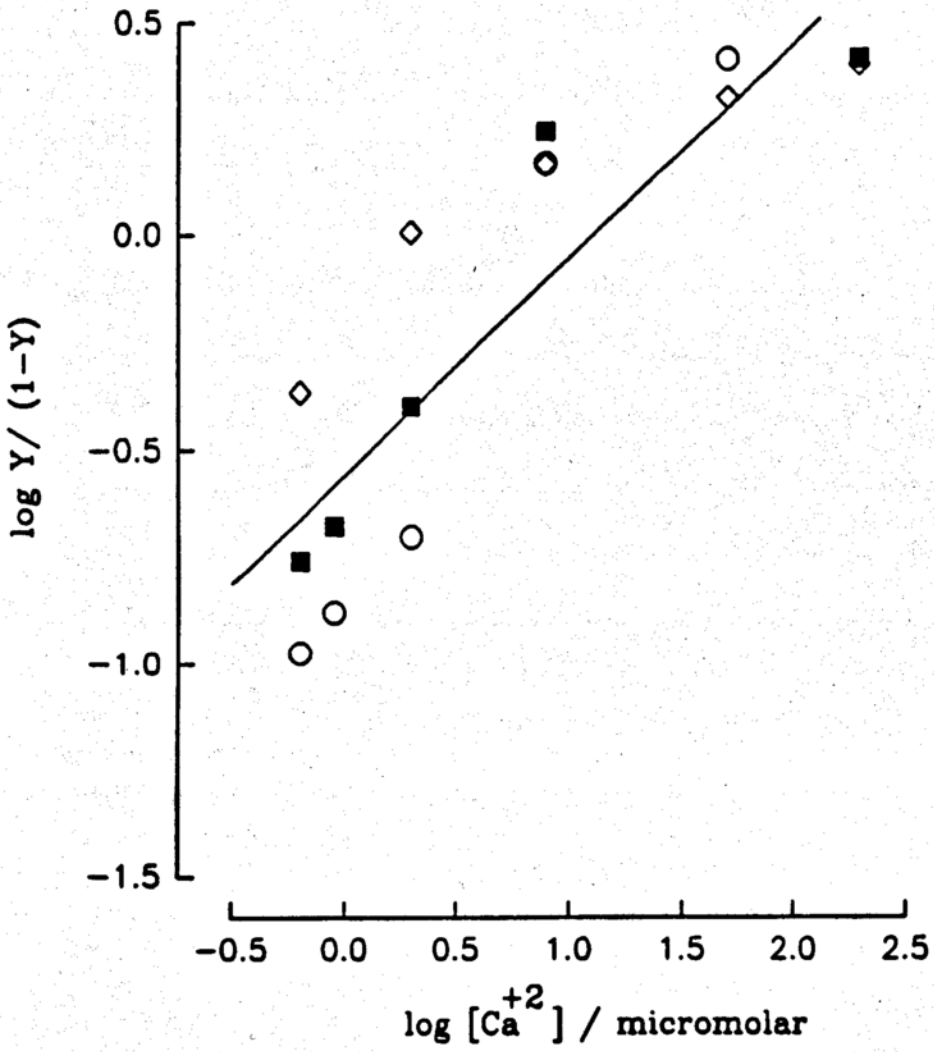

Table 1

Results of multiexponential data fitting of the open and closed dwell time histograms constructed based on the single channel current traces of a 49 pS ATP-activated K_{Ca} channel at five different intracellular ATP levels

(Also see Figure 21)

	[ATP]=0.33	[ATP]=0.57	[ATP]=1.7	[ATP]=2.55	[ATP]= 5.09
W1,o	239.66	405.03	357.50	1049.32	3568.82
W2,o	1644.57	2024.03	1810.62	3454.30	1464.54
W1,c	1917.92	3656.25	3957.39	4558.46	11543.07
W2,c	747.95	1422.89	1479.83	2017.53	2741.20
W3,c	801.83	748.24	422.26	638.62	1082.13
τ1,o	1.18	3.26	3.86	4.52	4.95
τ2,o	8.39	8.23	8.38	8.82	14.04
τ1,c	1.75	0.811	0.715	0.642	0.485
τ2,c	13.13	4.18	3.10	2.52	2.31
τ3,c	437.99	135.89	64.07	53.05	7.12

C. The 240pS ATP-activated channel

A K_{Ca} channel (Figure 52) with a large conductance (240 ps) also exhibited sensitivity to intracellular ATP (Figures 31, 32), the effects of which on channel opening were reversible (Figures 35). An intracellular ATP level of ~ 2 mM increased the probability of channel opening from a few percent to more than 90 % at membrane depolarization voltages (Figure 37). This channel was found to be highly selective to potassium ions (Figures 34 and 36): the potassium to sodium selectivity ratio calculated using the Goldman-Hodgkin-Katz equation is ~ 20 (Figure 33, 34).

This channel showed voltage sensitivity as well. As indicated in Figure 39, a shift of ~ -90 mV was observed in the dependence of channel opening on membrane voltage when the intracellular ATP concentration was increased from 0.5 mM to 4 mM. This shift appeared to be independent of the channel's gating charge since the charge factor ($Z\delta$), calculated based on the Boltzmann equation, remained constant ($Z\delta$ = -2.54) (Figure 40). This shift in voltage sensitivity of channel opening was presumably brought about by ATP binding (this will be discussed in the next paragraph). The increase in ATP concentration from 0.5 mM to 4 mM caused a binding difference to this channel that eventually led to a reduction, in the potential energy difference between the channel's initial open and its final closed states, by approximately 5 kCal (estimated using the Boltzmann equation:

$$\ln\left[\frac{Y}{1-Y}\right] = -\frac{Z\delta F}{RT}\,(V - V_0),$$

where Y is normalized channel response, F and RT have their usual meanings, and V is membrane voltage).

We found that the mechanism of ATP activation of this channel involves mediation via direct binding. The evidence for this is similar to that reported earlier for the 49 pS ATP-activated K_{Ca} channel. First, intracellular ADP or AMP at a

concentration of ~ 1-4 mM caused channel opening to increase (Figures 41, 42, and 45). As in the case of ATP, their effects were reversible. As mentioned earlier, since neither ADP nor AMP could serve as phosphate donors for protein phosphorylation, they could only activate the channel through direct binding. Second, hydrolysis of ATP was not required for activation. In the absence of intracellular Mg^{+2}, channel activity still increased with the concentration of sodium ATP on the intracellular side of the channel (Figure 44). In addition, a non-hydrolyzable ATP analog, AMP-PCP, at a concentration of ~ 2mM, had positive effects on channel opening (Figure 43). The Hill plot indicated that the channel's ATP sensitivity was the result of binding of at least 4 ATP molecules to the channel (Figure 38).

We analyzed the effects of ATP on the kinetics of channel gating using both burst analysis and regular kinetic data analysis. We used burst analysis because the channel exhibited substantial flickering once open (with a mean flickering opening duration of less than 2 ms), and the flickering appeared to be independent of ATP concentration; also, we felt that burst analysis might clarify the effects of ATP on channel opening since it appeared that ATP led to increased burst durations (Figure 32). In burst analysis, since brief events were relatively independent of ATP concentration, we ignored closed events with durations shorter than 1810 ms. (Note, 1810 ms was chosen based on the results obtained from the regular kinetic data analysis method discussed in the next paragraph. This method revealed that the smallest closed time constant for the closed state having the longest life time is about 2 ms.) This setting allowed closed events lasting longer than 1810 ms to be regarded as interburst gaps, and those shorter than 1810 ms to be ignored. We found that after limiting the closed events this way for analysis, the resultant mean burst duration increased linearly with the concentration of intracellular ATP (Figure 46), just as we

had speculated earlier. This burst analysis also revealed the ATP concentration dependency of the mean interburst gap; it increases with the reciprocal of the concentration of ATP (Figures 47, and 48).

When closed events were analyzed with no restriction imposed on their duration, as in regular kinetic data analysis, single channel data analysis revealed that this channel has three distinct closed states as well as three distinct open states. This method of data analysis, however, was expected not to provide very accurate estimates for the time constants associated with states having relatively long resident times since all dwell time histograms were dominated by events occurring within bursts due to the high degree of flickering associated with this channel's opening (Figure 31). In spite of this, useful information on channel kinetics was still obtained. This method of analysis indicated that the duration of flickery open was slightly dependent on ATP concentration; ATP increased the mean duration of flickery open at low ATP levels from ~0.7 - ~1.4 ms, but this short open duration began to decrease as ATP concentration continued to increase, from ~1.4 - ~0.6 ms (Figure 50). We compared the magnitudes of the three relevant closed time constants obtained from this method of data analysis to that of the one closed time constant obtained from the previously mentioned burst analysis, and rationalized that two of these closed states were associated with this channel's flickery closing during bursts and the other one closed state, with the interburst closed state revealed by burst analysis. This is because the mean dwell time for the longest closed state obtained appears to correspond well to the interburst closed state obtained using the mentioned burst analysis method; this mean closed time decreases with ATP concentration (Figure 51) (the time constant increase with the reciprocal of ATP concentration). This is the same kind of dependency seen for the interburst closed state revealed by burst analysis (Figure 48).

Figure 31 Single channel current traces and conductance plot for the 240 pS ATP-activated potassium channel

(a) Conductance plot

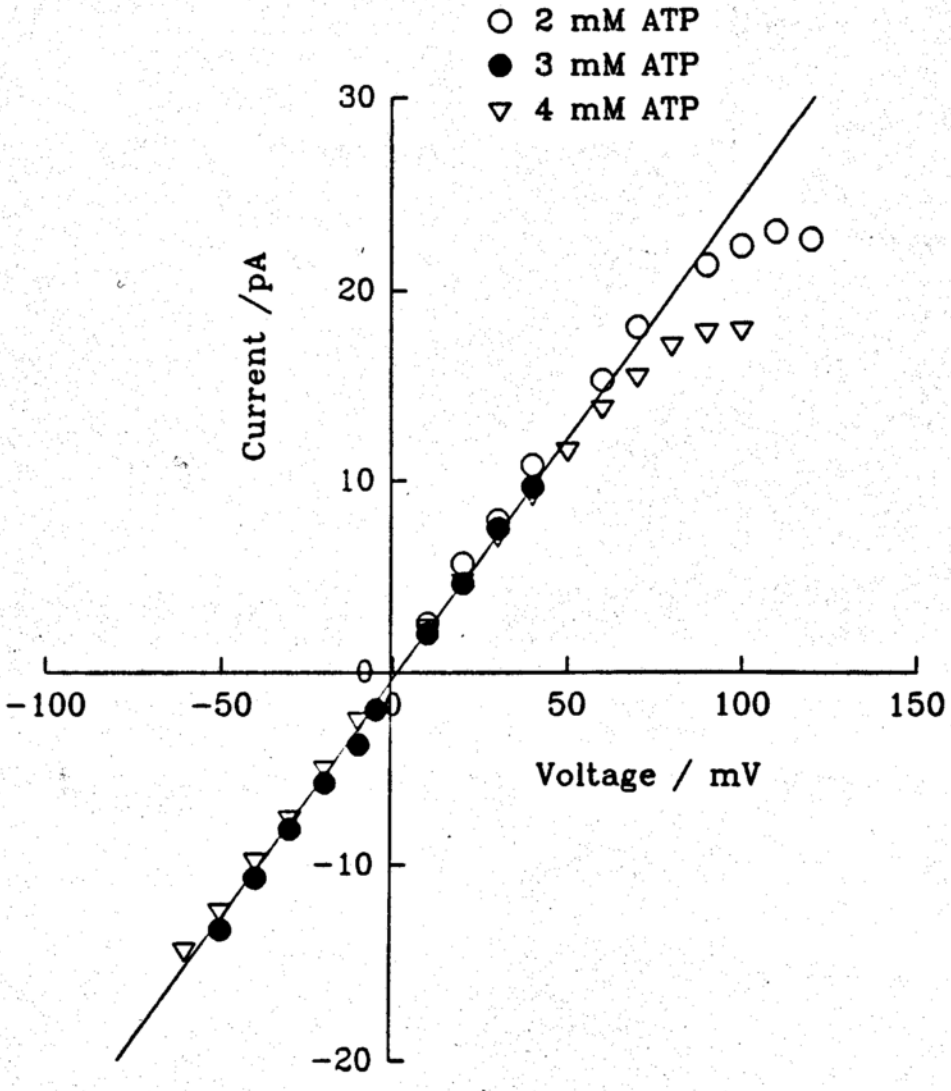

(b) Single channel current traces at various membrane voltages

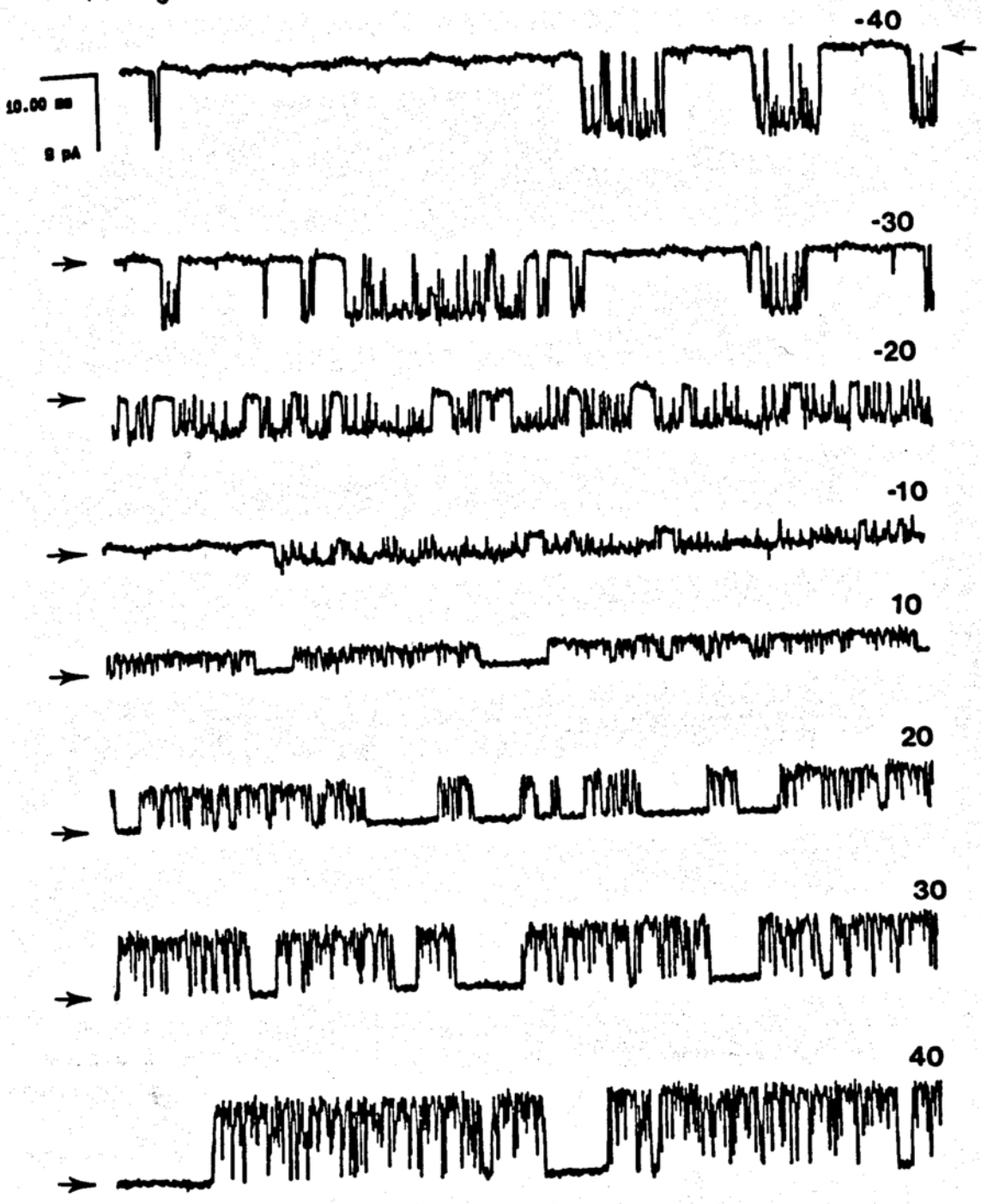

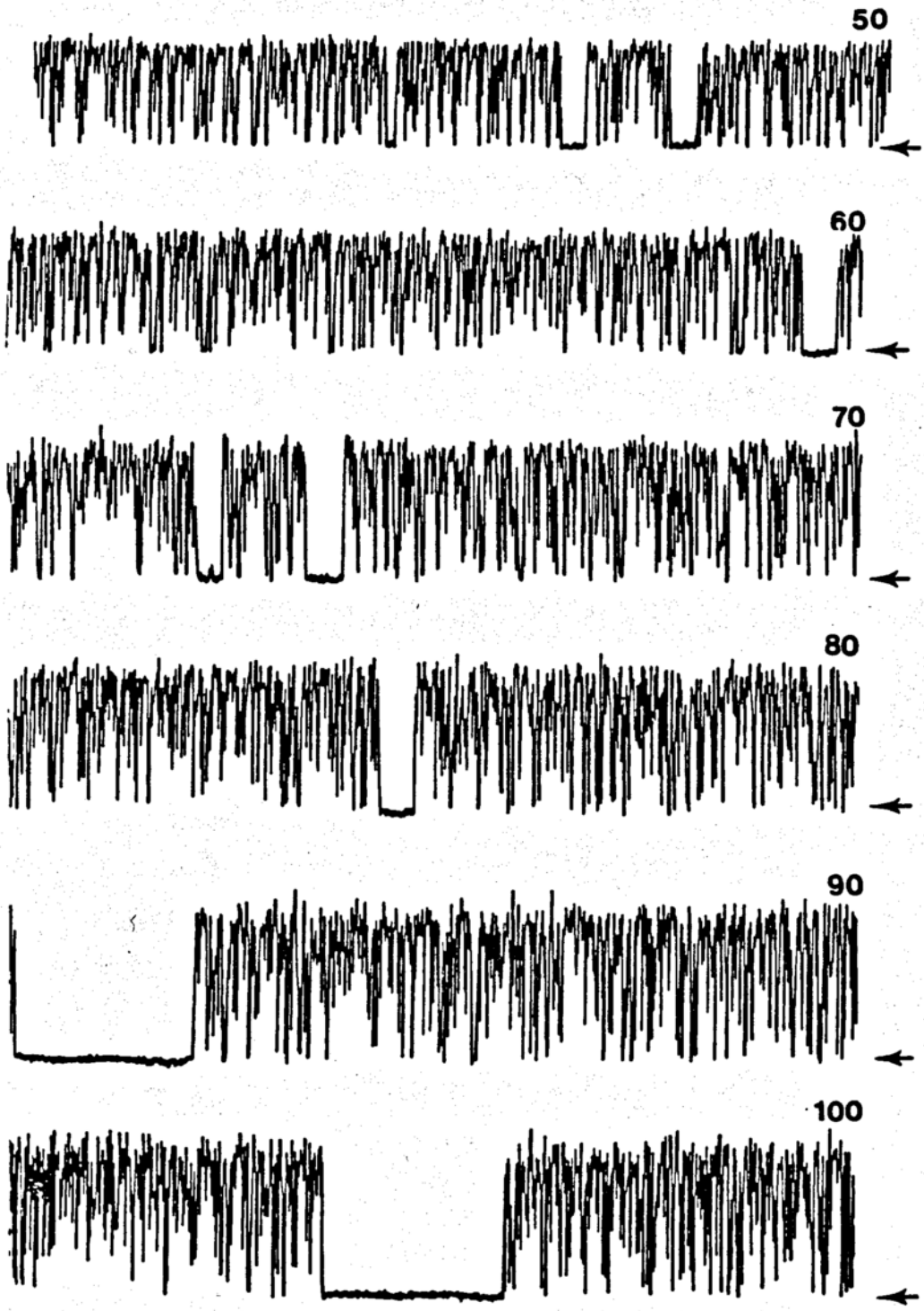
50
60
70
80
90
100

Figure 32 Change in channel opening as a function of intracellular ATP concentration. Notice that ATP binding causes little change in the time density of flickering within a burst, but significantly increases the duration of bursts.

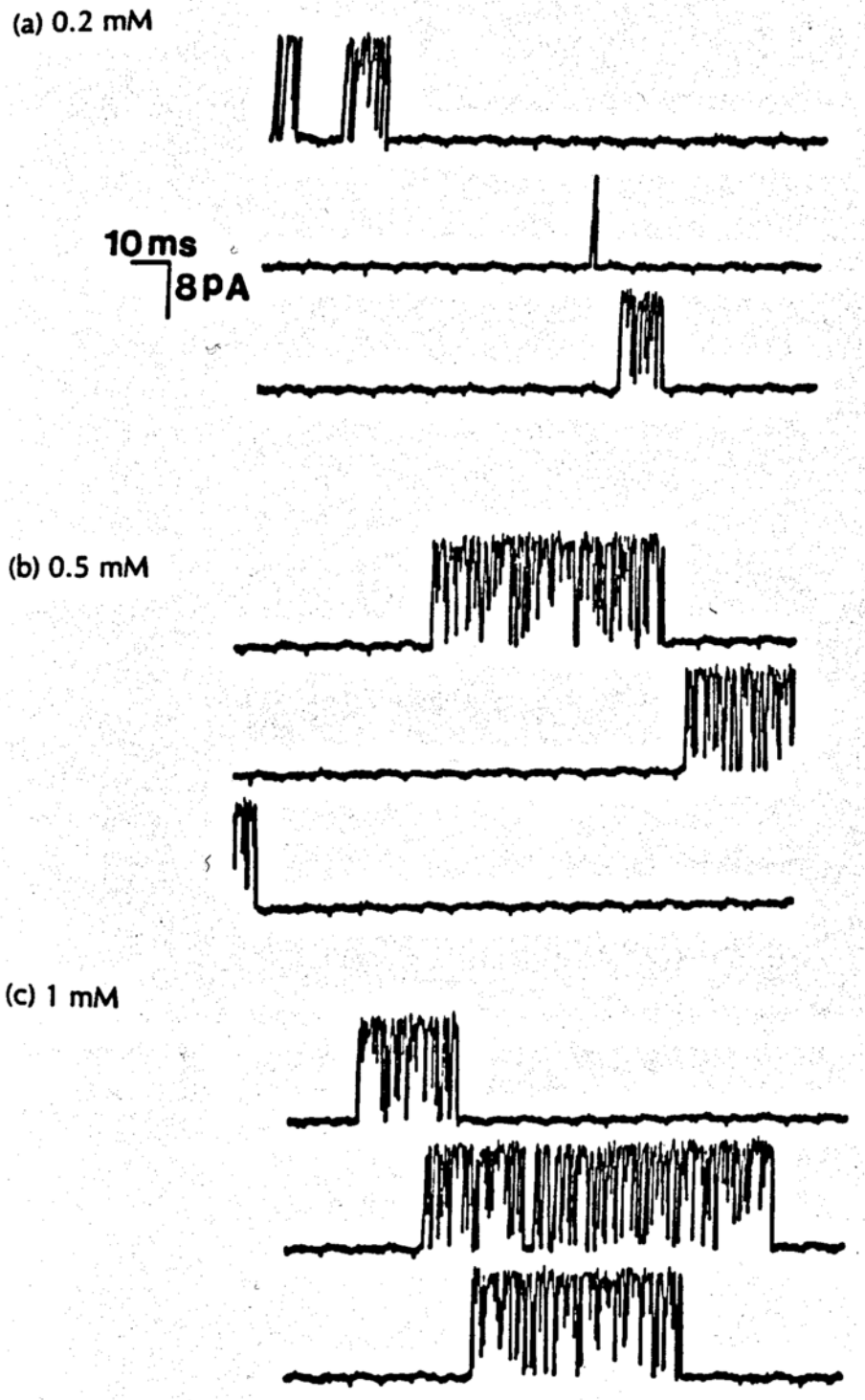

(d) 2 mM

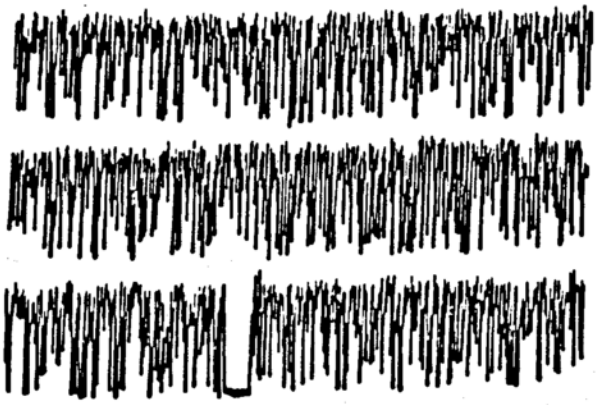

(e) 3 mM

(f) 4 mM

Figure 33 Single channel I-V relationship in various bathing conditions. The extracellular solution remains unaltered, with 160 mM potassium ions (100 % K); the intracellular solution contains either 50 % K and 50 % Na, or 75 % K and 25 % Na. The regression line indicates the I-V relationship when the channel is bathed in a symmetric high potassium solution of 160 mM.

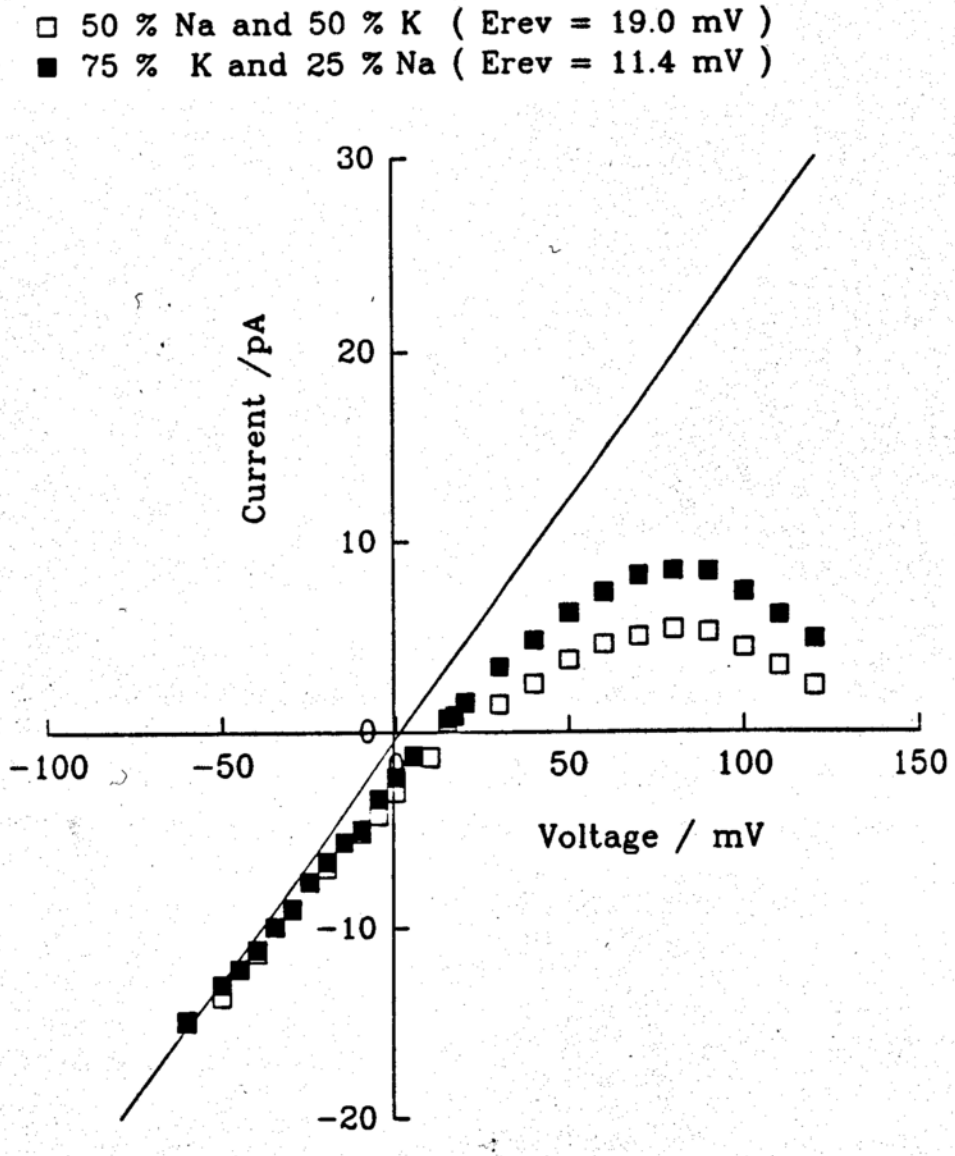

Figure 34 Reversal potentials derived based on various intacellular ionic compositions can be predicted by the Goldman-Hodgkin-Katz equation. The selectivity ratio (K : Na) is ~ 20.

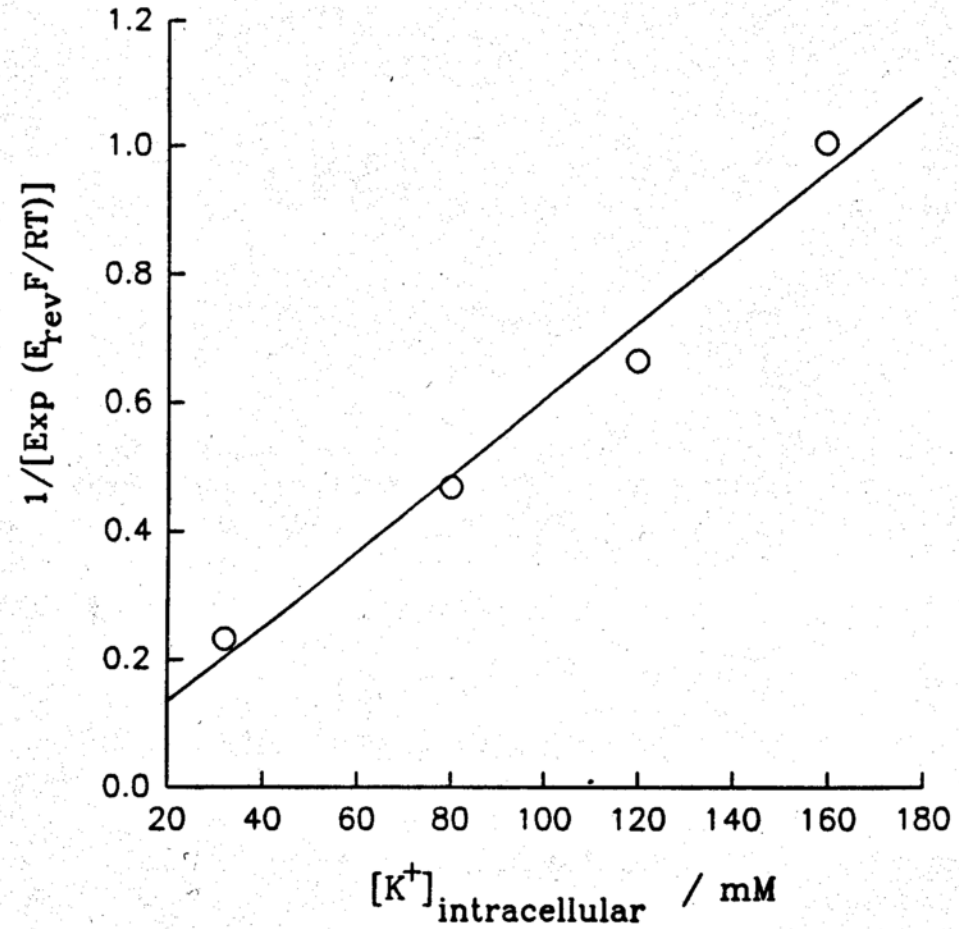

Figure 35 Reversible ATP effect on the opening of the 240 pS channel.

(a) Before the addition of ATP to the intracellular side of the channel.

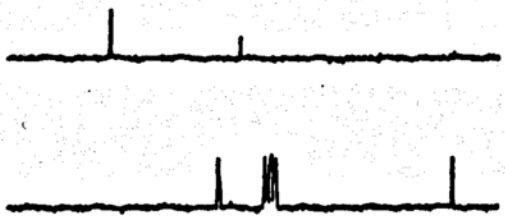

(b) Channel activity increases after the addition of intracellular ATP (~ 1.0 mM).

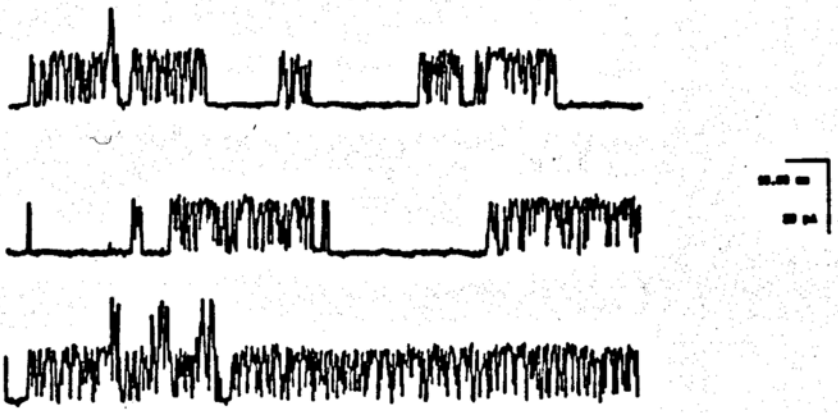

(c) Effect of ATP on channel activity is reversed by replacing ATP-containing bathing solution with ATP-free bathing solution.

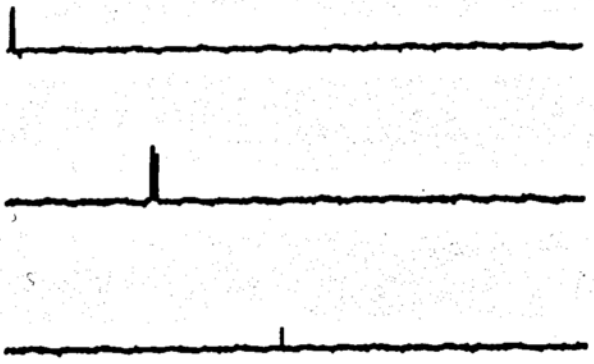

Figure 36 The specificity of the 240 pS ATP-activated potassium channel is demonstrated by using the specific potassium channel blocker TEA. The membrane patch is voltage clamped at 60 mV.

(a) Control

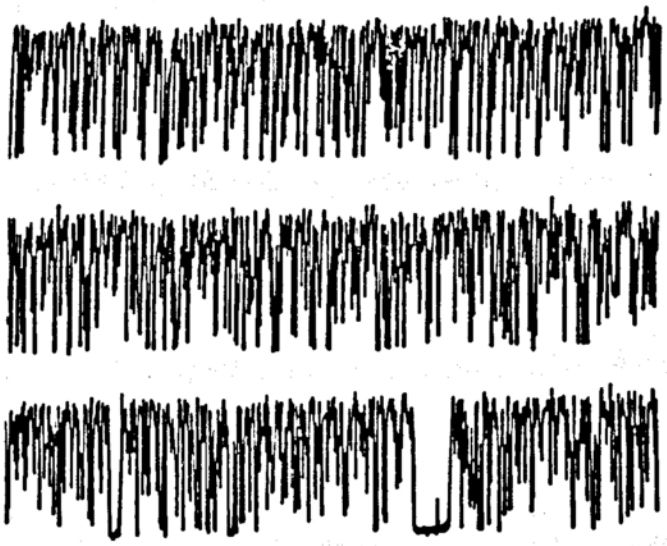

(b) Blocked by TEA

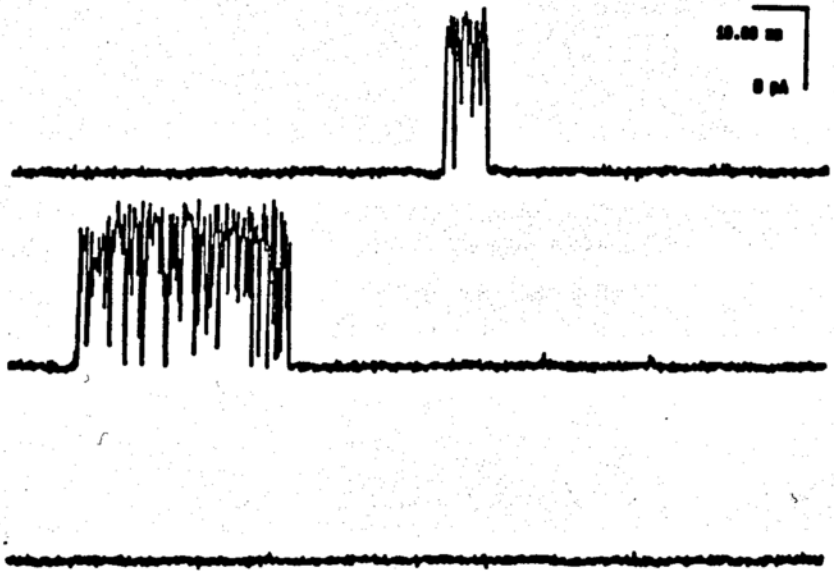

Figure 37 Dose-response curve of the 240 pS ATP-activated potassium channel

(a) Effect of ATP on six different patches each containing one 240 pS ATP-activated potassium channel.

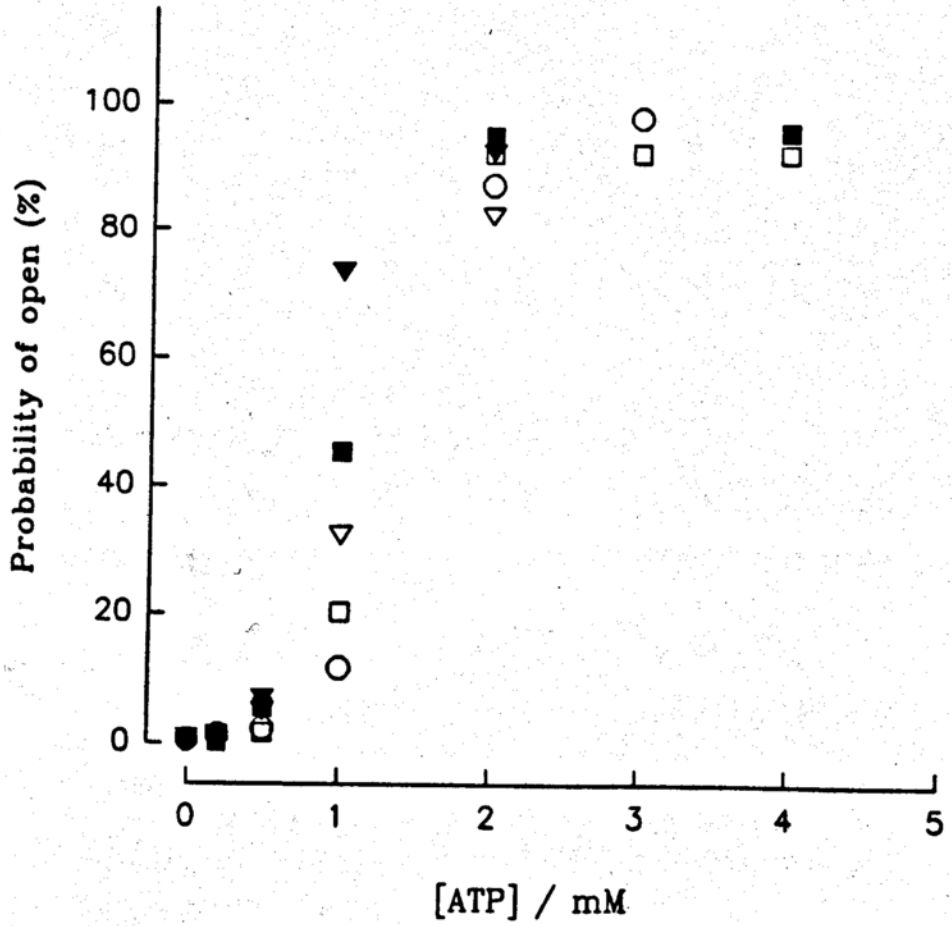

(b) Averaged dose-response

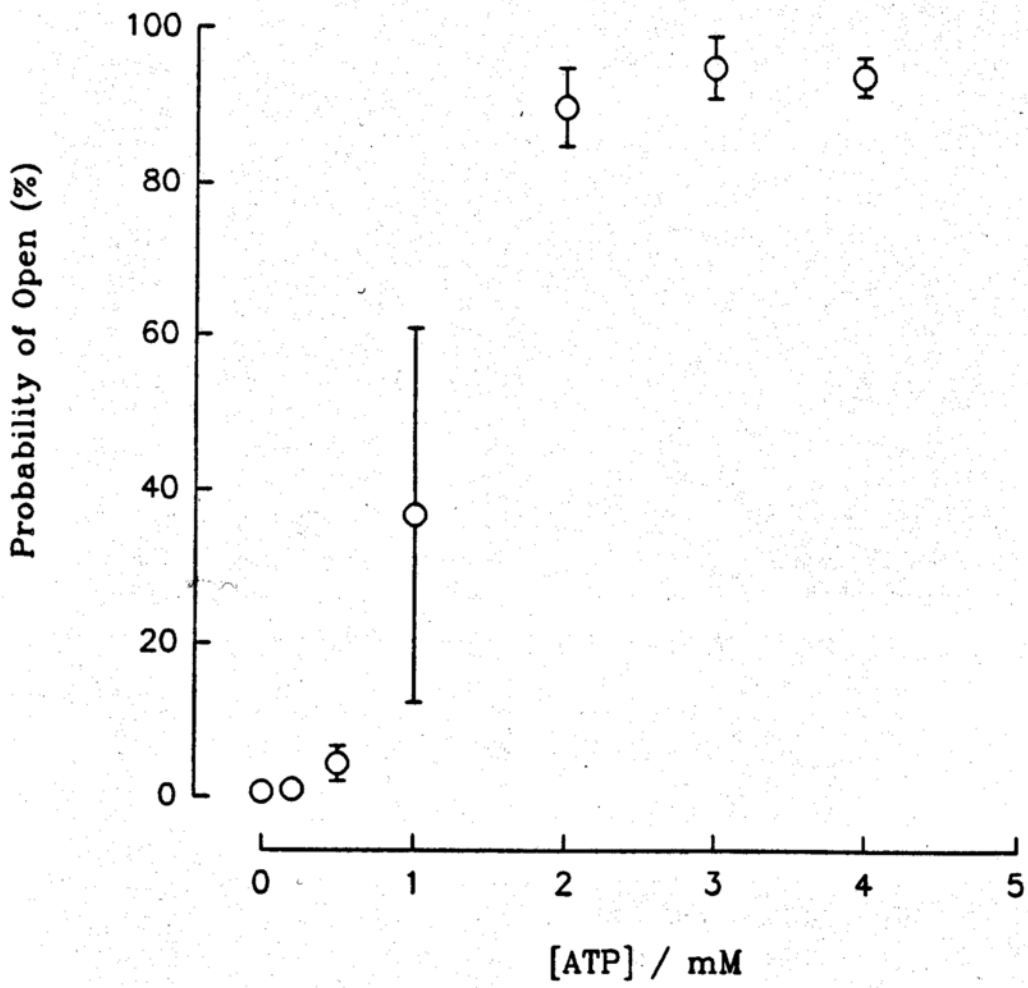

Figure 38 Hill's plot indicating that a minimum of 4 ATP bind to the 240 pS channel.

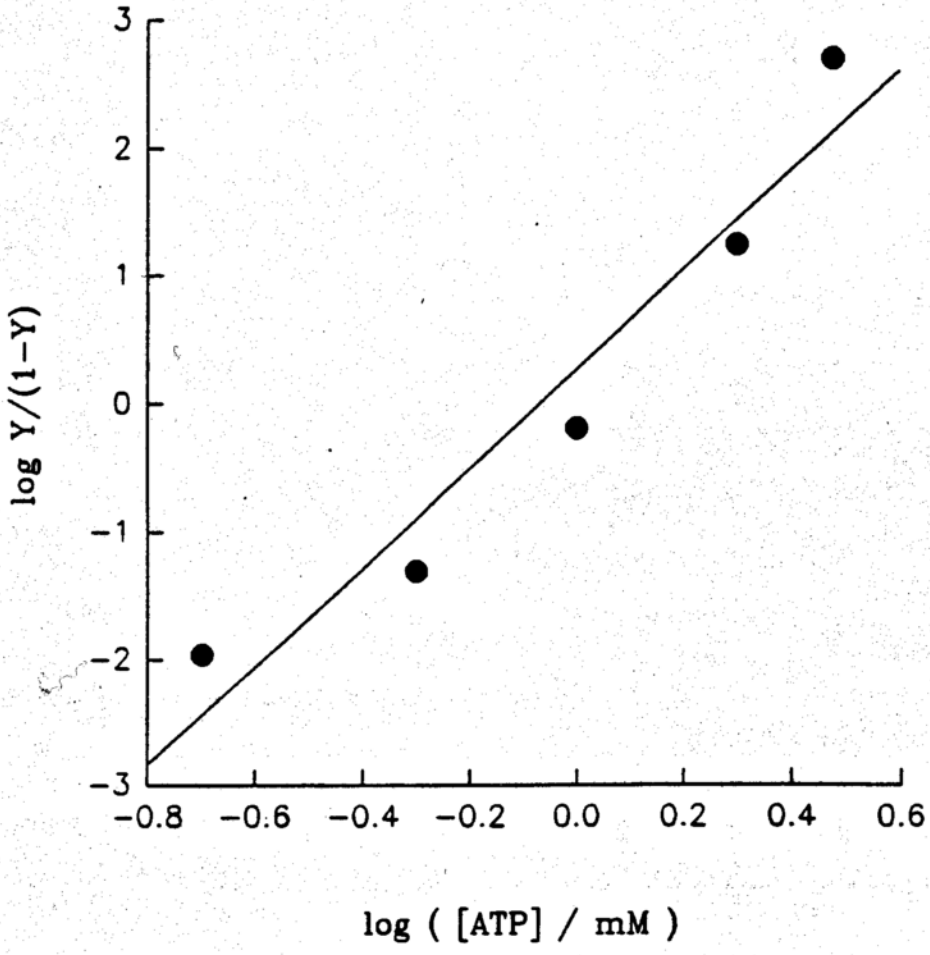

Figure 39 Effect of ATP on the voltage sensitivity of the 240 pS ATP-activated potassium channel. Notice the shift of membrane voltage toward hyperpolarization potential as a result of ATP binding.

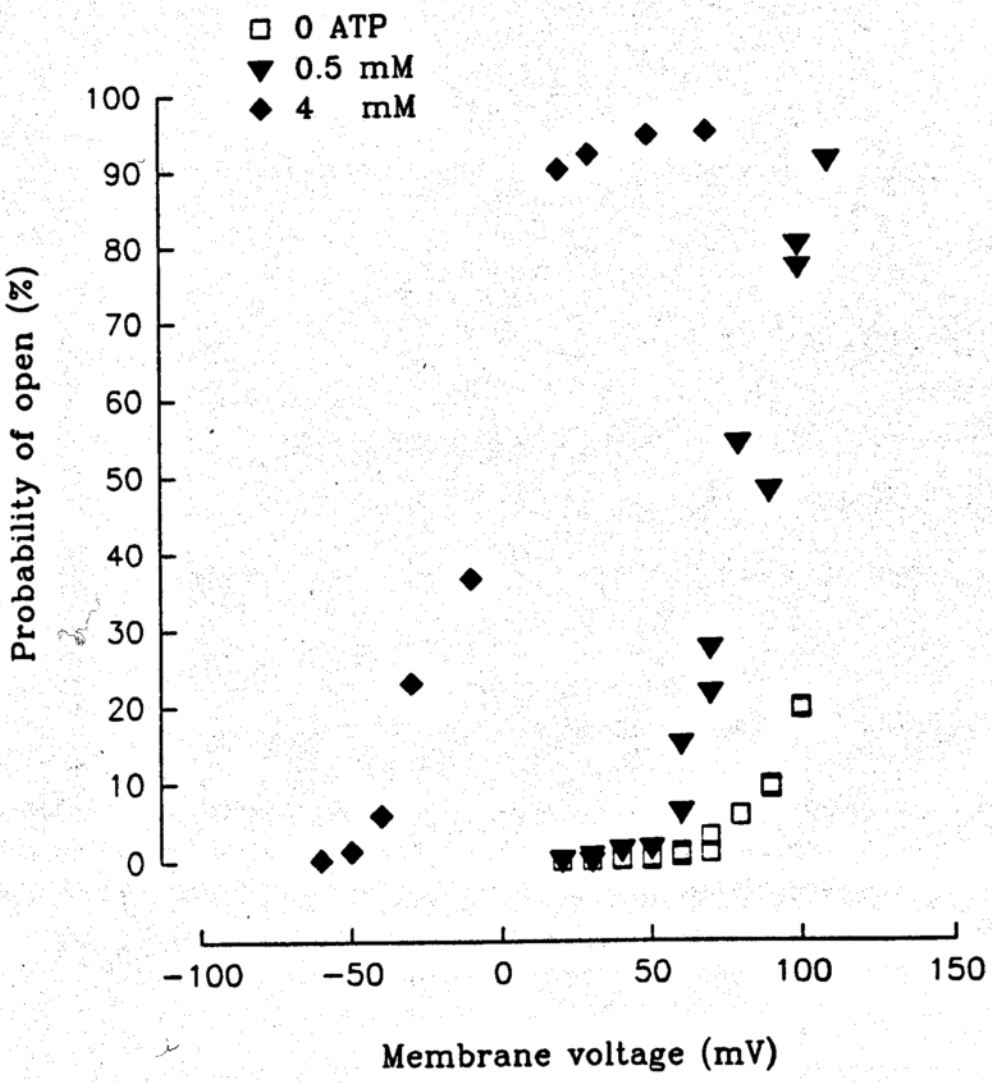

Figure 40 Voltage sensitivities in the presence of either 0.5 mM or 4 mM ATP are fitted to the Boltzmann equation. Notice that the slope of the Boltzmann plot remains unaltered despite the change in ATP concentration.

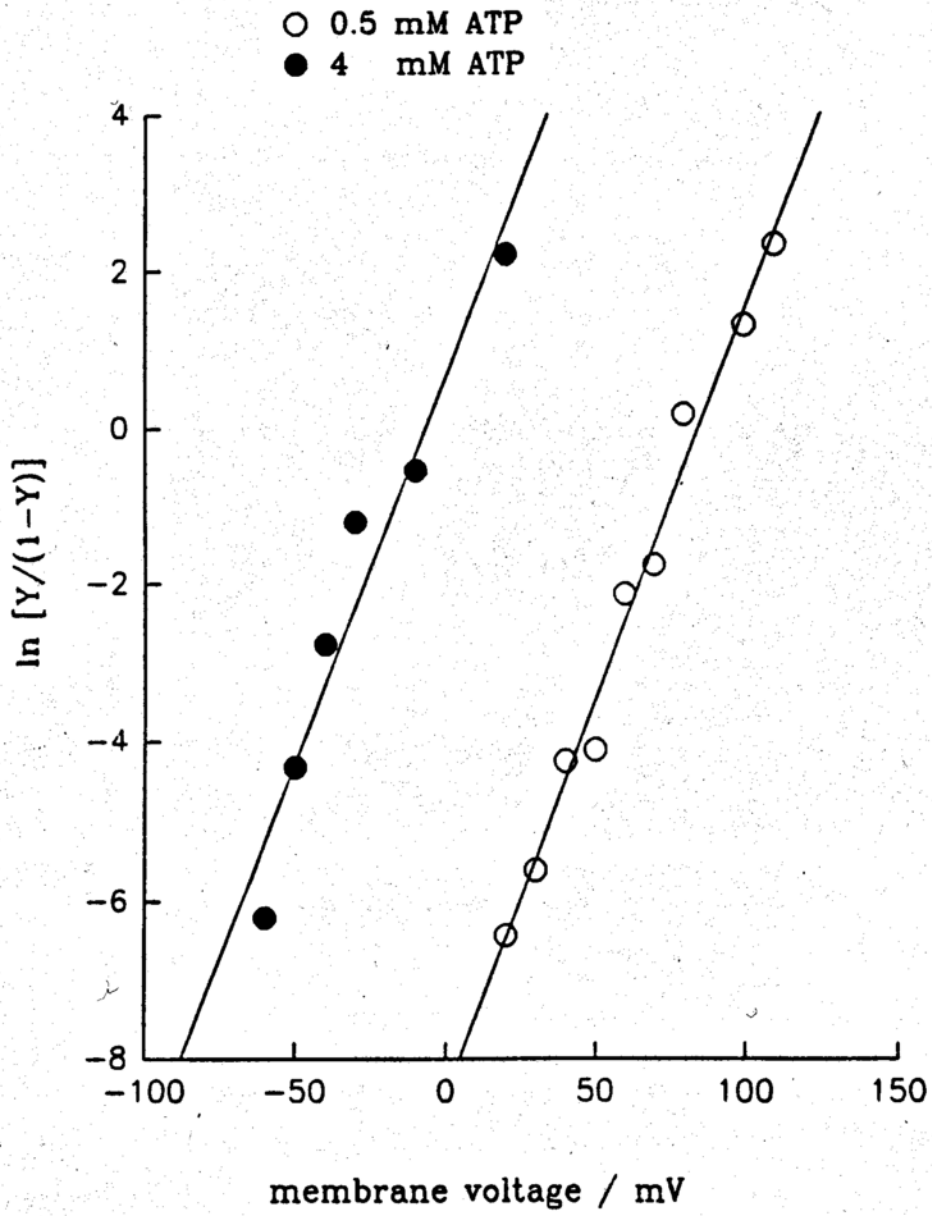

Figure 41 Reversible effect of AMP on the 240 pS channel activity

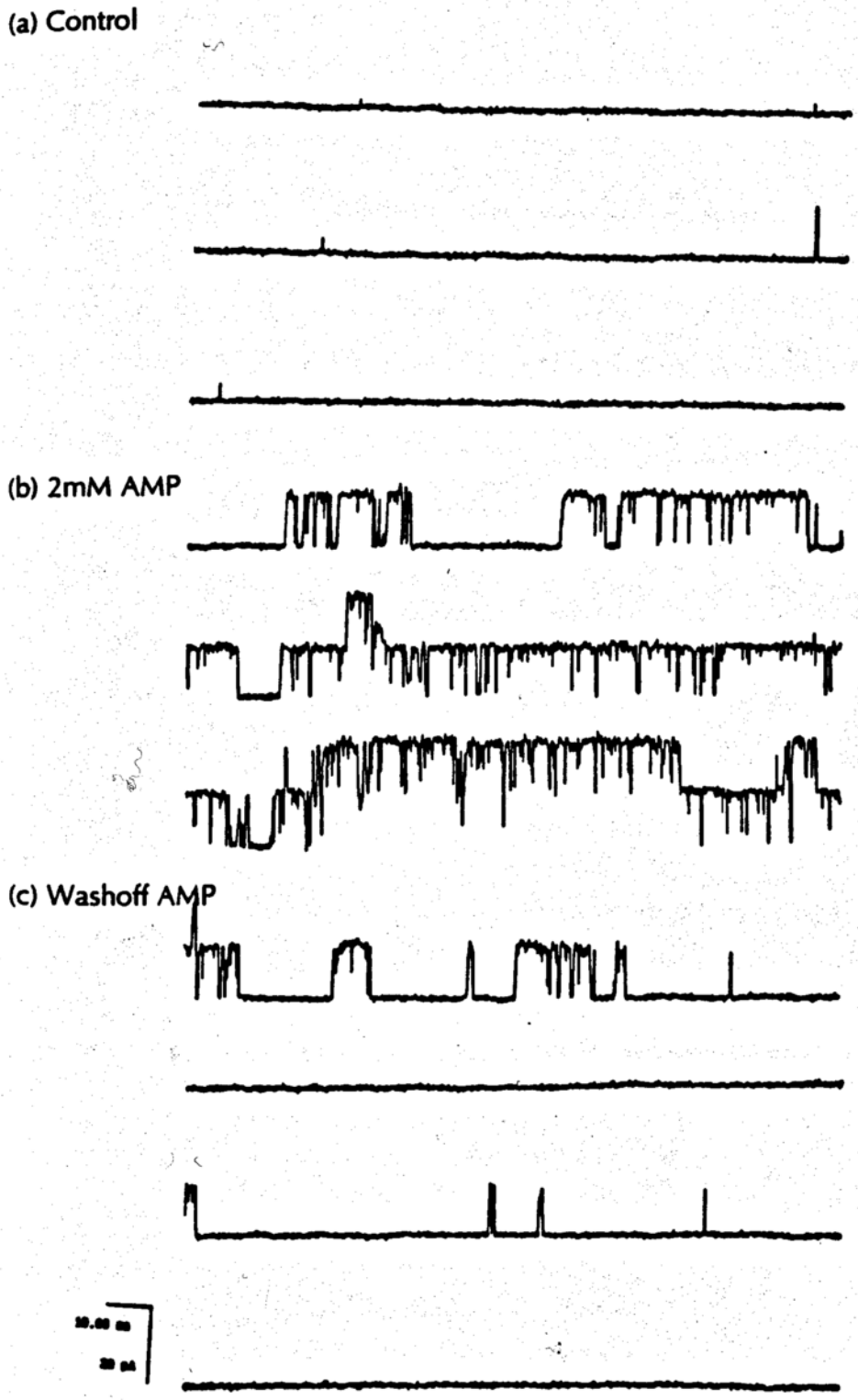

Figure 42 Reversible effect of ADP on the 240 pS channel activity

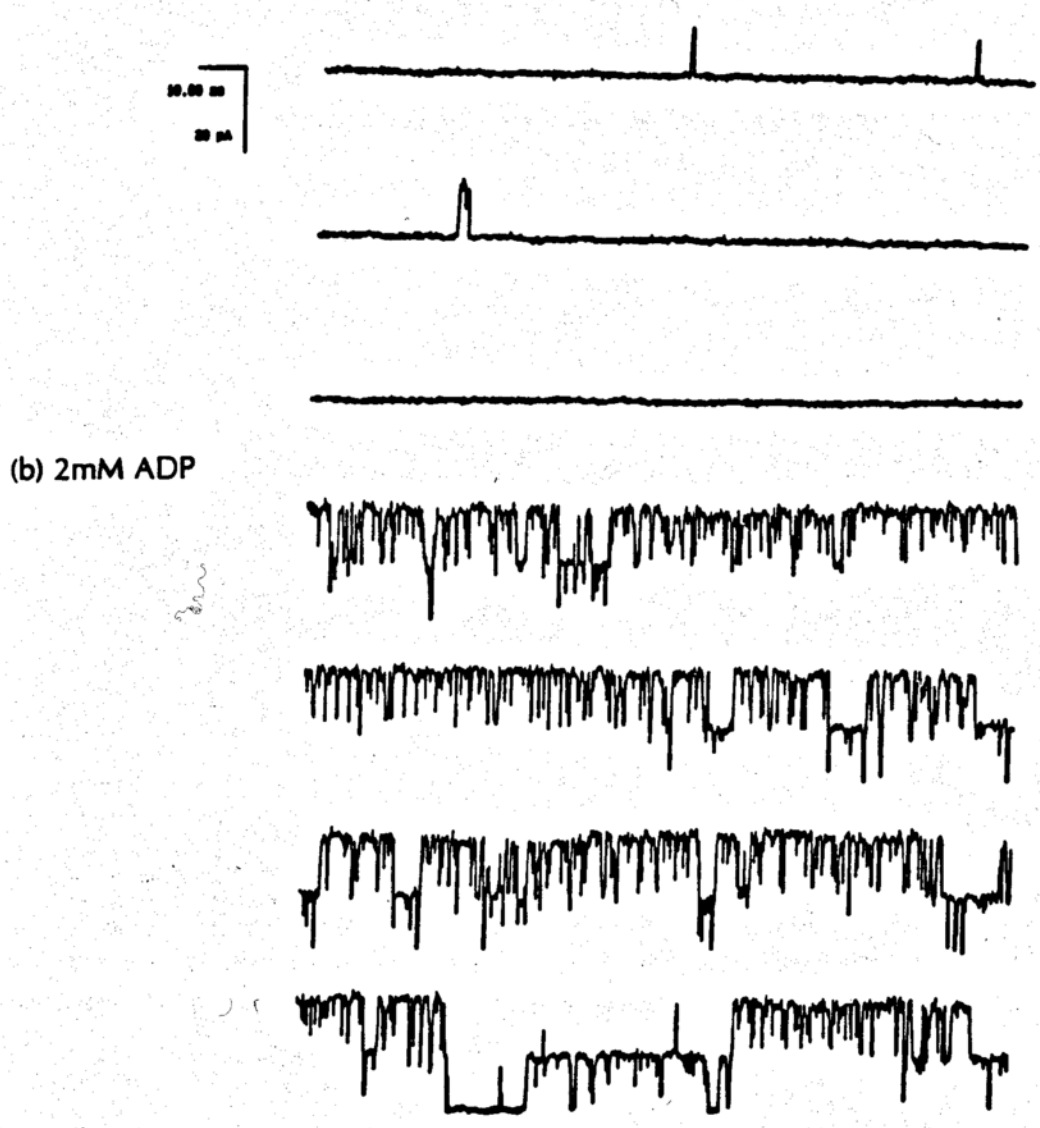

Figure 43 Reversible effect of AMP-PCP on the 240 pS channel activity

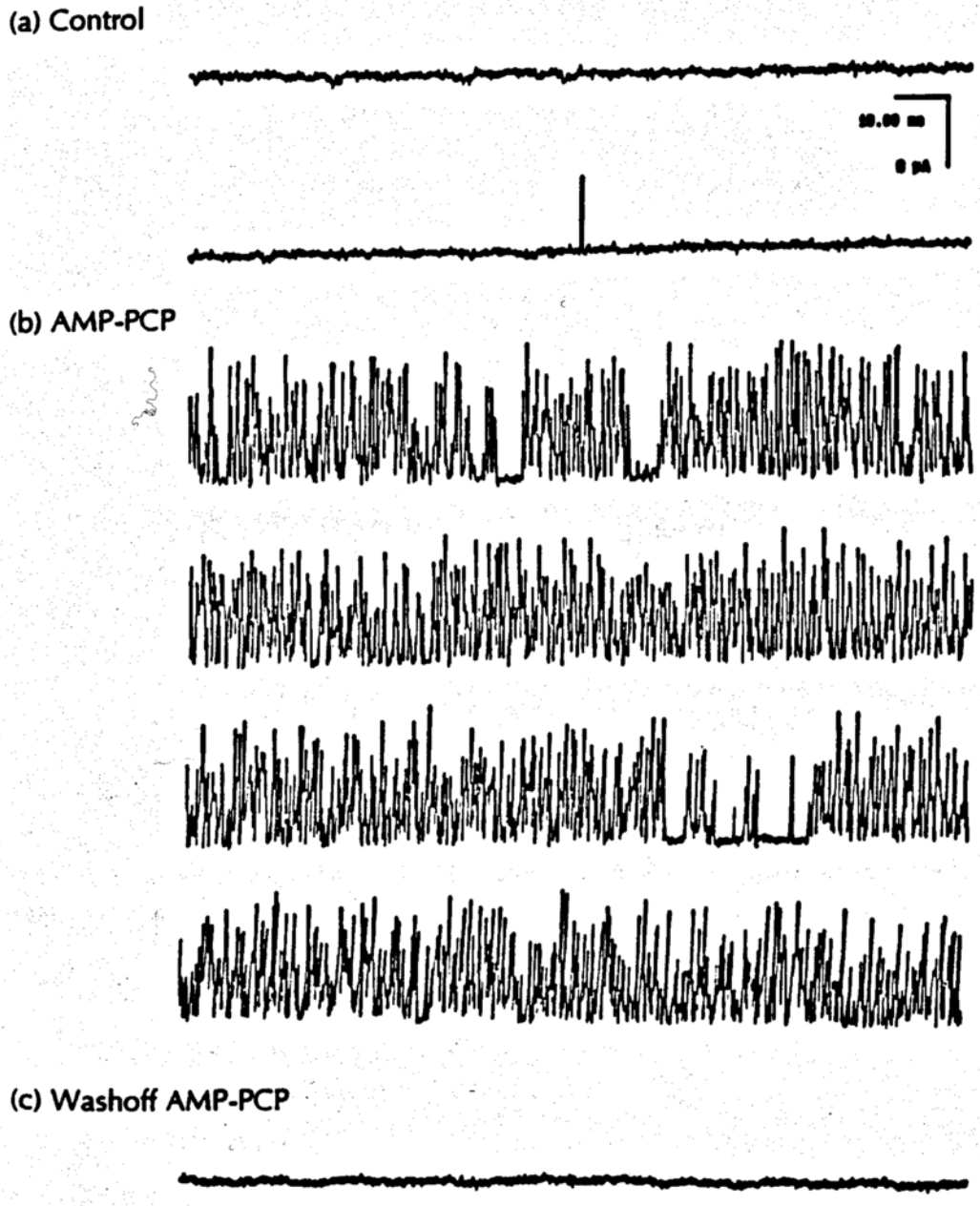

Figure 44 Mg^{+2} was not requiired for the channel activation induced by ATP

(a) Control single channel current without Mg^{+2}

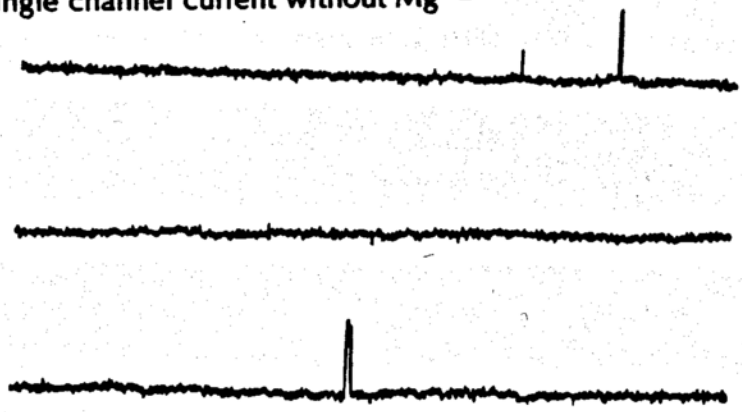

(b) Presence of ATP along (without Mg^{+2}) increased the channel activity

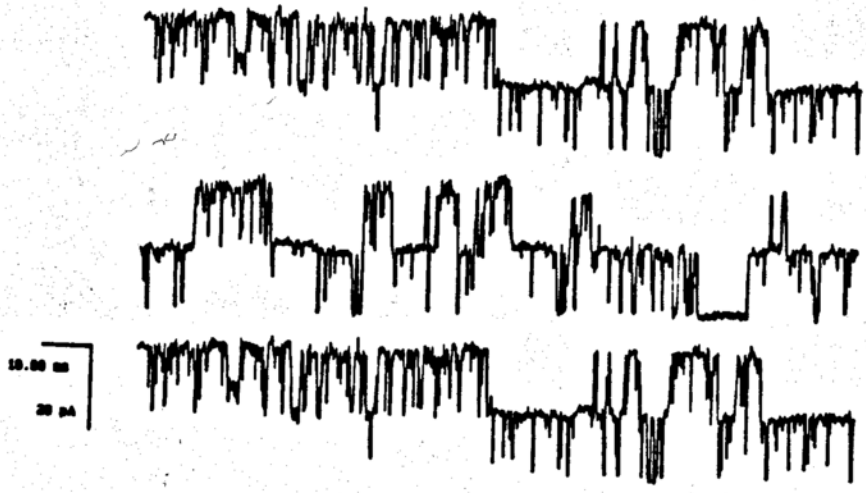

Figure 45 Responses of the 240 pS channel to various nucleotides with or without intracellular Mg^{+2}

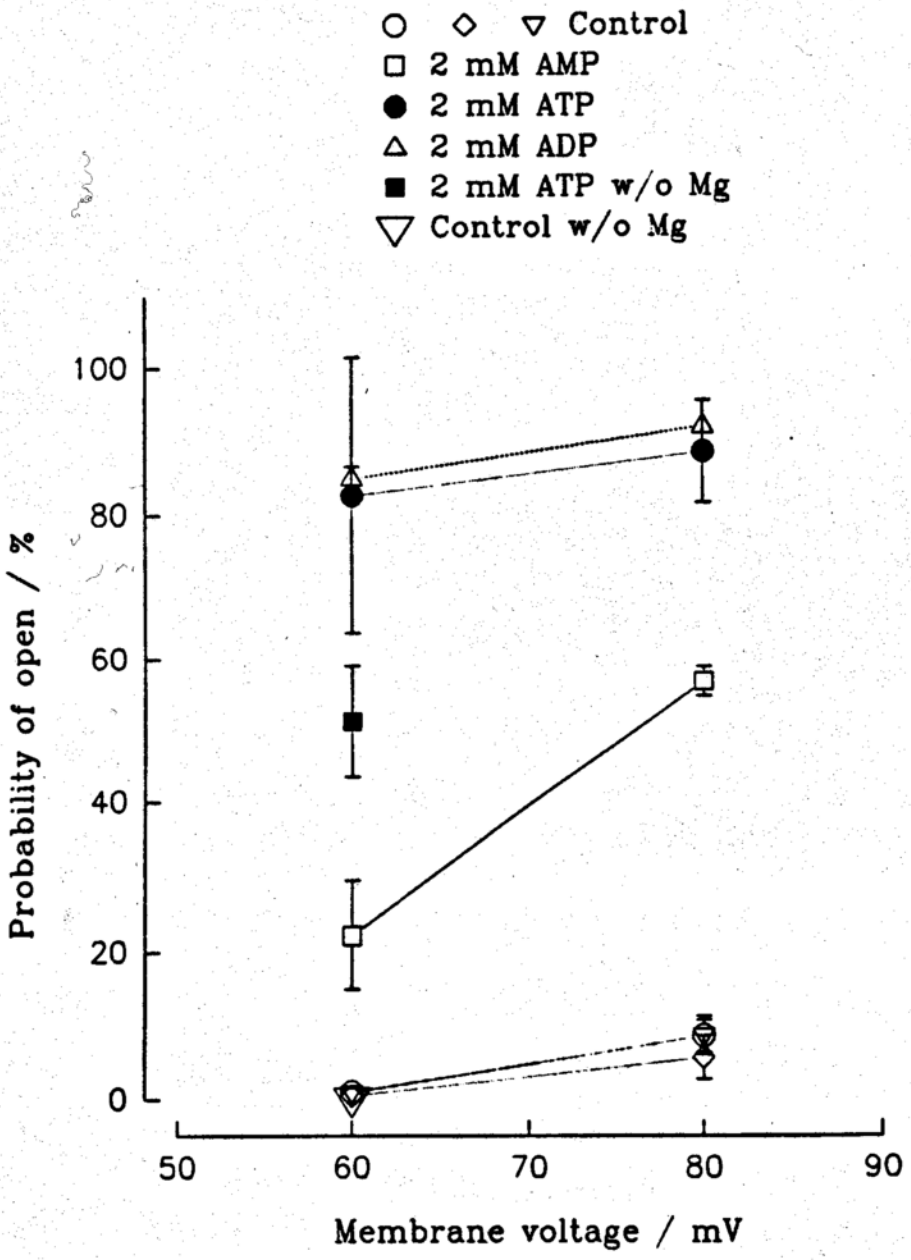

Figure 46 Using burst analysis, the resultant arithmetic mean opening time and the mean dwell time (obtained by fitting the open time histograms to an exponential expression) are both seen to increase with the intracellular ATP concentration.

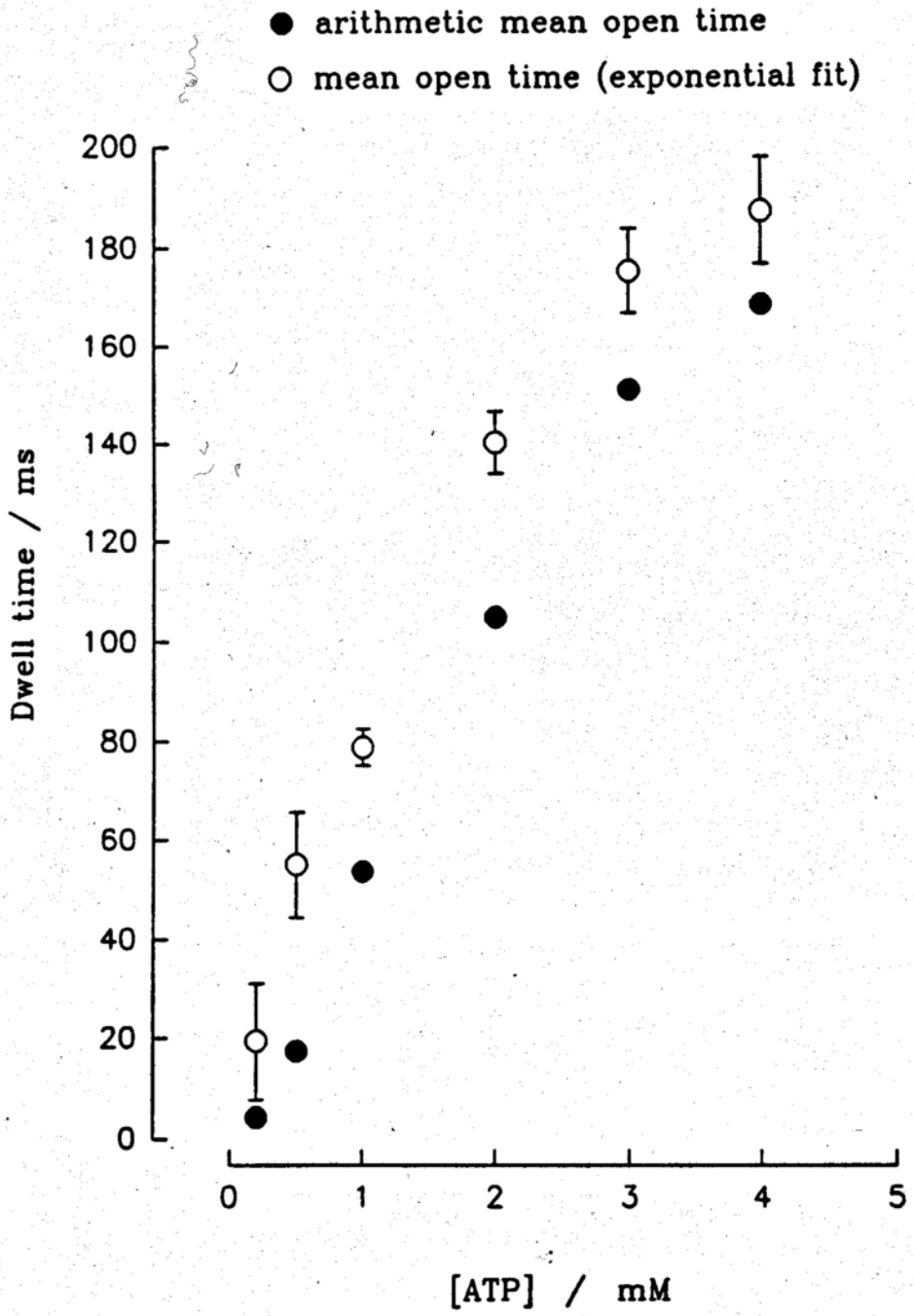

Figure 47 Average duration of the interburst gap, either calculated arithmetically or obtained by data fitting, decreases as the concentration of intracellular ATP increases.

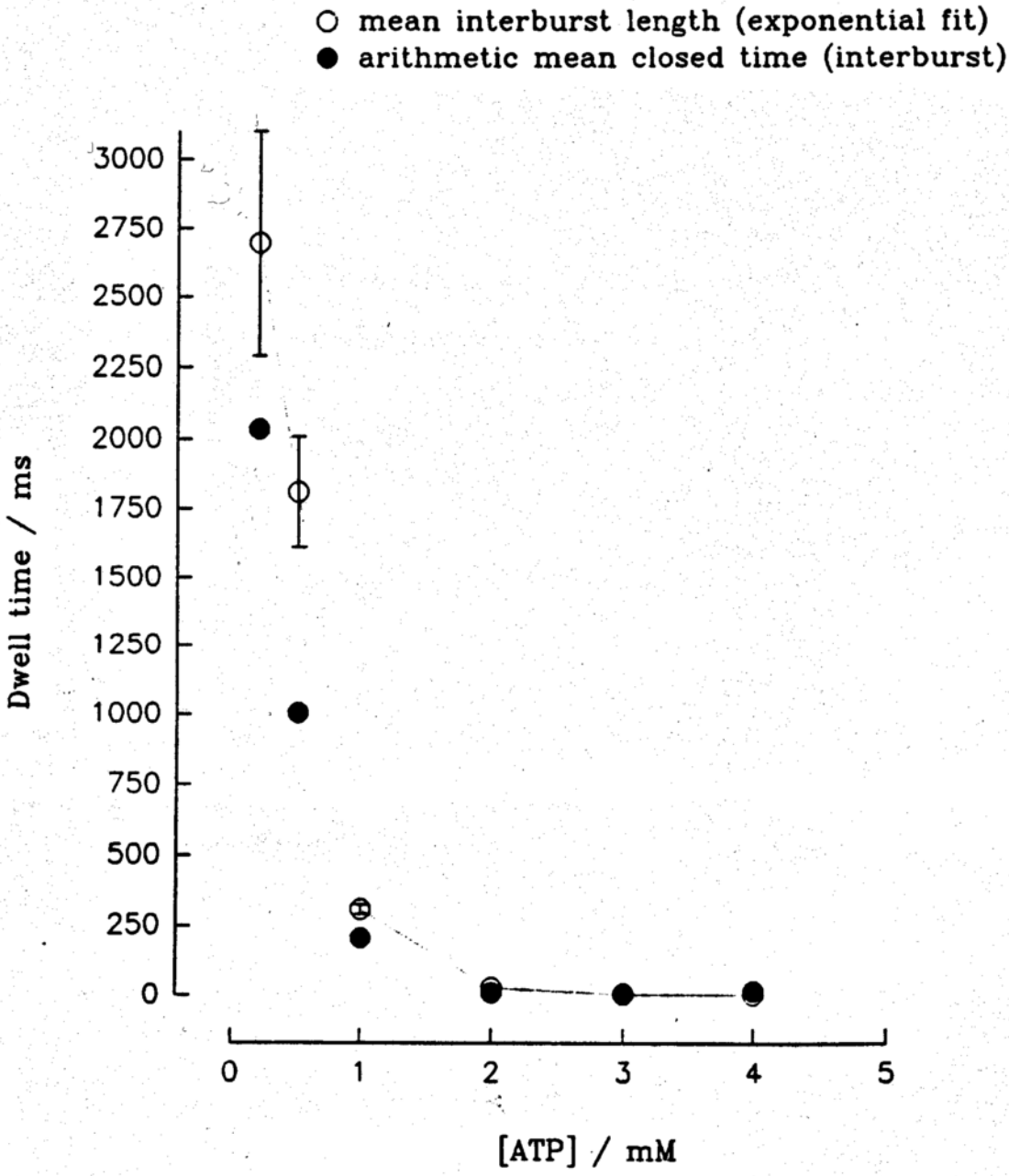

Figure 48 Average duration of the interburst gap appears proportional to the inverse of the ATP concentration.

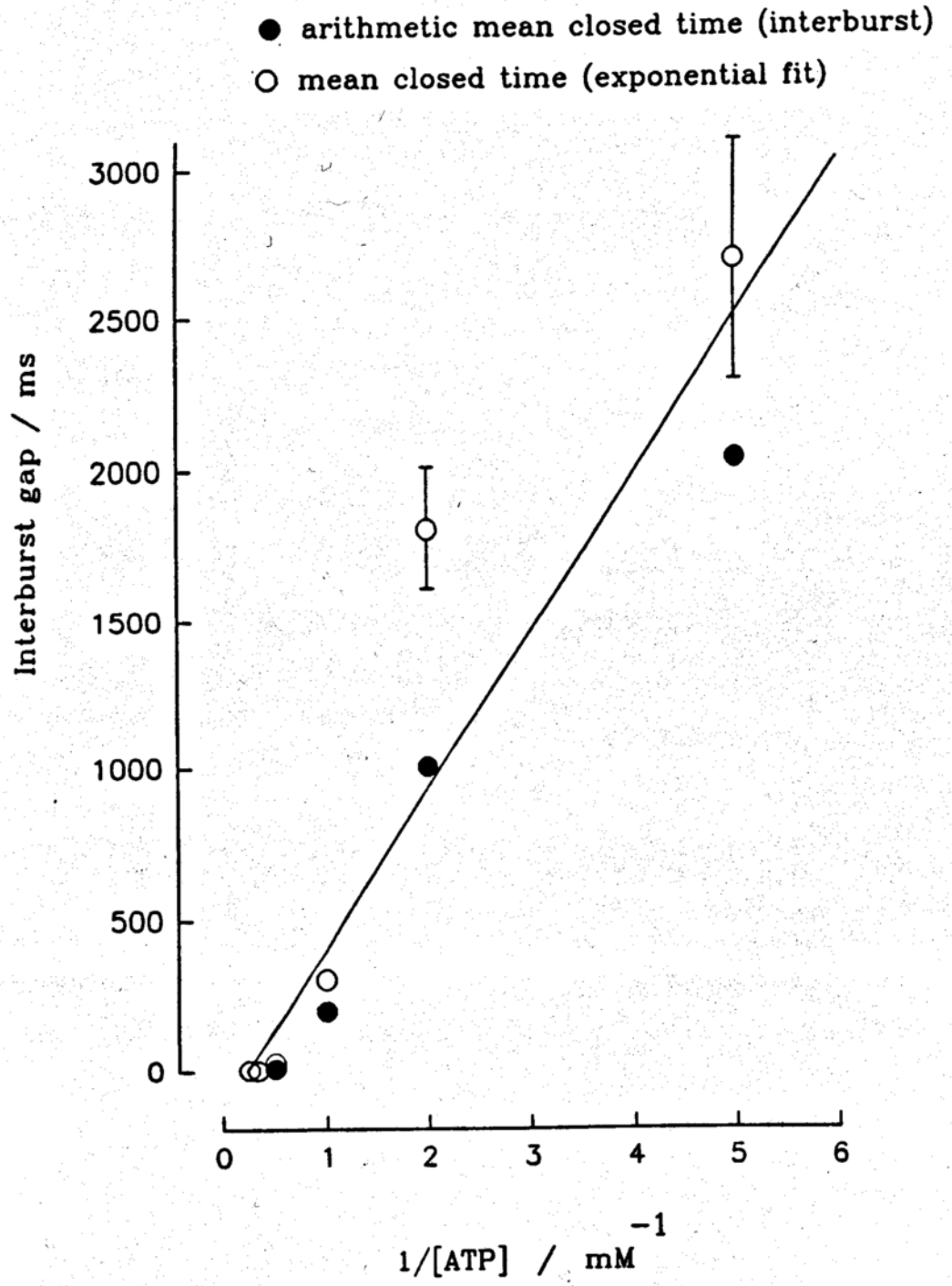

Figure 49 Logarithm of the Average duration of the interburst gap varies linearly with the ATP concentration

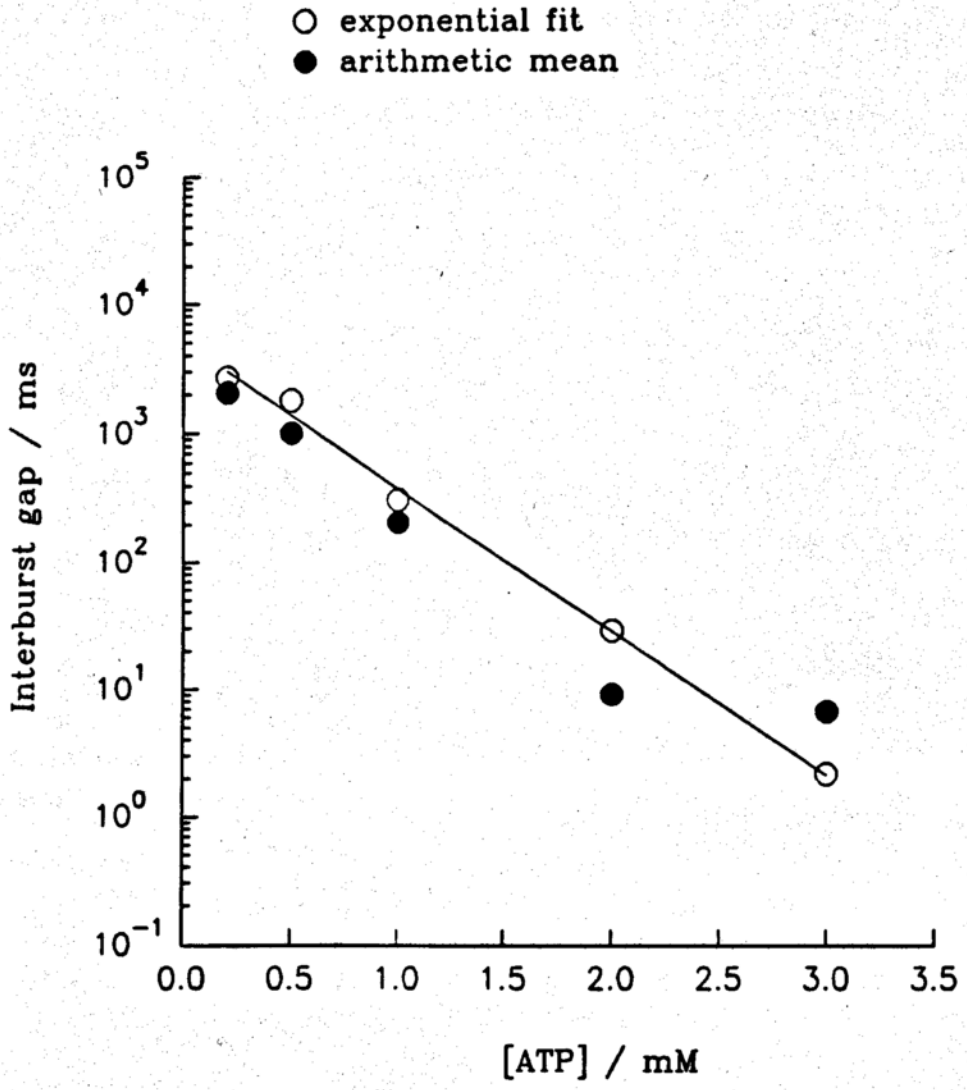

Figure 50 The duration of flickery opening shows a complex dependency on the concentration of ATP. The duration increases proportionally with the ATP concentration up to ~ 1mM, then decreases as the concentration of ATP further increases.

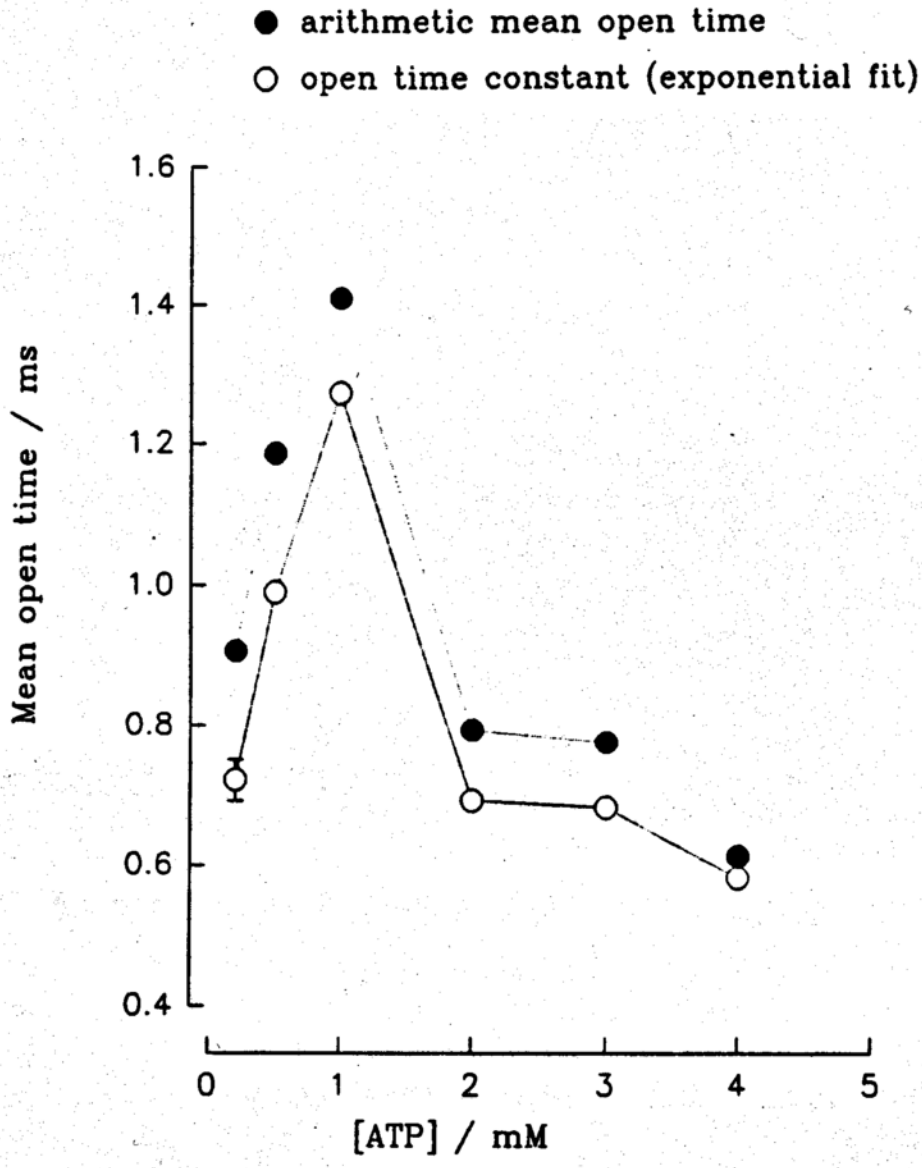

Figure 51 Three closed states can be deduced from analysis of closed events without constraints. Judging by values of the mean dwell time, two of the three states appear to be associated with closing of the channel within a burst. The third state, with the longest mean dwell time, reflects the interburst gap. The duration of flickery closure is independent of ATP concentration, while the duration of the third state appears to decrease as the concentration of ATP increases.

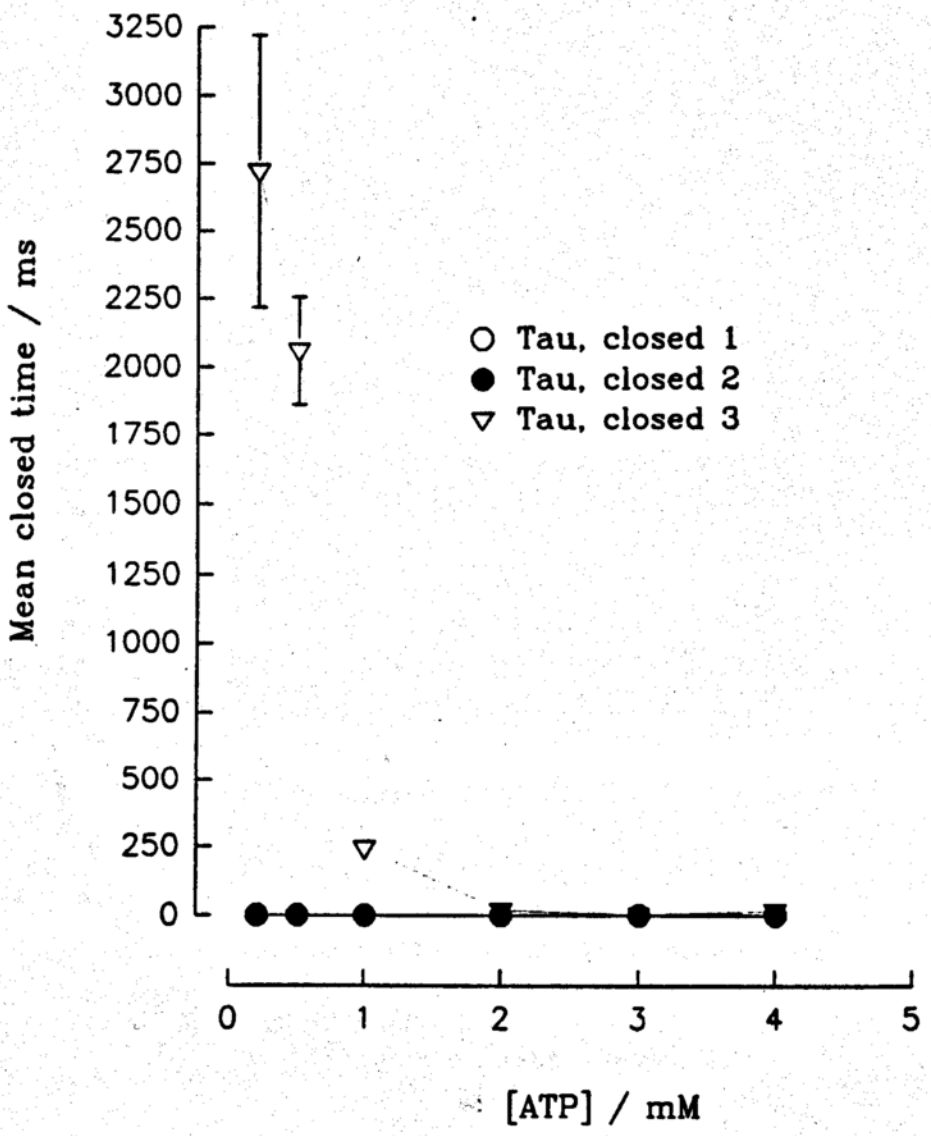

Figure 52 Calcium dose-response of the 240 pS ATP-activated K_{Ca} channel in the absence of ATP

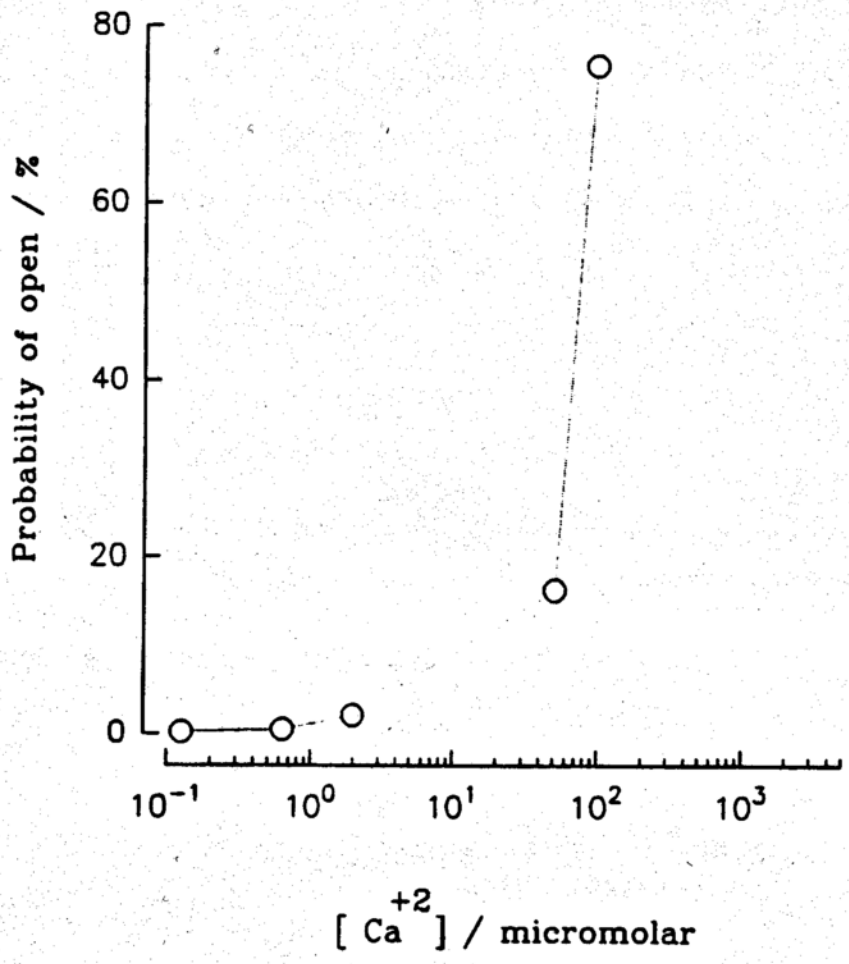

Discussion

As mentioned in the Results section, we identified three channels gated by ATP: two K_{Ca} and one K_{ATP} channel. The K_{ATP} channel, with a conductance of 40 pS, is different from the other two because it is not likely to be regulated by intracellular ATP in normal physiological conditions with high levels of intracellular K^+. In cell-free patches, with bathing solutions containing no K^+, channel opening is regulated (inhibited) by millimolar concentrations of intracellular ATP. However, normal physiological levels of intracellular K^+ inhibit this channel's activity, interfering with ATP regulation. Therefore, despite the fact that several other K_{ATP} channels have been identified in renal tubular cells from other sources, and tentatively have been assigned functional roles (4, 13, 28, 29, 30, 42), it is not clear that this 40 pS K_{ATP} channel in MDCK cells shares similar physiological roles with these other channels, since none of these channels appears to inactivate in the presence of normal levels of intracellular K^+. For this reason, this channel is not discussed further here.

Direct binding of intracellular ATP as a newly discovered mode of ATP-gated channel activation

The two K_{Ca} channels found in MDCK cells are activated by direct binding to intracellular ATP. In symmetric high potassium solutions of ~ 150 mM, one has a conductance value of 49 pS and the other, 240 pS. As discussed in the Results section, our evidence that ATP activates them through direct binding to channel proteins includes the facts that activation does not require the presence of Mg^{+2} along with ATP, and that AMP, ADP, and AMP-PCP, a nonhydrolyzable ATP analog, each can activate these channels. These two channels are different from all other ATP-gated channels reported so far because of their unique mechanism of activation.

I. Related phenomena

I.A. Effects of extracellular ATP

For a number of channels regulated by extracellular ATP, the mechanisms of regulation vary depending on how ATP affects these channels. Bean and Friel have summarized three main effects of extracellular ATP on various ionic channels: (a) activation of a family of channels in which current flow reverses near 0 mV; (b) activation of some highly potassium-selective channels; and (c) modulation of a variety of channels that are primarily controlled by other means (43). Each of these effects has been found to result from ATP interactions with these ion channels through different mechanisms.

The mechanism of the effects of extracellular ATP on the family of channels in which current flow direction is reversed near 0 mV is believed to be direct ATP binding, because these channels can be activated by ATP at concentrations as low as 10 nM and produce significant inward currents within less than 100 ms. These channels are thus ATP-specific receptor channels (43). The direct binding mechanism

is also indicated by results from ligand sensitivity studies. These studies reveal that these ATP receptor channels correspond well to P_2 purinoceptors, which are receptors specific to extracellular ATP binding (44).

External ATP activates some highly potassium-selective channels indirectly, because the current responses of these channels to extracellular ATP are much slower than those of the previous channels (ranging from less than a second to several seconds). In cardiac atrial cells, GTP-binding proteins have been found to be required in the pathway for channel activation; these proteins serve to couple ATP receptors to the activated potassium channels (43).

Little is known about the mechanisms of extracellular ATP's modulatory effects on ion channels. However, some studies suggest that these effects are secondary to stimulation via second-messenger pathways. For example, in MDCK cells, ATP's effects on channel activity have been attributed to elevated levels of intracellular Ca^{+2}, which result from ATP binding (45, 46). In frog sympathetic ganglion cells, Brown proposed the participation of some unknown second messenger systems in order to explain the inhibitory effects of extracellular ATP on a voltage-dependent potassium current (47).

I.B. Intracellular ATP regulation

I.B.i. Direct binding in K_{ATP} channels

In addition to extracellular ATP, intracellular ATP can also regulate ion channel activities. Two different mechanisms have been reported to be related to the regulation of ATP-gated channel activity by intracellular ATP: direct binding and phosphorylation. Direct binding is the mechanism most often associated with K_{ATP} channels, for the following reasons: (a) channel closure by ATP occurs in the absence of Mg^{+2}; (b) nonhydrolyzable analogs of ATP have an action similar to that of ATP itself; and (c)

other nucleotides mimic the action of ATP. This channel was first identified by Noma in cardiac muscle (48). Subsequently, similar channels were found in many other types of cells, including renal tubular cells. A general characteristic of these channels is that their open probability is low at resting physiological levels of intracellular ATP (~ 2-3 mM); however, a decrease in the level of intracellular ATP leads to higher channel open probabilities (27). Presumably, ATP binding to K_{ATP} channels causes them to close.

I.B.ii. Phosphorylation in K_{ATP} channels

ATP binding to K_{ATP} channels inhibits their activity, but in contrast, ATP-mediated phosphorylation activates many potassium channels, including K_{Ca} channels. In all the studies of ATP activation of K_{Ca} channels in which the mechanism is known, phosphorylation has been concluded to be the mechanism of activation because in some cases ATP hydrolysis is required for activation, and in other cases, addition of protein phosphatase can reverse ATP's activating effects. The levels of ATP required to activate these channels, in most cases, are in the micromolar concentration range. Only in three cases are millimolar concentrations (> 0.5mM) of intracellular ATP required to activate channels (38, 39, 40). These three cases involve activation of K_{Ca} channels obtained from rat brain (39), rat pulmonary artery (40) and opossum kidney cells (38).

However, on one occasion, phosphorylation caused by intracellular ATP was found to inhibit channel activity. This was reported by Wang and Giebisch using a K^+ channel with a conductance of 35 pS, located in the apical membranes of rat collecting ducts (49). They found that high concentrations of ATP (> 1 mM) could reduce the channel open probability through a mechanism requiring ATP hydrolysis, despite their other finding indicating that low concentrations of ATP (~ 0.05-0.1 mM)

could facilitate c-AMP-dependent phosphorylation, which helped to restore channel activity after channel rundown. They concluded that the inhibition at high ATP levels was mediated through phosphokinase A-dependent phosphorylation because ATP's inhibitory effect on channel activity could be blocked by adding exogenous catalytic subunits of phosphokinase A.

I.C. Summary

To summarize, we have identified a mode of activation of K_{Ca} channels not yet reported in the literature, by direct binding to intracellular ATP. Intracellular ATP thus appears to be capable of modulating potassium channel activity by direct binding or phosphorylation, depending on the individual channels.

II. Comparison of properties of K_{ATP} channels and the ATP-gated K_{Ca} channels in MDCK cells, and possible structural resemblances between the two

II.A. Structural resemblance

Since intracellular ATP can modulate channel activity via direct binding, one question to ask is whether direct binding sites for ATP exist in some ATP-gated channels. The only structural study of ATP-regulated channels was done by Ho et al. (41). In Xenopus oocytes, they expressed a polypeptide (ROMK1) synthesized from c-DNA clones made from rat kidney tissues, and found that ROMK1 gave rise to an inwardly rectified potassium channel of approximately 40 pS (in a symmetric potassium solution of 145 mM) that could be reversibly activated by MgATP at a concentration of 2.5-5 mM. In this study, no clear indications were presented pointing to either phosphorylation or direct binding as the mechanism for this ATP-induced channel activation although their structural study, in which the ROMK1 c-DNA was sequenced, indicated that phosphorylation, direct binding, or both may be involved in channel activation, because ROMK1 has a putative ATP binding site near a cluster of potential phosphorylation sites that are dependent on either PKA (phosphokinase A) or PKC (phosphokinase C). Whether K_{ATP} channels and the ATP-gated K_{Ca} channels in MDCK cells share structural similarities with ROMK1 channels is not known. However, it can be expected that even if such similarities exist, there will still be subtle local structural differences, which are likely to exist in locations regarded as regulatory domains, including ATP-binding site(s), phosphorylation sites or both. Hence, ATP binding to these regulatory domains can cause the ATP-gated channel to go from either open to closed or closed to open states.

Several kinds of evidence support the idea that structural similarities exist among channels regulated by ATP-binding. These include the following: first, except for the 240 pS ATP-activated Maxi K channels of the MDCK cells, all channels

regulated by ATP via direct binding have similar conductance values, ~ 40-80 pS (with symmetrical high potassium solutions of ~ 150 mM); second, again except for the 240 pS channel, these channels are inward rectifiers with open probabilities relatively independent of membrane voltage (50); and third, these channels can be regulated by other nucleotides such as ADP, AMP and non-hydrolyzable ATP analogs. In particular, the 49 pS K_{Ca} channel that we identified in MDCK cells may be structurally most similar to the ROMK1 channels. These two channels not only have similar conductance values, but are unique among ATP-gated channels in showing no inactivation at ATP concentrations above 2.5 mM.

However, the affinity of ATP for ATP-binding potassium channels indicates that there may also be significant differences between these channels. The affinity of K_{ATP} channels for intracellular ATP is an order of magnitude higher than that of the ATP-gated K_{Ca} channels reported here. The former have dissociation constants (K_i) in a concentration range of 20-500 μM while the latter have K_i values ranging from ~ 1 mM to 2 mM. Thus, it appears that K_{ATP} channels are capable of responding to lower intracellular ATP levels than the ATP-gated K_{Ca} channels.

II.B. Comparison of kinetic properties

Burst analysis of single channel events also reveals interesting similarities and differences in the properties of these two ATP-gated channels, and in ATP's effects on these channels. For example, the 49 pS ATP-gated K_{Ca} channel has the same number of conformational states as the K_{ATP} channel in muscle cells (51): two open and three closed states. The 240 pS ATP-gated K_{Ca} channel has only one less open state than these K_{ATP} channels.

ATP has opposite effects on the opening of the 240 pS ATP-gated K_{Ca} channel and that of the K_{ATP} channel in muscle cells, judging from comparisons based on the duration of long gaps between bursts and the number of openings per burst. For the K_{ATP} channels, the dominant effects of ATP include a decrease in the number of openings per burst and an increase in the duration of the long interburst gaps (27). Our study indicates that ATP increases both the burst duration and the number of openings per burst for the 240 pS K_{Ca} channel of MDCK cells. Our kinetic model indicates that this is probably due to ATP's effects on the open conformations of the channel.

Comparisons between the 49 pS K_{Ca} channel and the K_{ATP} channel reveal similarities as well as differences between the two channels. They are similar in their bursting patterns. These two channels have similar interburst mean resident closed times: 0.118 and 4.18 ms for the 49 pS channel, and 0.40 and 2.64 ms for the K_{ATP} channel at an ATP concentration of approximately 0.5 mM (51). The channels are different in that none of the open time constants of the 49 pS K_{Ca} channel vary with ATP concentration (Figure 23), yet all three of the closed time constants vary with ATP concentration. This indicates that one effect of ATP is to alter the closed times of the 49 pS K_{Ca} channel. This contrasts with ATP's effect on K_{ATP} channels; according to Spruce et al., ATP alters open times rather than closed times in K_{ATP} channels (27).

II.C. Summary

Although there are some indications that ATP-gated channels may share similar structures, ATP exerts different effects on different ATP-gated channels. In the case of K_{ATP} channels, ATP causes an increase in the average duration of the interburst gap and a decrease in the average number of openings per burst as the result of changing this channel's open time constants. In the case of the 49 pS K_{Ca} channel in MDCK cells, ATP affects only channel closed time constants; it leads to a higher open probability. In the case of the 240 pS channel, ATP increases the overall burst duration and decreases the overall interburst gap duration, and also leads to a higher channel open probability.

III. Kinetic models for ATP gating of the K_{Ca} channels, and comparison of effects of ATP on calculated channel energy levels

III.A. 240 pS ATP-gated K_{Ca} channel

We propose a kinetic model for the ATP-gated 240 pS K_{Ca} channel based on the results obtained from single channel burst analysis (Scheme III). We chose this model because some properties of the channel's opening and closing were consistent with the predictions of this model. These properties include the dependence of the mean burst duration and also of the interburst gap duration on ATP concentration. This kinetic model predicts a mean burst duration of $\frac{1}{\alpha}(1 + \frac{C}{K4})$ and a mean interburst gap duration of $\frac{1}{\beta}(1 + \frac{K1}{C})$, where C is the concentration of ATP (20, 52), and our data analysis reveals the same dependencies of the two durations on ATP concentration.

(Scheme III)

$$C \overset{K1}{\longleftrightarrow} C\bullet ATP \underset{\alpha}{\overset{\beta}{\rightleftharpoons}} O\bullet ATP \overset{K4}{\longleftrightarrow} O\bullet ATP_2$$

Despite this consistency, this model is still to be considered merely an initial step toward studying the effects of ATP on the channel's gating behavior. There are two reasons for this. First, the model is constructed based on results obtained from analyzing only the bursting pattern instead of the fine structure of the channel gating. This is the source of the inconsistency in the number of conformational states traversed by the channel from closed to open states, between that indicated in the model (two closed and two open states) and that implied by the results of our burst analysis (one

closed and one open state). It is possible that the cutoff duration for closed events in our burst analysis was too long, leading us to miss other conformational states that may well exist. Second, we assumed a linear relationship between the mean interburst duration and the reciprocal of ATP concentration, based on the high correlation coefficient, 0.915, obtained from linear regression. But a closer look at the dependency of the interburst duration on the reciprocal of ATP concentration reveals that the interburst duration actually decreases exponentially with the concentration of ATP (with an exponent of -1.1273; the correlation coefficient was 0.999 for this fit - see Figure 49), indicating that the reaction of ATP with the channel protein may be far more complex than in the simple model suggested here.

Nonetheless, we proceeded to calculate the dissociation constants (K_i) and the rate constants in this model. This was done by equating the two theoretical mean lifetime expressions, mentioned above, respectively to two linear equations describing the dependency of the mean burst duration and the mean interburst gap duration on either ATP concentration or the reciprocal of ATP concentration (see Equations 2 and 3). The resultant values for K1, K4, α, and β are as follows: $\alpha = 4.75 \cdot 10^{-2}$ ms^{-1}, $\beta = 1.53 \cdot 10^{-2}$ ms^{-1}, K1 = 7.313 mM, and K4 = $8.767 \cdot 10^{-4}$ mM.

$$\frac{1}{\alpha}\left(1 + \frac{C}{K4}\right) = a + b \cdot C \quad \text{(Equation 2)}$$

$$\frac{1}{\beta}\left(1 + \frac{K1}{C}\right) = p + \frac{q}{C} \quad \text{(Equation 3)}$$

where a,b, p and q are values obtained from fitting the plots of mean burst duration versus ATP concentration, and interburst gap versus reciprocal of ATP concentration, using linear regression.

III.B. 49 pS ATP-gated K_{Ca} channel

Based on the dependence of the closed time constants and the independence of the open time constants on ATP concentration, and based on a Hill coefficient of 2, we propose that the 49 pS channel can be described by the following kinetic scheme:

$$C \overset{K1}{\longleftrightarrow} C\bullet ATP \overset{K2}{\longleftrightarrow} C\bullet ATP_2 \underset{\alpha}{\overset{\beta}{\rightleftharpoons}} O_1\bullet ATP_2 \quad \text{(Scheme IV)}$$

One indication that Scheme IV is appropriate for describing ATP channel gating is that it predicts a mean open time independent of ATP concentration, and a mean closed time that is a function of the reciprocal of ATP concentration. According to Colquhoun and Hawkes, the mean open time (τ_o), sometimes referred to as the unconditional mean time in all open states (52), is $\frac{1}{\alpha}$, and the mean closed time (τ_c) is $\frac{1}{\beta} + \frac{K2}{\beta \bullet C} + \frac{K1\bullet K2}{\beta \bullet C^2}$, for this model (20).

Two different strategies were used to calculate the rate constants and the dissociation constants associated with this model. In the first strategy, we equated the coefficients of three terms in two different expressions for the mean closed time of the channel. The terms are in the form $\frac{1}{[ATP]^n}$, where n = 0, 1, or 2, giving three terms as follows: a constant term $(\frac{1}{1})$, $\frac{1}{[ATP]}$, and $\frac{1}{[ATP]^2}$. The two expressions are obtained

from two different sources: one is derived from the proposed kinetic model in Scheme III ($\tau_c = \frac{1}{\beta} + \frac{K2}{\beta \cdot [ATP]} + \frac{K1 \cdot K2}{\beta \cdot [ATP]^2}$); and the other was obtained from data fitting ($\tau_c = p + \frac{q}{[ATP]} + \frac{r}{[ATP]^2}$, as will be seen later). As mentioned in the Results Section, we found three closed states associated with this channel; the time constants of two of the states are proportional to $\frac{1}{[ATP]^2}$, and the other time constant, to $\frac{1}{[ATP]}$. Thus, we equated the three closed time constants with linear expressions in the form $ax + b$, where x is either $\frac{1}{[ATP]}$ or $\frac{1}{[ATP]^2}$ as the independent variable. Then we proceeded to calculate the overall mean closed time[1]. This gave the following expression: overall mean closed time = $p + \frac{q}{[ATP]} + \frac{r}{[ATP]^2}$, where p, q and r are values that can be calculated from the results of data fitting. We then equated the corresponding coefficients of the concentration-independent terms and of the terms dependent on $\frac{1}{[ATP]}$ and $\frac{1}{[ATP]^2}$ in the two expressions mentioned above (see Equation 4) and calculated the rate constants and the dissociation constants of our model from the three resulting equations in the forms $\frac{1}{\beta} = p$, $\frac{K2}{\beta} = q$, and

---

[1]Note that all the unconditional mean life times from the single channel data fitting were obtained using the following equation: $\tau = \sum_{i=1}^{n} \frac{A_i}{\lambda_i}$, where n is the number of exponential terms used in fitting the single channel event histogram; λ_i is the rate constant of the i^{th} exponential term; and A_i is the normalized pre-exponential weight for the i^{th} exponential term.

$\frac{K1 \cdot K2}{\beta} = r$. These equalities permitted us to determine the values of all the constants except α. We obtained its value by setting the equality described in Equation 5.

$$\frac{1}{\beta} + \frac{K2}{\beta \cdot [ATP]} + \frac{K1 \cdot K2}{\beta \cdot [ATP]^2} = p + \frac{q}{[ATP]} + \frac{r}{[ATP]^2} \quad \text{(Equation 4)}$$

$$\frac{1}{\text{arithmetic mean open time, 7.57 ms}} = \alpha. \quad \text{(Equation 5)}$$

This method of calculation gave the following results: K1 = 0.320 mM, K2 = 0.940 mM, $\beta = 1.578\ ms^{-1}$, and $\alpha = 0.132\ ms^{-1}$.

Notice that this model has one less open state than that suggested by the results of our data fitting, which indicates that there are two open states. One explanation for this is that the two open states can communicate without a change in ATP binding (see scheme V).

$$C \xleftrightarrow{K1} C \bullet ATP \xleftrightarrow{K2} C \bullet ATP_2 \underset{\alpha}{\overset{\beta}{\rightleftharpoons}} O_1 \bullet ATP_2 \xleftrightarrow{K4} O_2 \bullet ATP_2$$

(Scheme V)

In addition to the calculation strategy we used above in obtaining the individual rate or equilibrium constants, we also tried to obtain some of these values using a more rigorous treatment which involves the use of matrix algebra. We started by constructing a matrix, **Q**, based on three simultaneous differential equations written for the three

closed states of the model. We then imposed five different constraints to solve this 3X3 matrix containing five parameters corresponding to the various rate constants in the proposed model, including β, k1, k2, d1, and d2 (scheme V). Note that K_1 and K_2 of Scheme III, which respectively equal $\frac{d1}{k1 \cdot [ATP]}$ and $\frac{d2}{k2 \cdot [ATP]}$, are not the actual dissociation constants. These are, for the first two binding processes, K_1' ($= \frac{d1}{k1}$), and K_2' ($= \frac{d2}{k2}$), respectively. The five constraints used were as follows: (a) the determinant of the matrix must equal the product of the eigenvalues of the matrix, (b) the initial slope of the closed dwell time histogram must reflect the conformational transition from the $C \cdot ATP_2$ state to the open state, (c) the trace of the matrix **Q** must equal the trace of **Q** after diagonalization, (d) the second invariant of the matrix **Q** must equal the second invariant of **Q** after diagonalization, and (e) the ratio of the probability that the channel resides in any closed state to the probability of the open state must equal the ratio of the mean lifetime of all closed states to the mean lifetime of the open state.

This matrix method provided us with a basis for further determination of the individual dissociation constants as well as the value of β at various ATP levels. To obtain the two dissociation constants (K_i') , we first solved the matrix **Q** at the five different ATP levels studied, and then plotted the two apparent dissociation constants versus $\frac{1}{[ATP]}$ (Figure 53). The respective slopes of these two plots are the individual dissociation constants K_1' and K_2'; the value of K_1' is 0.3268, and of K_2', 0.0346. We obtained the values of β at various ATP levels directly by imposing the five constraints mentioned. We found that the value of β varies with ATP concentration approximately linearly ($\beta = 0.785 + 0.2447 \cdot [ATP]$, correlation coefficient = 0.914). This dependence

of β on ATP concentration indicates that in addition to the transition from the bound closed $C \cdot ATP_2$ state to an open state having two bound ATP molecules, there is also a transition from this bound closed state to yet another open state involving binding to a third ATP molecule. This is depicted in Scheme VI. As to the values of α_1 and α_2, since ATP binding to this channel leads to channel activation, it is reasonable to assume that the $O \cdot ATP_3$ state has a longer lifetime than the $O \cdot ATP_2$ state. Thus, from the two fitted open time constants, we computed the values of α_1 and α_2. These are 0.104 ms^{-1} and 0.281 ms^{-1}, respectively.

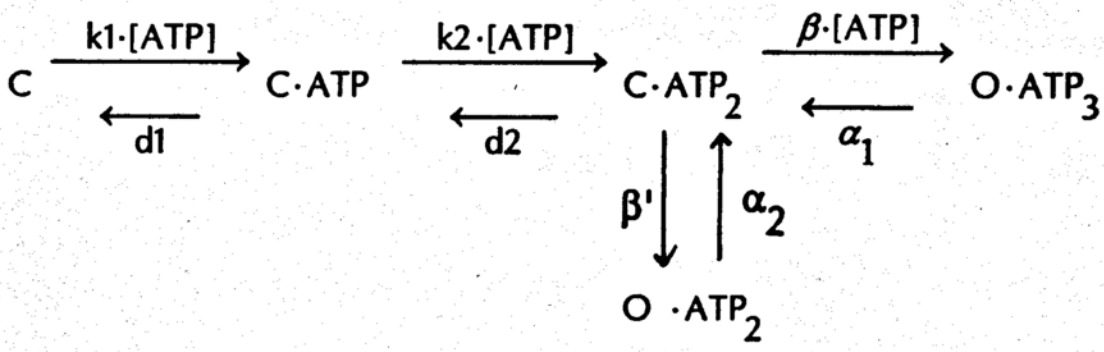

(Scheme VI)

We compared the individual values of K1, K2 obtained from the above two strategies, and found that these two methods gave very similar K1 and β values but very different K2 values. The values of K1 were 0.320 mM and 0.3268 mM,

respectively, for the first and second strategy used, and the β values[2] were 1.578 ms^{-1} and 1.29 ms^{-1}. The K2 values were 0.940 mM and 0.0346 mM. This difference appears to arise not from the methodology of the first strategy, but rather from the single channel data itself. Our calculation showed that, for this 49 pS K_{Ca} channel, the K2 value depends very strongly on the closed state with the largest time constant. The 49 pS channel had a very low probability (~ 0.42%) of residing in this long closed state at any ATP concentration. Thus, the time constant for this long closed state was obtained based on a very small number of closed events, and was subject to a large error. The combination of the channel's small probability of being in the long closed state and the large error associated with the estimated time constant renders the K2 value obtained from the first strategy invalid.

[2]The β value obtained from the latter strategy depends on the ATP concentration. An overall β value was calculated using the arithmetic mean of all β values at different ATP concentrations.

III.C. Comparison of effects of ATP binding on calculated energy levels of conformational states of the two ATP-gated K_{Ca} channels in MDCK cells

ATP binding leads to channel conformations with lower free energy levels than the initial closed states, in both the 240 ps and the 49 pS channels. This is shown in the energy diagrams depicted in Figure 55. These free energy differences are calculated based on our kinetic models described above. As can be seen from part (a) of the energy diagram, ATP binding to the 240 pS channel initially leads to a stable closed state which, with thermal energy, can easily be converted to the first open state, O·ATP, of the channel. Further ATP binding to the O·ATP conformation of the channel can lead to the conformational state with the lowest energy level, $O{\cdot}ATP_2$. This effect of ATP on the 240 pS channel is very similar to its effect on the 49 pS channel. As shown in part (b) of the energy diagram, all ATP-bound closed conformational states have lower energy levels than the initial closed state, C. Binding of two ATP molecules to this channel can lead to a closed state ($C{\cdot}ATP_2$), which is capable of undergoing conformational changes either to an open state without further ATP binding, or to another open state with a third ATP molecule bound to the channel.

However, between the two K_{Ca} channels, there is a slight difference in the energy levels of the conformations bound to ATP, which may help to explain why the opening of the 240 pS channel is more often interrupted by brief closing (flickering). Since the C·ATP state of the 240 pS channel is energetically more stable than its O·ATP state, it is to be expected that when the channel assumes the O·ATP state, it can go either forward or backward along the activation pathway to decrease its energy. Therefore, there can be very short closing events if the channel goes from the O·ATP state to the C·ATP state and back to the O·ATP state again. The situation is different for the 49 pS channel. Because all closed states of this channel have higher energy

levels than the final open states, the channel once open should stay open for some time. Hence, no short closing events are likely to occur.

Figure 53 Apparent dissociation constants calculated based on Scheme IV vary with reciprocal of ATP concentration.

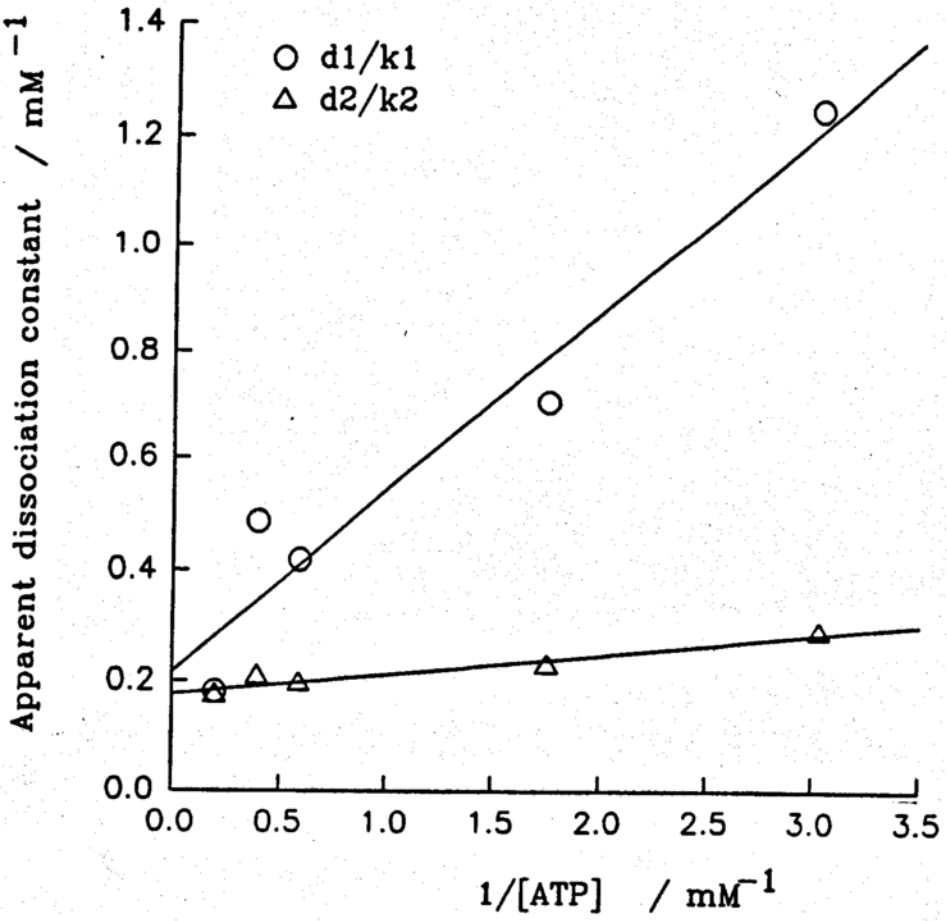

Figure 54 Rate constant β calculated based on Scheme IV varies linearly with ATP concentration.

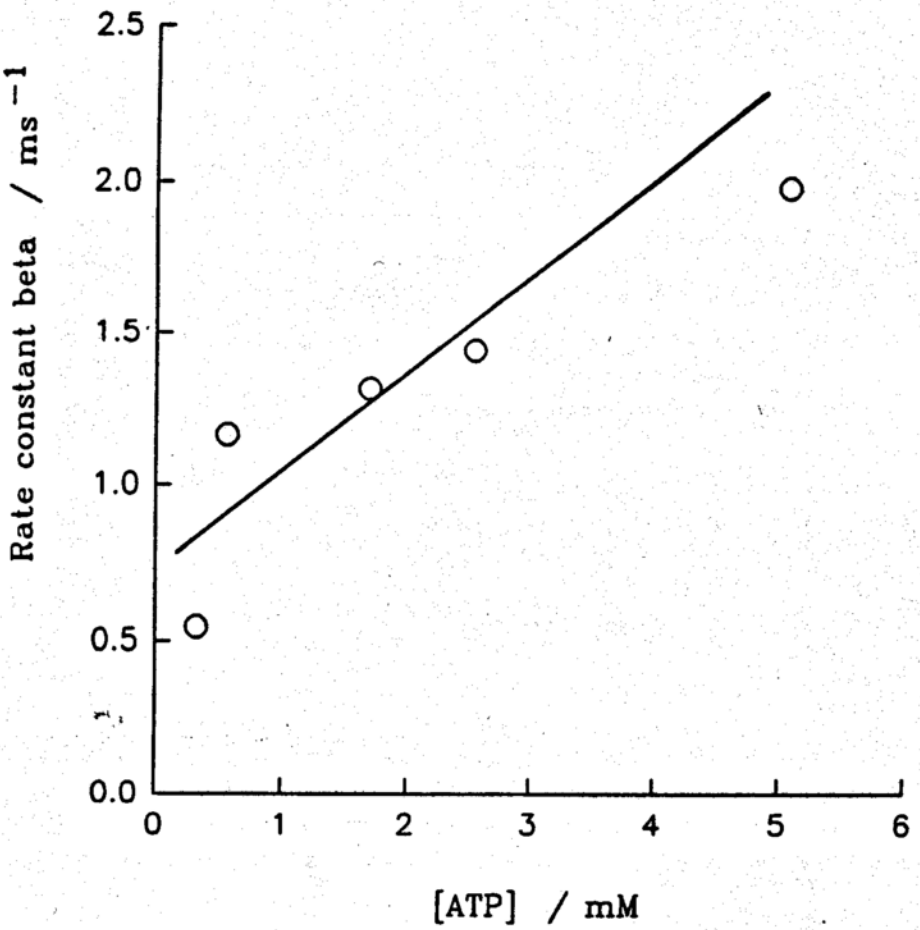

Figure 55 The relative potential energy levels of various states along the activation pathway from the initial closed state to an open state.

(a) 240 pS K_{Ca} channel. Quantities given in KCal.

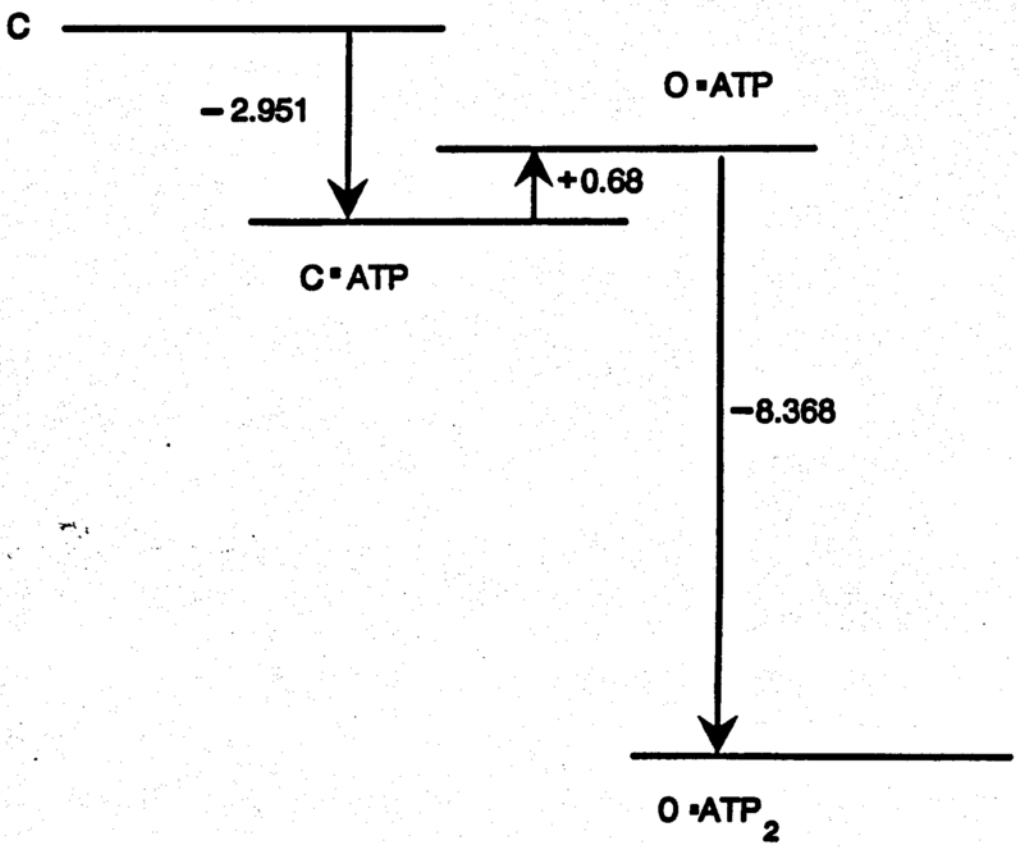

(b) 49 pS KCa channel. Quantities given in KCal.

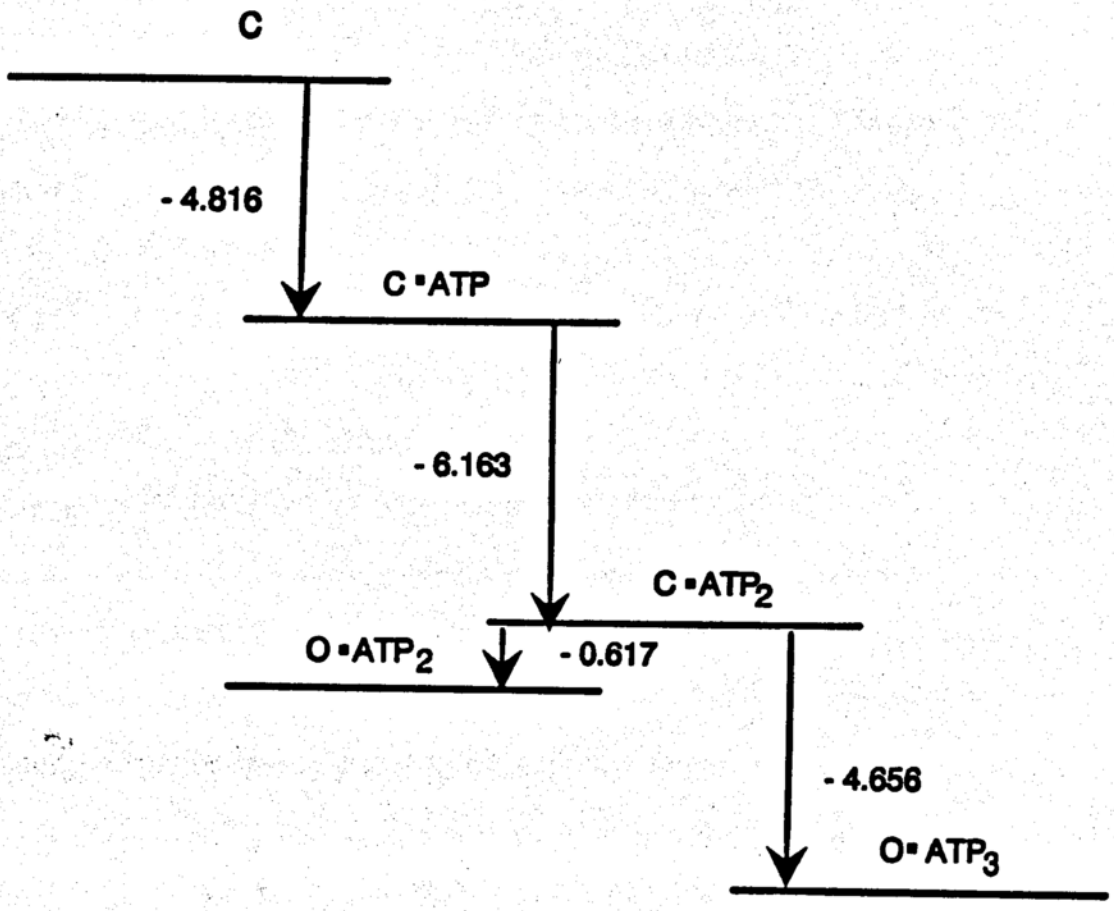

Conclusions

1. Three ATP-gated channels have been found in MDCK cells, with the following conductance values: 40 pS, 49 pS, and 240 pS.
2. The 40 pS channel is a K_{ATP} channel. This channel does not resemble other renal K_{ATP} channels in that it can be inactivated by intracellular K^+ at normal physiological levels.
3. The remaining two channels are ATP-gated K_{Ca} channels. These two channels are the only two channels reported so far that can be activated by ATP via direct binding.
4. In the case of the 240 pS K_{Ca} channel, ATP activation appears not to be mediated through changes in the gating charge of the channel since the charge factor remains unchanged at various ATP levels. In the case of the 49 pS channel, ATP appears not to interfere with channel gating through changes in the gating charge. This is because both before and after ATP activation, channel opening is voltage-independent.
5. For the large channel, ATP binding appears to cause a reduction in the value of $\Delta G^{\circ}_{\text{closed state to open state}}$ by 5 Kcal/mol. This is deduced by fitting the channel's opening at various voltages using the Boltzmann equation.
6. Our kinetic models for the two channels indicate that ATP binding to the channels has similar effects on the conformational stability of these two channels. That is, ATP binding to the channels causes changes in their potential energy levels, that eventually lead to stable open channel conformations.
7. For the 240 pS channel, the slightly higher energy level of the O·ATP state than of the neighboring closed state (C·ATP) may explain the flickering phenomenon.

References

1. Hsu, S. F. (1992). Control studies on MDCK cells using the patch-clamp. *M.S. thesis* University of Wisconsin-Madison.
2. Bolard, J. (1986). How do the polyene macrolide antibiotics affect the cellular membrane properties? *Biochim. Biophys. Acta* **864**, 257-304.
3. De Kruijff, B. and Demel, R. A. (1974). Polyene antibiotic-sterol Interactions in membranes of *Acholeplasma Laidlawii* cells and lecithin liposomes III. Molecular structure of the polyene antibiotic-cholesterol complexes. *Biochim. Biophys. Acta* **339**, 57-70.
4. Lang, F. and Rehwald, W. (1992). Potassium channels in renal epithelial transport requlation. *Physiological Reviews* **72** (1), 1-32.
5. Kone, B. C.; Brady, H. R. and Gullans, S. R. (1989). Coordinated requlation of intracellular K^+ in the proximal tubule: Ba^{+2} blockade down-regulates the Na^+, K^+-ATPase and up-regulates two K^+ permeability pathways. *Proc. Natl. Acad. Sci. USA* **86**, 6431-6435.
6. Kubota, T.; Biagi, B. A. and Giebisch, G. (1983). Intracellular potassium activity measurements in single proximal tubules of Necturus kidney. *J. Membr. Biol.* **73**, 51-60.
7. Lang, F.; Oberleithner, H. and Giebisch, G. (1986). Electrophysiological heterogeneity of proximal convoluted tubules in amphiuma kidney. *Am. J. Physiol.* **251**, F1063-F1072.
8. Boulpaep, E. L. (1976). Electrical phenomena in the nephron. *Kidney Int.* **9**, 88-102.
9. Boulpaep, E. L. and Sackin H. (1979). Equivalent electrical circuit analysis and rheogenic pumps in epithelia. *Fed. Proc.* **38** (6), 2030-2036.

10. Kolb, H. A. (1990). Potassium channels in excitable and non-excitable cells. *Rev. Physiol. Biochem. Pharmacol.* **115**, 51-91.

11 Lang, F.; Messner, G.; Wang, W. and Oberleithner, H. (1983). Interaction of intracellular electrolytes and tubular transport. *Klin. Wochenschr.* **61**, 1029-1037.

12. Lang, F.; Messner, G. and Rehwald, W. (1986). Electrophysiology of sodium coupled transport in proximal renal tubules. *Am. J. Physiol.* **250**, F953-F962.

13. Wang, W.; Sackin, H. and Giebisch, G. (1992). Renal potassium channels and their regulation. *Annu. Rev Physiol.* **54**, 81-96.

14. Guggino, S. 1986. Channels in kidney epithelial cells. In: *Ionic channels in cells and model systems*. (Latorre, R. ed.). pp 207-220. Plenum Press, New York and London. .

15 Latorre, R. (1991). Metabolic control of K^+ channels: an overview. *J. bioenergetics and biomembranes* **23** (4), 493-497.

16. McManus, O. B. (1991). Calcium-activated potassium channels: Regulation by calcium. *J. bioenergetics and biomembranes* **23** (4), 537-560.

17. Lang, F; Friderich, F; Paulmichl, M.; Schobersberger, W., Jungwirth, A., Ritter, M., Steidl, M., Weiss, H., Woll, E., Tschernko, E., Paulmichl, R., and Hallbrucker, C. (1990). Ion channels in Madin-Darby canine kidney cells. *Renal Physiol. Biochem.* **13**, 82-93.

18. Morel, F. (1981). Sites of hormone action in the mammalian nephron, *Am. J. Physiol.* **240**, F159-F164.

19. Fernandez-Castelo, S., Bolivar, J. J., Lopez-Vancell, Beaty, G. and Cereijido, M. (1985). Ion transport in MDCK cells. In *Tissue culture of epithelial cells.* (Taub M. ed.). pp 37-50. Plenum Press, New York and London.

20. Moczydlowski, E., Latorre, R. (1983). Gating kinetics of Ca^{+2}-activated K^+ channels from rat muscle incorporated into planar lipid bilayers. *J. Gen. Physiol.* **82**, 511-542.

21. Moczydlowski, E., Alvarez, O., Vergara, C. and Latorre, R. (1985) *J. Memb. Biol.* **83**, 273-282.

22. Bolotina, V., Omelyanenko, V., Heyes, B., Ryan, U. and Bregestovski, P. (1989). *Pflugers Arch.* **415**, 262-268.

23. McManus, O. B., and Magleby, K. L. (1988). Kinetic states and modes of single large-conductance calcium-activated potassium channels in cultured rat skeletal muscle. *J. Physiol.* **402**, 79-120.

24. Vaca, L. Toro, L. amd Stefani, E. (1989). *Biophys. J.* **55**, 536a.

25. Reinhart, P. H., Chung, S. and Levitan, I. B. (1989). *Neuron* **2**, 1031-1041.

26 Colquhoun, D. and Hawkes, A. G. (1983). The principles of the stochastic interpretation of ion channel mechanisms. In *Single Channel recording* (Sakmann B. and Neher E. eds.). pp. 135-175. Plenum Press. New York.

27. Davies, N. W., Standen N. B. and Stanfield, P. R. (1991). ATP-dependent potassium channels of muscle cells: their properties, regulation and possible functions. *J. bioenergetics and biomembranes* **23** (4), 509-535.

28. Wang, W., White, S., Geibel, J. and Giebisch G. (1990). A potassium channel in the apical membrane of rabbit thick ascending limb of Henle's loop. *Am. J. Physiol.* **258**, F244-F253.

29. Wang, W., Schwab, A. and Giebisch G. (1990). A potassium channel Regulation of small-conductance K^+ channel in apical membrane of rat cortical collecting tubule. *Am. J. Physiol.* **259**, F494-F509.

30. Bleich, M., Schlatter, E. and Greger, R. (1990). The luminal K^+ channel of the thick ascending limb of Henle's loop. *Pflugers Arch* **415**, 449-460.

31. Fernandez-Castelo, S., Bolivar, J. J., Lopez-Vancell, R., Beaty, G., and Cereijido, M. (1985). Ion transport in MDCK cell, in *Tissure Culture of Epithelial Cells* (Taub, M. ed.). pp 37-50. Plenum Press. New York.

32. Valentich, J. D. (1981). Morphological similarities between the dog kidney cell line MDCK and the mammalian cortical collecting tubule, *Ann. New York Acad. Sci.* **81**, 384-405.

33. Rindler, M. J., Chuman, L. M., Schaeffer, L. and Saier, M. H. Jr. (1979). Retention of differentiated properties in an established dog kidney epithelial cell line (MDCK), *J. Cell Biol.* **81**, 635-648.

34. Richardson, J. C. W., Scalera, V. and Simmons, N. L. (1991). Identification of two strains of MDCK cells which resemble separate nephron tubule segments, *Biochim. Biophys. Acta* **673**, 26-36, 1991.

35. Bolivar, J. J., and Cereijido, M. (1987). Voltage and Ca^{+2}-activated channel in cultured epithelial cells (MDCK). *J. Membrane Biol.* **97**, 43-51.

36. Ponce, A., and Cereijido, M. (1991). Polarized distribution of cation channels in epithelial cells. *Cell Physiol. Biochem.* **1**, 13-23.

37. Sabra, R., and Branch, R.A. (1990). Amphotericin B nephrotoxicity. *Drug Safty* **5**(2), 94-108.

38. Ohno-Shosaku, T., Kubota, T., Yamaguchi J., Fukase, M., Fujita, T. and Fujumoto, M. (1989). Reciprocal effects of Ca^{+2} and Mg-ATP on the 'run-down' of the K+ channels in opossum kidney cells. *Pflugers Arch* **413**, 562-564.

39. Chung, S., Reinhart, P. H., Martin, B. L., Brautigan, D., and Levitan, I. B. (1991). Protein kinase activity closely associated with a reconstituted Calcium-activated potassium channel. *Scinece* **253**, 560-562.

40. Robertson, B. E., Corry, P. R., Nye, P. C. G. and Kozlowski, R. Z. (1992). Ca^{+2} and Mg-ATP activated potassium channels from rat pulmonary artery artery. *Pflugers Arch* **421** (1), 94-96.

41. Ho, K., Nichols, C. G., Lederer, W. J., Lytton, J., Vassilev, P. M., Kanazirska, M. V. and Hebert, S. C. (1993). Cloning and expression of an inwardly rectifying ATP- regulated potassium channel. *Nature* **362** (4), 31-38.

42. Hirsch, J., Leipziger, J., Frobe, U., and Schlatter, E. (1993). Regulation and possible physiological role of the Ca^{+2}-dependent K^+ channel of cortical collecting ducts of the rat. *Pflugers Arch* **422**, 492-498.

43. Bean, B. P. and Friel, D. D. (1990). ATP-activated channels in excitable cells. In *Ion Channels* Volume 2 (Narahashi T., ed.), pp. 169-203. Plenum Press. New York.

44. Bean, B. P. (1992). Pharmacology and electrophysiology of ATP-activated ion channels. *TiPS*, **13**, 87-90.

45 Friedrich, F., Weiss, H, Paulmichl, M., and Lang, F. (1989). Activation of potassium channels in renal epithelioid cells (MDCK) by extracellular ATP. *Am. J. Physiol.* **256**, C1016-C1021.

46. Friedrich, F., Weiss, H, Paulmichl, M., Woll, E., Waldegger, S. and Lang, F. (1989). Further analysis of ATP-mediated activation of K+ channels in renal epitheloid Madin Darby canine kidney (MDCK) cells. *Pflugers Arch* **418**, 551-555.

47. Brown, D. A. (1988). M currents. In *Ion channels*, Volume 1 (Narahashi, T., ed.). pp. 55-94. Plenum Press. New York.

48. Noma, A. (1983). ATP-regulated K^+ channels in cardiac muscle. *Nature* **305**, 147-148.

49. Wang, W., Giebisch, G. (1991). Dual effect of adenosine triphosphate on the apical small conductance K^+ channel of the rat cortical collecting duct. *J. Gen. Physiol.* **98**, 35-61.

50. Rorsman, P., and Trube, G. (1990). Biophysics and physiology of ATP-regulated K^+ channels (K_{ATP}). In *Potassium channel: structure, classification, function and therapeutic potential*. (Cook, N. S., ed.). pp. 97-116. Ellis Horwood. Chichester.

51. Spruce, A. E., Standen, N. B. and Standfield, P. R. (1985). Voltage-dependent ATP-sensitive potassium channels of skeletal muscle membrane. *Nature* **316** (22), 736-738.

52. Colquhoun, D. and Hawkes, A. G. (1977). Relaxation and fluctuations of membrane currents that flow through drug-operated channels. *Proc. R. Soc. Lond. B.* **199**, 231-262.

Chapter Two

Amphotericin B

Abstract

The MDCK cell line of distal kidney cells was used as the cell model to study the effects of Amphotericin B on distal tubules in the kidneys. Our data suggest that the toxicity of Amphotericin B is related to its ability to disturb normal protein functioning rather than to the formation of Amphotericin B pores in cell membranes. In whole cells, we observed increased ion conductance across cell membranes in two types of MDCK cells after bathing the cells with electrolyte solutions containing Amphotericin B. Prior to bathing with Amphotericin B, these two types of cells exhibited different whole cell currents in response to a series of voltages ranging from -80 mV to 90 mV, clamped to the cells. Type I cells showed no significant whole cell currents at any voltage level or over time. Type II cells showed outward currents at these voltages, and these currents decreased over time. Whole cell currents in Type II cells began to increase after bathing with Amphotericin B. Whole cell conductance for Type I cells increased on average 1070% (n=3). Conductance in Type II cells increased on average 269% ± 116% (n=6). At the single channel level, we found that Amphotericin B led to higher channel activity in both inside-out and outside-out patches. At a low cytoplasmic Ca^{+2} level (~ 130 nM), the channel opening probability, recorded using inside-out membrane patches, increased from 0 to ~ 80% at hyperpolarization potentials (n=4). Similar increases were observed in outside-out patches. Single channel kinetic studies indicated that the increases in channel activity were associated with changes in the mean closed and open times of the channels.

Introduction

Amphotericin B was reported in 1956 by Gold et al. to have a potent antifungal action (1). After more than thirty years of clinical use in the treatment of most systemic fungal infections, Amphotericin B remains the drug of choice despite the introduction of several newer antifungal agents such as Miconazole and Ketoconazole (2, 3, 4). This may be because Amphotericin B has caused few types of resistance. In spite of this fact, its toxicities are of primary concern in patient treatment. The most detrimental of these is nephrotoxicity, which is manifested as disturbances in both glomerular and tubular functioning (3). Patients treated with Amphotericin B commonly exhibit symptoms such as a reduced glomerular filtration rate (GFR), azotemia, renal tubular acidosis, impaired renal concentration, and electrolyte abnormalities, especially those involving potassium and sodium ions.

The mechanisms of Amphotericin B-induced nephrotoxicity are poorly understood. Researchers speculate that it may result from both direct and indirect forms of action by Amphotericin B (5). The direct action is believed to affect lipid membranes primarily. The indirect action is thought to lead to effects secondary to activation of intrarenal mechanisms such as tubuloglomerular feedback (TGF) and the release of messenger mediators such as the Ca^{+2} ion. The mechanisms proposed to explain the indirect action of Amphotericin B emphasize an interplay of the different segments in a nephron, which is believed eventually to cause acute decreases (~ 40 - 80%) in renal blood flow and GFR, and an increase in renal vascular resistance. While the mechanisms of these indirect forms of action are still in dispute, the direct membrane effects have been extensively studied in various model systems. For this reason, we restricted our investigation to the direct membrane action of Amphotericin B.

One explanation for the direct membrane action of Amphotericin B is the sterol hypothesis (6). According to this hypothesis, Amphotericin B binds to sterol molecules such as cholesterol in the cell membranes of tubular cells; this binding is believed to induce increases in ion permeabilities, leading to a loss of electrolytes from the interior of a cell. Some have suggested that Amphotericin B molecules, in complexes with the membrane sterol, can form aqueous pores of approximately 40-105 nm in diameter (7, 8). Several lines of evidence indicate the formation of such an aqueous pore. In planar lipid bilayer studies, the electrical resistances of sterol-rich membranes treated on both sides with Amphotericin B (in a concentration range of $5 \cdot 10^{-8}$ to $2 \cdot 10^{-7}$ M) decreased one million times, whereas untreated membranes remained unchanged, and the correlation between aqueous salt concentration and resistance was found to approach -1 (6, 9). This is similar to the correlation observed in bulk water. Also, chloride ion fluxes across black lipid membranes treated on both sides with Amphotericin B were found to obey the Goldman-Hodgkin-Katz field equation (10). Since this equation was derived to describe ion fluxes across aqueous pores imbedded in a nonpermeable barrier, it was concluded that aqueous pores formed as a result of Amphotericin B treatment.

Another convincing piece of evidence of pore formation is the on-off patterns of current flow driven by potential differences across single Amphotericin B defects in different ionic environments. These current traces resemble those of typical transport protein channels (11, 12), and suggest that the interaction between Amphotericin B and sterol molecules results in a dynamic Amphotericin B channel whose conductive property, reflecting an equilibrium between dissociation and association, depends on the ionic environment bathing the channel.

The sterol hypothesis is supported by the following evidence. First, results obtained from monolayer studies indicate a preferential interaction between sterol molecules and several polyene antibiotics which are structurally similar to Amphotericin B (28). For example, nystatin and filipin can penetrate cholesterol monolayers and mixed lipid monolayers containing cholesterol. Second, results from studies of *Acholeplasma Laidlawii* and liposomes indicate that planar sterol molecules having a 3β- OH group and a hydrophobic side chain at C_{17} were required for Amphotericin B to induce leakage of small molecules and ions from these cells and liposomes. These molecules include K^+, Na^+, Rb^+, Li^+, ribose, xylose, and urea (15). *Acholeplasma Laidlawii* is unique in that it can grow and synthesize membranes with or without a sterol component. Because it cannot synthesize its own sterols, when grown in a sterol-containing medium, *Acholeplasma Laidlawii* can integrate the added exogenous sterol into its membrane. It can therefore be used as a membrane model whose cholesterol composition can be controlled. Other evidence came from studies of Amphotericin B in aqueous solutions. UV absorption spectra revealed that the addition of free cholesterol to aqueous solutions of Amphotericin B resulted in decreased absorptivities at certain absorption maxima, indicating that binding may occur. This phenomenon has not been observed in the absence of cholesterol (25). Also, Witzke et al. (28) and Strauss (29) studied the strength of binding between lipids and Amphotericin B. They found that the total binding strength increased with the cholesterol content of the lipids.

However, some researchers have challenged the idea that sterol is required for Amphotericin B molecules to create membrane defects that allow bulk flow of ions because both Amphotericin B-phospholipid binding and permeability increases have been observed in sterol-free small unilamellar and multilamellar vesicles (30, 31).

Doubts have also been raised concerning the in vivo formation of Amphotericin B pores as a result of Amphotericin B treatment, because of the following conflicting evidence. Indications of the existence of Amphotericin B pores have been observed only in black lipid membranes, both sides of which were treated with solutions containing Amphotericin B. These pores were anion selective, with typical anion transfer numbers averaging approximately 0.9 in solutions with various concentrations of KCl and NaCl (13). Across these channels, the permeability ratio of K^+/Cl^- was 0.15, and that of K^+/NO_3^- was 0.37 (10). However, this anion selective property has been contradicted by indications from both cell and liposome studies which reveal that the major side effect of Amphotericin B is a loss of cations, especially K^+ (14, 15, 16, 17, 18).

Results obtained from bilayer membrane models treated with Amphotericin B on only one side of the membrane may better reflect the effects of Amphotericin B in vivo (for example, its effects on kidney tubular cells). Many membrane models bathed with Amphotericin B on only one side of the membrane exhibit cation-selective leakage that seems to parallel the findings observed in patients undergoing Amphotericin B treatment. These models include black lipid membranes, using either the cis or the trans side of a bilayer membrane; cells, using the extracellular side of the cell membrane; liposomes, using the exterior surface of a liposome. Therefore, in vivo, Amphotericin B is likely to interact with a cell only on the extracellular side of the membrane.

Structural studies, regarding the one-sided effects of Amphotericin B on lipid membranes, showed structural variation in Amphotericin B-lipid complexes formed in bilayer membranes as a result of bathing the membranes with Amphotericin B. This lack of a consistent structure indicates that the Amphotericin B pore is probably not the

mechanism of the increased membrane permeability associated with Amphotericin B treatment, because the Amphotericin B pore, it has been pointed out, has an unvarying structure in lipid membranes (13), as concluded from various spectroscopic studies, using liposomes. For example, circular dichroism has detected the formation of more than one type of complex as a result of Amphotericin B binding to lecithin-sterol small unilamellar vesicles (32, 33, 34, 35). The quantitative importance of each membrane-Amphotericin B complex species was shown to depend on parameters including the ratio of Amphotericin B to lipid, the time elapsed after mixing of Amphotericin B and sterol, the amount of sterol present, and the properties of the sterol present. The role of each of these complexes in relation to the permeability increase of the membrane, however, is not known.

Results from black lipid membranes treated on one side with Amphotericin B also support the idea of non-pore membrane defects. Cass et al. have reported that the one-sided action of Amphotericin B, even in successive black lipid membranes formed using the same membrane-forming solution, was "highly irreproducible", based on resistance measurements. The variation in membrane resistance exceeded a thousand-fold (9). This implied that no channel had formed, because the membrane resistance resulting from the two-sided action of Amphotericin B on black lipid membrane is highly reproducible (within 10% of the mean resistance value) and can be achieved in 30 minutes. These observations are consistent with the findings of Borisova et al. (10), who reported that upon the addition of 10^{-4} M Amphotericin B (a relatively high concentration) to one side of a cholesterol-containing film, the membrane conductance increased about 10-fold, but no discrete current jumps were observed. These facts indicate that Amphotericin B is able to enter the membrane structure and disrupt its integrity via a non-pore-forming mechanism.

In summary, although the effect of Amphotericin B in various membrane models is always to cause an increase in the permeability of these membranes to small molecules and ions, the nature of the membrane defects created by Amphotericin B is not known, despite extensive studies designed to elucidate the structures of Amphotericin B-lipid complexes.

Statement of the problem

Amphotericin B has been the drug of choice for systemic fungal infections. However, its side effects, especially nephrotoxicity, often force termination of the treatment, increasing the risk of recrudescence of the infectious disease. The nephrotoxic action of Amphotericin B is believed to occur as a consequence of its ability to modify the structures of cell membranes. It has been proposed that Amphotericin B can interact with the sterol molecules in a cell membrane resulting in the formation of aqueous channels approximately 40 - 100 nm in diameter (7, 8, 15). These channels, termed Amphotericin B channels, in the lipid membranes are believed to cause electrolyte leaks from intact kidney cells and eventually to lead to electrolyte imbalances as observed clinically (3, 36).

However, certain evidence indicates that the formation of Amphotericin B channels cannot be the mechanism for the electrolyte loss seen clinically. The Amphotericin B channel has been characterized as anion selective (10), and found to exist only when both sides of a lipid membrane are exposed to Amphotericin B. Therefore, it is not likely that Amphotericin B channels can form in the membranes of kidney tubular cells since Amphotericin B has never been observed to translocate across these lipid membranes. Even if anion-selective pores do form in the apical membranes of tubular cells, the expected consequences of these pores cannot explain certain clinical manifestations. Since, under normal physiological conditions, the concentration of Cl^-, the main anion in urine, is higher than in plasma, it is logical to assume that the presence of Amphotericin B channels in kidney tubules will cause a larger than usual Cl^- influx into kidney tubular cells. Two consequences are expected to ensue from the Cl^- movement:

1) More Na^+ in the glomerular filtrate will move across the tubular cell membranes and enter the tubular cells through the existing transcellular pathways, driven by the increase in the electrical driving force created by the Cl^- influx.
2) Cl^- uptake by the body will increase.

These consequences suggest that in patients undergoing Amphotericin B treatment, the levels of Na^+ and Cl^- will be higher than in patients not undergoing treatment. This, as we know, is the reverse of what is seen clinically. As a matter of fact, Na^+ supplements (to counteract the Na^+ wasting caused by Amphotericin B) have been found to reduce Amphotericin B's nephrotoxicity (3, 4).

Another line of evidence against pore-forming as the mechanism of Amphotericin B's toxicity is the observation that cells such as erythrocytes treated with Amphotericin B always generate cation leaks, in particular K^+ leaks, from the interiors of the cells (14). This further denies the role of an anion-selective Amphotericin B channel in causing Amphotericin B-induced electrolyte wasting.

To explain the electrolyte wasting caused by Amphotericin B, non-pore mechanisms must be invoked. For example, disruption of the lipid ordering in the membrane structure after Amphotericin B treatment may constitute a non-pore mechanism responsible for Amphotericin B's toxicity in vivo. We propose a new way to study the Amphotericin B-induced changes in ion transport across the cell membrane. The activity of an ion channel (K^+) is used to quantify the extent of such change. The reason for using a K^+ channel is that its function has been associated with acidosis, one of the commonly seen Amphotericin B toxicities. We believe that the functioning of this protein channel is influenced by Amphotericin B.

To quantify the extent of cation leakage, we propose using both the changes in resting cell membrane potential and membrane current as ways to evaluate the degree of cation loss from cells. Since, as mentioned previously, cation leakage is usually associated with Amphotericin B treatment, we suspect that this outward movement of cations may cause a shift in the resting membrane potential.

The experimental protocol for this study is as follows:

1) To measure the membrane potential change induced by Amphotericin B and thus to quantify the degree of cation leakage.
2) To evaluate the effects of Amphotericin B on membranes via transport protein markers, specifically K^+ channels.

We expect that

1) If the cation leakage induced by Amphotericin B is pronounced enough, a hyperpolarization of the membrane potential may occur as a result of the loss of intracellular potassium.
2) The activity of the channel marker may change since the channel, after the Amphotericin B treatment, is in a somewhat disturbed lipid environment.
3) If 2 is found to be true, then we will see a change conductance at the whole-cell level after Amphotericin B treatment.

In summary, the goal of this study is to elucidate the mechanism of Amphotericin B toxicity in kidney tubular cells, using the patch-clamp technique, in the conditions most similar to those found in vivo. We use MDCK cells as the cell model for distal kidney tubular cells because it is a well-established epithelial cell line that in many respects resembles distal tubular cells (19, 20, 21, 22). The patch-clamp technique, developed by Hamill et al. (23), offers advantages over other electrical recording methods in that it allows electrical recording in either a live cell or a patch

of cell membrane obtained from a live cell. Because a tight seal is formed between the recording micropipette and the membrane patch under investigation, current fluctuations measurable in picoamperes can be detected. This allows us to discern whether pore formation is the mechanism responsible for the nephrotoxic effects of Amphotericin B.

Experimental

Tissue culture

The experimental procedures concerning cell culture are identical to those described in Chapter One.

Electrolyte solutions and solutions containing Amphotericin B

The pipette solution bathing the cytoplasmic face of the membrane, used in both outside-out single channel recording and whole cell current recording, contained (in mM): NaOH, 10; KOH, 141; Methanesulfonic acid, 154; $Ca(OH)_2$, 2; $Mg(OH)_2$, 1; glucose, 10; and Hepes, 10. The solution bathing the extracellular face of the membrane, also used in both outside-out single channel recording and whole cell current recording, contained (in mM); NaOH, 146; KOH, 5; Methanesulfonic acid, 154; $Ca(OH)_2$, 1.54; $Mg(OH)_2$, 1; EGTA (ethylene glycol bis(β-aminoethyl ether) N, N, N', N'-tetraacetic acid), 2.3; glucose, 10; and Hepes (N-2-hydroxyethylpiperasine-N'-2-ethylsulfonic acid), 10. Channel blocking solutions were prepared by spiking the prepared patch clamp solutions with 10 mM of individual channel blockers, either TEA or CsCl. The solution used to investigate the effects of Amphotericin B on channel kinetics in inside-out membrane patches was a symmetric high potassium solution with a free Ca^{+2} level of 2 μM. This solution contained (in mM): K gluconate, 150; glucose, 10; Hepes, 10; $CaCl_2$, 1; and EGTA, 1.03. The rest of the inside-out patch clamp study used a symmetric high potassium solution with a low Ca^{+2} level of ~ 130 nM. It contained (in mM): NaOH, 10; KOH, 141; Methanesulfonic acid, 154; $Ca(OH)_2$, 2; $Mg(OH)_2$, 1; glucose, 10; and Hepes, 10.

Saturated solutions containing Amphotericin B were prepared by spiking 10 ml of appropriate bathing solutions with 4 mg of Amphotericin B (Sigma, St. Louis, MO).

In order to eliminate possible side effects of surfactants such as sodium deoxycholate on the cell membranes and proteins, we avoided using them to increase Amphotericin B's solubility in the electrolyte solutions. The amounts of Amphotericin B dissolved in these electrolyte solutions were estimated by UV spectrometer. The concentration of Amphotericin B in the various bathing solutions was approximately $6.8 \cdot 10^{-8}$ M.

In studies of Amphotericin B using various membrane configurations, control currents were first recorded immediately after achieving the desired patch clamp configurations. The original bathing solutions were then replaced by the Amphotericin B bathing solution in order to monitor the effects of Amphotericin B on the patches. Because of the instability of the gigaseals, all experiments had to be limited to two hours.

Single channel recording

The experimental procedures concerning single channel recording are identical to those described in Chapter One.

Voltage control and data aquisition system

The experimental procedures concerning the voltage control and data aquisition system are identical to those described in Chapter One.

Results

Three different membrane configurations were used to study the effects of Amphotericin B on MDCK cells. Two types of cell-free membrane patches were used: inside-out and outside-out. The third configuration used whole cells. A control study was performed using each patch or whole cell prior to the addition of Amphotericin B to the membrane bathing solution. Before and during exposure to Amphotericin B, current traces were obtained by means of voltage clamping and simultaneous monitoring of membrane currents, or else membrane potentials were measured using current clamping.

I. Potential measurements

The average resting membrane potential of MDCK cells measured using the traditional micropuncture technique has been reported to be -40.5 ± 1.5 mV (37). However, using the patch clamp technique, our measurements of resting membrane potential, which ranged from +20 mV to -90 mV, showed a significant deviation from the reported average value. We have not been able to explain this wide range of observed resting membrane potentials. We decided that only the cells exhibiting resting membrane potentials close to the reported average would be used to evaluate the effects of Amphotericin B on resting membrane potential. Figure 1 shows the typical effect of Amphotericin B on the resting membrane potential of an MDCK cell. As shown in Figure 2, the average resting membrane potential prior to Amphotericin B treatment was -38.4 ± 16.4 (n=7) mV while the average resting membrane potential after Amphotericin B treatment was found to be -53.7 ± 26.6 (n=7) mV.

II. Effects of Amphotericin B on single potassium channel activity

II.A. Effects of Amphotericin B on the activity of single channels in outside-out patches

The results of our Amphotericin B studies using outside-out membrane patches fall into four categories. First, some outside-out patches showed no channel activity at all prior to treatment with Amphotericin B, and bathing them with Amphotericin B solutions until the end of the experiments did not alter even the DC level of the baseline currents across these membrane patches. We interpreted this as indicating the absence of ion channels in the patch, which meant that only membrane lipids were present. This seemed to indicate both that , in terms of ion leakage, Amphotericin B had very limited effects on the lipid components of a cell membrane, and that the gigaseal between the measuring pipette and the membrane patch was stable during the treatment.

The second category is similar to the first except that the experiments in this case were terminated due to gradual loss of the tight seal. Two factors may account for this loss: instability of the cell-free patches, and effects of Amphotericin B on the patches. We believe that the loss is due mostly to the first factor - the intrinsic instability of a tight seal - since we observed in many instances that Amphotericin B could bathe channel-free membrane patches for more than 2 hours without altering channel-free current traces (the DC level of the current traces).

In the third category, there was no channel activity before addition of Amphotericin B, but channel events were detected after treatment with Amphotericin B (Figure 3, (a) and (b)). Since we monitored channel activity prior to treatment for ~ 20-30 minutes, these channel events appear to have been caused by Amphotericin B.

In the fourth category, channel opening was observed prior to the addition of Amphotericin B, and the opening probability increased further after its addition. The characteristics of single channel activity both before and after the addition of Amphotericin B are listed in Table 1 for two different patches, each containing only one channel. The change in channel opening is shown in Figure 3(c) and 3(d). We also observed that the increase in channel activity in the latter two categories occurred only after more than half an hour.

In summary, our observations indicated that Amphotericin B had minimal effects on outside-out membrane patches lacking protein channels, but it led to greater single channel activity in outside-out patches with protein channels. The evidence for Amphotericin B's minimal effects in the first case is that Amphotericin B caused no detectable changes, in either the DC levels of the currents or the noise levels associated with these currents, in patches showing no single channel activity. Our observations thus contradict the theory of the Amphotericin B pore as the mechanism for Amphotericin B toxicity. However, our observations do not eliminate the possibility that bathing the membranes with Amphotericin B may cause the formation of small aqueous pores in the membranes. Instead, the findings here suggest that Amphotericin B affects membrane proteins more than it does membrane lipids; hence, changes in the functioning of membrane proteins may largely account for the in vivo toxic action of Amphotericin B. The results of our further studies using both inside-out and whole cell membranes support this explanation.

II.B. Effects of Amphotericin B on the activity of single channels in inside-out patches

The results of the inside-out patch studies were similar to the findings observed in the outside-out patches. Channel activity increased at various voltage levels as a result of bathing with Amphotericin B. Like those observed in the outside-out patches, the increases did not occur immediately after Amphotericin B treatment, but were observed after more than half an hour. Figure 4 shows the average increases in channel activity at various voltage levels for four different patches. In all four of the patches, the probability of opening was zero prior to Amphotericin B treatment.

The effects of Amphotericin B on channel kinetics were studied in one inside-out patch where an inwardly rectified K_{Ca} channel of 52 pS was identified before Amphotericin B was added to the bathing solution (Figure 5). In order to compare changes in channel kinetics before and after Amphotericin B treatment, we recorded single channel current fluctuations throughout the entire experiment in the presence of moderate levels of free Ca^{+2} (~ 2 μM), in contrast to all the other experiments reported here, in which we used low levels of free Ca^{+2} (~ 130 nM). This prevented a complete rundown of channel activity prior to Amphotericin B treatment, and allowed us to analyze the kinetic properties of a channel prior to Amphotericin B treatment. As indicated in Figure 6, we found that at four different voltage levels, the opening probability increased over time. The most dramatic effects of Amphotericin B appear to be associated with channel gating at the lowest voltage level investigated (-40 mV) and at the longest recorded elapsed time after Amphotericin B treatment (Figure 7). Notice also that prior to Amphotericin B treatment, opening occurred more frequently at higher membrane voltages. This trend was reversed after Amphotericin B treatment.

The change in opening probability may be explainable by reference to changes in the kinetic properties of a channel. Through kinetic analysis, we realized that the effect of Amphotericin B was partly related to a change in the average dwell time of the longest closed state of the channel. We found that closed events of the channel both before and after Amphotericin B treatment could be described by a single sum of three exponential terms. The two shorter closed time constants remained unchanged throughout the experiment at all voltages studied, but the longest closed time constant changed dramatically at lower voltages (Figure 8). Since the pre-exponential weights for the three closed time constants did not vary significantly (not shown), the decrease over time of the longest time constant caused by Amphotericin B was an important factor that contributed to the channel's increased opening probability. The changes in open time constants due to Amphotericin B also played a part in altering the opening probability of this channel. This is because of the finding that a histogram of the number of events versus the open duration before Amphotericin B treatment could be described by a single exponential decay, whereas for a histogram after treatment, a sum of two exponential terms was required (Figure 9). At all voltages studied, the additional exponential terms with the longer time constants had larger pre-exponential weights, indicating an increase in the overall average duration of an open event (see Figure 9 legend).

At the single cell level, in both the inside-out and outside-out configurations, Amphotericin B thus appeared to have widespread effects on ion channels. The addition of Amphotericin B to either the cytoplasmic side or the extracellular side of a cell membrane, through the use of cell-free patches, caused similar increases in channel activity. Amphotericin B caused changes in the channel activity of both Ca^{+2}-activated and non-Ca^{+2}-sensitive channels. Some of the channels studied were

not Ca^{+2}-activated channels because they opened even though all but one of the patches were studied in solutions with low Ca^{+2} levels (~ 130 nM). Also, the time required for the effects of Amphotericin B to appear, in most cases longer than half an hour, indicated that Amphotericin B did not interact with any of the channels as a specific ligand but rather as a non-specific agent, through a partitioning process with these channels. This partitioning may be mediated by membrane lipids or it may occur within the hydrophobic domain of the protein channels itself.

III. Effects of Amphotericin B on whole cell currents

In the control whole cell study, we found two types of current responses to a series of clamped voltage levels (Figure 10a). Based on the current profiles, we categorized the MDCK cells into two different types. Type I cells had no obvious conductances at any voltage level tested, while Type II cells showed significant whole cell conductances. In many Type II MDCK cells, whole cell currents decreased over time at all voltage levels tested (Figure 10b). These differences in whole cell currents in individual cells from a cloned cell line could be due to a dependence of channel expression in cell membranes on factors such as the cell cycle. Moody et al. have observed cyclic expression of various channels during the development of an Ascidian egg (27).

One reason for the disappearance of whole cell currents among the Type II cells over time may be washout. In general, the washout observed during whole cell patch clamping is thought to occur due to a loss of certain important intracellular signaling molecules because of the cell's exposure of its cytoplasm to the pipette solution. Whole cell patch-clamping allows fast free diffusion to occur between the pipette solution and the cell's cytoplasm (24). We suspect that in our experiment, the signaling molecule involved in the decrease in Type II whole cell currents was Ca^{+2}, because EGTA, a Ca^{+2} chelater, was added to the pipette solutions to prevent resealing of the membrane patch after the whole cell configuration had been achieved. It is likely that the EGTA in the pipette solution diffused into the cytoplasm of the cell and bound to all the intracellular free Ca^{+2} needed to generate channel currents. A decrease in intracellular Ca^{+2} has been shown to lead to the closing of many types of Ca^{+2}-dependent channels. As to the Type I cells, since the whole cell conductances

started out as insignificant, washout of any signaling molecules should have a minimal effect on channel conductances. In fact, this was what we observed.

We tested the effects of Amphotericin B on the whole cell currents of both types of cells. Type I whole cell currents at all voltage levels tested increased as a result of Amphotericin B treatment. Figure 11 illustrates one series of current recordings. In this cell, controlled currents at eighteen different voltage levels, ranging from -80 mV to 90 mV in steps of 10 mV, were first recorded immediately after forming the whole cell configuration for patch-clamping. Four and a half minutes later, the original bathing solution was replaced by a bathing solution containing Amphotericin B, and currents at each voltage level were then recorded as a function of elapsed time for another hour. The average responses from three whole cells are shown in Figure 12. It is evident that, in Type I cells, Amphotericin B caused a dramatic increase in whole cell conductance.

Detailed examination of the increases in whole cell conductance of Type I cells revealed that Amphotericin B brought about different patterns of current increase in different cells. As illustrated in Figures 11 and 13 for the Type I cells, Amphotericin B could induce a whole cell conductance that was either linear or showed inactivation at high depolarization levels. These induced currents were similar to some of the whole cell currents recorded in the control studies of Type II cells (not shown). This phenomenon indicates that Amphotericin B might only be capable of modifying the activity of channels already present in the membrane instead of creating new conduction pathways, and channel expression in the cell membrane might still depend on factors such as the cell cycle and the maturity of the epithelial monolayer, which are entirely independent of the presence of Amphotericin B. Conductance changes in the Type II cells support this idea because the increase in whole cell conductance

remained similar in shape (linear, inactivation or outward rectification) after Amphotericin B treatment.

Another feature associated with the responses of MDCK cells to Amphotericin B treatment is shown in Figure 13. Decreases in current responses occurred at t = 28, 37, and 41 minutes. These decreases were observed soon after recording dramatic increases in whole cell conductances caused by Amphotericin B. The conductances following these decreases were found to be larger than those just before the decreases. These phenomena may relate to the cell's attempts to maintain homeostasis.

A positive effect of Amphotericin B on Type II whole cell conductance was observed in six out of the eight cells studied. In these six cells, we observed net current increases as a result of adding Amphotericin B to the bathing solution (Table 2). One such whole cell response is shown in Figure 14. The average increase in conductance for the six cells was from 2.903 ± 1.519 to 7.137 ± 4.610. Note that the conductance values reported for those prior to Amphotericin B treatment were recorded just before the addition of Amphotericin B to the cells. This represents an overall average increase in conductance of 269%. In two other cells, net conductance decreases were observed even after the addition of Amphotericin B. These conductance decreases may be due to termination of current recordings before the effects of Amphotericin B could be observed.

In summary, the observed increases in whole cell conductance due to the presence of Amphotericin B again support our conclusion that the in vivo toxic effects of Amphotericin B are caused by changes in membrane proteins instead of membrane lipids, and are predicted by the single channel studies. This increase was observed in all Type I cells, and in 75% of the Type II cells. The results obtained from both the Type I and the Type II cells reflect these effects of Amphotericin B. As previously

mentioned, the Type I cells exhibited no current at any of the clamped voltage levels before bathing with Amphotericin B, and their negligible whole cell currents at various voltage levels showed no time dependency. Also, before bathing with Amphotericin B, the Type II currents either decreased or remained stable as time elapsed.

Figure 1 Effect of Amphotericin B on the resting membrane potential of a MDCK cell as a function of time.

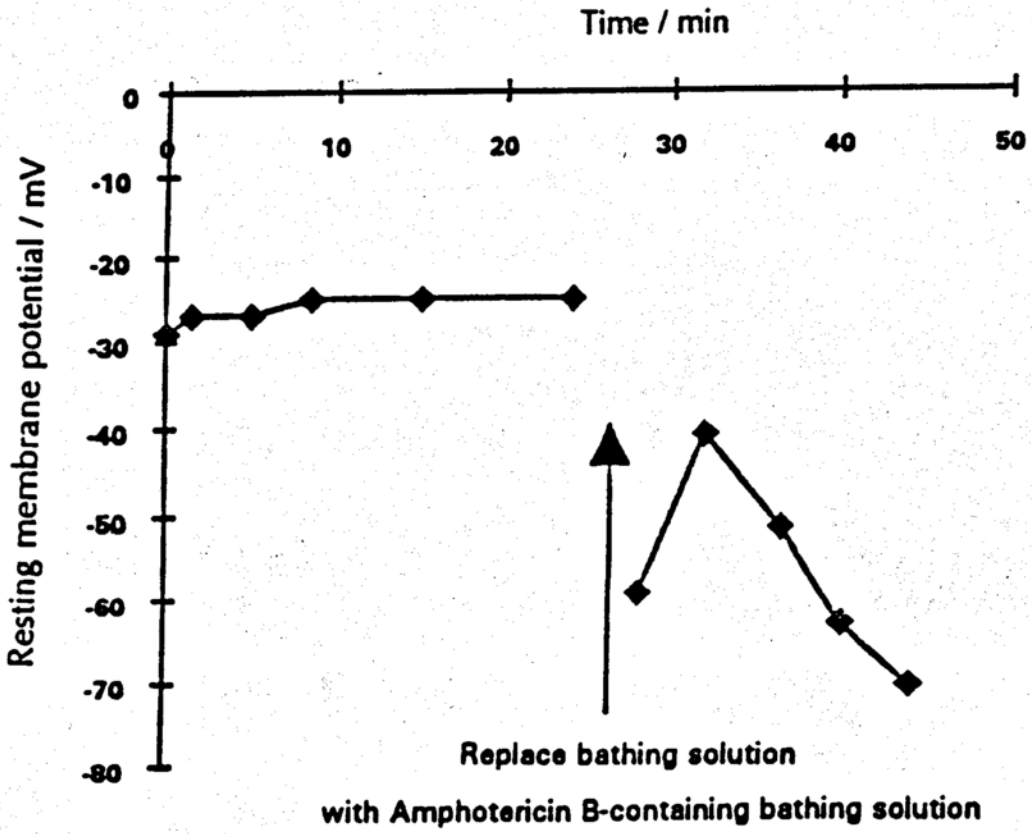

Figure 2 The average resting membrane potential* before and after Amphotericin B treatment

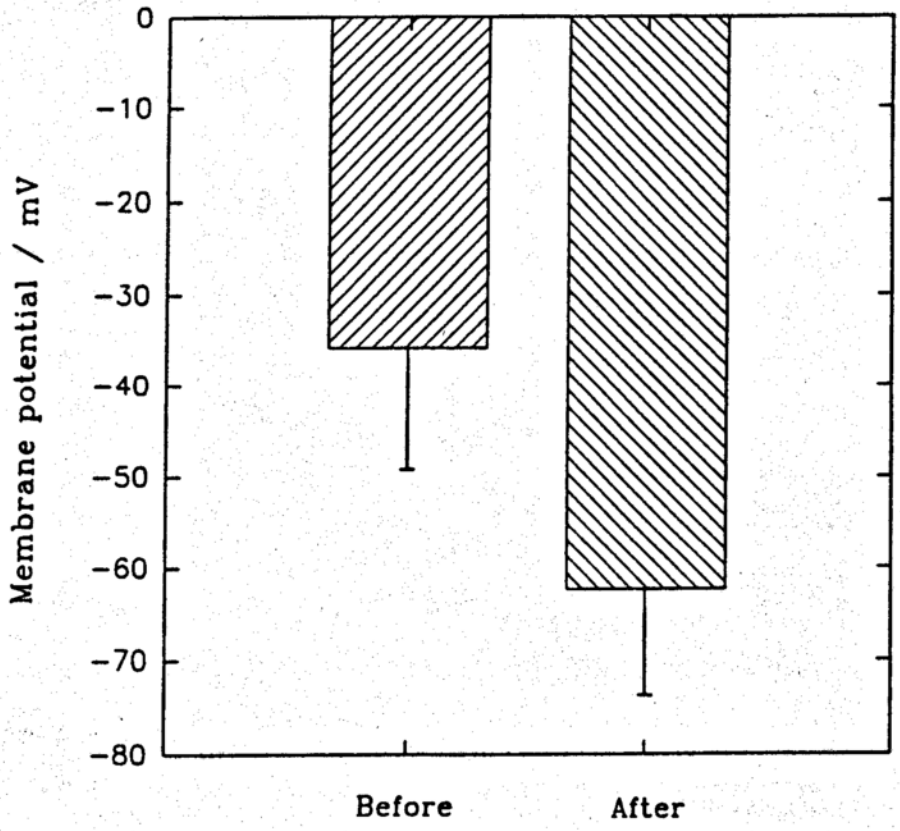

* The average membrane potential after Amphotericin B treatment was calculated using the highest hyperpolarization levels achieved during Amphotericin B treatment. The average membrane potential before Amphotericin B treatment was calculated based on the membrane potentials right before replacing the bathing solutions with the Amphotericin B containing bathing solutions.

Figure 3. Effects of Amphotericin B on outside-out membrane patches. (a) and (b) are current traces obtained from a patch that originally showed no channel activity at a holding potential of 80 mV. (c) and (d) are current traces from another patch, containing a channel whose opening probability was ~ 30 % at 75 mV prior to addition of Amphotericin B. (a) Single channel current recording showed no channel opening prior to exposure to a saturated solution of Amphotericin B. (b) In the same membrane patch, single channel currents appeared at approximately 45 minutes after addition of Amphotericin B. (c) In another outside-out membrane patch, the opening probability prior to addition of Amphotericin B was ~ 30 %. (d) In the same membrane patch as in (c), the opening probability at the same holding voltage, +75 mV, doubled after addition of Amphotericin B to the bathing solution.

(a) Holding at 80 mV prior to the treatment of Amphotericin B

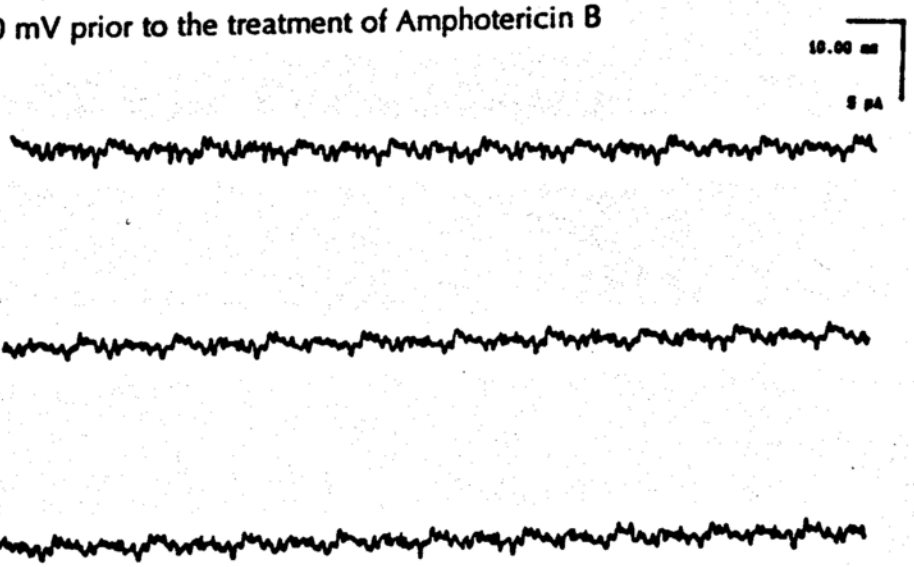

(b) Holding at 80 mV after the treatment of Ampbotericin B

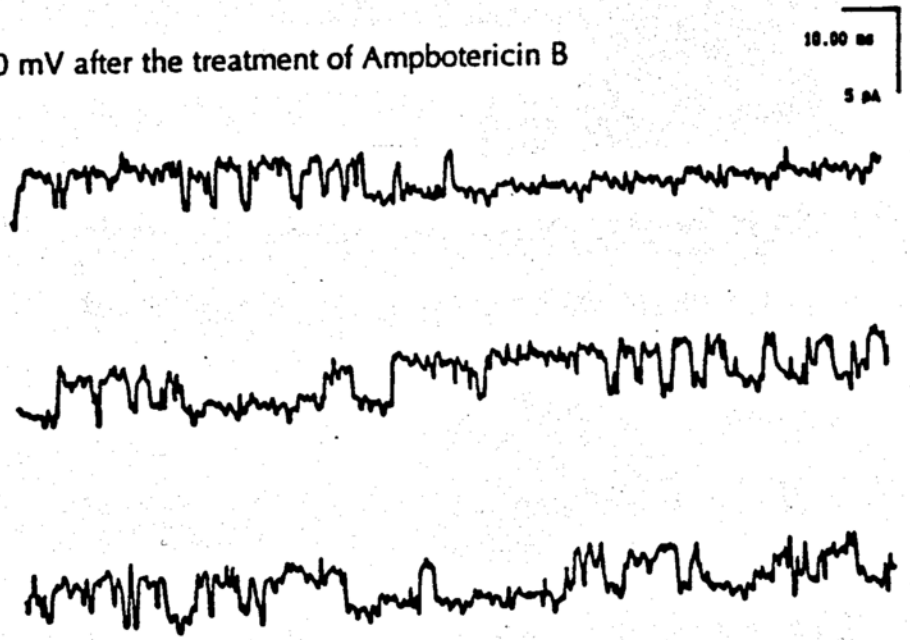

(c) Prior to the Amphotericin B treatment at 75 mV

(d) After the Amphotericin B treatment at 75 mV

Figure 4. Effects of Amphotericin B on inside-out membrane patches. Prior to addition of Amphotericin B, the open probabilities of these channels were zero at all voltage levels studied. After addition of Amphotericin B, the opening probabilities eventually increased to ~ 80% (n=4) at hyperpolarization membrane potentials. These channels appeared to be inwardly rectified because no opening events were observed at depolarization membrane potentials.

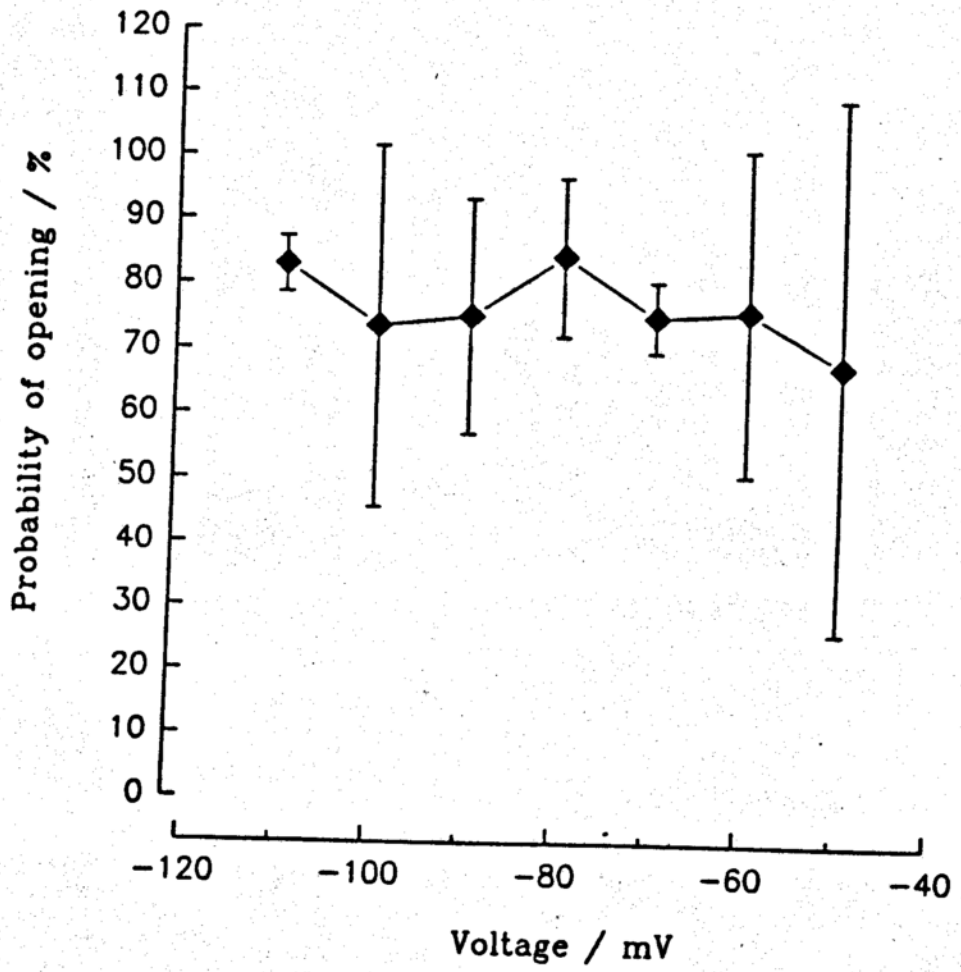

Figure 5 Conductance and calcium dose-response characteristics of the 53 pS channel used in studying the effects of Amphotericin B on channel kinetics using the inside-out configuration

(a) Conductance plot

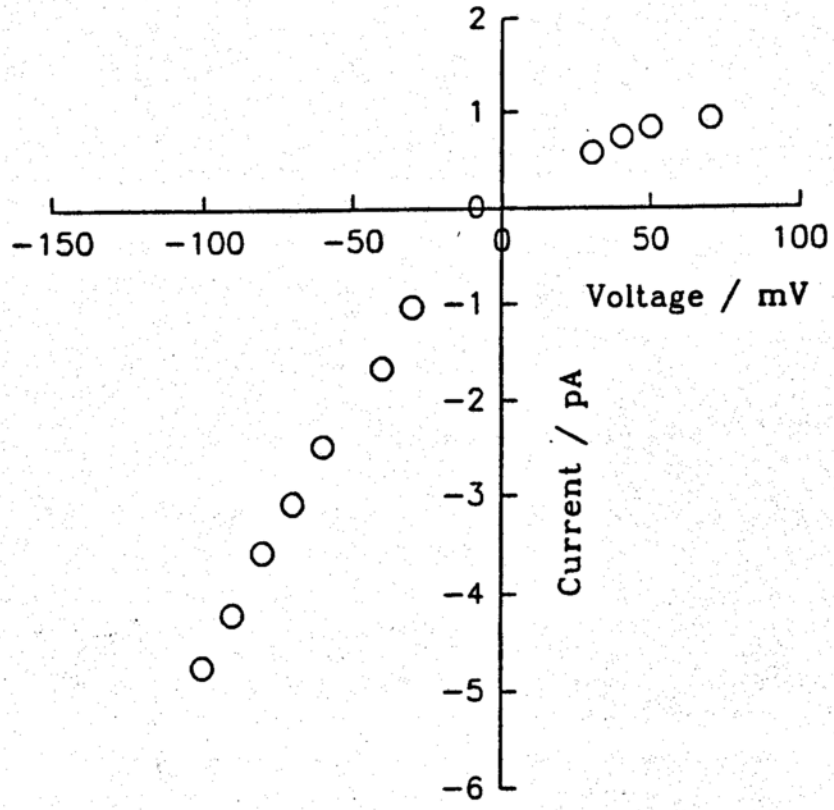

(b) Calcium dose-response curve

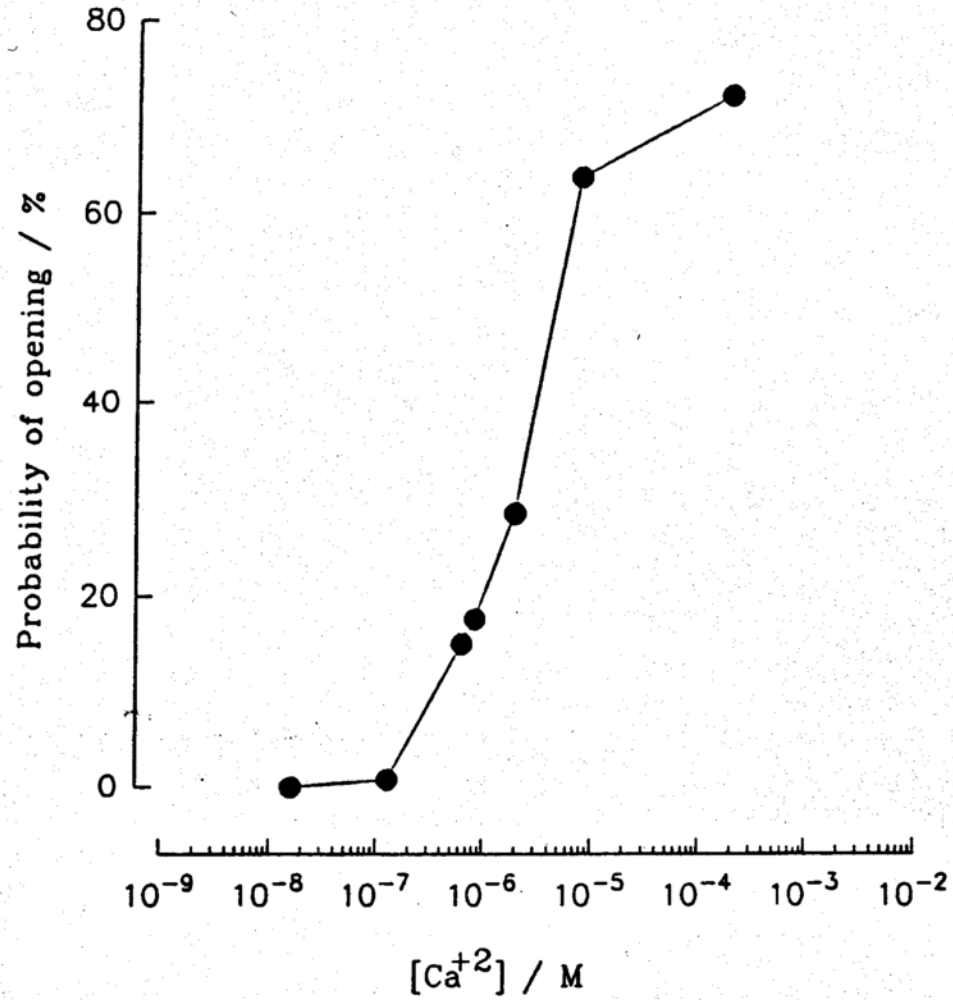

Figure 6 Change in channel opening probability over time at 4 different voltage levels, as a result of Amphotericin B treatment.
Notice that the increase at -40 mV is the most dramatic while that at -100 mV is much less pronounced.

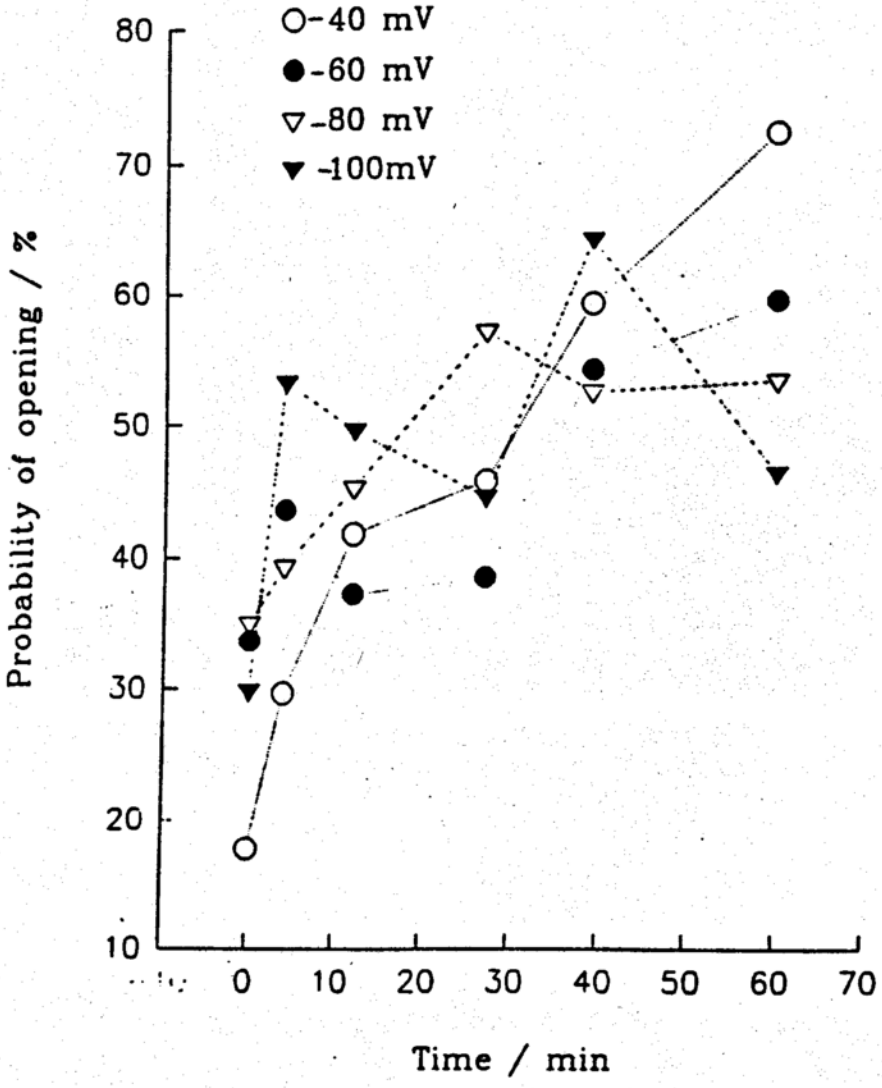

Figure 7 Change in voltage dependency of opening probability as a result of Amphotericin B treatment.
Prior to treatment, opening probability is greater at larger hyperpolarization potentials, but after treatment, it is reversed.

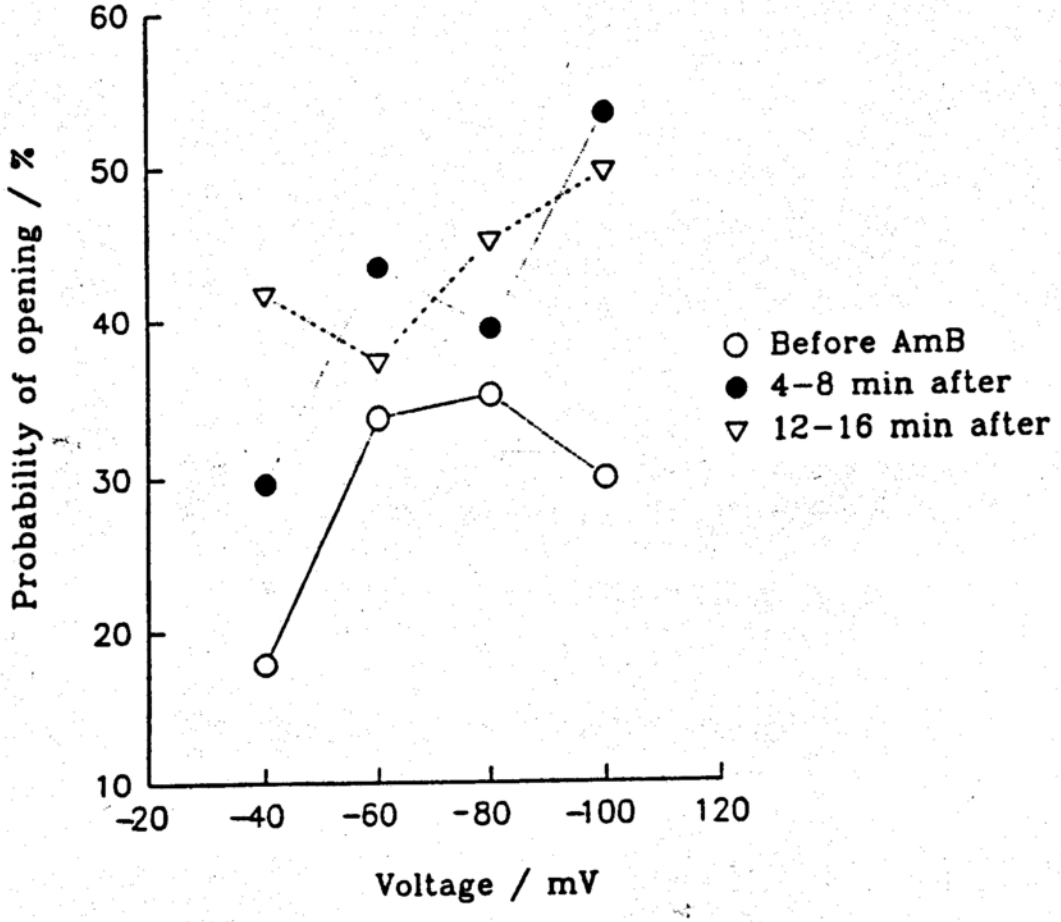

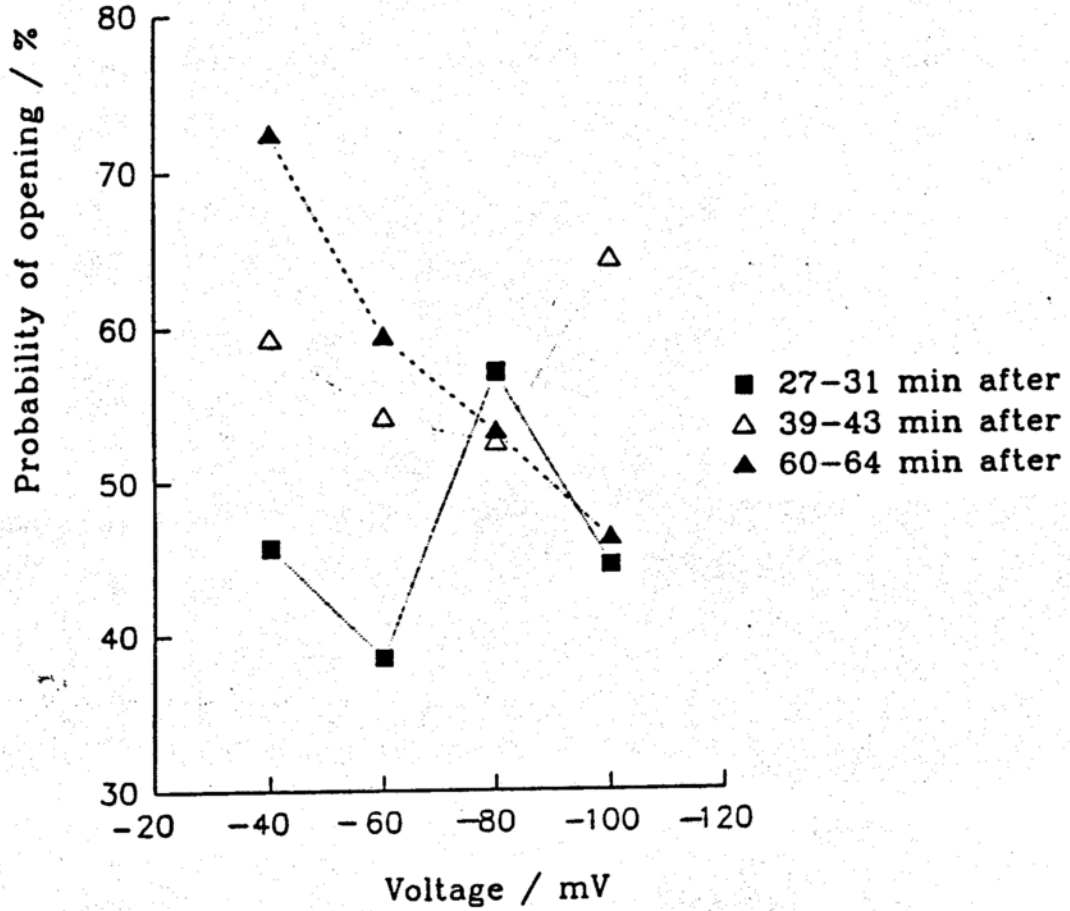
Probability of opening / %
80
70
60
50
40
30
-20
-40
-60
-80
-100
-120
Voltage / mV
27–31 min after
39–43 min after
60–64 min after

Figure 8 Change in the three closed time constants as a result of Amphotericin B treatment.

(a) At -40 mV

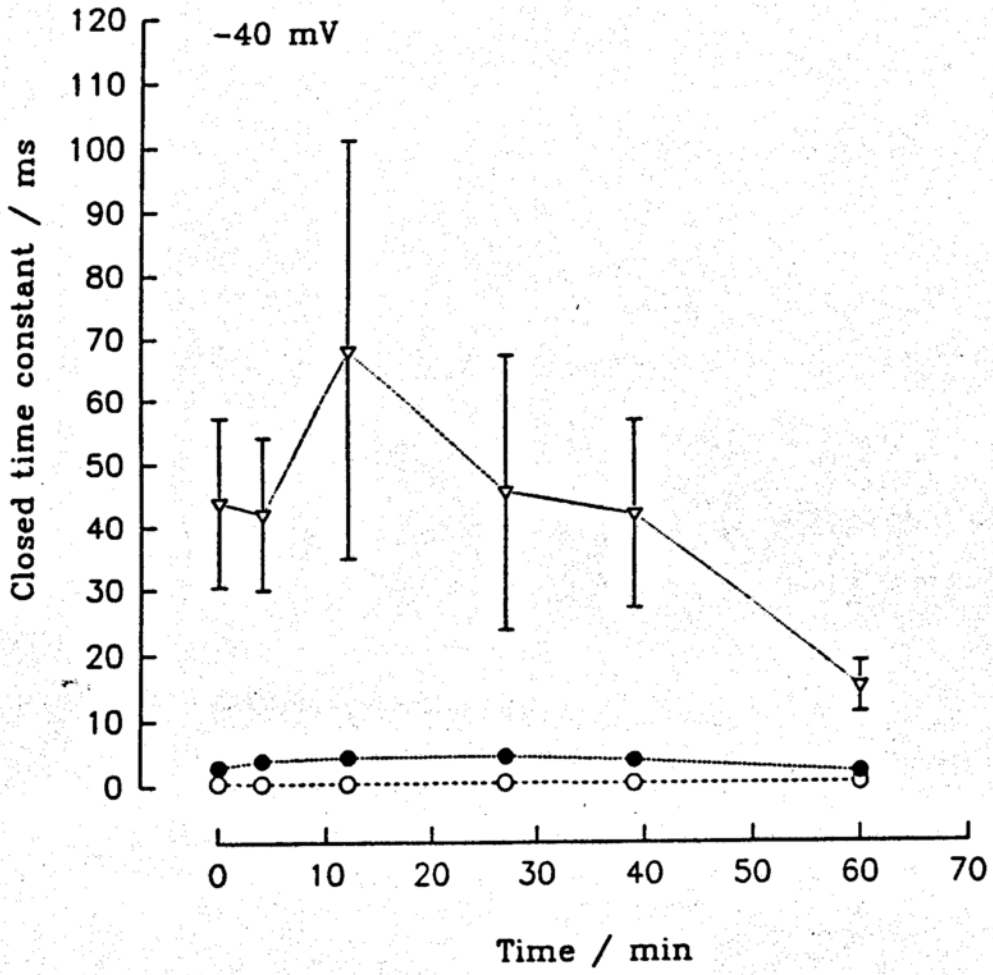

(b) At -60 mV

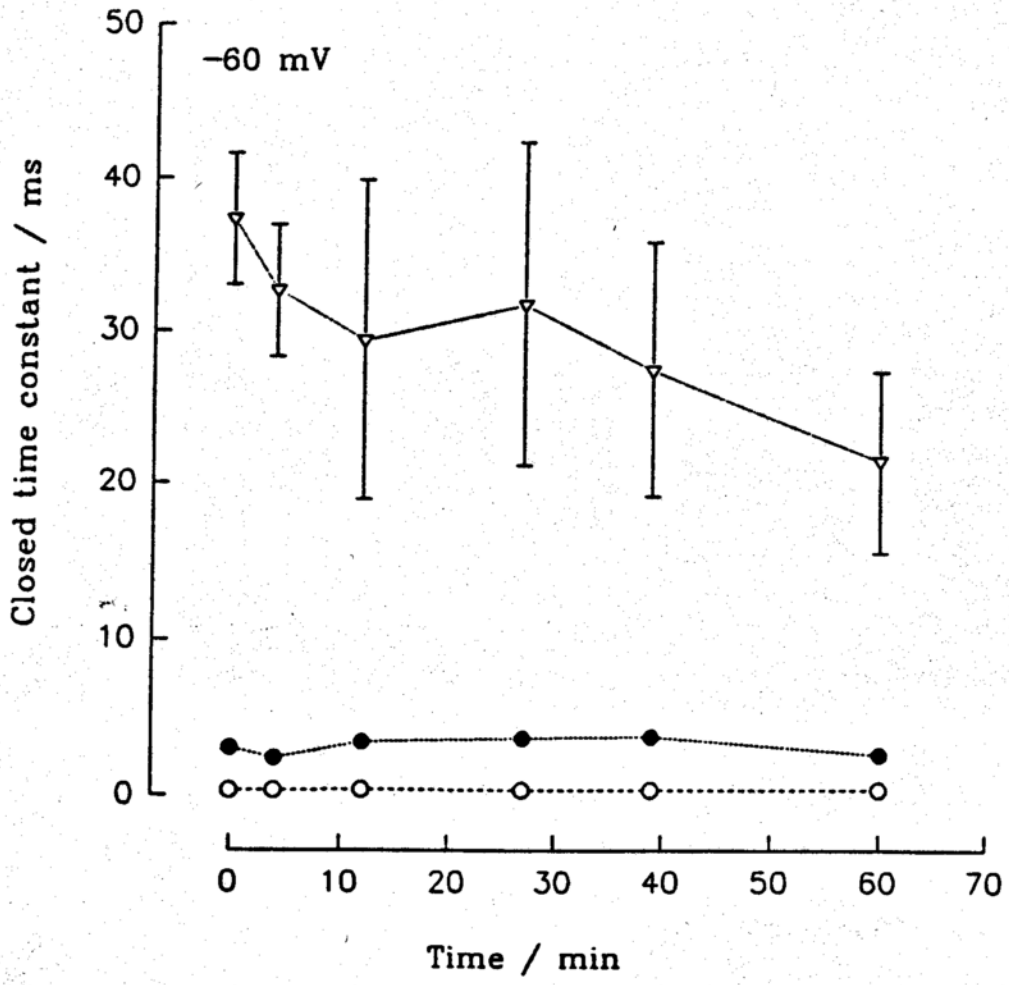
−60 mV
Closed time constant / ms
50
40
30
20
10
0
0
10
20
30
40
50
60
70
Time / min

(c) At -80 mV

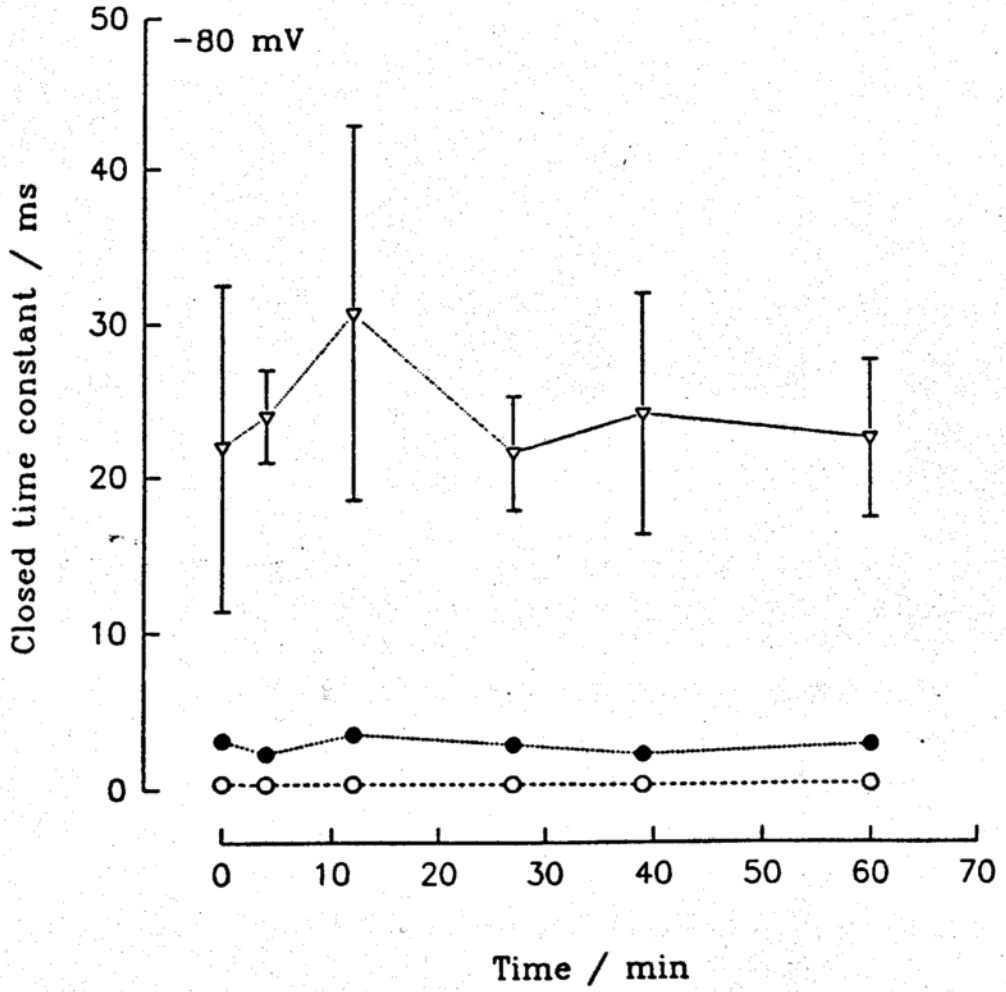
50
40
30
20
10
0
−80 mV
Closed time constant / ms
0
10
20
30
40
50
60
70
Time / min

(d) At -100 mV

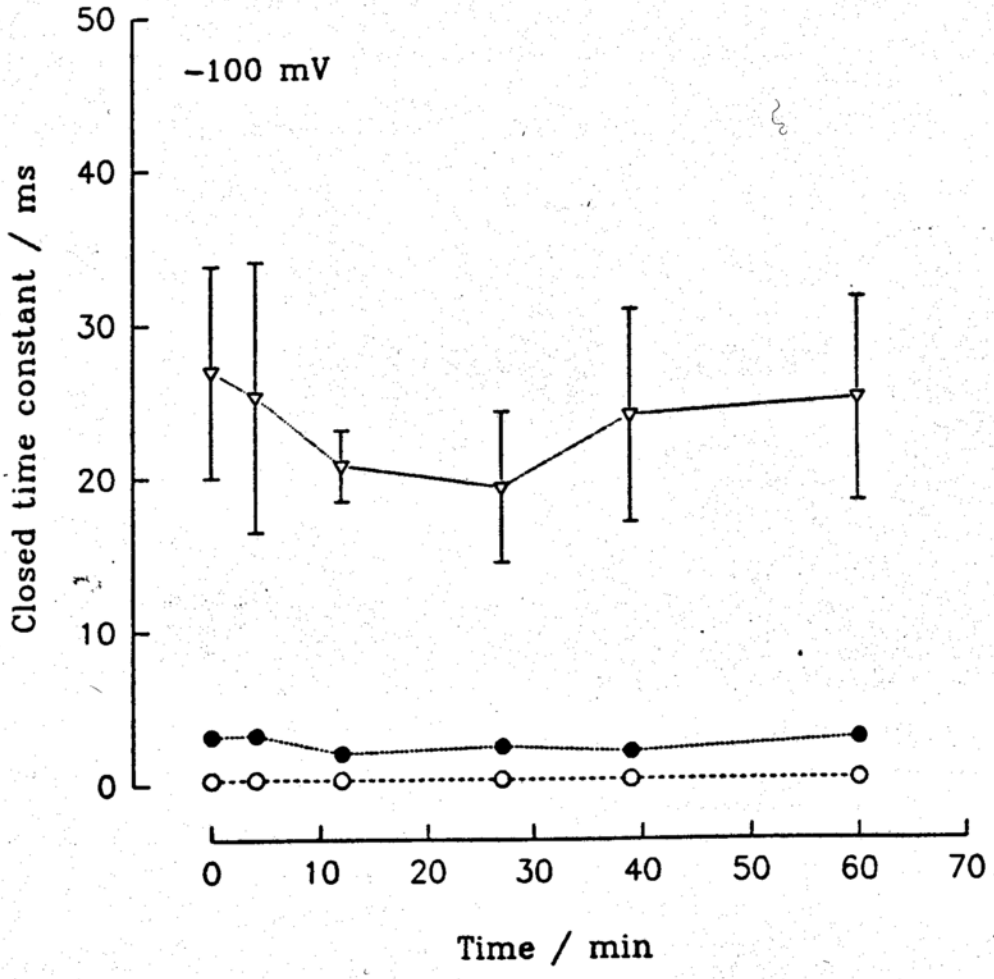
50
40
30
20
10
0
−100 mV
Closed time constant / ms
0
10
20
30
40
50
60
70
Time / min

Figure 9. The effects of Amphotericin B on open time constants at the four voltage levels studied. Prior to bathing with Amphotericin B, the channel in the patch had only one open state (hence, one time constant); after bathing with Amphotericin B, two open states were required to described the opening events of the channel. The overall opening probability increased at all four voltage levels partly because more than 50 % of the channel open events had longer open durations after Amphotericin B treatment. At -40 mV, -60 mV, -80 mV, and -100 mV, 61.3 %, 71.17 %, 55.41 %, and 60 % respectively of the open events were primarily attributable to the open state with the longer mean open resident time.

(a) -40 mV

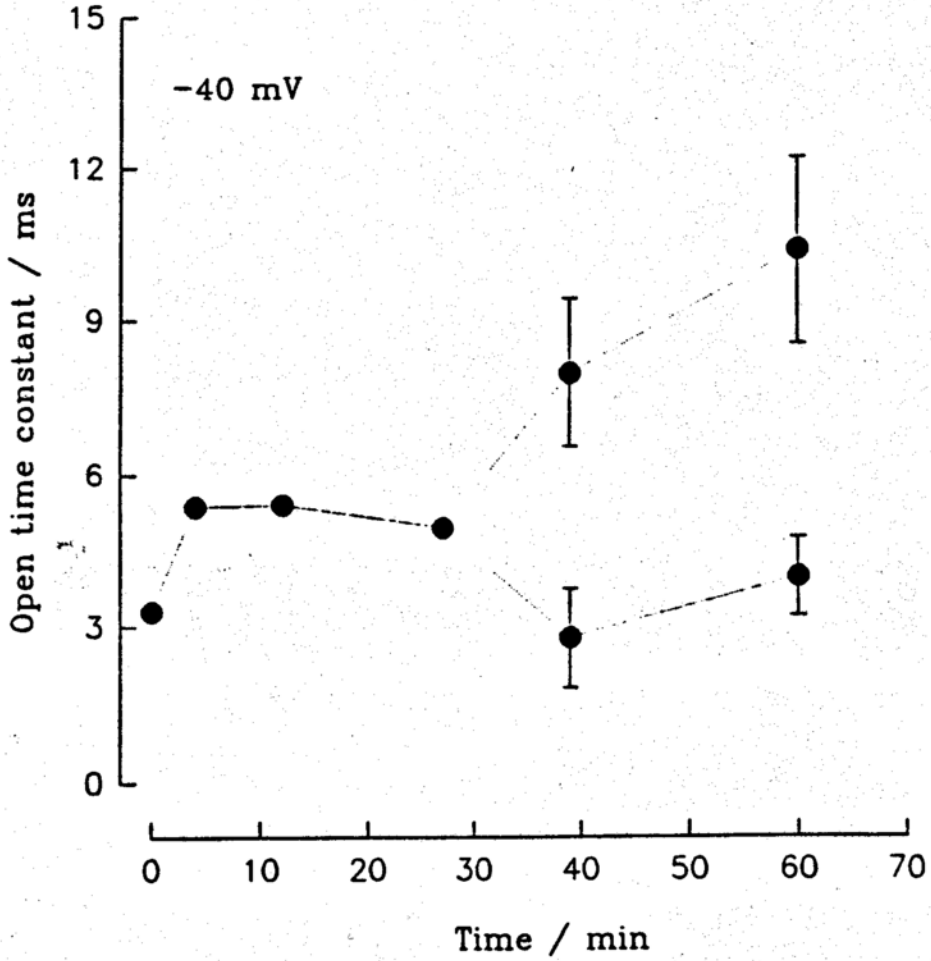
-40 mV
Open time constant / ms
15
12
9
6
3
0
0
10
20
30
40
50
60
70
Time / min

(b) At -60 mV

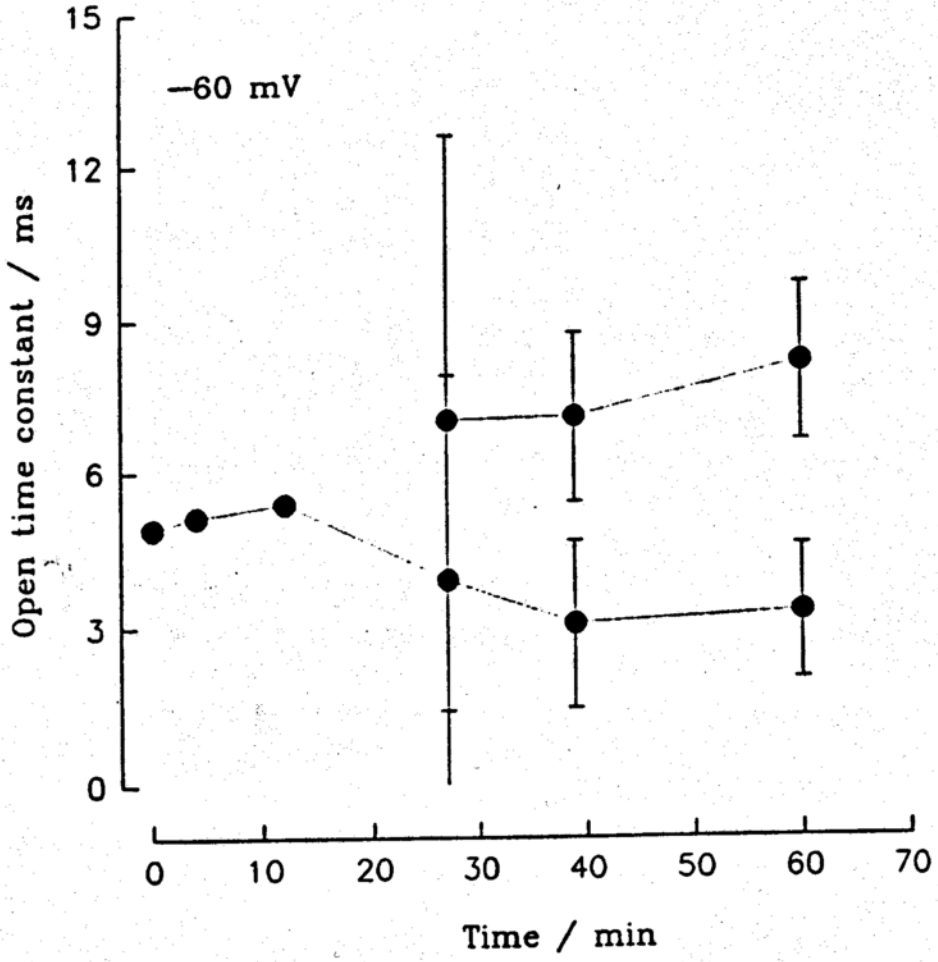
15
12
9
6
3
0
−60 mV
Open time constant / ms
0
10
20
30
40
50
60
70
Time / min

(c) At -80 mV

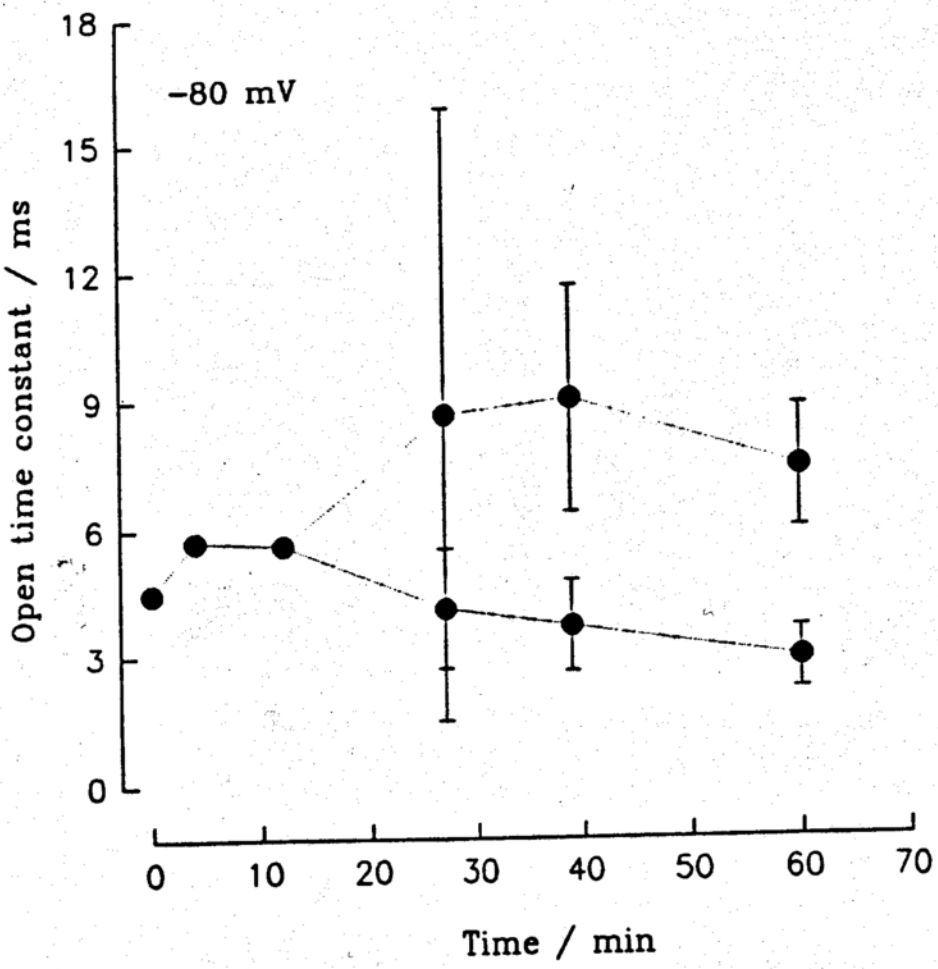
−80 mV
Open time constant / ms
Time / min
0
3
6
9
12
15
18
0
10
20
30
40
50
60
70

(d) At -100 mV

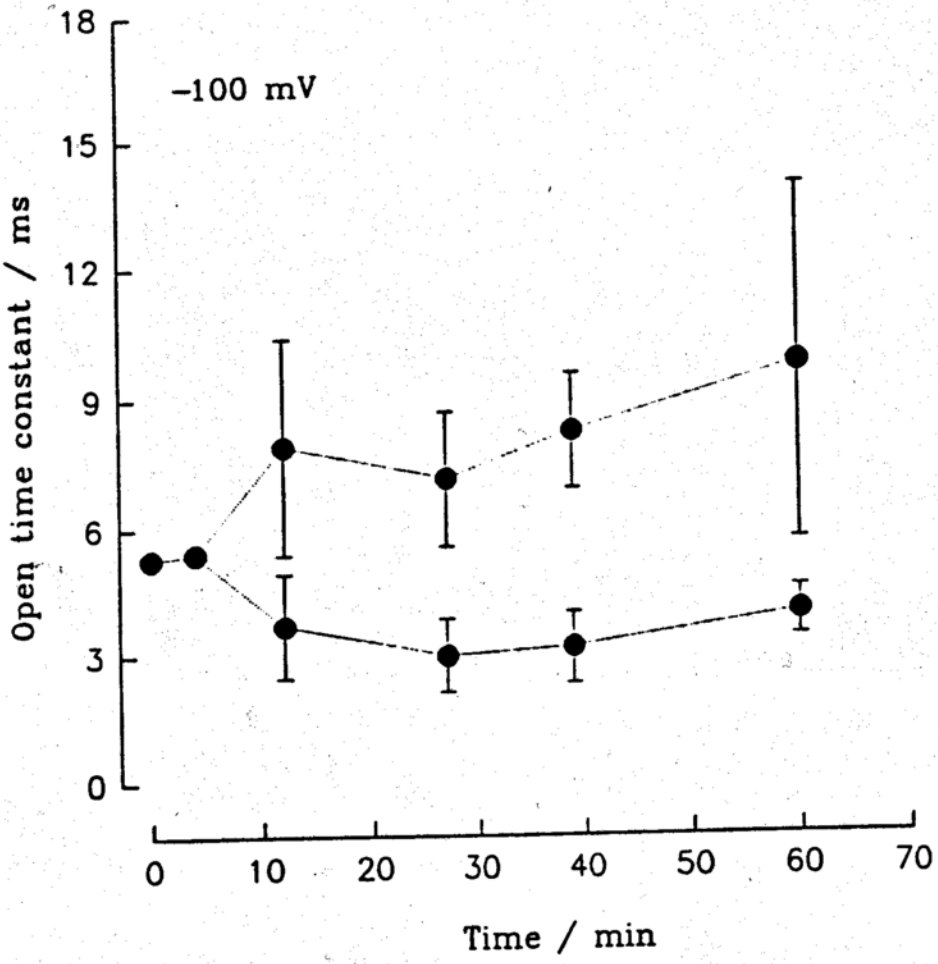
−100 mV
Open time constant / ms
Time / min
0
3
6
9
12
15
18
0
10
20
30
40
50
60
70

Figure 10. Two types of whole cell conductances were found in cloned MDCK cells.

(a) The Type I cells showed no significant conductances at membrane voltages ranging from -100 mV to +100 mV (O), whereas the Type II cells had conductances larger than a few nS (●). (b) The conductances of the Type II cells decreased over time, time = 0 minutes (O), 2 minutes (●), 9.8 minutes (▽), 15.5 minutes (▼), 20.3 minutes (□), 25 minutes (■), 27.5 minutes (△).

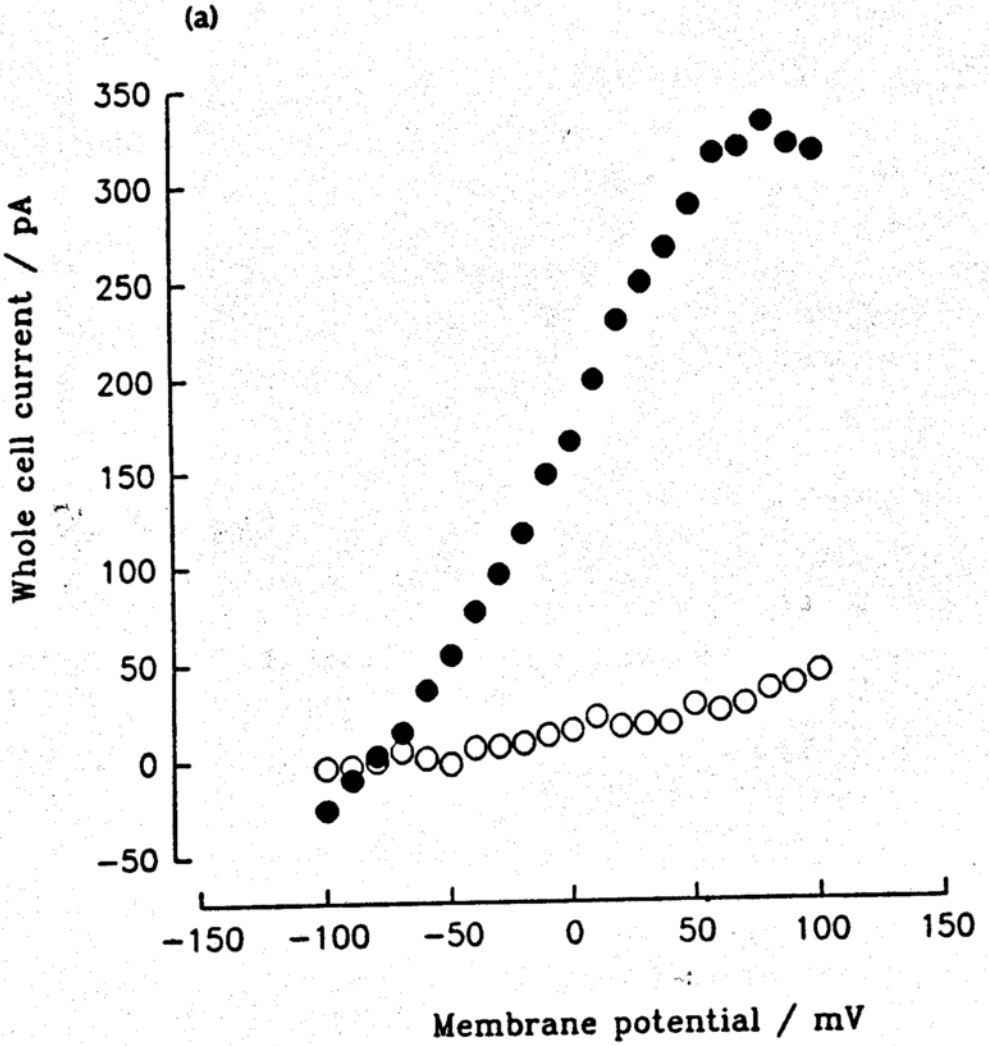

(b)

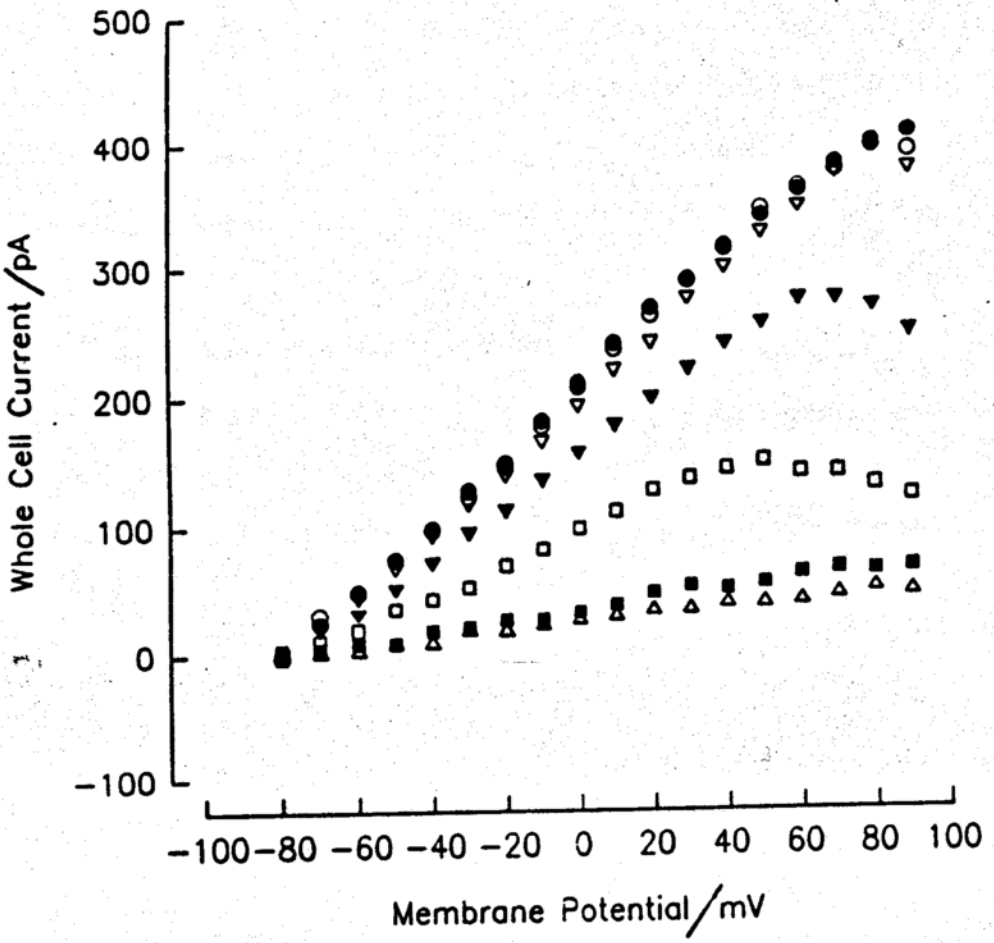
500
400
300
200
100
0
−100
Whole Cell Current /pA
−100 −80 −60 −40 −20 0 20 40 60 80 100
Membrane Potential /mV

Figure 11. Effects of Amphotericin B on Type I whole cell currents over time. (a) Before adding Amphotericin B to the solution bathing the whole cell, at times zero and 1 minute, whole cell currents were recorded, and whole cell conductances were found to be insignificant (Type I). After 4.5 minutes, Amphotericin B was added to the solution bathing the membrane patch. The increase in conductance became apparent at 12 minutes. The increase in conductance continued for approximately another hour. In this cell, there were at least two distinct conductive pathways for K^+ to translocate across the whole cell membrane, judging from the individual current traces at various time points and voltage levels. Amphotericin B appeared to have distinct effects on these two pathways. For example, compare the current records at 36 minutes and 66 minutes; over time, Amphotericin B caused larger increases in currents responding to higher clamped voltage levels than those clamped at lower voltage levels. (b) The associated whole cell conductance plots before and after bathing the cell with Amphotericin B, control at time = 0 minutes (O), and 1 minute (●), and after bathing with Amphotericin B at time = 5 minutes (▽), 12 minutes (▼), 18 minutes (□), 28 minutes (■), 36 minutes (△), 44 minutes (▲), 54 minutes (◊).

(a)

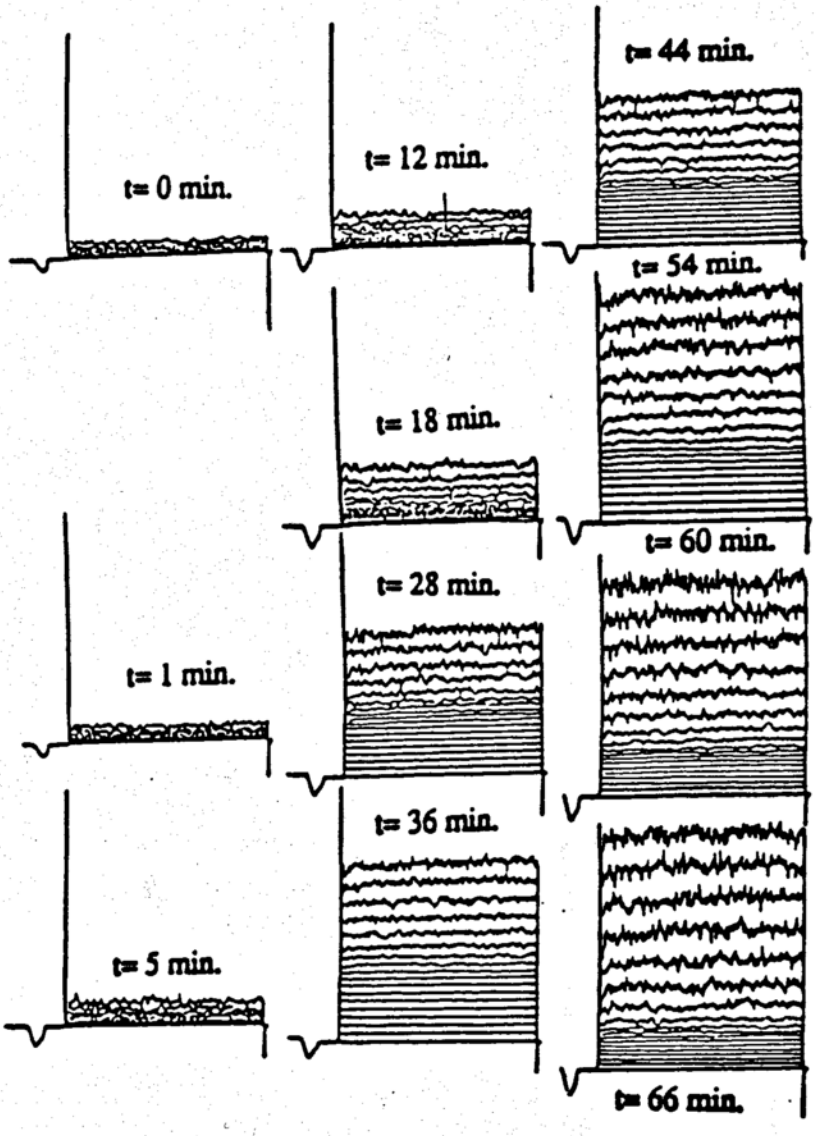
t= 0 min.
t= 12 min.
t= 44 min.
t= 54 min.
t= 18 min.
t= 60 min.
t= 28 min.
t= 1 min.
t= 36 min.
t= 5 min.
t= 66 min.

(b)

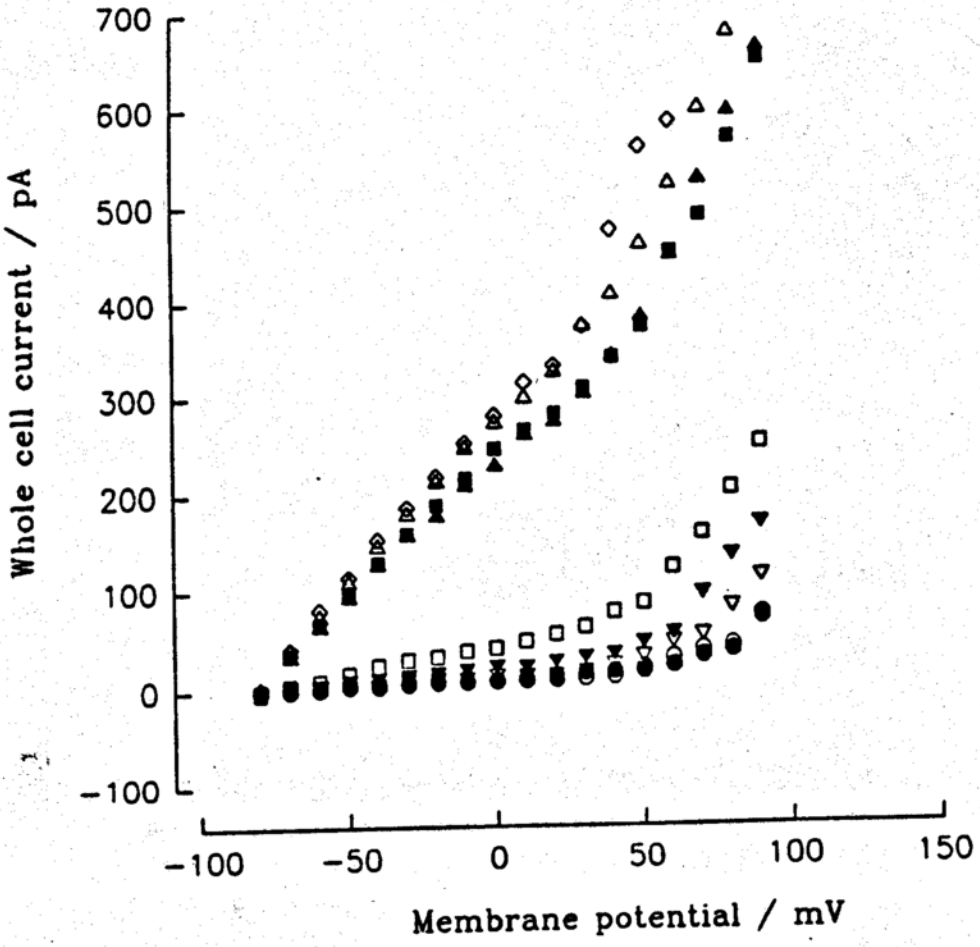
Whole cell current / pA
700
600
500
400
300
200
100
0
−100
−100
−50
0
50
100
150
Membrane potential / mV

Figure 12. Amphotericin B caused the average Type I whole-cell conductance to increase from 0.395 ± 0.153 nS (O) to 4.622 ± 0.769 nS (●) (n=3), corresponding to an average net increase of 1070%.

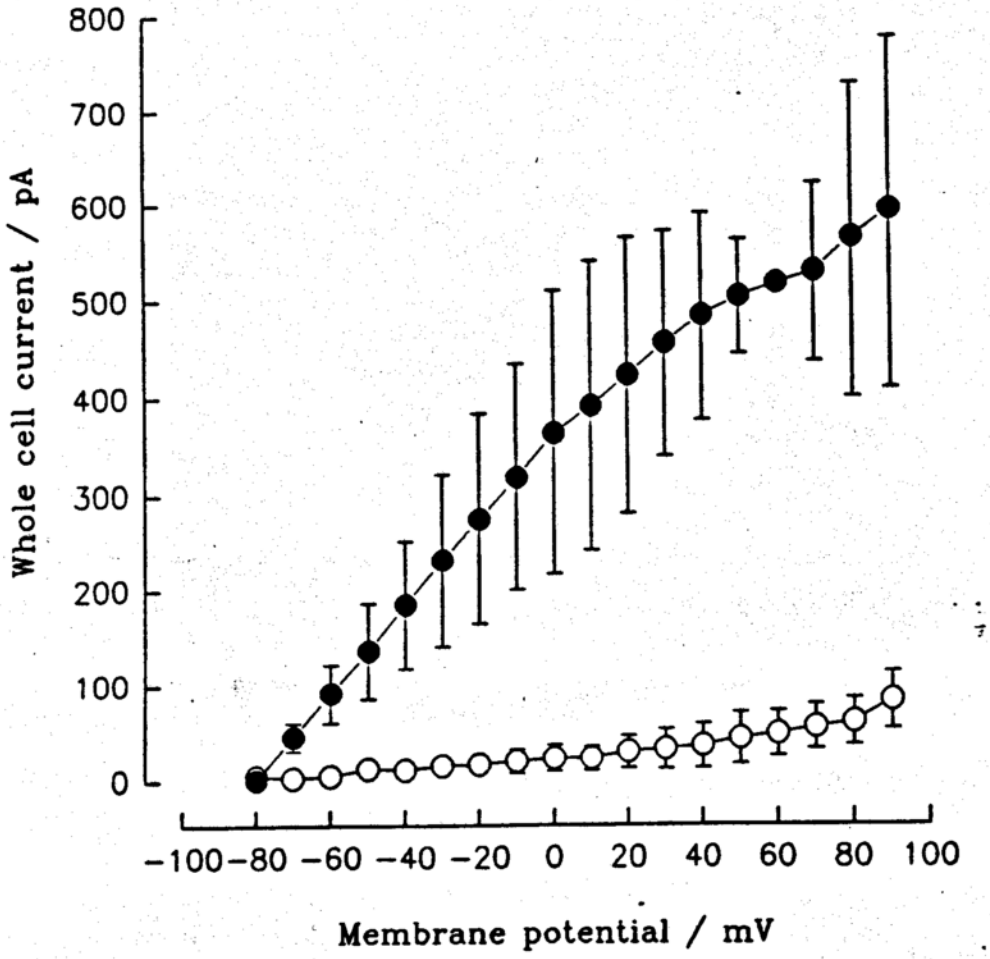

Figure 13. Effects of Amphotericin B on another Type I MDCK cell. (a) In this cell, the whole cell currents prior to bathing with Amphotericin B, were obtained immediately after applying suction and gaining access to the interior of the cell. Three minutes later, Amphotericin B was introduced into the bathing solution for the cell. Although an increase in whole cell conductance did occur over time after addition of Amphotericin B, the shape of the induced whole cell conductance was very different from that shown in Figure 8. This Type I cell exhibited K^+ currents which inactivated at high depolarization voltage levels.

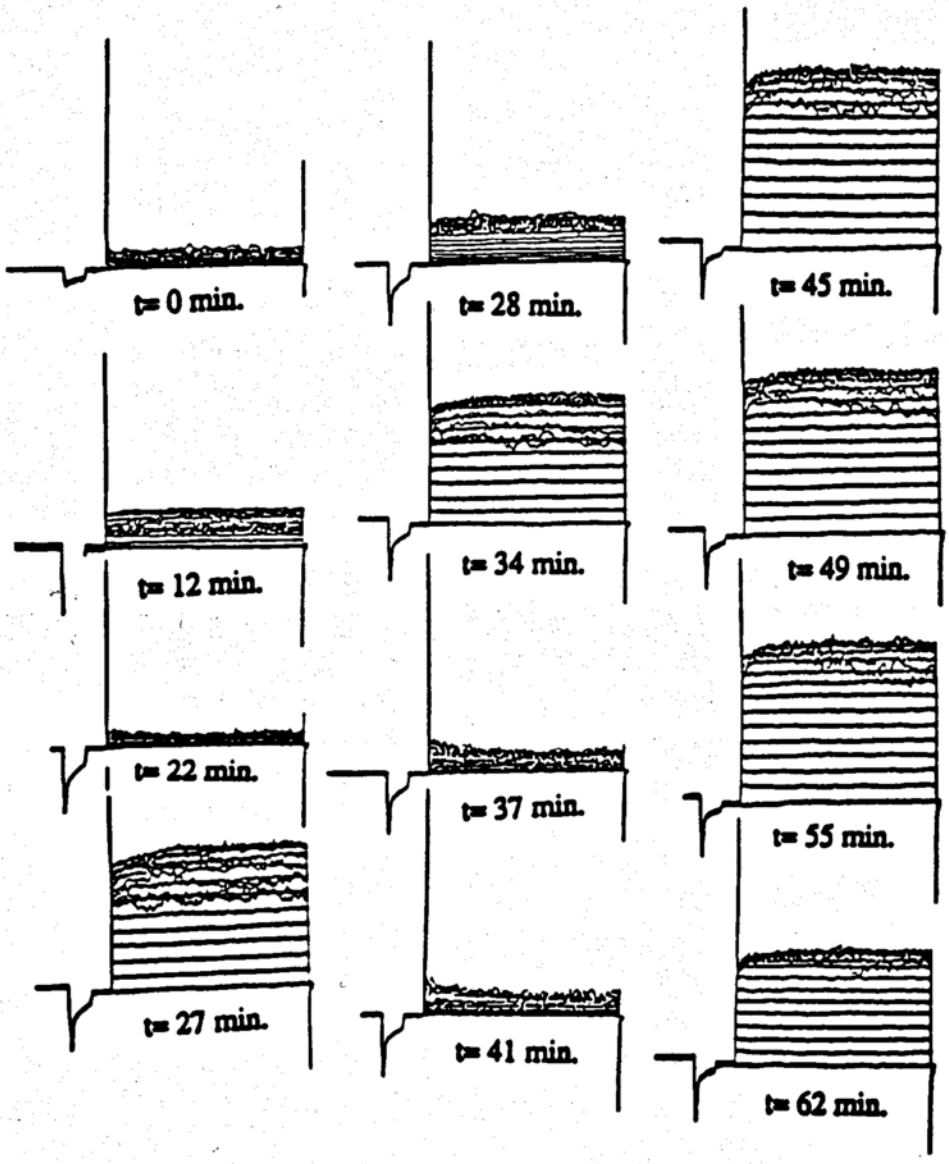

(b) The associated whole cell conductance plots before and after bathing the cell with Amphotericin B, control at time = 0 minutes (O), and after bathing with Amphotericin B at 12 minutes (●), 27 minutes (▽), 34 minutes (▼), 45 minutes (□), 49 minutes (■), 55 minutes (△).

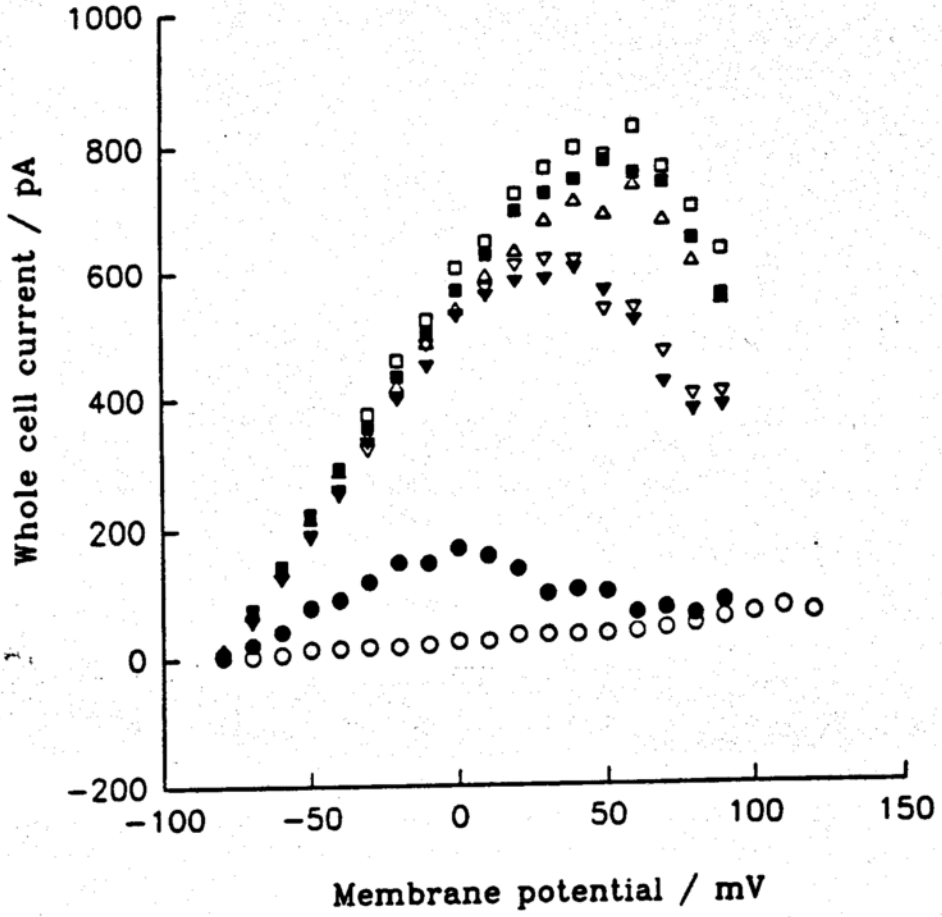

Figure 14. Effects of Amphotericin B on Type II whole cell currents. (a) Prior to bathing with Amphotericin B, the whole cell currents decreased over time, a phenomenon often referred to as rundown. Twenty-two minutes later, Amphotericin B was introduced to bathe the whole cell, and increases of whole cell currents became apparent approximately 20 minutes later.

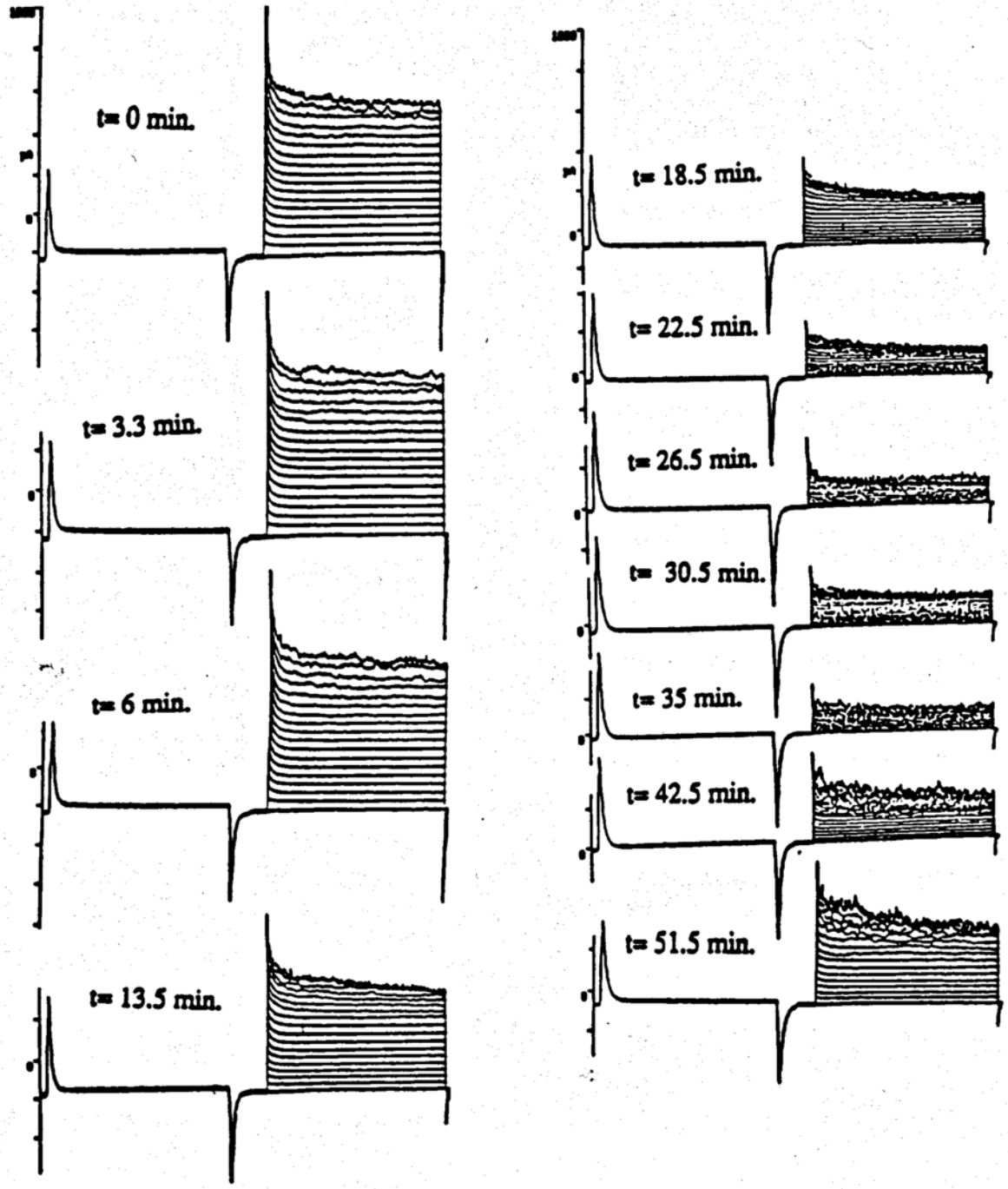

(b.) The associated whole cell conductance plots before and after the cell was bathed with Amphotericin B, control at time = 0 minutes (O), 3.3 minutes (●), 6 minutes (▽), 13.5 minutes (▼), 18.5 minutes (□), and after bathing with Amphotericin B at time = 22.5 minutes (■), 26.5 minutes (Δ), 30.5 minutes (▲), 35 minutes (◊), 42.5 minutes (◆) and 51.5 minutes (O).

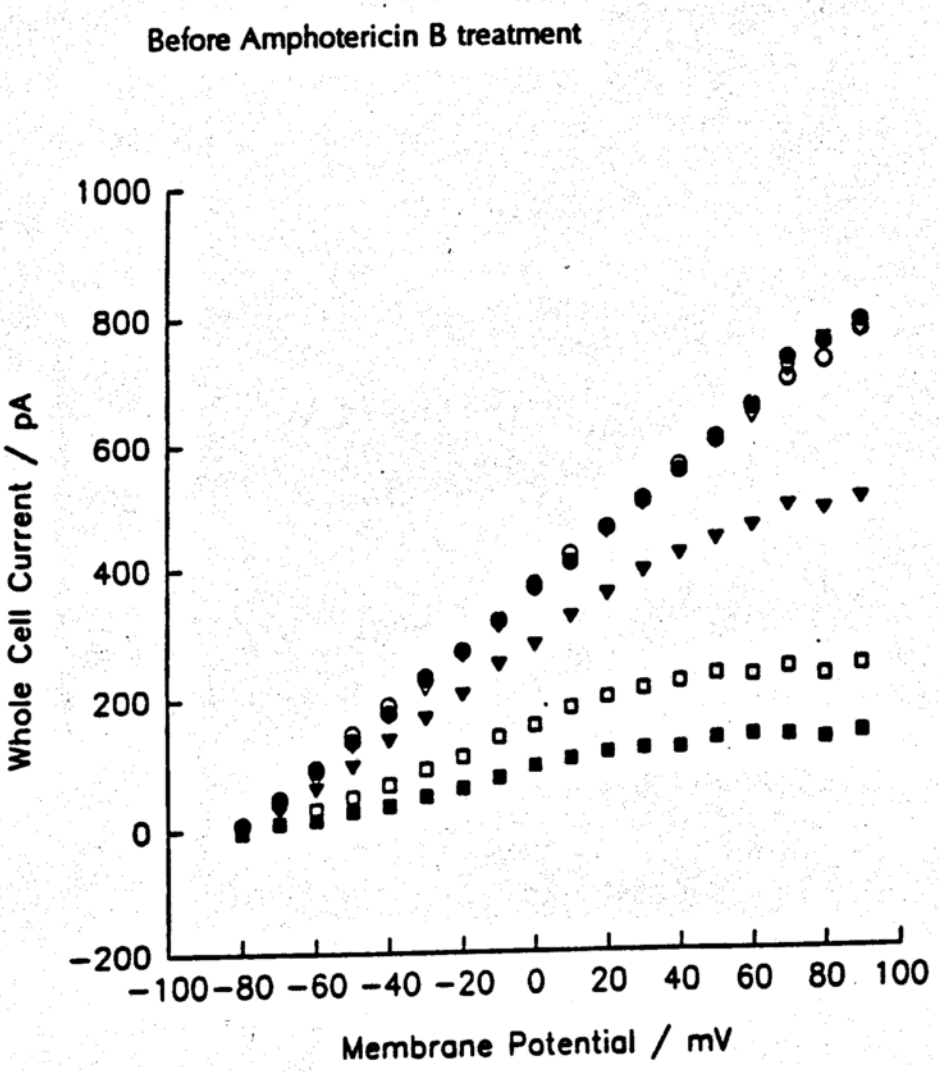

After Amphotericin B treatment

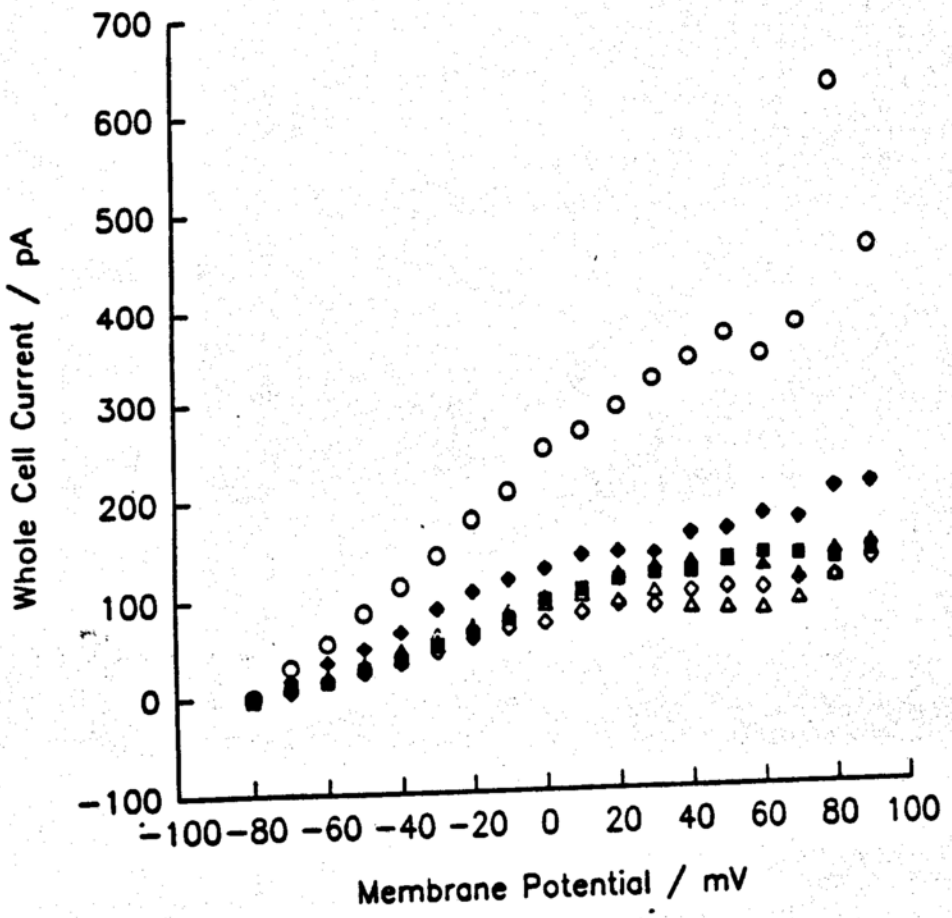

Table 1

Single channel parameters in outside-out membrane patches before and after the addition of Amphotericin B to the extracellular side of the membrane patch

	Opening probability (%)		Single channel current amplitude (pA)		Open time constant (ms)		Closed time constant (ms)	
	Before	After	Before	After	Before	After	Before	After
membrane held at + 69 mV	~ 0	35.3	----	----	----	1.14 6.63	----	1.00 11.39
membrane held at + 75 mV	33	83.8	13.14	17.76	2.65 16.07	1.79 8.32	1.64 23.35	0.66 2.49

Table 2

Addition of Amphotericin B led to increase in whole-cell conductance over time in six different Type II MDCK cells

In three of the six cells, the whole cell conductances decreased over time prior to treatment with Amphotericin B. After Amphotericin B treatment, conductances increased over time. In the remaining three cells, before Amphotericin B treatment, no conductance decreases over time were observed; however, conductances increased after Amphotericin B treatment as time elapsed.

	Conductance at time zero (nS)	Conductance prior to addition of AmB (nS)	Conductance after addition of AmB (nS)
cell #1	4.5	1.1 (22.5 min.)	2.86 (51.5 min.)
cell #2	2	1 (1 min.)	5 (22.5 min.)
cell #3	1.78	0.79 (4 min)	2.82 (15 min.)
cell #4	4.44	NC	9.3 (55 min.)
cell #5	1.7	NC	8 (18 min.)
cell #6	3.57	NC	14.84 (23.5 min.)

NC, no change.

Discussion

For the past three decades, studies of the mechanism of action of Amphotericin B on fungal cells have indicated that Amphotericin B can increase cell membrane permeability to ions. Many researchers believe that this capability is due to the formation of aqueous pores by Amphotericin B and the sterol molecule ergosterol, which is found in the cell membrane (5). This interaction is also thought to account for Amphotericin B's toxicity to the fungal host cells since mammalian cell membranes contain cholesterol molecules, which also have been shown to interact with Amphotericin B (25).

However, a closer look at the properties of the Amphotericin B pore reveals several lines of evidence against the Amphotericin B pore mechanism. For example, the selectivity of the Amphotericin B pore indicates that pores may not be responsible for the Amphotericin B toxicity seen in certain isolated cells. These pores turn out to be anion-selective. This feature contradicts the experimental observations of potassium leakage in cells treated with Amphotericin B. This can be understood as follows: Suppose that as a result of Amphotericin B treatment, these anion-selective pores formed in the membranes of these isolated cells. In a normal physiological environment, these cells are bathed in an extracellular fluid containing high levels of Na^+ and Cl^-, so that the concentration gradient would drive extracellular chloride ions into the cells through these pores. This would hyperpolarize the membrane potential and thus create an unusually large driving force for inward movement of Na^+, which would also inhibit K^+ efflux. Hence, anion pores in the cell membrane cannot explain the cellular K^+ leakage caused by Amphotericin B.

Several mechanisms may contribute to the cation leakage. When an Amphotericin B molecule comes into contact with a cell, it remains in the cell

membrane because of its amphiphilic nature. The presence of Amphotericin B molecules in the cell membrane disturbs the membrane lipid structure (5). Several lines of evidence suggest that this disturbance arises because the Amphotericin B molecule interacts preferentially with membrane sterol molecules, leading to cation-selective membrane defects that allow cytoplasmic K^+ to flow out of the cell (5). However, it remains to be determined whether this preferential interaction leads to attraction of membrane sterol molecules away from certain locations, where they are needed to provide membrane structural integrity, toward the Amphotericin B molecules. A study using fluorescent labelling of sterol molecules would help to determine whether such depletion occurs in bilayer membranes.

Two alternative hypotheses may also explain the cation leakage. The first hypothesis is that some of the sterol molecules in a cell membrane may be involved in creating proper environments for normal membrane protein functioning. If Amphotericin B moves these sterol molecules from their normal locations, then normal protein functioning should be disrupted. The other hypothesis involves direct interaction between Amphotericin B and membrane proteins, altering their normal functioning. Our single channel studies indicate that the cation leakage is related to these two hypotheses involving channel proteins of the cell, but do not enable us to distinguish between them as explanations for Amphotericin B toxicity.

Studies at the whole cell level add to the evidence against the pore mechanism. We found that if whole cell currents were abolished by a channel blocker TEA, Amphotericin B had no effect on the whole cell current (not shown). Similar results were observed using LLP-CK_1 cells (26). These results indicate that even at the whole cell level, Amphotericin B has no effect on the ionic permeability of lipid membranes once the ionic current through channel proteins is eliminated. The increase in whole

cell conductance was thus mediated by an increase in the activity of ion channels in the cell membrane. These observations at the whole cell level are consistent with the results obtained from single channel studies.

We believe that the positive effects of Amphotericin B on ion currents as observed involve interactions between Amphotericin B and various types of K^+ channels in MDCK cells, because of the results obtained from the whole cell control studies and the single channel control studies (not shown). We determined that the MDCK whole cell currents were mostly K^+ currents through the following observations. First, the whole cell currents could be blocked completely by specific K^+ channel blockers such as TEA, Cs and 4-AP; and second, in single channels, current traces could always be blocked by extracellular TEA or intracellular Cs^+. The presence of channel currents while Cl^- ions were replaced by gluconate ions eliminates the possibility that these channels are Cl^- channels. Further evidence came from the fact that the measured reversal potentials of the channels were consistent with those predicted by the Nernst equation for K^+-specific channels. Hence, we believe that the effects of Amphotericin B on whole cell currents reflect its interaction with an ensemble of K^+ channels in MDCK cells.

In summary, we have shown that Amphotericin B has a minimal effect on ion transport in lipid membranes devoid of ion channels. Instead, it acts mainly on the ion channels present in cell membranes. The effects of Amphotericin B on whole cell currents are dependent on the magnitude of depolarization and are different for different cells. This may be due to the fact that the various cells we clamped expressed different channels in their membranes. Because the whole cell current profile shapes after Amphotericin B treatment were similar to the shapes before the treatment, it is likely that, at least within the experimental time frame, Amphotericin B affected only

channel activity and not channel expression. Finally, based on these studies, we think that the K^+ wasting seen in Amphotericin B-treated patients may be caused by higher K^+ channel activity induced by a change in the lipid environment surrounding the channel protein. The change in the lipid environment may be due to preferential interaction between certain lipid components and Amphotericin B.

Conclusions

1. In MDCK cells, Amphotericin B causes increases in potassium channel activity, regardless of whether it is in contact with the intracellular or the extracellular side of a cell-free membrane patch. The potassium channels affected by Amphotericin B include some K_{Ca} channels, and also some potassium channels not regulated by intracellular Ca^{+2}.
2. Amphotericin B also causes whole cell conductance to increase. The conductance increase can be seen in cells that initially exhibit no significant whole cell currents, as well as in cells that exhibit significant outward currents, but decrease over time prior to Amphotericin B treatment.
3. The effects of Amphotericin B on single channel currents and whole cell currents appear to be mediated by potassium channels in MDCK cells, because when whole cell currents are blocked by TEA, Amphotericin B does not induce current increases.
4. Recordings of the current flowing through cell free membrane patches bathed with Amphotericin B may have minimum noise at constant DC levels for more than two hours, indicating that no non-selective leakage has occurred as a result of bathing with Amphotericin B. Based on these recordings and on recordings of channel currents, we believe that the toxicity of Amphotericin B is more probably related to its ability to disturb normal protein functioning than to the creation of aqueous pores.

References

1. Martin. A. R. (1977). Antibiotics. In *Textbook of organic medicinal and pharmaceutical chemistry* (Wilson, C. O., Gisvold, O. and Doerge, R.F., eds.). pp. 269-348. Lippincott Press, Philadelphia, PA.
2. Medoff, G., Brajtburg, J., and Kobayashi, G. S. (1983). Antifungal agents useful in therapy of systemic fungal infections. *Ann. Rev. Pharmacol. Toxicol.* **23**, 303-30.
3. Sabra, R., and Branch, R.A. (1990). Amphotericin B Nephrotoxicity. *Drug Safty* 5(2), 94-108.
4. Gallis, H. A., Drew, R. H., and Pickard, W. W. (1990). Amphotericin B: 30 years of clinical experence, *Review of Infectious Diseases* **12**(2), 308-329.
5. Bolard, J. (1986). How do the polyene macrolide antibiotics affect cellular membrane properties? *Biochim. Biophys. Acta* **864**, 257-304.
6.. Andreoli, T.E., and Monahan M. (1968). The interaction of polyene antibiotics with thin lipid membranes, *J. Gen. Physiol.* **52**, 300-325.
7. Andreoli, T.E. (1973). On the anatomy of Amphotericin B-cholesterol pores in lipid bilayer membranes, *Kidney Int.* **4**, 337-345.
8. Andreoli, T.E. (1974). The structure and function of Amphotericin B-cholesterol pores in lipid bilayer membranes. *Ann. New York Acad. Sci.* **235**, 448-468.
9. Cass A., Finkelstein A. and Krespi V. (1970). The ion permeability induced in thin lipid membranes by the polyene antibiotics nystatin and Amphotericin B, *J. Gen. Physiol.* **56**, 100-124.
10. Borisova, M.P., Brutyan, R.A., and Ermishkin, L.N. (1988). Mechanism of anion-cation selectivity of Amphotericin B channels, *J. Membrane Biol.* **90**, 13-

11. Ermishkin, L. N. , Kasumov, Kh. M.,and Potzeluyev, V. M. (1976). Single ion channels induced in lipid bilayers by polyene antibiotics Amphotericin B and nystatin, *Nature* **262**, 698-699.

12. Ermishkin, L. N., Kasumov, Kh. M., and Potseluyev, V. M. (1977). Properties of Amphotericin B channels in lipid bilayer, *Biochim. Biophys. Acta* **470**, 357-367.

13. Dennis V.W., Stead N.W., and Andreoli T.E. (1970). Molecular aspects of polyene- and sterol-dependent pore formation in thin lipid membranes, *J. Gen. Physiol.* **55**, 375-400.

14. Butler, W. T., and Cotlove, E. (1971). Increased permeability of human erythrocytes induced by Amphotericin B, *J. Infectous Diseases* **123**(4), 341-350.

15. De Kruijff, B. and Demel, R. A. (1974). Polyene antibiotic-sterol interactions in membranes of *Acholeplasma Laidlawii* cells and lecithin liposomes III. Molecular structure of the polyene antibiotic-cholesterol complexes. *Biochim. Biophys. Acta* **339**, 57-70.

16. Wietzerbin, J., Szponarski, W., Borowski, E., and Gary-Bobo, C. M. (1990). Kinetic study of interaction between ^{14}C-Amphotericin B derivatives and human erythrocytes: Relationship between binding and induced K^+ leak, *Biochim. Biophys. Acta* **1026**, 93- 98.

17. Szponarski, W., Wietzerbin, J., Borowski, E. and Gary-Bobo, C. M. (1988). Interaction of ^{14}C-labeled Amphotericin B derivatives with human erythrocytes: Relationship between binding and induced K+ leak, *Biochim. Biophys. Acta* **938**, 97-106.

18. Hartsel, S. C., Benz, S. K., Peterson, R. P. and Whyte, B. S. (1991). Potassium-selective Amphotericin B channels are predominant in vesicles regardless of sideness, *Biochem.* **30**, 77-82.

19. Fernandez-Castelo, S., Bolivar, J. J., Lopez-Vancell, R., Beaty, G., and Cereijido, M. (1985). Ion transport in MDCK cell, in *Tissure Culture of Epithelial Cells* (Taub, M. ed.). pp. 37-50. Plenum Press. New York.

20. Valentich, J. D. (1981). Morphological similarities between the dog kidney cell line MDCK and the mammalian cortical collecting tubule, *Ann. New York Acad. Sci.* **81**, 384-405.

21. Rindler, M. J., Chuman, L. M., Schaeffer, L. and Saier, M. H. Jr. (1979). Retention of differentiated properties in an established dog kidney epithelial cell line (MDCK), *J. Cell Biol.* **81**, 635-648.

22. Richardson, J. C. W., Scalera, V. and Simmons, N. L. (1991. Identification of two strains of MDCK cells which resemble separate nephron tubule segments, *Biochim. Biophys. Acta* **673**, 26-36, 1991.

23. Hamill, O. P., Marty, A., Neher, E., Sakmann, B. and Sigworth, F. J. (1981). Improved patch-clamp techniques for high-resolution current recording from cells and cell- free patches, *Pflugers Arch* **391**, 85-100.

24. Penner, R., Pusch, M., and Neher, E. (1987). Washout phenomena in dialyzed mast cells allow discrimination of different steps in stimulus-secretion coupling. *Biosci. Reports* 7(4), 313- 321.

25. Norman, A.W., Spielvogel A.M., Wong, R.G. (1976). Polyene antibiotic-sterol interaction in *Advances in Lipid Research* (R. Paoletti, and D. Kriechevsky, eds.). **14**, pp. 127-170. Academic Press, New York.

26. Boontaveekul, S. (1992). The characterization of the LLC-PK_1 cell line and a preliminary study of Amphotericin B's effects on this cell line. MS thesis. University of Wisconsin- Madison.

27. Block, M. L., and Moody, W. J. (1990). Voltage-dependent chloride currents linked to the cell cycle in Ascidian embryos, *Science* **247**, 1090-1092.

28. Witzke, N. M., Bittman, R. (1984). Dissociation kinetics and equilibrium binding properties of polyene antibiotic complexes with phosphatidylcholine/sterol vesciles. *Biochemistry* 23, 1668-1674.

29. Strauss, G. (1981). Can. J. Spectroscopy 26, 95-102.

30. Whyte, B. S., Perterson, R. P., and Hartsel, S. C. (1989). Amphotericin B and Nystatin show different activities on sterol-free vesicles, *Biochem. Biophys. Res. Commun.* 164(2), 609-614, 1989.

31. Bolard, J., Seigneuret, M.,and Boudet, G. (1980). Interaction between phospholipid bilayer membranes and the polyene antibiotic Amphotericin B. lipid state and cholesterol content dependence, *Biochim. Biophys. Acta* 599, 280-293.

32. Bolard, J. and Cheron, M. (1982). Can. J. Biochemistry. 60, 782-789.

33. Vertut-Croquin, A., Bolard, J., Chabbert, M. and Garybobo, C. M. (1983). Biochemistry 22, 2939-2944.

34. Bolard, J., Seigneuret, M. and Boudet, G. (1980). Biochim. Biophys. Acta 599, 280-293.

35. Chen, W. C., Sud, I. J., Chou, D. and Feingold, D. S. 91977). Biochim. Biophys. Res. Commun. 74, 480-487.

36. Benson, J. M. and Nahata, M. C. (1988). Clinical use of systemic antifungal agents. *Clinical Pharmacy* 17, 424-438.

37. Gonzalez-Mariscal, L. Borboa, L., Lopez-Vancell, R., Beaty, G. and Cereijido, M. (1985). Electrical Properties of MDCK cells, in *Tissue Cultrue of Epithelial Cells* (Taub, M. ed.). pp. 25-36. Plenum Press. London.